Journal of Cardiovascular Magnetic Resonance (2006) **8,** 117–210

ISSN: 1097-6647 print / 1532-429X online
DOI: 10.1080/10976640500479011

Friday Posters

321. THE PREVALENCE OF MYOCARDIAL SCAR IN PATIENTS NO PRIOR HISTORY OF CARDIAC DISEASE DETECTED BY DELAYED-ENHANCEMENT CARDIAC MAGNETIC RESONANCE

Simon Greulich, MD,[1] Igor Klem, MD,[1] John F. Heitner, MD,[2] Holger Vogelsberg, MD,[1] Srivani Ambati, MD,[3] Martina Mangin, MD,[1] Udo Sechtem, MD[1]. [1]***Robert-Bosch-Krankehaus, Stuttgart, Germany,*** [2]***New York Methodist Hospital, New York, NY, USA,*** [3]***Duke University Medical Center, Durham, NC, USA.***

Background: Patients with myocardial scar (scar) are at increased risk for cardiovascular mortality and morbidity. Delayed enhancement cardiac magnetic resonance imaging (DE-CMR) is highly accurate in the detection of scar. The pattern of myocardial scar can be divided into 2 groups: 1. Coronary artery disease (CAD) based on location, ie extending from subendocardium to subepicardium; and 2. Non-CAD based on mid-myocardial or epicardial location. The prevelance of these patterns of scar in patients with no prior history of infarction or CAD is unknown.

Purpose: To assess the prevalence of scar (both CAD and Non-CAD) by DE-CMR in patients with clinically suspected CAD and no previous cardiac disease.

Methods: We prospectively enrolled 42 consecutive patients (pts) without a prior history of cardiac disease including myocardial infarction who were referred for elective coronary angiography (CA) based on clinical suspicion of CAD. DE-CMR was performed in all patients within 24 hrs of CA. DE-CMR images were scored visually, blinded to patient identity, using a 17-segment model. The presence of silent MI by DE-CMR was defined as the presence of hyperenhanced myocardium in a pattern typical of CAD. Non-CAD pattern of hyperenhancement was defined as either midmyocardial or epicardial HE representing primary myocardial disease. Patients were considered positive for CAD if there was $\geq$70% coronary stenosis on CA.

Results: The prevalence of CAD by CA was 38% (16 pts). DE-CMR showed evidence of HE in 9 pts (21%). Four (44%) patients had a HE pattern consistent with CAD, and 5 pts. (56%) had Non-CAD type of HE. The mean silent MI size was 9.4% of total LV mass, the mean size of scar in the Non-CAD group was 1% of total LV mass. Of the 4 pts. with evidence of silent MI by DE-CMR, three had significant stenosis on CA, and one pt. had non-obstructive disease on CA. Among the 5 pts. with evidence of Non-CAD type of scar, 4 had no CAD on CA, one pt. with HE in the midmyocardial basal septum (0.8% of LV mass) had evidence of obstructive CAD (posterior descending artery) on CA.

Conclusion: There is a high prevalence of scar in patients with clinically suspected CAD but without previously known cardiac disease. DE-CMR has additive diagnostic value for the evaluation of patients with clinical suspicion of CAD.

322. CARDIOVASCULAR SAFETY OF EVP 1001-1 (SEEMORE™), AN INTRACELLULAR AGENT FOR MAGNETIC RESONANCE IMAGING OF THE ISCHEMIC HEART

Peter R. Seoane, PhD, Phillip P. Harnish, PhD. ***Eagle Vision Pharmaceutical Corp., Exton, PA, USA.***

Introduction: Manganese (Mn) has demonstrated potential utility for imaging of the heart from the early days of magnetic resonance imaging. Mn has been shown to distribute rapidly from the blood to myocardium, providing a persistent pattern of enhancement that reflects local perfusion at the time of intracellular uptake. Unfortunately, Mn activity at calcium channels depresses the heart and relaxes blood vessels at doses and rates of administration relevant for imaging. This results in acute decreases in blood pressure, electrical disturbances such as prolonged P-R and Q-T intervals and ventricular arrhythmias. One may improve the cardiac safety of Mn via chelation while sacrificing two key advantages of Mn, rapid tissue uptake and high relaxivity. These factors significantly limit the utility of chelated Mn for imaging the ischemic heart. Through formulation with calcium, EVP 1001-1 mitigates the undesired cardiovascular effects associated with Mn while retaining the kinetic and magnetic properties that enable imaging of the ischemic heart.

Purpose: To evaluate the cardiovascular safety of EVP 1001-1 administered to beagle dogs at rest and under peak pharmacologic stress.

Methods: Groups of three anesthetized beagle dogs were dosed with EVP 1001-1 (120 μmol/kg IV over one minute) at rest, at peak dipyridamole stress (142 μmol/kg/min IV for 4 minutes) and at peak dobutamine stress (40 μg/kg/min IV for 20 minutes). Blood pressure, heart rate and electrocardiogram (ECG) were continuously monitored from induction of anesthesia through up to one hour following administration of EVP 1001-1. ECG recordings (12 Lead) were obtained and P-R, R-R and Q-T intervals measured at predetermined timepoints prior to stressor administration, during stress induction and for up to one hour following EVP 1001-1 administration. QTc was derived from Q-T and R-R measurements using Fridericias's correction.

Results: When animals were dosed with EVP 1001-1 at rest, a small increase in mean arterial blood pressure was noted that resolved within minutes of administration. The animal's heart rate was not affected and no significant changes were noted on ECG. In animals that were underwent maximal stress with

either dipryridamole or dobutamine, EVP 1001-1 did not exacerbate the hemodynamic stress, alter ECG or result in cardiac rhythm changes. Thus the No Observable Adverse Event Level (NOAEL) for EVP 1001-1 is greater than 120 μmol/kg, or more than 12 times the anticipated maximum clinical dose.

Conclusions: Cardiac MRI with EVP 1001-1 may be accomplished without the cardiac depression or ECG changes typically associated with Mn, even when given under peak pharmacologic stress. Previous studies have shown that the magnetic and pharmacokinetic properties of EVP 1001-1 are consistent with the requirements for steady state imaging of the ischemic heart. Thus, EVP 1001-1 may be safely administered under exercise or pharmacologic stress away from the magnet, with full cardiac monitoring. Imaging of the stress induced pattern of enhancement, which evolves shortly after administration of EVP 1001-1 and persists for more than 90 minutes, may be performed once the patient has returned to the resting condition. Imaging of the perfusion deficit may be performed as desired during this period without the need for additional stress or doses of EVP 1001-1. Studies in patients are currently underway.

Acknowledgment: This work was supported in part by the National Heart Lung and Blood Institute/NIH, Grant # R44HL63518.

323. CLINICAL SAFETY EVALUATION OF CARDIAC MRI EARLY AFTER CORONARY STENT IMPLANTATION IN ACUTE MYOCARDIAL INFARCTION PATIENTS

Paula Tejedor,[1] Alberto San Román,[2] Itziar Gómez,[2] José Sierra,[3] Juan Manuel Durán,[1] Francisco Fernández-Avilés.[2] ***[1]Hospital General Yagüe, Burgos, Spain, [2]Hospital Clínico Universitario, Valladolid, Spain, [3]Centro Diagnóstico Valladolid, Valladolid, Spain.***

Introduction: MRI provides helpful information in patients in the inmediate post-stent PCI (percutaneous coronary intervention) period. However, current "information for use guidelines" recommend to wait at least 8 weeks for the MRI to be safe, because of theoretical concerns of stent dislodgment when exposed under a magnetic field. Most clinicians perform cardiac MRI before 8 weeks, although information on safety is lacking.

Purpose: To determine whether to perform a cardiac MRI in the first 2 weeks after stent-PCI in patients with the diagnosis of AMI is a safe procedure.

Methods: We retrospectively study 409 postAMI patients. Mean age was 62 ± 11, 85% were males. 43% of all the patients were treated by primary PCI (percuataneous coronary intervention) and 76% by facilitated PCI (thrombolysis followed by PCI within 24 hours). Cardiac MRI was performed in 86 patients (group 1, n = 86) according to physician's criteria an average of 14 ± 11 days after the stent implantation. MRI was not performed in group 2(n = 312). All MRI examinations were performed in a 1.5 Tesla scan. Cine-MRI images were obtained using an ultra-fast gradient-echo sequence (FIESTA^{TM}, General Electric). Safety outcomes included occurrence of stent thrombosis, myocardial infarction, target vessel revascularization and rehospitalization during index hospitalization and at 6 and 12 months after the AMI.

Table 1

Variables	Group 1 (MRI, n = 86)	Group 2 (No MRI, n = 321)	p
Anterior AMI, n (%)	58 (67.4)	117 (36.4)	<0.001
Baseline angiographic EF, mean ± SD	51 (11)	55 (11)	0.008
Primary PCI, n (%)	23 (27.7)	76 (23.7)	0.44
Facilitated PCI, n (%)	60 (72.3)	245 (76.3)	0.44
Stainless steel stents, n (%)	81 (98.8)	321 (100)	0.9
CPK-MB, gr	343.99	293.73	0.09
Target vessel revasc, n (%) at 12 months	4 (4.7)	19 (5.9)	0.79
Reinfarction, n (%) at 12 months	2 (2.3)	7 (2.2)	0.99
Death, n (%) at 12 months	0	11 (3.4)	0.13

Results: Baseline and cardiovascular risk factors were not different in both groups. Reperfusion therapy was similar in both groups of patients (Table 1). Infarct size determined by quantification of cardiac markers was also quite similar between the two groups. Baseline angiographic mean ejection fraction (EF) was slightly inferior in group 1 (EF = 51 ± 11%) than in group 2 (EF = 55 ± 10, $p < 0.008$). The vast majority of the implanted stents were 316 L stainless steel in both groups of patients. There was no significant difference in the percentage of patients receiving double antiplatelet therapy (aspirine plus clopidogrel) for at least one month after the stent implantation. No clinical complication was described in the post-inmediate MRI procedure. During index hospitalization, 3 acute stent thrombosis were registered, all of them in group 2 (no CMR). At 12 months, MACE (including death, reinfarction, rehospitalization and revascularization) was 14% in group 1 and 15.6% in group 2 ($p = 0.7$) (Table 1).

Conclusions: Cardiac MRI performed within 2 weeks of stent-PCI in the postAMI setting appears to be a safe procedure, with a very low risk of MACE. Delaying MRI in the immediate post stent implantation period does not appear to be necessary.

324. MICROVASCULAR OBSTRUCTION IN AN EXPERIMENTAL REPERFUSED ACUTE MYOCARDIAL INFARCTION AT THE VERY EARLY STAGE: EVALUATION USING A MODIFIED T1 PREP LOOK-LOCKER SEQUENCE

Yuesong Yang, MD, PhD, Warren D. Foltz, PhD, John Graham, MD, Jay S. Detsky, BSc, Alexander J. Dick, MD, Graham A. Wright, PhD. ***Sunnybrook and Women's College Health Sciences Centre, Toronto, ON, Canada.***

Introduction: The concept of microvascular obstruction (MO) or the "no-reflow" phenomenon in the infarcted myocardium was proposed decades ago using a canine model. However, the linkage between the MO and unfavorable clinical prognosis has

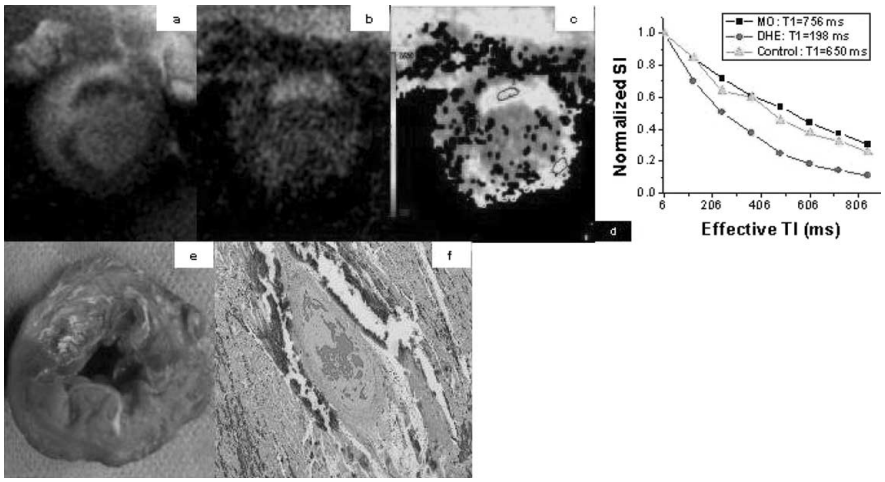

FIG. 1. a. DE-MRI: MO as hypo-enhanced region (TI = 250 ms). b. One T1 prep difference image (post-Gd, TI = 606 ms): MO was positive enhanced area. c. T1 map: ROI 1: MO, ROI 2: DHE, ROI 3: Control region. d. Normalized signal intensity changes over eight data points. e. TTC staining. f. Histology (HE statining): necerosis and hemorrhage present. A small arteriole totally occluded by disrupted red blood cells, platelet and fibrin was observed in MO region.

been established only in recent years using TIMI flow, myocardial contrast echocardiography and MRI. Delayed enhanced MRI (DE-MRI) has been widely used for myocardial viability determination. The MO in acute myocardial infarctions (AMI) has been detected as hypoenhanced regions. A noninvasive MRI technique with positive enhancement of MO would be preferred.

Purpose: To investigate a modified T1 prep Look-Locker sequence before and during a Gd-DTPA infusion for evaluation of MO in a porcine model of reperfused AMI.

Methods: In seven Yorkshire pigs (22–28 kg) a reperfused AMI was produced under X-ray guidance using a 90-minute percutaneous balloon occlusion of the distal LAD, followed by reperfusion. MRI studies were performed on a GE 1.5T Signa Excite system. All pigs underwent a baseline MRI examination including a SSFP functional study and T1 mapping. The T1 map uses a modified Look-Locker sequence acquiring a set of 8 spiral images, corresponding to the differences between signals in a train of 20-deg excitations at intervals of 120 ms, obtained with and without a preceding inversion at the same cardiac phase. The signal difference isolates the T1 contribution from the approach to steady-state in the small-tip train, so that longer T1 values yield bright signal at later points (effectively longer TI). After the intervention, SSFP and T1 mapping sequences were repeated in the same location. First pass myocardial perfusion (FPMP) was obtained immediately after a Gd-DTPA bolus injection (0.2 mmol/kg) followed by a continuous intravenous drip of Gd-DTPA. DE-MRI was performed 30 minutes post-injection and T1 mapping was applied 45 minutes post-injection. Pigs were sacrificed for TTC staining and histology. SSFP LV function, FPMP and DE-MRI analysis were conducted using Mass Plus software (Medis). T1 change was calculated from the MO, DE-MRI hyperenhanced (DHE), control segments and LV with the following formula: [(T1 at baseline—T1 at steady state post Gd-DTPA)/T1 at baseline] using manually drawn regions-of-interest and custom or commercial fitting algorithms (Xcinema, Stanford; Functool 2, GE).

Results: MO was seen in six of seven pigs. MO was defined as the persistent hypoenhanced area in the infarcted myocardium in FPMP and DE-MRI (Fig. 1a). Upon the modified Look-Locker technique post-contrast, MO was identified as bright regions in

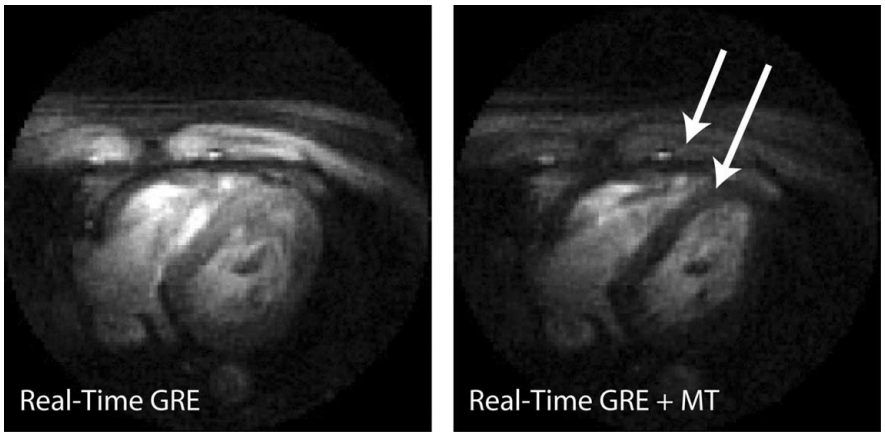

FIG. 1.

later difference images while the surrounding DHE regions appeared dark (Fig.1 b–c). Figure 1d shows the typical signals from MO, DHE and control regions in difference images across the small tip train. MO areas calculated from the DE-MRI (1.46 ± 0.84 cm^2) and T1 images (1.54 ± 0.91 cm^2) in the same location were comparable with a trend toward greater area in the T1 images although no statistical significance was reached ($p = 0.20$, paired *t*-test). T1 reduction (%) in MO regions (23.5 ± 21.8) was small compared to measurements from the control segments (38.2 ± 7.3, $p = 0.13$), DHE regions (72.8 ± 14.5, $p = 0.0004$) and LV (83.5 ± 10.9, $p = 0.005$) using a paired t-test. Pre-contrast T1 values across the myocardial segments were the same. All pigs had an AMI demonstrated by TTC staining and histology and occluded microvessels were seen in MO (Fig. 1e–f).

Conclusions: MO at early stages of reperfused AMI can be identified as a bright area on images from a modified T1 prep Look-Locker sequence post-contrast. Observations suggest reduced Gd-DTPA distribution volume in MO relative to both control and DHE regions. Quantitative results yield greater specificity while positive contrast may help identify even partial volumes of MO.

REFERENCES

1. Kloner RA. JCI 1974;54:1496.
2. Topol EJ. Circulation 2000;101:570.
3. Hombach V. EHJ 2005;26:549.
4. Wright GA. 4th ISMRM Proceedings 1996;1474.

325. VENTRICULAR FUNCTION WITH REAL-TIME MTC

Juan M. Santos,[1] Bob S. Hu,[2] John M. Pauly[1]. [1]*Stanford University, Stanford, CA, USA,* [2]*Palo Alto Medical Foundation, Palo Alto, CA, USA.*

Introduction: The evaluation of ventricular function is one of the most important applications of cardiac magnetic resonance imaging. Earlier imaging sequences frequently employed spoiled gradient-recalled fast imaging techniques. While the method is useful, contrast between the blood and myocardium was frequently inadequate in the presence of slow flow. Recently, the introduction of fast SSFP imaging sequences to cardiac imaging has considerably improved the delineation of myocardium and blood. However, SSFP imaging suffers from significant artifacts in the presence of rapid blood flow. SSFP is also more susceptible to artifacts at higher field strength. An alternative cardiac imaging technique that provides good contrast between the myocardium and blood, does not depend on inflow refreshment, and possesses good off-resonance properties would be a welcome addition to the current sequences. One mechanism for producing good blood to myocardium contrast is magnetization transfer (1). MT contrast is flexible and can be used in the pulsed mode. We developed a cardiac imaging sequence using a flexible real-time architecture that allows MT pulses to be interleaved with a gradient-recalled fasting imaging sequence. This sequence reliably improves the blood-myocardial contrast while remaining highly resistant to flow and susceptibility artifacts.

Purpose: To obtain real-time ventricular function images without flow artifacts and with good myocardium blood contrast.

Methods: Pulsed mode MT contrast uses RF pulses to saturate the macromolecule pool, while minimizing the effect on the liquid pool. Net zero degree excitation pulses accomplish this by using the short T2 characteristic of the macromolecule pool. Alternatively, off-resonance excitation can take advantage of the high bandwidth of the macromolecule pool by shifting the excitation band where the water pool is minimally sensitive. Contrast is then obtained by saturation of the liquid pool on some tissues due to a magnetization exchange process. We have added an off-resonance MT pulse at the end of a real-time GRE sequence that continually saturates the macromolecule pool. One of the challenges of MT contrast imaging is to optimize the MT pulse parameters. We take advantage of the dynamic nature of the real-time system (2) by tuning the parameters during the course of the experiment. We have added control over the pulse width, center frequency and RF power. With these parameters, the tradeoff between SAR, water pool direct saturation and pure MTC can be optimized.

Results: To observe the effect of MTC in real-time, an axial view of the heart was acquired every 75–95 ms (depending on the duration of the MT pulse). The pulse parameters were interactively optimized to obtain the best possible myocardium saturation, while minimizing the effect on blood, the SAR and the pulse duration. The Fig. shows two frames of the experiment before and after the application of the MT pulse.

Conclusions: Magnetization transfer is a mechanism for contrast production that is independent of conventional T1 and T2 imaging. MT produces contrast that is often similar to T2 weighted images. We have shown that MT when applied to the heart can provide additional benefits beyond the currently available sequences. Its principal disadvantage is the increased SAR, which can be minimized to well within the FDA limits.

REFERENCES

1. Wolff, et al. MRM 1989;10:135–144.
2. Santos, et al. IEEE EMBS 2004;1048.

326. RAPID MR ANGIOGRAPHY WITH RANDOMLY UNDER-SAMPLED 3DFT TRAJECTORIES AND NON-LINEAR RECONSTRUCTION

Michael Lustig, David L. Donoho, PhD, John M. Pauly, PhD. *Stanford University, Stanford, CA, USA.*

Introduction: Recently, we proposed a rapid imaging method using under-sampled randomly perturbed spirals and non-linear reconstruction (1). This method is inspired by theoretical results in sparse signal recovery (2, 3, 4) showing that sparse or compressible signals can be completely recovered from randomly under-sampled frequency-domain data. We now propose a rapid 3D Cartesian imaging method based on similar ideas. Pure random sampling in 2D is impractical for MRI hardware, however,

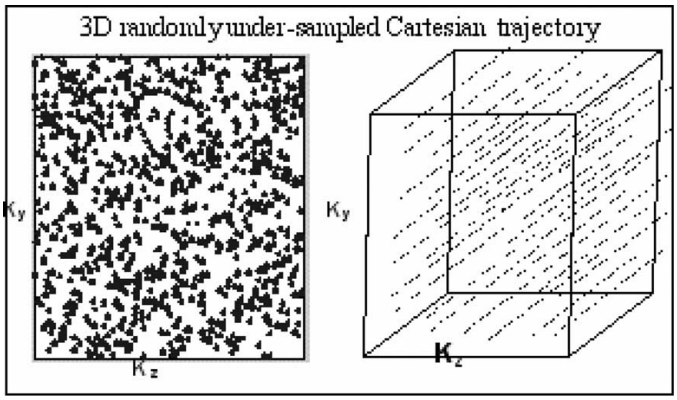

FIG. 1. Under-sampling is achieved by randomly throwing away phase encodes in the $k_y - k_z$ plane (left).

randomly under-sampling the two phase encodes in a 3D Cartesian scan is practical, involves no overhead, is purely random in two dimensions and is simple to implement by minor modification of existing product pulse sequences. We reconstruct by minimizing the L_1 norm of a transformed image subject to data fidelity constraints. We apply this method for magnetic resonance angiography where the images are truly sparse and short scan time is crucial. We demonstrate in vivo SSFP angiograms (5) acquired with a scan-time reduction of more than three.

Theory: Medical images in general and angiograms specifically often have a sparse representation in some domain (such as finite differences, wavelets, etc.). Aliasing artifacts due to random under-sampling are incoherent and appear as additive noise in the sparse domain. Therefore, the sparse coefficients can be recovered by a non-linear reconstruction scheme based on minimizing the L_1 norm, as described in (1–4). Sparsity is exploited by constraining our reconstruction to have a sparse representation and be consistent with the measured k-space data.

Methods: Angiograms have high signal from blood vessels and particularly low background signal. In fact, the images are mostly piece-wise constant. Therefore, we use a reconstruction as described in (1–4) with an L_1 Total-Variation (TV) (1, 2, 6, 7) penalty—a penalty known to preserve edges (6, 7) and represent piece-wise object sparsely. To validate our approach we considered a non-contrast T_2 prepared fat suppressed SSFP angiogram (5) of a leg (TR/TE 4.6/2.3). A full data set was acquired and under-sampled to 33% retrospectively by randomly throwing away phase encodes as illustrated in Fig. 1. The data was reconstructed with L_1 TV reconstruction implemented with finite derivatives. Results were compared to a linear reconstruction by zero filling and the original fully sampled reconstruction. Our reconstructions used a non-linear conjugate gradient solver (6). The experiment was performed on a 1.5T GE Signa scanner.

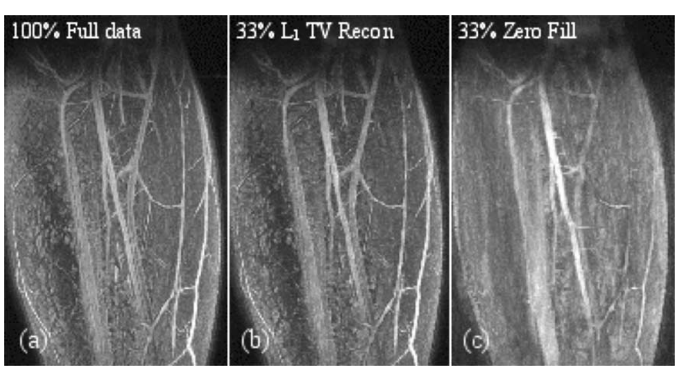

FIG. 2. Maximum intensity projection of non-contrast T_2 prepared fat suppressed SSFP angiogram of the leg. (a) Reconstruction from full data. (b) Our L_1 TV reconstruction from 33% of data. (c) Reconstruction by zero-filling the missing data.

Results and Discussion: Figure 2 illustrates a maximum intensity projection (MIP) of the reconstructions. As expected, reconstruction from by zero filling is severely degraded by aliasing artifacts and most vessels do not show in the MIP. On the other hand, the L_1 reconstruction was able to recover the sparse signal and produces a similar quality MIP to the fully sampled reconstruction but with only 33% of the data. In conclusion, L_1 -penalized image reconstruction, recovers sparse images even with severe under-sampling. The non-linearity of the L_1 norm and the random sampling is the key; however our method is more computationally intensive than traditional linear methods. In the current, rather inefficient Matlab™ implementation we are able to reconstruct a $128 \times 128 \times 256$ volume in 120 minutes. This approach can be used to reduce scan time, or to gain spatial or temporal resolution.

REFERENCES

1. Lustig, et al. 12th ISMRM 2004:685
2. Candès, et al. Robust uncertainty principles: Exact Signal Reconstruction from Highly incomplete Frequency Information." Available at: http://www.math.ucla.edu/~tao/preprints/Exact4.pdf. Accessed 2004.
3. Donoho DL. Compressed Sensing. Available at: http://www-stat.stanford.edu/~donoho/Reports/2004/ExtCS-102204.pdf. Accessed 2004.
4. Tsaig, et al. Extensions of Compressed Sensing. Available at: http://www-stat.stanford.edu/~donoho/Reports/2004/ExtCS-102204.pdf. Accessed 2004.
5. Bangerter, et al. 12th ISMRM 2004:11.
6. Bronstein, et al. IEEE TMI 2002;21:1395–1401.
7. Rudin, et al. Phys D 1992;60:259–268.

327. PTAGs: COMBINING PARTIAL TAGGING WITH SSFP

Vinay M. Pai, PhD,[1] Maureen Hogan, MS,[2] Roderick Pitts, BS.[1] [1]*New York University School of Medicine, New York, NY, USA,* [2]*Oxford University, Oxford, United Kingdom.*

Introduction: Myocardial tagging is an established approach for evaluating cardiac wall function. However, several hurdles still exist in developing tools for analyzing tagged datasets. These include difficult in segmenting epicardial and endocardial contours, and analysis of early systolic phases when SSFP-based sequences are considered. We present here a partial tagging approach which may alleviate these problems. In this multi-echo SSFP approach, the central region of k-space is acquired in a non-tagged manner, and the outer regions of k-space are acquired with tagging on.

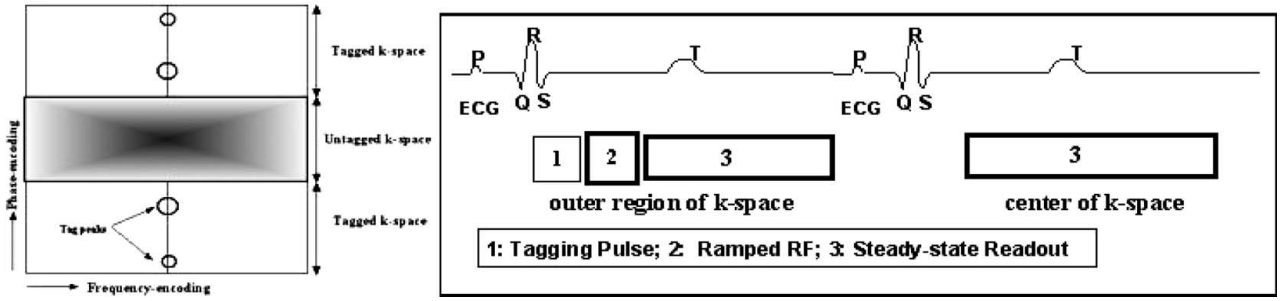

FIG. 1.

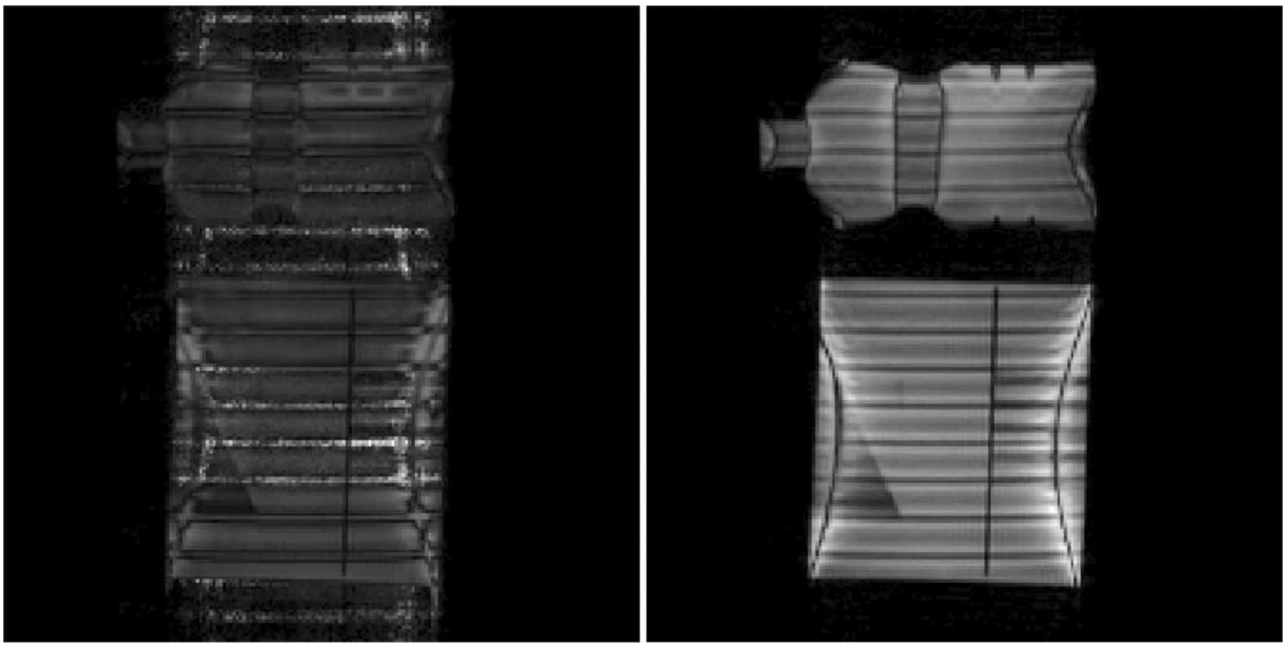

FIG. 2.

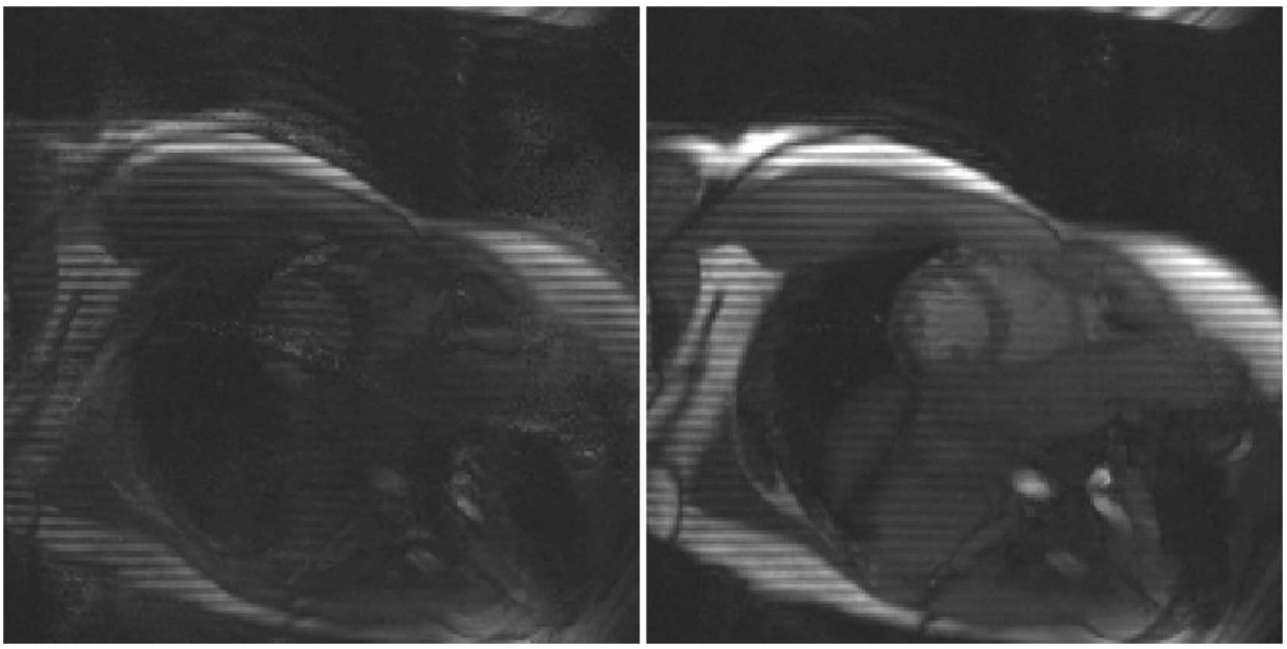

FIG. 3.

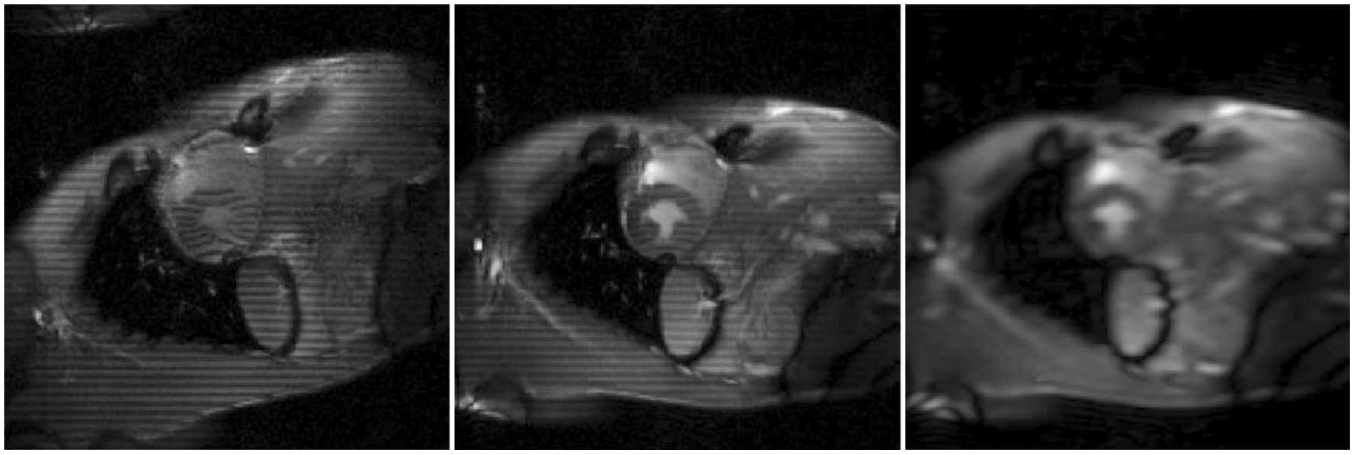

FIG. 4.

Purpose: A partial tagging approach could automatically provide tagged and untagged datasets from the same acquisition; the untagged dataset may then be used to generate the epicardial and endocardial contours for the tagged dataset. Since the center of k-space is acquired in a steady-state approach without any interruptions due to the tagging pulse, the transition artifact arising through such interruptions may be minimized, permitting analysis of the early systolic phases.

Methods: Due to the non-isotropic in-plane resolution, conventional tagging techniques acquire tagging echoes along the readout direction in k-space to minimize scan duration. However, use of an isotropic resolution imaging technique such as multiecho SSFP implemented with the phased array approach to ghost elimination (PAGE) (MESSFP-PAGE) permits acquisition of tagging echoes along the phase-encode direction in k-space, in short breathhold scan durations. Figure 1 shows the partial tagging (PTAG) approach when considered with the MESSFP-PAGE sequence. In this approach, the segments of the image data in the center of k-space are acquired in a steady-state manner with no tagging pulse applied, while the data segments farther away from the center of k-space are acquired with tagging pulses applied. For the tagging segments, the interruption to steady-state is minimized by using a ramped RF flip angle approach to reach steady-state subsequent to the tagging pulses. For reconstructing the tagged image, the data from the entire k-space is used; while the untagged image is reconstructed from the segments of the data acquired with no tagging pulse applied. Phantom and human studies were performed on Siemens Avanto and TIM Trio systems (Siemens Medical Solutions, Malvern, PA).

Results: The first image in the phantom and human cine acquisition with MESSFP-PAGE (Fig. 2a, 3a) and PTAG (Fig 2b, 3b) approaches are shown in Fig. 2 and 3 respectively. Since the center of k-space is acquired in steady-state in PTAGS, the image quality is considerably enhanced as compared to the conventional MESSFP-PAGE acquisition (which is affected by the ramped RF approach). Figure 4 compares the tagged data from MESSFP-PAGE and the PTAG approaches, along with the reconstructed untagged image from the PTAG data. Since the central k-space data and the tagged data are acquired in independent cardiac cycles, a higher flip angle can be used to acquire the central k-space data (60 in Fig. 4b, c), and a lower flip angle can be used to acquire the tagged portion of the k-space (45 in Fig. 4b, c), thus providing better myocardium-to-blood contrast. Figure 5 shows the contrast (= Mean Signal [tagged]—Mean Signal [untagged]) for the water phantom. Due to the band-pass filtering effect of the PTAGs approach, the tag contrast is reduced compared to the conventional MESSFP-PAGE technique.

Conclusions: Partial tagging when combined with SSFP readout approaches can be used to obtain tagged and untagged images simultaneously; the untagged image may be used to segment the epi- and endocardium in the tagged image; use of partial tagging minimizes/eliminates the transition artifacts seen in early systolic phases when SSFP tagging is used. This may make it useful to study myocardial wall function in early systolic phases.

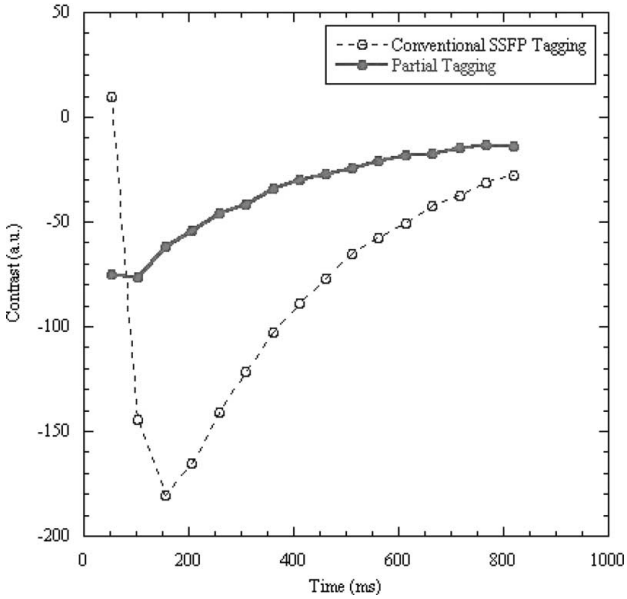

FIG. 5.

328. COMPARISON OF DELAYED ENHANCEMENT IMAGE QUALITY AT 1.5T AND 3T

Puneet Sharma, PhD, Josh Socolow, MD, Mushabbar Syed, MD, John N. Oshinski, PhD. ***Emory University, Atlanta, GA, USA.***

Introduction: The improved signal-to-noise ratio (SNR) at 3T compared to 1.5T has been observed in cardiac MRI applications (1), which can be used to improve visualization of small pathologies. For the assessment of myocardial viability, this can be a particular advantage, since quantification of infarct size has a direct correlation with patient prognosis (2). However, delayed enhancement is not only reliant on SNR and resolution, but also contrast-to-noise ratio (CNR) between enhanced infarct tissue (MI) and viable myocardium and/or the left-ventricular (LV) blood pool. Since the T1 relaxation time and T2* effects increase at 3T, question remains whether these trade-offs will compromise the image signal and contrast of delayed enhancement imaging at 3T.

Purpose: Our goal was to quantify the mean SNR of infarct tissue, the CNR between infarct and normal myocardium, and the relative signal contrast (RSC) between infarct and blood at 1.5T and 3T.

Methods: Seven individuals with known MI were recruited. The protocol was approved by the university's internal review board and all subjects gave written consent prior to the study. Each subject underwent two MRI exams: the first at 1.5T (Philips Intera, Best, The Netherlands) to confirm the presence and location of the MI, and the second exam at 3T (Philips Intera or Siemens Trio, Erlangen, Germany). Following localization of the short-axis plane, 0.2 mmol/kg Gd-DTPA-BMA (Omniscan, Amersham, Oslo, Norway) was administered intraveneouosly. Acquisition of delayed enhancement images began 10 minutes post-contrast and continued for approximately 25 minutes. The protocol was a segmented inversion recovery (IR) spoiled gradient echo (2D-FLASH) sequence with a 350 mm field of view, 256 matrix (75–100% phase encode acquisitions), TR/TE/α = 5 ms/2 ms/20°, 10 mm slice thickness, 16 lines/segment, 2 heartbeats/segment, inversion time (TI) = 250–300 ms, and 225 Hz/pixel bandwidth. The pulse sequence parameters were kept similar at 3T in light of SAR constraints and differences in gradient performance. Key 3T changes were TR/TE = 4.6 ms/2.3 ms, 448 Hz/pixel bandwidth, and TI = 250–310 ms. Region-of-interest measurements of the mean signal intensity were made in the LV blood pool, enhanced infarcted tissue, and normal myocardium (adjacent and remote to MI). SNR was quantified as the mean signal value divided by the standard deviation, which can be approximated in phased array receiver systems from the mean value of the background noise (3). CNR was measured as the SNR difference between two tissues, while the RSC was the ratio of infarct-to-blood signal strengths.

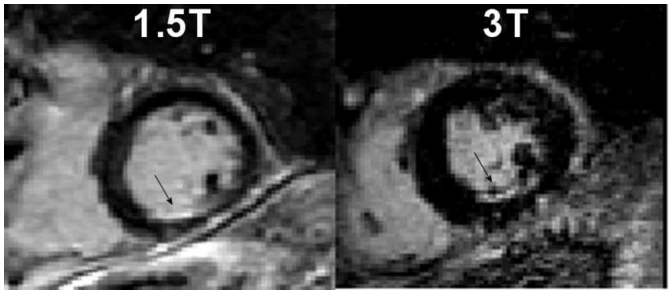

FIG. 1.

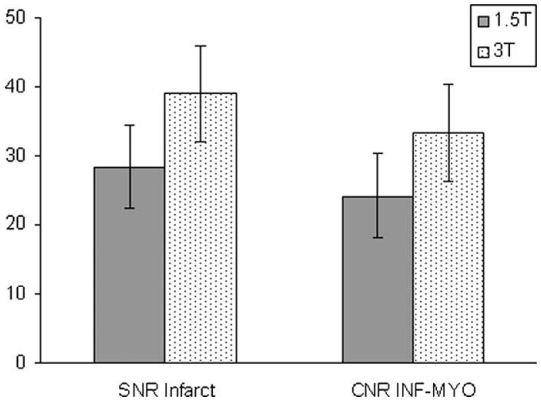

FIG. 2.

Results: Two subjects did not complete the 3T examination, leaving 5 subjects with SNR and CNR measurements. An example of delayed enhancement imaging at 1.5 T and 3T is shown in Fig. 1. There is improved visualization of the inferior MI at 3T and distinction with the blood pool. However, this trend was not evident in all subjects. In one particular subject, MI enhancement was much greater at 1.5 T, possibly due to a very high contrast agent concentration, which may have induced significant T2* dephasing at 3T. However, on average, the mean SNR of infarct tissue was higher at 3T (39.0 ± 14.6 vs. 28.4 ± 13.3), along with CNR between infarct and normal myocardium (33.3 ± 13.9 vs. 24.3 ± 11.4) (Fig. 2). The mean infarct-to-blood RSC also favored 3T (1.63 vs. 1.38), possibly enabling distinction of small subendocardial infarcts adjacent to the blood pool.

Conclusions: This preliminary investigation of delayed enhancement imaging at 3T reveals an average increase in infarct SNR and CNR relative to 1.5T in the same subjects and dose. This study suggests that 3T may provide additional benefits of improved resolution and infarct-to-blood contrast for the visualization of small subendocardial infarcts.

REFERENCES

1. Noeske R, et al. MRM 2000;44:978–982.
2. Kim RJ, et al. NEJM 2000;343:1445–1453.
3. Constantinides CD, et al. MRM 1997;38:852–857.

329. FREE-BREATHING DELAYED ENHANCEMENT MR CORONARY VESSEL WALL IMAGING IN PATIENTS WITH SUSPECTED CORONARY ARTERY DISEASE

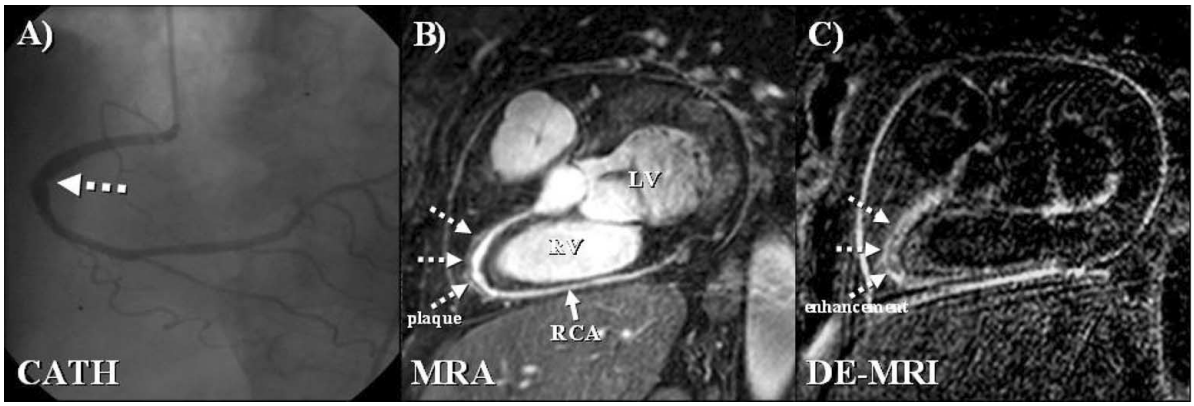

FIG. 1. 77 Years old patient with luminal/stenotic irregularities (A). B) Corresponding contrast enhanced coronary MRA showing an irregular lumen overlaid by an iso-intense layer suggestive for outward remodelling. C) Delayed enhancement vessel wall image demonstrates contrast uptake in the proximal and mid RCA suggestive for diffuse atherosclerosis.

Tareq Ibrahim,[1] Josef Dirschinger,[1] Silvia Schachoff,[2] Albert Schomig,[1] Markus Schwaiger,[2] Rene Botnar.[2]
[1] German Heart Center, Technical University Munich, Munich, Germany, [2] Department of Nuclear Medicine, Technical University Munich, Munich, Germany.

Introduction: Assessment of coronary plaque burden and stability is of major clinical interest in the diagnosis of coronary artery disease (CAD). Native MR coronary vessel wall imaging has been shown to allow measurement of vessel wall thickness in patients with CAD but widespread use was so far limited because of the long scan times, lack of robustness, and need for high spatial resolution. Contrast enhanced plaque imaging is flow insensitive, relatively fast and thus potentially a more robust technique. In addition, contrast enhanced vessel wall imaging may allow reducing the imaging task to the detection of the presence/absence of contrast uptake, thereby reducing the requirements on spatial resolution. Thus, we recently introduced a delayed enhancement approach for the assessment of contrast uptake in the coronary vessel wall.

Purpose: We sought to investigate the relationship between conventional coronary angiography and delayed enhancement coronary vessel wall imaging (DE-MRI) in patients with suspected CAD.

Methods: Twelve patients (64 ± 13 years) that had undergone invasive coronary angiography were examined. Nine (75%) patients had angiographically confirmed coronary artery stenoses. All subjects were imaged in supine position using a 1.5T Phillips ACS-NT scanner equipped with a cardiac coil and a cardiac software package (R11). Approximately 30 minutes prior to MR scanning, 0.2 mmol/kg Gd-DTPA (Magnevist) was administered. Coronary MRA of the left and right coronary artery was performed using a magnetization prepared (T2prep, fatsat) 3D SSFP technique. Imaging parameters included spatial resolution = 1.25 × 1.25 × 3 mm, TR/TE = 5.4 ms/2.7 ms, flip angle = 110°, and slices = 20. Motion compensation was performed using ECG triggering and navigator gating and correction. Data were acquired using a patient specific mid-diastolic trigger delay. For determination of the inversion delay, a Look Locker sequence was performed. Subsequently (~60 min. post Gd injection), DE-MRI of the left and right coronary vessel wall was performed using a T1 weighted 3D inversion recovery fast gradient echo technique. Imaging parameters were identical to the coronary MRA sequence, except for: TR/TE = 6.1/1.9 ms, flip angle = 30° and inversion time ~280 ms. For MR image analysis, the three major coronary vessels were subdivided into a total of 8 segments. The intensity of contrast enhancement within the vessel wall was assessed for each segment according to a semi-quantitative score (0 = no, 1 = mild, 2 = moderate, 3 = severe) by consensus reading and compared with the corresponding invasive angiogram. Image quality was assessed on a scale from 1–4 with 1 being very good.

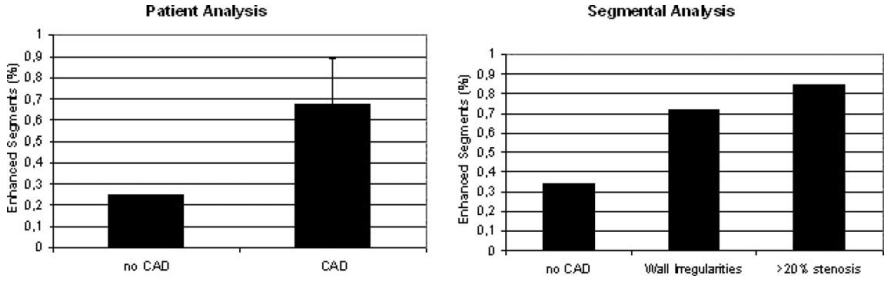

FIG. 2. Patient based and segmental analysis of vessel wall enhancement. In patients with CAD, contrast uptake was observed in ~68% of the evaluated segments while in patients with no angiographically detectable CAD, ~25% were enhanced.

Results: Image quality was good for both MRA (2.0 ± 0.4) and DE-MRI (1.7 ± 0.8) (Fig. 1). Altogether, 92 coronary artery segments in 12 patients were evaluated (1 segment not evaluated due to stent, 3 segments not available). MR contrast enhancement within the coronary vessel wall was significantly more often found in patients with CAD than in those with a normal x-ray angiogram (5.4 ± 1.7 vs. 2.0 ± 0 segments, $p = 0.008$) (Fig. 2a).

The enhancement score correlated with the severity of CAD ($r = 0.65$). Based on the segmental analysis, 85% of stenotic segments showed contrast enhancement within the coronary artery wall. However, the incidence of coronary contrast enhancement was also high in segments with only minimal wall irregularities (72%) and even in segments without detectable abnormalities (34%) by coronary angiography (Fig. 2b).

Conclusions: Delayed enhancement imaging is a promising technique for the non-invasive visualization of the coronary vessel wall. The good correlation of coronary vessel wall enhancement with clinically evident CAD suggests that contrast uptake may be associated with an increased distribution volume in the altered vessel wall, which is likely related to plaque formation. Coronary vessel wall imaging by DE-MRI thus may provide an estimation of coronary plaque burden and may allow detection of subclinical CAD. Further studies are now warranted to better understand the underlying pathophysiology of these observations.

330. QUANTITATIVE ASSESSMENT OF SUBEBDOCARDIAL PERFUSION ABNORMALITY IN HYPERTROPHIC CARDIOMYOPATHY: CORRELATION WITH MYOCARDIAL SCAR

Kakuya Kitagawa, MD,[1] Hajime Sakuma, MD,[1] Masaki Ishida, MD,[1] Tairo Kurita, MD,[1] Katsuya Onishi,[1] Takeshi Nakano, MD,[1] Atsushi Nozaki, PhD,[2] Kan Takeda, MD.[1]
[1]Mie University Hospital, Tsu, Japan, [2]GE Yokogawa Medical Systems, Tokyo, Japan.

Introduction: Previous studies demonstrated that myocardial ischemia occurs in patients with hypertrophic cardiomyopathy (HCM), despite of angiographically normal coronary arteries (1). A study employing ^{15}O-water PET indicated that subendocardial hypoperfusion could be an important mechanism of myocardial ischemia in patients with HCM (2). However, PET assessment of endocardial/epicardial (endo/epi) flow ratio was only feasible in the markedly hypertrophied septum. Quantitative analysis of first-pass contrast enhanced MRI permits assessment of transmural distribution of myocardial blood flow (MBF) for the entire LV myocardium.

Purpose: The purposes of this study were to determine the endo/epi flow ratio in HCM patients and to clarify the relationship between subendocardial hypoperfusion and myocardial scar.

Methods: Nine patients (6 men, mean age of 56 ± 17 years) with HCM were evaluated with a 1.5 T MR system. First-pass contrast-enhanced MRI was performed during ATP stress and in the resting state by using a saturation recovery prepared steady-state sequence (TR 3.0 ms; TE 1.2 ms, TI = 180 ms), following an intravenous bolus injection of gadolinium-contrast agent (0.05 mmol/kg, 4 mL/sec). After correcting saturation of the blood signal and coil sensitivity profile, arterial input and myocardial output time-intensity curves were analyzed with a Patlak plot method to quantify tissue K1, which represents product of tissue plasma flow and extraction fraction of extracelluar MR contrast media. Cine MRI and delayed-enhancement MRI were acquired on the same imaging planes and image analysis was performed by using a 16 segment model.

Results: In HCM patients, the endo/epi flow ratio was 0.99 ± 0.13 in the resting state, and significantly decreased to 0.92 ± 0.14 during stress ($p < 0.001$), which showed a good agreement with those reported by the previous radio-water PET study (2). No significant correlation was observed between the endo/epi flow ratio and end-diastolic wall thickness. In the 17 segments exhibiting delayed hyperenhancement, the endo/epi ratio was significantly reduced in comparison with the segments without delayed hyperenhancement both in the resting state and during vasodilator stress (0.91 ± 0.10 vs 1.00 ± 0.13 at rest; $p = 0.005$, 0.82 ± 0.12 vs 0.94 ± 0.13 during stress; $p = 0.001$).

Conclusions: While no transmural gradient of myocardial perfusion was observed in the resting state, subendocardial myocardial perfusion was significantly impaired during vasodilator stress in patients with HCM. Subendocardial perfusion abnormality during pharmacological stress had a close relationship with scar formation in HCM.

REFERENCES

1. Cannon RO, et al. Circulation 1991;83:1660–1667.
2. Choudhury L, et al. Basic Res Cardiol 1999;94:49–59.

331. IMPROVED WALL MOTION ASSESSMENT USING CINE DELAYED ENHANCEMENT MRI

Randolph M. Setser, DSc,[1] Yiu Cho Chung, PhD,[2] Arthur E. Stillman, MD, PhD,[1] Orlando P. Simonetti, PhD,[3] Richard D. White, MD[1]. ***[1]The Cleveland Clinic Foundation, Cleveland, OH, USA, [2]Siemens Medical Solutions, Chicago, IL, USA, [3]The Ohio State University, Columbus, OH, USA.***

Introduction: Cine delayed enhancement (CINE-DE) magnetic resonance imaging (MRI) has been proposed as a technique for simultaneous visualization of left ventricular (LV) wall motion and myocardial scar extent (1). However, the technique has previously been limited by inconsistent contrast between image frames and undersampling of ventricular systole in some patients, particularly in cases where heart rate is variable. Thus, we have now incorporated pre-pulses for better image contrast and alternate triggering strategies for better systolic coverage.

Purpose: To improve characterization of LV systolic function using CINE-DE imaging.

Methods: The CINE-DE technique is based on inversion recovery (IR), single-shot, balanced steady state free procession (TrueFISP) imaging. Each frame of the cine series is acquired during a separate heart beat using a constant inversion time (TI). However, the trigger delay (TDEL) is varied between images, resulting in a series of single-shot images, each from a different phase of the cardiac cycle. The first image in each cine series is acquired at TDEL = TI; because of the IR pulse, systolic images have been acquired in a subsequent heart beat (after diastolic images are acquired). However, now image acquisition is triggered using either a pulse oximeter signal, or using an ECG signal with a fixed delay time to begin imaging in mid-to-late diastole, to ensure that adequate systolic images are acquired. Furthermore, an "intelligent" trigger detection scheme is employed which detects ECG triggers throughout the acquisition to ensure that every heart beat is counted and that a consistent time interval between IR pulses is maintained. The sequence has been implemented on a 1.5T Sonata scanner (Siemens, Germany) using the following typical acquisition parameters: α 50°, TR 2.5 ms, TE 1.1 ms, BW 1090 Hz/pixel, FOV 380 mm, RFOV 75%, acquisition matrix 192 × 115 (frequency, phase). Fifteen image frames are acquired for each cine, with a variable temporal spacing to cover the cardiac cycle. Each cine series is acquired during a single breath-hold. A non-selective "dummy" IR pulse is applied before image acquisition for consistent image contrast throughout the cine series (increases breath-hold duration by 1 heart beat). Mid-ventricular short-axis CINE-DE images were acquired in 10 patients undergoing clinical assessment of myocardial viability, 10–25 minutes after intravenous injection of 40 mL 0.5 mmol/mL gadopentetate dimeglumine (Magnevist, Berlex Imaging), using an IRB approved protocol with waiver of individual consent. TrueFISP cine images were also acquired in each patient at anatomic levels matching the CINE-DE images. Two readers independently evaluated wall motion using the CINE-DE and cine TrueFISP images; each reader was blinded to other imaging results during analysis. Three myocardial segments were evaluated per short-axis slice, representing the LAD, LCX and RCA coronary territories. Segmental wall motion was graded as follows: normal (0), hypokinetic (1), akinetic/dyskinetic (2). In addition, the mass, end-diastolic volume (EDV), end-systolic volume (ESV), stroke volume (SV) and ejection fraction (EF) of each slice were computed.

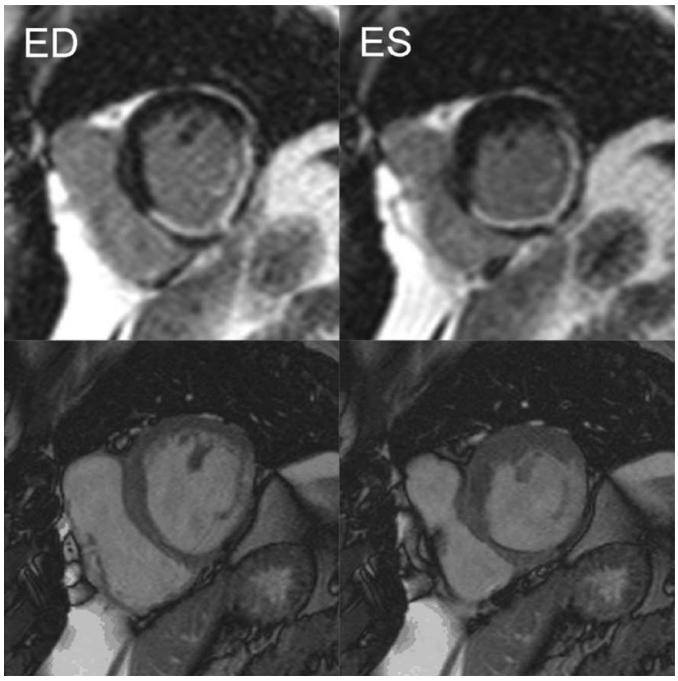

FIG. 1A.

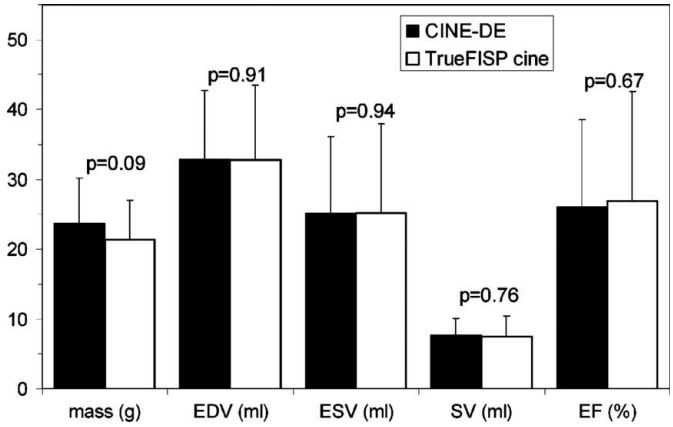

FIG. 1B.

Results: Temporal spacing of images averaged 64 ± 30 msec. Images from a single patient with non-transmural infarct are shown below left: CINE-DE images (top row) at end-diastole (ED) and end-systole (ES), and corresponding TrueFISP cine images (bottom row). For Reader 1, CINE-DE wall motion scores matched cine TrueFISP results in 24/30 segments (80%), and differed by ± 1 in 6/30 segments (20%). For Reader 2, CINE-DE wall motion scores matched cine TrueFISP results in 19/30 segments (63%), and differed by ± 1 in 11/30 segments (37%). As shown in the Figure 1 below right, there were no significant differences between image types in any quantitative parameter.

Discussion/Conclusions: "Intelligent" triggering schemes enable accurate quantification of LV systolic function using CINE-DE imaging.

REFERENCE

1. Proc/SMRM 2005;236.

332. THE EXTENT OF MYOCARDIAL SCAR IDENTIFIES PATIENTS WITH LEFT VENTRICULAR SYSTOLIC DYSFUNCTION WHO HAVE PERSISTENT ADVERSE VENTRICULAR REMODELING DESPITE PHARMACOLOGICAL TREATMENT: A CARDIAC

MAGNETIC RESONANCE STUDY WITH DELAYED ENHANCEMENT

Nikolay P. Nikitin, MD, PhD, Poay Huan Loh, MB ChB, MRCP, Ramesh de Silva, MB ChB, MRCP, Elena Lukaschuk, MSc, Duncan F. Ettles, MB ChB, MRCP, Andrew L. Clark, MA, MD, FRCP, John G. F. Cleland, MD, FRCP, FACC. ***University of Hull, Kingston Upon Hull, United Kingdom.***

Introduction: In chronic heart failure (CHF), beta-blockers and ACE inhibitors improve LV systolic function but not all patients respond.

Purpose: We sought to establish whether scar extent, assessed by cardiac magnetic resonance (CMR) with delayed enhancement (DE), can determine the risk of persistent adverse left ventricular (LV) remodeling despite standard pharmacological treatment.

Methods: Thirty-eight patients with CHF due to LV systolic dysfunction and already receiving treatment with ACE inhibitors/angiotensin receptor antagonists and beta-blockers underwent CMR with DE which was repeated after 12 months.

Results: DE on CMR (interpreted as scar tissue) was present in 24 patients. The scar mass was 24 ± 9 g (range 9–43 g) and scar extent (% of LV mass) was 17 ± 7% (range 6–31%). At baseline, there were no differences in clinical or CMR-derived indices between patients showing DE (DE + group) and no DE (DE − group). After 12 months, LV volumes and ejection fraction (EF) were unchanged in the DE+ group. In the DE− group, LV end-diastolic and end-systolic volumes fell (231 ± 83 to 196 ± 71 mL, $p = 0.018$ and 161 ± 74 to 120 ± 68 mL, $p = 0.007$, respectively) and EF increased (32 ± 11 to 41 ± 11%, $p = 0.003$). No DE- patients showed deterioration in EF of ≥5%. Eight DE+ patients who demonstrated deterioration in EF had higher scar extent than 17 DE + patients with no deterioration (22 ± 8 vs. 14 ± 3%, $p = 0.03$). There was a strong negative correlation between scar extent and change in EF ($p < 0.001$, $r = -0.77$).

Conclusions: In patients with LV systolic dysfunction, scar extent predicts the risk of persistent adverse LV remodeling despite conventional pharmacological treatment.

333. THREE-DIMENSIONAL VELOCITY OF THE MYOCARDIUM MEASURED BY MR PHASE VELOCITY MAPPING IN PATIENTS WITH VENTRICULAR DYSSYNCHRONY

Jana G. Delfino,[1] Mohit Bhasin,[2] Angel R. Leon,[2] Robert L. Eisner,[2] John N. Oshinski[1]. [1]***Georgia Insitute of Technology/ Emory University, Atlanta, GA, USA,*** [2]***Emory University, Atlanta, GA, USA.***

Introduction: Tissue Doppler imaging (TDI) has been proposed as a tool to detect ventricular dyssynchrony and to predict which patients will respond to Cardiac Resynchronization Therapy (CRT). However, several characteristics of TDI limit its ability to evaluate dyssynchrony, including difficulty evaluating radial velocities, inability to obtain adequate windows in some patients, and low reproducibility. Measurement of myocardial tissue velocity by magnetic resonance (MR) phase velocity mapping could potentially overcome some of these limitations.

Purpose: The purpose of this study was to examine three-dimensional myocardial tissue velocity in both normal volunteers and patients with ventricular dyssynchrony scheduled for CRT.

Methods: Twenty-eight patients with ventricular dyssynchrony (age = 64 ± 15) scheduled for CRT and 17 normal volunteers (age = 28 ± 7) participated in this study. MRI scans were performed on a Philips Medical Systems Intera CV MRI scanner. A segmented, navigator-echo and ECG-gated sequence was used to acquire three-directional myocardial velocity from a mid-basal short axis slice. Regions of interest (8 × 8 mm) were selected in the septal, lateral, anterior and inferior walls of the left ventricle. Values of velocity vs. time in these regions were exported to a spreadsheet for analysis. The acquired velocities were converted into radial velocity (positive toward the center of the LV blood pool), longitudinal velocity (positive toward the apex), and circumferential velocity (positive for clockwise rotation when viewed from the apex). Peak systolic and diastolic velocities, as well as the *time to peak* systolic and diastolic velocities were computed for all subjects. Normal and patient values were compared using a two-tailed t-test, with p-values < 0.005 considered statistically significant (denoted as *).

Results: Both peak radial and longitudinal velocities were greater in the normal volunteers than the dyssynchrony patients, both during systole and diastole. No significant differences were observed in the magnitude of peak circumferential velocity between the normal volunteers and the dsysynchrony patients, either during systole or diastole, Table 1. A significant delay in *time to peak* systolic velocity was observed in the *lateral* wall of dyssynchrony patients, Fig. 1. This delay was seen in both the longitudinal and radial directions, but not in the circumferential

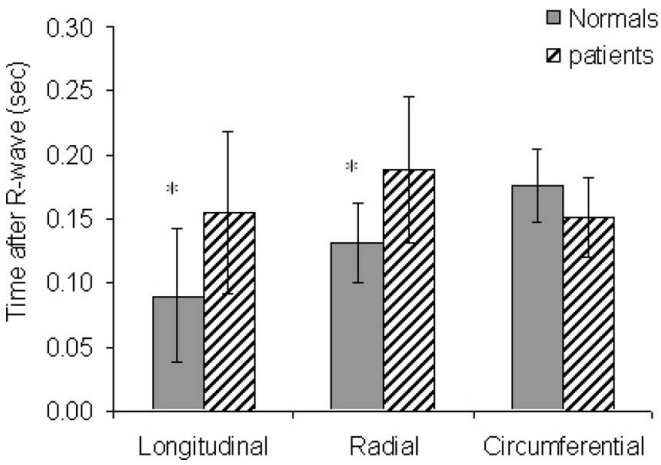

FIG. 1. Time to peak sytolic velocity in the lateral wall.

	Longitudinal velocity (cm/s)		Radial velocity (cm/s)		Circumferential velocity (cm/s)	
	Systole	Diastole	Systole	Diastole	Systole	Diastole
Normals	8.7 ± 2.8	−15.9 ± 4.1	5.4 ± 1.9	−8.2 ± 3.0	4.3 ± 1.6	−4.8 ± 2.3
Patients	5.1 ± 1.9	−5.8 ± 3.1	4.1 ± 1.7	−5.8 ± 3.0	4.2 ± 1.8	−4.9 ± 2.1
	$p < 0.001$	$p < 0.001$	$p < 0.001$	$p < 0.001$	p = NS	p = NS

direction. No significant differences in time to peak systolic velocity were observed in any of the other walls. Since the majority of patients had a left bundle branch block, a delay in peak velocity is expected in the lateral wall. The reason for the lack of significance in circumferential velocity may due to the location of the velocity measurement slice, as circumferential velocity varies greatly along the long axis of the LV.

Conclusions: Peak radial and longitudinal myocardial velocities were greater in magnitude in the normal volunteers than the dyssynchrony patients. No significant difference was observed in the magnitude of peak circumferential velocity. A significant delay in *time to peak* systolic contraction velocity was observed in the *lateral* wall of dsyssynchrony patients. This preliminary study indicates that 3-directional MR PVM may provide a new method to detect regional ventricular dyssynchrony.

334. A NEW ECG CLASSIFICATION TO ASSESS MYOCARDIAL INFARCTION LOCATION: VALIDATION BY CONTRAST-ENHANCED CMR

Sandra Pujadas, Juan M. Cino, Francesc Carreras, Mariana Noguero, Xavier Garcia-Moll, Ruben Leta, Guillem Pons-Llado, Antoni Bayes de Luna. ***Hospital de la Santa Creu i Sant Pau, Barcelona, Spain.***

Background: Electrocardiographic (ECG) location of myocardial infarction (MI) is based on early studies by Myer appeared in the mid 20th century. Despite the proven accuracy of contrast-enhanced cardiovascular magnetic resonance (CeCMR) to depict and locate infarcted myocardium, no global study has yet been conducted with the aim of correlating ECG patterns of Q-wave MI and infarct location. In the present study, a new ECG classification (as proposed by Bayés de Luna) is validated by means of CeCMR.

Material and Methods: Fifty-one patients with a first ST-elevation MI were studied by CeCMR 6 months after the event. A 12 lead ECG was also performed within the same week. The location of necrosis assessed by Ce-CMR was compared with the following 7 predefined ECG patterns of infarct location from the new classification, including 4 corresponding to the anteroseptal region (A-1, A-2, A-3, A-4) (n = 23) and 3 in the inferolateral zone (B-1, B-2, B-3) (n = 28):

A-1 *septal;* ECG pattern of necrosis in V1-V2 (QS, qrs or Qr)
A-2 *apical* and/or *anteroseptal;* ECG pattern of necrosis in V1-2 to V4-V6 (QS or Qr V1-V4)
A-3 *extensive anterior*; ECG pattern of necrosis in V1-V2 to V4-V6, I and/or VL (QS or QR until V4)
A-4 *limited antero-lateral;* ECG pattern of necrosis in I and/or VL (qs, qr, r) and sometimes "q" in V2-3
B-1 *lateral;* ECG pattern of necrosis (qr, r) in I, and/or VL and/or V5-6, and/or R (RS) in V1
B-2 *inferior;* ECG pattern of necrosis in II, III, VF (QS, QR, qR) without R (RS) in V1
B-3 *infero-lateral;* ECG pattern of necrosis in II, III, VF and/or V5-6, I, VL and/or R (RS) in V1

Results: The number of patients within the 7 defined ECG patterns and their concordance with the CeCMR location are shown in the following Table:

Globally, the concordance between ECG patterns and CeCMR for MI location, assessed by the Cohen's unweighted Kappa Index was 86%; 95% CI: (0.75- 0.97).

Conclusions:

1. The new predefined ECG patterns of MI location matched well with their corresponding infarcted area as detected by CeCMR.
2. Particularly noticeable findings were that the MI previously known as posterior (RS in V1) is due in fact to high lateral

	CeCMR location							
ECG pattern	Septal	Apical-anteroseptal	Extensive anterior	Limited anterolateral	Lateral	Inferior	Inferolateral	Total
A-1	6	2	0	0	0	0	0	8
A-2	0	7	1	0	0	0	0	8
A-3	0	0	4	0	0	0	0	4
A-4	0	0	0	3	0	0	0	3
B-1	0	0	0	0	4	0	1	5
B-2	0	0	0	0	0	9	1	10
B-3	0	0	0	0	0	1	12	13
Total	6	9	5	3	4	10	14	51

MI, and that the one known as high lateral MI (QS in VL) corresponds to a mid-anterior and mid-lateral MI.

335. MIXED MICELLES: A VERSATILE PLATFORM FOR MULTIMODALITY CT AND MRI IMAGING

Juan Carlos Frias, PhD, Karen C. Briley-Saebo, PhD, Venkatesh Mani, PhD, Fabien Hyafil, PhD, Jean-Francois Toussaint, PhD, Zahi A. Fayad, PhD. ***Mount Sinai School of Medicine, New York, NY, USA.***

Introduction: Mixed micelles offer a very flexible platform for the delivery of imaging contrast agents that may facilitate the study of atherosclerotic plaques. The size of the micelles can be easily modified by choice of the micelle components such as the phospholipid used (POPC or DPPC). Antibodies or peptides can be attached to the micelle surface allowing specific cellular uptake and molecular targeting. Although primary focus has been related to gadolinium mixed-micelles for MRI, it is also possible to incorporate other imaging materials, such as iodine, into or on the micelle surface. The resulting gadolinium-iodine micelles may potentially allow for CT/MR evaluation of plaque in all vessel types, including the coronary arteries.

Purpose: The purpose of this study was to synthesize and characterize gadolinium-iodine micelles for multimodality imaging with CT and MR.

Methods: Iodination of phospholipids is well described and the sonicated dispersion of phospholipids in water is found to form a 1:1 molecular complex with iodine when the concentration of phospholipids is above the critical value. Gadolinium(Gd)-iodine (I) micelles were prepared by incubating iodine with gadolinium micelles (7 w/w% of GdDTPA-$(C_{18})_2$), surfactant (Tween 80, 14 w/w%) and 79 w/w% POPC. Prior to iodine addition, the micelles exhibited the following physical and chemical properties: hydrated particle diameter = 106.5 Â ± 0.2 nm, r_1 blood = 13.0 Â ± 0.5 $s^{-1}mM^{-1}$ (63 MHz, rt), and Gd/micelle = 4,100. The micelles were incubated for 12 hours at 4 Â°C. Following the incubation, dialysis was performed to remove excess iodine. Micelles with constant gadolinium (2 mM Gd) and variable iodine concentrations (3–8 mg I/ml) were prepared in whole human blood. Omnipaque (GE Healthcare, a commercially available iodine CT contrast agent) was prepared in blood at 9-24 mg I/ml for comparison. CT images were obtained on a 64-slice scanner at 130 Kv, 163 mA and 0.6 s. MR imaging was performed on phantoms with iodine concentrations of either 0 or 8 mg I/ml and variable gadolinium concentration (0.1-0.5 mM Gd) in blood. Samples of GdDTPA (Magnevist, Berlex) in blood were also prepared for comparison. All MR imaging was performed at 1.5T using T1-w TSE sequences with TR/TE/flip = 300 ms/4.7 ms/90Â° and 4 NEX.

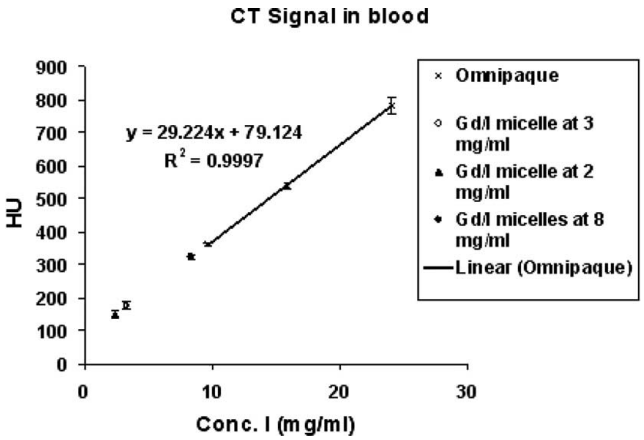

FIG. 1. Gd/l micelle, Gd concentration constant at 2 mM Gd.

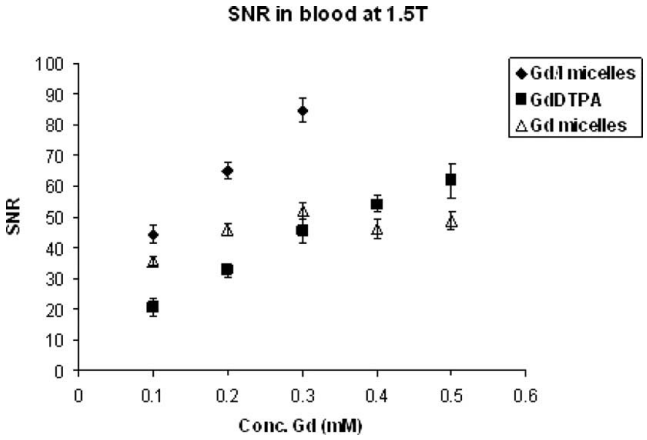

FIG. 2. SNR at 1.5T (TSE TR/TE = 300/4.7).

Results: Fig. 1 shows that the gadolinium-iodine micelle is able to significantly attenuate the CT signal. A linear relationship between CT signal and iodine concentration was observed. The MR phantom revealed that the Gd-I micelles significantly increase the SNR of blood, relative to both the Gd-micelles and GdDTPA (Fig. 2).

Conclusions: Preliminary phantom results suggest that the simultaneous incorporation of iodine and gadolinium complexes into mixed micelles could result in a new combined MRI-CT contrast agent that may be useful for the multimodality imaging of atherosclerotic plaques and cardiovascular disease.

336. SHOULD WE CONSIDER LV VOLUME INDICES WHEN DIAGNOSING LEFT VENTRICULAR DIASTOLIC HEART FAILURE: ANSWERS FROM A 3D CARDIOVASCULAR MAGNETIC RESONANCE EVALUATION

Vikas K. Rathi, MD,[1] Michael R. Zile, MD,[2] Mark Doyle, PhD,[1] Ketheswaram Caruppannan, MD,[1] June Yamrozik,[1] Ronald Williams,[1] Geetha Rayarao,[1] Diane A. Vido,[1] Robert W. W. Biederman, MD[1]. ***[1]Allegheny General Hospital, Pittsburgh, PA, USA, [2]Medical University of South Carolina, Charleston, SC, USA.***

Introduction: The conventional understanding of diastolic heart failure (DHF) suggests that left ventricular (LV) indices and ejection fraction (EF) are within normal range in these patients. However, some studies now suggest that patients with DHF (compensated or decompensated) will have increased LV volumes leading to increased LV end-diastolic pressures. On the contrary, most believe that LV volumes should be in the normal range and DHF is due to LV myocardial relaxation abnormality leading to increased LV EDP, not *vice versa*. However, the majority of these considerations are derived from 1 and 2D data. We performed 3D cardiovascular MRI (CMR) volume and mass measurement in DHF patients to resolve the true LV geometry and volume indices associated with DHF.

Methods: Thirty patients (male 15; female 15) (mean age 55 ± 19) with clinical evidence for DHF and LVEF >50%, who were not in overt heart failure, underwent 3D CMR on a 1.5T scanner (GE, Milwaukee, WI). Standard FIESTA cine sequence and phase velocity mapping (PVM) of mitral valve and pulmonary vein flow were performed to categorize the stage of diastolic dysfunction (DD), both quantitatively and morphologically. Double oblique multiplanar LV imaging, along with 3D LV short-axis cine images, was performed. The LVEF, LV end-diastolic volume index (LVEDVI), LV end-systolic index (LVESVI) and LV mass index (LVMI) were calculated using Simpson's rule.

Results: All patients completed the CMR with PVM. DD was categorized into impaired relaxation (IR), pseudonormal (PN) and restrictive (R). There were 19 IR, 5PN, and 6R. The mean LVEF was 65 ± 9%. The LVEDVI and LVESVI were normal (77 mL/m^2 ± 22 and 30 mL/m^2 ± 12, respectively) and not different from age matched CMR reference values (71 mL/m^2 ± 13 and 28 mL/m^2 ± 7). The LVMI and ratio of LVMI/LVEDVI, as expected, were slightly high at 85 g/m^2 ± 26 and 1.13 ± 0.3, respectively.

Conclusions: Patients with abnormal diastolic filling in the setting of normal systolic function demonstrate normal LVEDVI and LVESVI. The LVMI was high, reflecting the etiology of DHF. Despite varied DD categories, the LV geometry, as well as LVEF, remained in the normal reference standard for all. This supports the hypothesis that the primary abnormality in DHF is abnormal LV compliance with an abnormal operating stiffness.

337. ANTIBODY-CONJUGATED IRON OXIDE MICROPARTICLES QUANTIFY VCAM-1 EXPRESSION IN MOUSE ENDOTHELIAL CELLS IN VITRO USING MAGNETIC RESONANCE IMAGING

Martina A. McAteer, PhD, Jürgen E. Schneider, PhD, Nicholas Warrick, PhD, Keith M. Channon, MD FRCP, Stefan Neubauer, MD FRCP, Robin P. Choudhury, DM MRCP. ***Wellcome Trust Centre for Human Genetics, Oxford, United Kingdom.***

Introduction: Intracellular superparamagnetic microparticles of iron oxide (MPIO) have been shown to be useful for murine cell tracking using magnetic resonance imaging. Conjugating MPIOs to specific antibodies may allow targeted molecular MR imaging of extracellular epitopes, such as VCAM-1, a marker of endothelial inflammation.

Purpose: To investigate whether covalent conjugation of primary rat anti-mouse VCAM-1 antibody to MPIO (4.5 μm diameter) can specifically detect and quantify TNF-alpha induced VCAM-1 expression in cultured mouse endothelial (sEND) cells using high resolution MRI.

Methods: Mouse sEND cells (8×10^5) were stimulated *in vitro* for 20 hr with TNF-alpha (0.1, 1, 10 or 50 ng/ml respectively) to induce endothelial VCAM-1 expression. The cells were then incubated in duplicate with either anti-VCAM-1-MPIO complexes or isotype anti-IgG-1-MPIO negative controls (1.2×10^6) for 30 min. Unbound beads were removed by extensive washing with phosphate buffered saline. The cells were examined for MPIO binding using light microscopy and the number of MPIO bound to sEND cell surfaces in 4 fields of view were quantified for each dose of TNF-alpha using Image-Pro plus. The cells were then embedded in 2% agarose and MRI of cell phantoms was performed using an 11.7 T vertical magnet and a 40 mm probe with a home built sample holder allowing for imaging of up to 10 samples simultaneously. A 3D gradient echo sequence was used (TR/TE = 4/90 ms, field of view 30 × 30 × 30 mm, matrix size $(512)^3$, two averages, imaging time ~13 h overnight) with a final isotropic resolution of 29.3 μm^3 (after image reconstruction). The area of signal voids corresponding to MPIO in individual 2-D images was quantified (8 images per sample selected at slice intervals of 293 μm) using a semi-automated histogram based approach.

Results: Using light microscopy, anti-VCAM-1-MPIO bound specifically to TNF alpha stimulated sEND cells. No binding of anti-IgG-MPIO was observed. The number of anti-VCAM-1-MPIO binding to sEND cell surfaces increased significantly in response to increasing doses of TNF alpha stimulation (Fig. 1. $r^2 = 0.94$, $p = 0.03$). By MRI, the area of anti-VCAM-1-MPIO in cell phantoms was also observed to significantly increase in a linear fashion in response to increasing dose of TNF-alpha stimulation (Fig. 2. $r^2 = 0.98$, $p = 0.01$).

Conclusions: Anti-VCAM-1 antibody conjugated MPIO bind specifically and in a TNF-alpha dose-dependent manner to sEND cells *in vitro* as quantitatively assessed by light microscopy and MRI. The conjugation of VCAM-1 monoclonal antibody to MPIO may therefore be a useful strategy for targeted MRI investigation of VCAM-1 expression in mice in vivo.

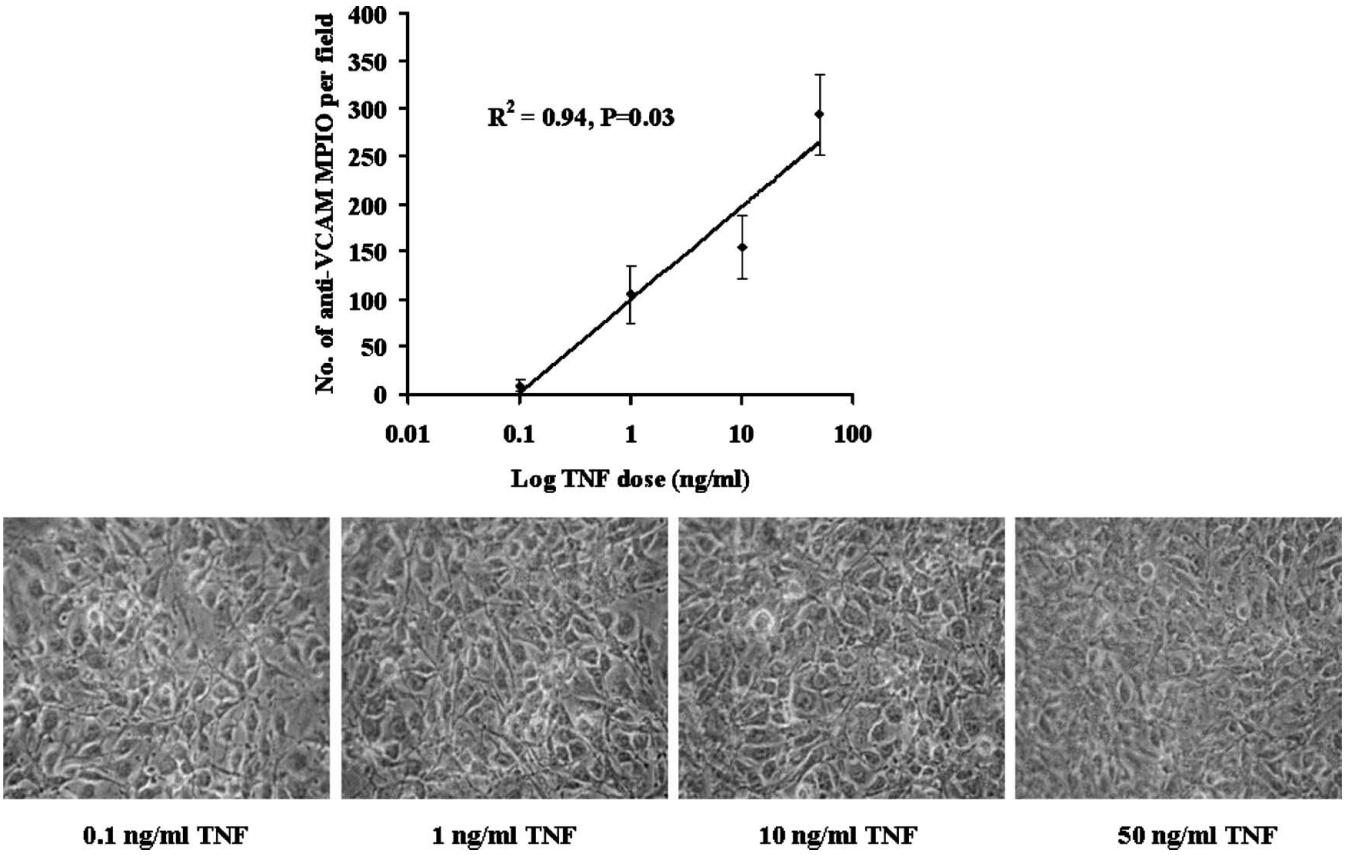

FIG. 1. Number of anti-VCAM-1 MPIO binding to sEND cells stimulated with increasing doses of TNF alpha.

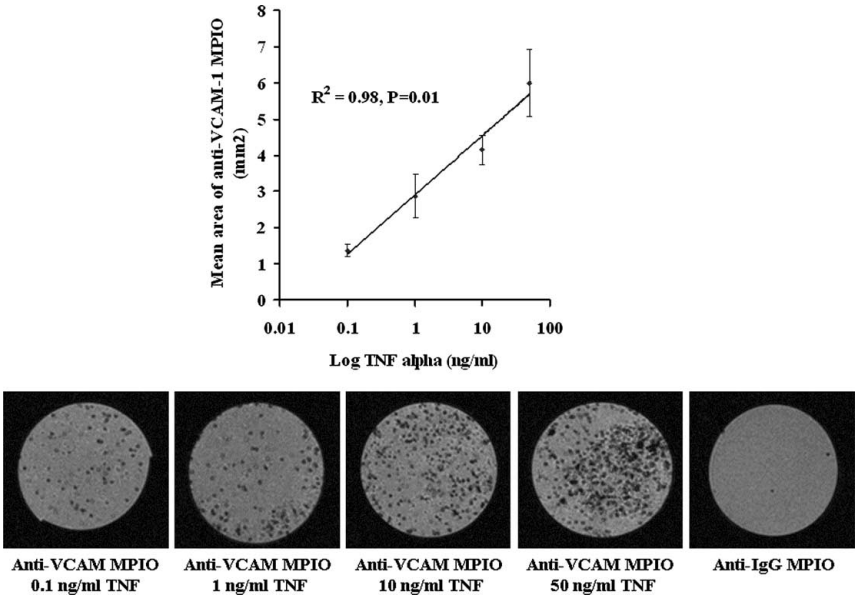

FIG. 2. MRI quantification of area of anti-VCAM-1 MPIO binding to sEND cells stimulated with increasing doses of TNF alpha.

338. SEX-SPECIFIC CHARACTERISTICS OF CARDIAC FUNCTION, GEOMETRY AND MASS IN YOUNG ADULT ELITE ATHLETES

Steffen E. Petersen,[1] Lucy E. Petersen, MA, MRCP,[1] Matthew D. Robson, PhD,[1] Helen A. Doll, Dphil,[1] Jane M. Francis, DCRR, DNM,[1] Frank Wiesmann, MD,[1] Bernd A. Jung, PhD,[2] Juergen Hennig, PhD,[2] Hugh Watkins, MD, PhD, FRCP,[1] Stefan Neubauer, MD, FRCP[1]. [1] *University of Oxford, Oxford, United Kingdom,* [2] *University of Freiburg, Freiburg, Germany.*

Introduction: Principal differences between male and female hearts are at least partly a reflection of opposing modulating cardiac effects of estrogen and testosterone. Estrogen has an antiproliferative and testosterone a proliferative stimulus in situations of cardiac pathological remodeling. In contrast, little data exist for sex-specific effects on chronic physiological remodeling. We studied young adult elite athletes with age- and sex-matched sedentary controls to assess sex-specific differences for LV and RV dilatation and hypertrophy as well as for LV contraction and relaxation. We hypothesized that structural and functional adaptive changes to chronic physiological cardiac remodeling would be sex-specific.

Methods: Twenty-three male athletes (mean age 25 ± 4 years, training 22 ± 7 hours/week in rowing, swimming or triathlon) and 20 female athletes (mean age 24 ± 4 years, training 19 ± 5 hours/week in rowing, swimming or triathlon) and age-sex matched sedentary controls (21 male/17 female) underwent cardiovascular magnetic resonance (CMR) imaging (1.5 Tesla). LV and RV volumes and mass were determined on the basis of a complete short axis stack using steady state free precession cines (TE/TR 1.5/3.0 ms, flip angle 60 degrees, slice thickness 7 mm, 3 mm interslice gap, in plane resolution 1.5×1.5 mm, temporal resolution 45 ms) in end-expiration (Fig. 1). Contraction and relaxation was assessed in three short axis planes (basal, mid-ventricular and apical) using cine phase contrast velocity magnetic resonance imaging applying a black blood k-space

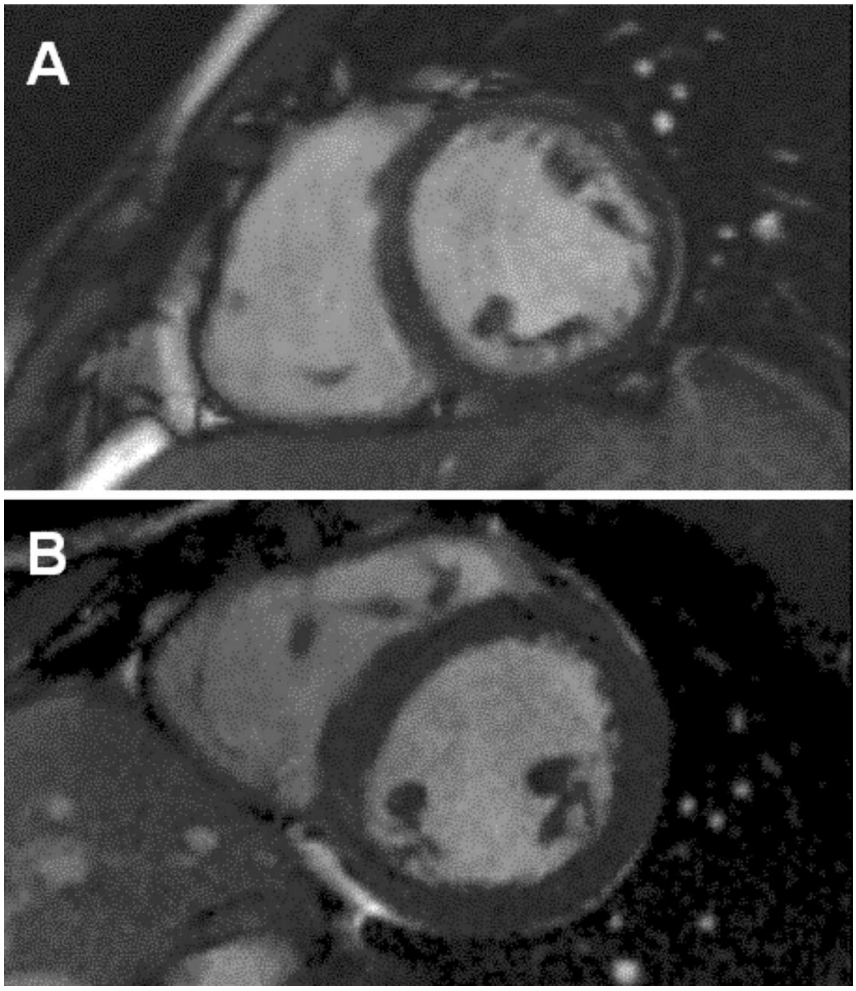

FIG. 1. End-diastolic still frames of steady-state free precession cines in a male sedentary control (A: Body surface area 1.84 m^2, LV end-diastolic volume 158 mL, LV mass 98 g, RV end-diastolic volume 193 mL RV mass 37 g) and a male elite athlete (B: Body surface area 2.37 m^2, LV end-diastolic volume 317 mL, LV mass 345 g, RV end-diastolic volume 331 mL, RV mass 63 g).

segmented gradient echo sequence (TE/TR = 4.5/6.2 ms, flip angle 15 degrees, in-plane resolution 1.3 × 1.3 mm, slice thickness 8 mm, temporal resolution of 37–87 ms adjustable to breath-holding capabilities) with first-order flow compensation in all dimensions. A univariate general linear model with fixed effects for sex and training (athlete vs. sedentary control) was used to test whether differences between age-and sex-matched athletes and sedentary controls were sex-specific.

Results: Male (22 ± 7 hours/week) and female athletes (19 ± 5 hours/week) showed similar increases in LV and RV volume and mass indices when compared to controls (ranging between 15 and 42%). No sex-specific differences in training effect on LV and RV volumes, mass indices and ejection fractions, as well as LV to RV ratios of these volume and mass indices (parameters of balanced LV and RV dilatation and hypertrophy) were observed (all p for interaction >0.05). Similarly, no sex-specific differences in training effect on cardiac contraction and relaxation were found (all p for interaction >0.05).

Conclusions: Adaptive structural and functional changes to exercise training in young adult elite athletes are not sex-specific. This is in accordance with the benign nature of the hypertrophy associated with athlete's heart.

339. DISCORDANT RISK STRATIFICATION FOR INCREASED LEFT VENTRICULAR MASS BY VOLUMETRIC AND GEOMETRIC-FORMULA METHODS

Carol J. Salton, BA,[1] Christopher J. O'Donnell, MD, MPH,[2] Kraig V. Kissinger, BS, RT (R), (MR),[1] Loryn S. Feinberg, MD,[1] Daniel Levy, MD,[2] Warren J. Manning, MD,[1] Michael L. Chuang, MD[1]. [1]*Beth Israel Deaconess Medical Center, Boston, MA, USA,* [2]*NHLBI's Framingham Heart Study, Framingham, MA, USA.*

Introduction: Increased left ventricular (LV) mass is an independent predictor of cardiovascular morbidity and mortality. To date, the large imaging studies from which this conclusion has been drawn have used linear echocardiographic measurements in conjunction with a cubed-power geometric formula to determine LV mass. We and others have shown that cubed-formula methods overestimate LV mass relative to volumetric imaging, but it is not known whether these 2 methods risk-stratify individual patients in the same manner, as there is wide individual variation in the amount of overestimation.

Purpose: To determine whether a commonly used geometric formula for LV mass (Penn) ranks members of a given cohort concordantly with ranking by volumetric mass; a positive finding might allow development of a correction formula between the 2 methods, whereas discordance would make it unlikely that Penn and volumetric measures could reliably be compared for individuals.

Methods: Adult subjects from the Framingham pilot CMR study (N = 292; aged 59.5 ± 9.0 years, range 36–78; 151 women, 141 men) underwent contiguous multislice ECG-triggered FFE-EPI breathhold cine CMR imaging in the LV short-axis orientation in a 1.5-T scanner using cardiac array coil for RF signal reception. Imaging parameters included: TR = RR, TE = 9 ms, FA = 30°, THK = 10 mm, GAP = 0 mm, in-plane resolution 1.25 × 2.0 mm^2. For volumetric analysis, epi and endocardial borders were traced at end-diastole and volumetric mass (Mvol) was determined using a summation of disks method. The Penn formula ($Mpenn = 1.04[(EDD + IVS + PWT)^3 - EDD^3] - 13.6$) was used to determine geometric mass, where end-diastolic diameter (EDD) and septal (IVS) and posterior wall (PWT) thicknesses were measured from the CMR short-axis slice immediately basal to the papillary muscle tips at end-diastole. Statistical analyses were performed by gender and $p < 0.05$ was considered significant. Mvol and Mpenn are summarized by mean ± SD and were compared using Student's *t*-test. For each gender subjects were ranked by Mvol and Mpenn; agreement between the 2 rankings was assessed using Spearman correlation, r_s. Finally, subjects were divided into quartiles of LV mass and the proportion of subjects whose quartile-classification differed between volumetric and Penn measures was tabulated.

Results: Mpenn was significantly greater than Mvol for both women (163 ± 37 g vs 110 ± 22 g, $p < 0.001$) and men (230 ± 59 g vs 158 ± 28 g, $p < 0.001$). LV mass was greater in men than women for both Mpenn ($p < 0.001$) and Mvol ($p < 0.001$) measures. Gender-dependent Penn and volumetric rankings of individual subjects were significantly but only modestly correlated, women: $r_s = 0.43$, $p < 0.001$, men: $r_s = 0.55$, $p < 0.001$. Ranking subjects by quartile of LV mass (Fig.) showed that approximately two-thirds of subjects were placed into the same quartile of mass by Penn and volumetric measures ("Same"), but nearly one quarter of subjects differed by one quartile ("1Q"), and approximately one in ten subjects differed by 2 or 3 quartiles ("2Q" or "3Q"). Discordance by quartile-crossover was similar between men and women.

Conclusions: Penn formula and volumetric measures of LV mass are not interchangeable on a gram-to-gram basis; the former overestimates the latter. Ranking subjects by quartile of mass showed that one-third of subjects were assigned to different quartiles; this was consistent with the finding that Spearman

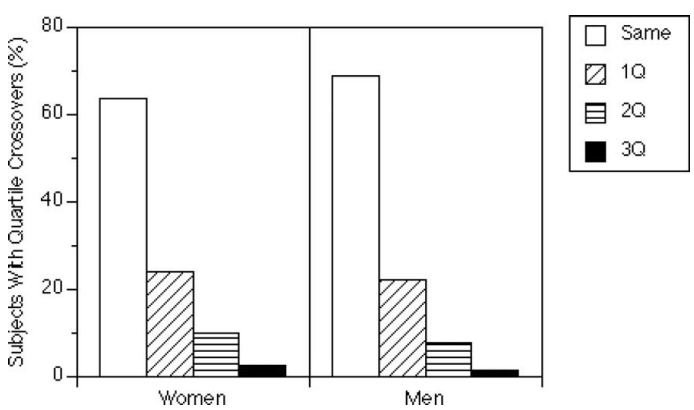

FIG. 1.

correlations between Mvol and Mpenn were only modest for both women and men. These findings suggest that any correction formula between Penn and volumetric LV mass is unlikely to be applicable on an individual basis, although such a formula may have value when applied to aggregates of subjects. Finally, it remains to be determined whether volumetric imaging will better predict excess morbidity and mortality associated with elevated LV mass than geometric-formula methods; several large studies using volumetric CMR for LV mass are underway and may provide insight into this question in the near future.

340. ASSESSMENT OF LEFT VENTRICULAR STRUCTURE AND FUNCTION BY CARDIAC MRI IN CHRONIC HEMODIALYSIS PATIENTS. IS IT CLINICALLY RELEVANT?

Roger T. Getts, MD, Shawn M. Hazlett, MD, Sandeep B. Sharma, MD, Robert W. W. Biederman, MD, Rita L. McGill, MD, Steve E. Sandroni, MD, Richard J. Marcus, MD. ***Allegheny General Hospital, Pittsburgh, PA, USA.***

Introduction: Echocardiographic assessment of LV mass and geometry in hemodialysis patients is operator dependent, requires an acoustic window and widely varies over the course of hemodialysis. We reasoned that cardiac MRI (CMR) may provide more accurate, detailed and reproducible images of the LV while less affected by operator skill and volume status. Yet, a paucity of CMR data is available detailing LV mass, geometry and function in chronic hemodialysis pts.

Methods: We performed 3D CMR on 28 stable hemodialysis patients on a GE scanner. LV mass, length, diameter, EF, wall thickness, volumes and LV geometry were determined using FIESTA sequences with contiguous short axis slices via Simpson's rule, a combination of 2, 4, and 5 chamber views with all related to patients demographics. The metrics were then compared to an age matched CMR reference population.

Table 1. LV Indices by CMR in hemodialysis patients

	Males (n = 19)	Females (n = 9)	CMR age matched reference group (n = 150)
Age (years)	57 ± 17	66 ± 14	51 ± 15
Systolic blood pressure (mmHg)	140 ± 21	145 ± 26	118 ± 11
EF (%)	56 ± 15	58 ± 19	60 ± 5
End-diastolic volume index (mL/m^2)	100 ± 40	91 ± 34	71 ± 13
LV mass index (g/m^2)	100 ± 37	76 ± 17	62 ± 10
LV end-diastolic mass/volume (g/mL)	1.04 ± 0.25	0.87 ± 0.19	0.915 ± 0.196
Relative wall thickness (RWT)	0.52 ± 0.19	0.60 ± 0.20	0.35 ± 0.09
LV sphericity index	2.05 ± 0.28	2.09 ± 0.36	2.00 ± 0.21

Results (Table 1)*:* No values were found to be statistically significant when controlling for age, gender, diabetes mellitus or CAD while reproducibility of LV mass index on a repeat 15% subset 9 months later demonstrated a precision of 5g (range 0.7–16%; $R^2 = 0.94$) as compared to the echocardiographic standard of 17–26 g.

Conclusion: Relative to a reference CMR population, there was a marked increase in LVMI, RWT, in the setting of low normal EF all occurring in the face of preserved 3D, not 2D LV geometry but detectable by the low variability CMR exam. This supports the notion that this gender neutral hemodialysis population, due to its extraordinarily high cardiovascular morbidity and mortality, may benefit clinically from a systematic cardiac interrogation with a reproducibility that far exceeds echocardiography.

341. MRI FINDINGS IN PATIENTS WITH FAT DISSOCIATION SYNDROME OF THE RIGHT VENTRICLE

Robson Macedo, MD, Prakasa Kalpana, MD, Harikrishna Tandri, MD, Joao A. C. Lima, MD, Hugh Calkins, MD, David A. Bluemke, MD, PhD. ***Johns Hopkins Hospital, Baltimore, MD, USA.***

Introduction: Fatty infiltration of the right ventricular (RV) wall with RV dysfunction detected by MRI is considered as one of the morphologic hallmarks for arrhythmogenic right ventricular dysplasia (ARVD). Small amounts of RV fat with normal RV function are seen in normal individuals, but individuals with large amounts of RV fatty infiltration and normal function have been described as "fat dissociation syndrome."

Purpose: The purpose of this study was to describe the MRI findings in "fat dissociation syndrome."

Methods: The study included a total of 12 patients referred for second opinion due to fatty infiltration of the RV free wall. None of the patients met the Task Force criteria for ARVD as evaluated by a senior clinical cardiologist. All studies were obtained at 1.5T MRI. ECG gated black blood images of the myocardium were acquired in the transaxial and/or short axis plane using either double inversion recovery fast/turbo spin echo technique or spin echo T1 or proton density weighted images. Fat suppressed images were obtained using either chemical shift fat suppression or inversion recovery technique. The cardiac morphology and RV wall signal intensity were analyzed and post processed with the Efilm software (version 1.8.3 Patch 3). ECG gated bright blood cine images were obtained using steady state free precession images, (eg, TrueFISP, Fiesta, balanced fast field echo) in the transaxial and short axis planes. RV function and volumes were determined with the software program MASS (version 6.1, Medis, The Netherlands). Two observers independently

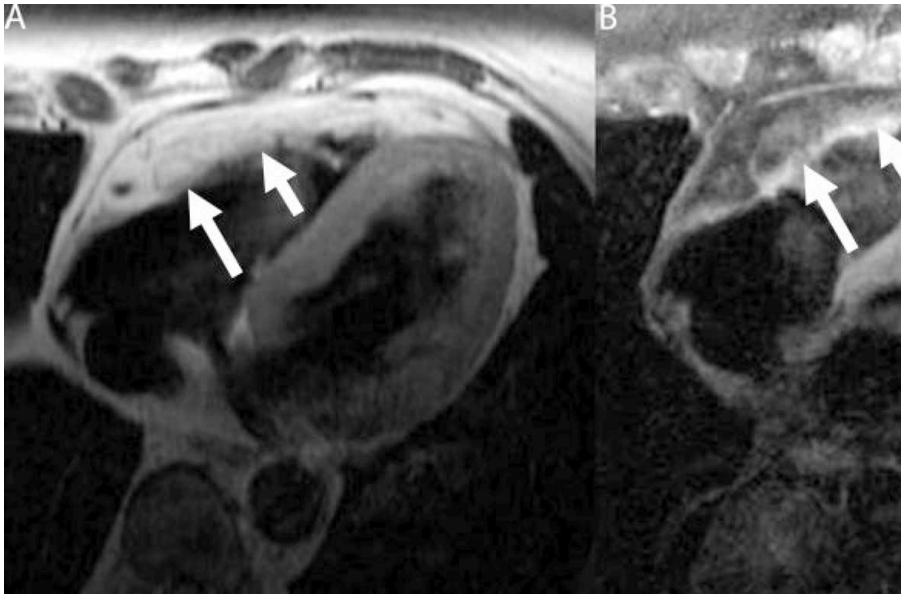

FIG. 1. A—Long axis dark-blood without fat saturation image showing fat replacement of the entire RV wall (arrows). The fatty replaced RV wall appears thickened. B—Long axis dark-blood with fat saturation image shows suppression of the fatty component of the RV wall. A thin portion of non fatty RV wall is now seen (arrows).

analyzed the MR images in a blinded fashion. RV function was compared to 20 asymptomatic volunteers free of clinical cardiovascular disease.

Results: The RV out flow tract, basal, middle and inferior walls showed MRI signal changes compatible with fat in 58% (n = 7), 83% (n = 10), 83% (n = 10), 66% (n = 8) and 50% (n = 6) of the patients, respectively. In 3 cases, there was transmural replacement of the RV wall by fat. (Fig. 1) There was no evidence of left ventricular fat in any of the patients. There were no statistically significant differences for the RV end diastolic volumes and RV ejection fractions between the fat dissociation syndrome group and the control group (Fig. 2). No wall motion abnormalities were present in the patient group, including in the area of the RV fat.

Conclusion: Our study suggests that fat dissociation syndrome is seen on MRI as abundant fatty infiltration of the RV wall without RV dysfunction and without wall motion abnormalities. Adoptions of strict diagnostic criteria for ARVD are therefore warranted in MRI cases with RV fat to avoid unnecessary pharmacologic or ICD intervention in patients suspected for ARVD.

Acknowledgement: This work was supported by The Johns Hopkins ARVD program, the Bogle Foundation and the National Institutes of Health Research Grant 1 UO1 HL65594-01A1.

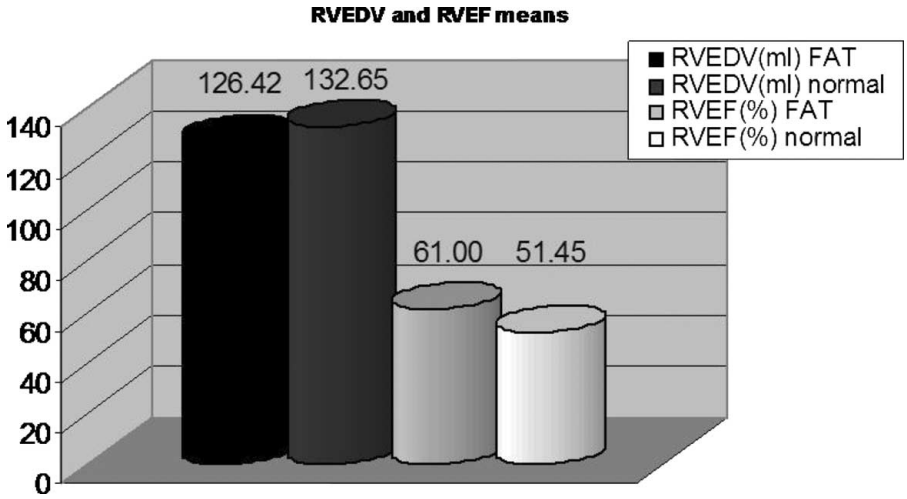

FIG. 2. There were no statistically significant differences for the RV end diastolic volumes and RV ejection fractions between the fat dissociation syndrome group (FAT) and the normal group ($p > 0.05$).

342. LEFT VENTRICULAR TORSION IS INCREASED IN PATIENTS WITH DUCHENNE MUSCULAR DYSTROPHY INDEPENDENT OF CHANGES IN LV SYSTOLIC FUNCTION

William M. Gottliebson, MS, MD, Larry Markham, MD, Janaka Wansapura, PhD, Eric Crotty, MBBCh, Robert Fleck, MD, Amy Tipton, BS, Linda Cripe, MD. ***Cincinnati Childrens Hospital and Medical Center, Cincinnati, OH, USA.***

Introduction: In normal subjects, shortening of oblique left ventricular (LV) fibers results in counterclockwise torsion of the left ventricular apex during systole relative to the base, with concomitant recoil during diastole. The degree of this apical torsion has previously been characterized via several methods, including cine tagged-cardiac magnetic resonance imaging (CMRI). A simplified technique, using the degree of displacement of the mid-papillary muscles (PM) relative to each other from simple short-axis cine MRI images, has been described as a reliable surrogate to tagged CMRI analysis in determining the net left ventricular torsion. Previous reports state that the maximum twist at the mid-PM level is 4–6 degrees. We sought to apply this torsion-measurement analysis technique to the CMRI studies of young patients with Duchenne Muscular Dystrophy (DMD), some of whom have not yet manifested the progressive dilated cardiomyopathy ubiquitous to DMD.

Methods: Thirty-three male patients (mean age 15.6 ± 4.7 yrs) with DMD underwent a total of 38 CMRI scans ordered for clinical indications. Scans were performed on a 3T Siemens *Trio*. Breath hold cine SSFP cine 2 chamber, 4 chamber, and short axis stack loops were obtained. For each study, the SSFP slice end-systolic and end-diastolic frames at mid-papillary level were determined. The raw DICOM images were analyzed utilizing the angle measurement tool available in the GE PACS system workstation. Mid PM twist was defined as the angle of rotation between the mid-papillary line at end-diastole versus end-systole (Fig. 1). This value was compared to the patient's age and MRI-derived LV ejection fraction (EF), as well as each patient's recent (within 3 months) echocardiograhically-determined LV wall stress (WS) and LV isovolumic relaxation time (IVRT) via separate linear regressions.

Results: The mean counterclockwise mid-PM twist for all DMD patients was 12.5°± 3.9°. For the subset with abnormal LV EF (EF > 55%, n = 19), the mean mid-PM was 11.43°± 3.01°. For those patients with LVEF <55%, (n = 19) the mean mid-PM was 13.18°± 4.4°). There were no statistically significant correlations between mid-PM twist angle and patient age, LVEF, LV IVRT, or LV WS (r^2 range .06–.24).

Conclusions: The mid-PM twist is increased in patients with DMD as compared to previously-published normal values, validating the common qualitative appearance of exaggerated diastolic recoil seen in the short axis cine SSFP images of these patients. The lack of correlation of this value with other indexes of LV systolic and diastolic function suggests that the amount of mid-PM twist may be an independent indicator of myocardial abnormality, such as early fibrosis or abnormal myocardial energetics. Further CMRI study of these patients via delayed contrast enhancement and MR spectroscopy is in progress.

343. INTRA- AND INTER-PLATFORM REPRODUCIBILITY OF 1.5T SIEMENS, GE AND PHILLIPS SCANNERS FOR CLASSIFYING CAROTID ATHEROSCLEROTIC LESION TYPE USING MODIFIED AHA CRITERIA

Tobias Saam, MD,[1] Thomas S. Hatsukami, MD,[2] Hunter Underhill, MD,[1] Baocheng Chu, MD/PhD,[1] Norihide Takaya, MD/PhD,[1] Jianming Cai, MD/PhD,[1] Vasily L. Yarnykh, PhD,[1] William S. Kerwin, PhD,[1] Dongxiang Xu, PhD,[1] Nayak L. Polissar, PhD,[3] Wendy K. Hamar, BS,[4] Jeffrey Maki, MD/PhD,[5] Dennis W. Shaw, MD,[1] Robert Buck, PhD,[6] Phil Wastall, BSc,[6] Marika Mychajluk, BSN,[6] Brad Wyman, PhD,[6] Chun Yuan, PhD.[1] ***[1]Dept. of Radiology, University of Washington, Seattle, WA, USA, [2]VA Puget Sound Health Care System & Dept. of Surgery, University of Washington, Seattle, WA, USA, [3]The Mountain-Whisper-Light Statistical Consulting, Seattle, WA, USA,***

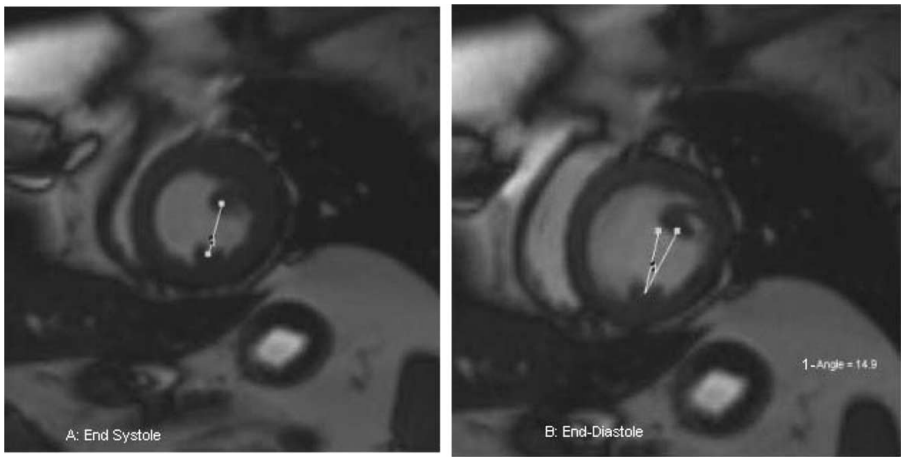

[4] *Dept. of Surgery, University of Washington, Seattle, WA, USA,* [5] *VA Puget Sound Health Care System & Dept. of Radiology, University of Washington, Seattle, WA, USA,* [6] *Pfizer Global Research & Development, Ann Arbor, MI, USA.*

Introduction: Previous studies have demonstrated that in vivo multi-contrast MRI is capable of distinguishing advanced from early and intermediate carotid atherosclerotic lesions by using modified American Heart Association (AHA) criteria with high intra-platform reproducibility on 1.5T GE MRI scanners. To establish the AHA lesion type characterization as a viable clinical tool, the reproducibility of this method has to be established on other scan manufacturers.

Purpose: The goal of this study was to determine 1) the intra-platform reproducibility of the AHA lesion type on Siemens and Philips scanners, and 2) inter-platform reproducibility of the AHA lesion type between (a) GE and Philips and (b) GE and Siemens scanners.

Methods: Thirty-two individuals with $\geq$15% carotid stenosis by duplex ultrasound were each imaged three times over a period of two weeks using a multi-contrast carotid MRI protocol and identical phased-array carotid coils. Each person was scanned once on a 1.5T GE scanner (Signa Horizon EchoSpeed) and either twice on a 1.5T Phillips scanner (Philips Intera) or twice on a 1.5T Siemens scanner (Siemens Symphony). Expert readers, blinded to subject information, scanner type, and time point used the same image processing software (CASCADE) to review the cross-sectional images. The AHA lesion type assessment was based on the relative tissue intensities in T1-, T2-, PD- and TOF-weighted images.

Results: Intra-platform agreement, as measured by Cohen's κ, was 0.76 for the Siemens and 0.75 for the Phillips scanner. For inter-platform agreement, Cohen's κ was 0.74 for GE vs. Siemens and 0.66 for GE vs. Phillips.

Conclusions: The intra- and inter-platform reproducibility shown in this study suggests that the AHA lesion type can be consistently identified across two scans on the same platform and across platforms from different manufacturers.

344. MRI ASSESSMENT OF REGIONAL RIGHT VENTRICULAR WALL MOTION IN PATIENTS AFTER REPAIR OF TETRALOGY OF FALLOT

Karen G. Ordovas, MD, Mario Morales, MD, Gautham P. Reddy, MD, MPH, Charles B. Higgins, MD. ***UCSF, San Francisco, CA, USA.***

Introduction: Pulmonary regurgitation is one of the most common complications after correction of tetralogy of Fallot. It is known that chronic pulmonary regurgitation causes deterioration of right ventricular (RV) function (1). MRI has been used to evaluate the severity of pulmonary regurgitation after surgical correction of tetralogy of Fallot, as well as right ventricular function (2). It has been demonstrated that replacement of the insufficient pulmonary valve can improve right ventricular function in these patients (3). However, parameters to determine the need and the best time for replacement are still under investigation. Regional RV functional abnormalities can be seen in these patients and may precede a loss of RV ejection fraction. The purpose of this study was to compare right ventricular regional function in normal volunteers and patients with pulmonary regurgitation after surgically corrected tetralogy of Fallot.

Patients and Methods: Twenty-three patients with pulmonary artery regurgitation after repair of tetralogy of Fallot were

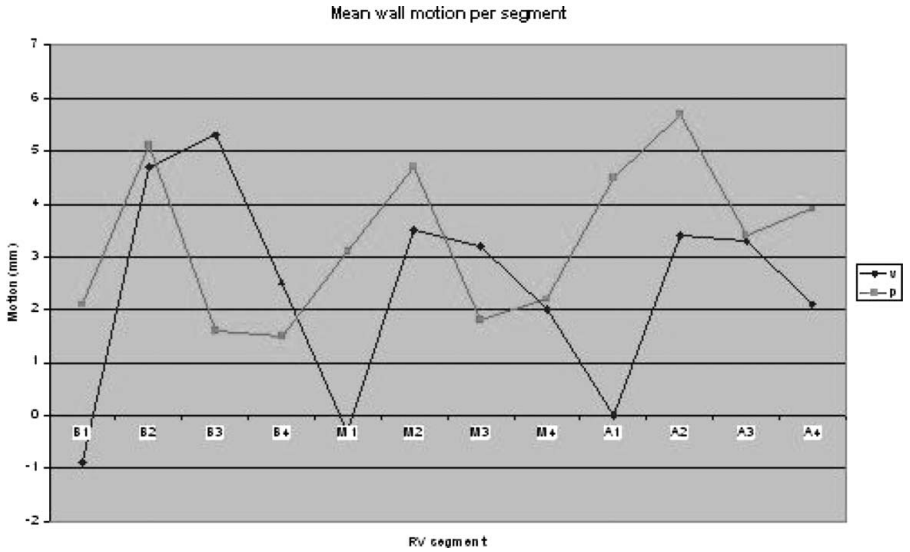

FIG. 1. Comparison of RV segmental wall motion in patients and normal volunteers. p = patients; v = volunteers; B1 = septal segment at the base; B2 = inferior segment at the base; B3 = ventral segment at the base; B4 = anterior segment at the base; M1 = septal segment at the midventricle; M2 = inferior segment at the midventricle; M3 = ventral segment at the midventricle; M4 = anterior segment at the midventricle; A1 = septal segment at the apex; A2 = inferior segment at the apex; A3 = ventral segment at the apex; A4 = anterior segment at the apex.

referred for MRI studies between May 2002 and July 2005. We also recruited 10 normal volunteers. Cine MR images were obtained in the short-axis plane in order to evaluate RV function. A method of RV segmentation was developed and 12 segments were defined: septal wall, inferior wall, ventral wall and anterior wall segments at the base, midventrical and apex. The outlet portion of the RV was not evaluated since this region is severely altered by operative procedures (such as outlet patch). RV regional motion during the cardiac cycle was measured in each of RV segments of patients and volunteers. The means of absolute motion for each segment of the right ventricular wall was compared between normal volunteers and patients with repaired tetralogy of Fallot.

Results: Compared to normal volunteers, patients with postoperative tetralogy of Fallot had severely impaired wall motion of the ventral wall segments at basal and midventricular levels ($p \leq 0.01$). On the other hand, there was increased wall motion of septal segments in basilar, midventricular and apical levels. Moreover, at the apical regions all segments except ventral had significantly ($p < 0.01$) greater wall motion compared to normal volunteers (Fig. 1).

Conclusion: Patients with pulmonary regurgitation after repair of tetralogy of Fallot have a different regional wall motion pattern when compared to normal volunteers. This pattern can be systematically assessed by MRI. Increased wall motion of apical segments and the septum appear to compensate for severe dysfunction of the ventral wall. The segmentation of the RV as proposed in this study may be useful for tomographic evaluation of RV regional function.

REFERENCES

1. Geva T, Sandweiss BM, Gauvreau K, Lock JE, Powell AJ. Factors associated with impaired clinical status in long-term survivors of tetralogy of Fallot repair evaluated by magnetic resonance imaging. J Am Coll Cardiol 2004;43:1068–1074.
2. Helbing WA, de Roos A. Clinical applications of cardiac magnetic resonance imaging after repair of tetralogy of Fallot. Pediatr Cardiol 2000;21:70--79. Review.
3. Van Straten A, Vliegen HW, Hazekamp MG, Bax JJ, Schoof PH, Ottenkamp J, van der Wall EE, de Roos, A. Right ventricular function after pulmonary valve replacement in patients with tetralogy of Fallot. Radiology. 2004;233:824–829.

345. CONTRAST-ENHANCED MRI OF OCCLUSIVE ARTERIAL DISEASE

Kevan J.T. Anderson,[1] General Leung,[1] Nigel Munce,[1] Beiping Qiang,[2] Erin McMillan,[3] John Graham,[3] Alan R. Moody,[3] Alexander J. Dick,[3] Bradley H. Strauss,[2] Graham A. Wright.[3] [1]***University of Toronto, Toronto, ON, Canada,*** [2]***St Michael's Hospital, Toronto, ON, Canada,*** [3]***Sunnybrook and Women's College Health Sciences Centre, Toronto, ON, Canada.***

Introduction: Percutaneous treatment of arterial occlusive disease is gaining popularity in recent years with the dramatic reduction in restenosis rates attributed to the use of drug-eluting stents. Despite the benefits of percutaneous treatment, clinicians often do not attempt the crossing of an occlusion due the technical difficulty, primarily inability to cross a chronic occlusion with a guide wire. MRI has a significant potential role in characterization of occlusion attributes such as inflammation and neovascularization. These may be critical determinants of successful guide-wire crossings and may also be important considerations in treatment selection. This study investigates the use two different MRI contrast agents, Omniscan (Nycomed, Denmark) and Clariscan (GE Healthcare, UK), for characterizing occlusive arterial disease in an animal model of total occlusion.

Materials and Methods: Total occlusions were created in 11 rabbit femoral arteries by surgically isolating the arteries with ligatures and then occluding these arteries with local injections of bovine thrombin (Serologicals, USA). These occlusions were confirmed angiographically at the time of the procedure. This occlusion model shares several characteristics with human coronary occlusions including development of mature fibrous tissue and multiple small intraluminal vascular channels (1, 2). The femoral vein adjacent to the occlusion was removed at the time of surgery to avoid venous signal contamination during imaging. Imaging was performed on a 3T GE Excite Scanner using a custom 3-cm surface coil. Occlusions of varying age (1–18 weeks) were imaged using an elliptic centred FSPGR sequence (TR/TE/flip = 8.3/2.1/30, 31 kHz bandwidth, resolution of 0.25 mm in plane, 1 mm through plane). Images were obtained before and at 4 s after the injection of 0.1 cc/kg Omniscan. After allowing 40 min for the Omniscan to clear, imaging was repeated as above at a higher resolution (0.4 mm resolution 0.7 mm in plane) 16 s after the injection of 0.05 cc/kg Clariscan. Regions of interest were then selected within the occlusion and the relative volume distribution of contrast agent was determined using methods similar to (3). Specimens were sent for serial histological staining.

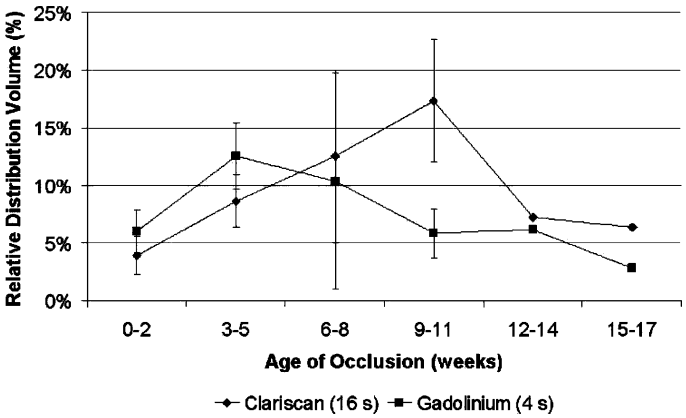

FIG. 1. Relative volume distribution of Clariscan (imaged 16 s after injection) and Omniscan (imaged 4s after injection) plotted as a function of occlusion age.

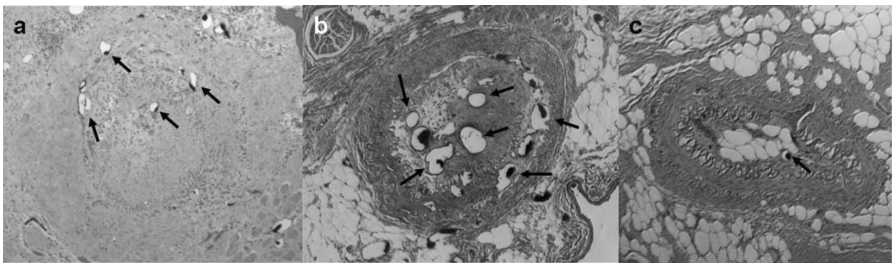

FIG. 2. A) Histology slide of a 2 week olds occlusion induced in a rabbit femoral artery stained with H+E. Small microvessels can be seen (arrows). B) 5 week old occlusion stained with Massons trichrome. More microvessels are present in this occlusion (arrows). C) Histology slide of a 15+ week old occlusion. Distinct lack microvessels is seen when compared to A) and B).

Results and Discussion: Figure 1 depicts the calculated volume distribution of Clariscan and Omniscan against the age of the occlusion. The volume distribution of Omniscan, a Gadolinium based extra-cellular contrast agent, 4s after injection is likely related to the directly filled microvasculature and interstitial volume adjacent to highly permeable vasculature within the occluded vessel. The volume distribution of Clariscan, a physically larger and intra-vascular agent, is likely related to complete vascular volume (given the longer filling time). Based on this interpretation, the data suggest that endoluminal neovascularization increases over the initial 10 weeks and is followed by a progressive collapse of these neovessels. These data also suggest that an increase in permeability and associated interstitial space (possibly inflammation) is experienced over the initial 2 weeks and subsides over time. This is consistent with current theories of the progression of occlusive disease (4) and is confirmed by initial histological samples (Fig. 2, Fig. 3). A second set of images was obtained 60s after Omniscan injection. In all cases, the volume distribution was found to be substantially greater than the 4-s time point and the 16-s Clariscan measurement suggesting that Omniscan eventually reaches a more extensive vascular and interstitial space.

Conclusion: The use of contrast-enhanced MRI was investigated in the characterization of occlusive disease. The volume distribution of Omniscan and Clariscan were calculated within the occluded vessels of varying ages to provide a direct characterization of interstitial volume and vascular volume respectively. These measurements may play an important role characterizing lesions as well as improving the prediction of guide-wire crossing success.

REFERENCES

1. Strauss BH. Circulation 2003;108:1259–1262.
2. Srivatsa SS. J Am Coll Cardiol 1997;29:955–963.
3. Schwarzbauer C. Magn Reson Med 1993;29:709–712.
4. Strauss BH. J Interv Cardiol 2005;18.

346. DETERMINANTS AND IMPACT OF MICROVASCULAR OBSTRUCTION IN SUCCESSFULLY REPERFUSED ST-SEGMENT ELEVATION MYOCARDIAL INFARCTION

Maria Kalantzi, MD, Stefaan Janssens, Steven Dymarkowski, Frank E. Rademakers, Frans Van de Werf, Jan Bogaert. ***Gasthuisberg University Hospital, Leuven, Belgium.***

Introduction and Purpose: Microvascular obstruction is an important and independent determinant of post-infarct remodeling. We sought to evaluate the determinants of MVO in patients with a successfully reperfused ST-segment elevation acute myocardial infarction (MI).

Methods: Fifty-two patients were studied with serial magnetic resonance imaging (MRI) in the first week (1W) and at 4 months (4M) post-infarction.

Results: On early, ie, 2–5 min, post-contrast MRI, MVO was detected in 32 patients (volume: 7.5 ± 6.5g, transmurality of 51 ± 18%, MVO to infarct ratio: 36.3 ± 24.9%). On late, ie, 10–25 min, post-contrast MRI, MVO was detected in only 27 patients, with significantly lower values (volume: 4.1 ± 4.8 g, $P = 0.03$; transmurality: 32.4 ± 17.8%, $P = 0.0002$; MVO to infarct ratio: 15.9 ± 13.9%, $P = 0.0003$) than on the early enhanced images. MVO infarcts were associated with higher cardiac enzymes (troponin I, $P = 0.016$), and lower pre-revascularization TIMI-flow ($P = 0.018$) than non-MVO infarcts. Infarct size was larger in MVO infarcts (25.0 ± 14.3 g) than non-MVO infarcts (12.5 ± 7.9 g), $p = 0.0007$. Systolic wall thickening in the infarct and peri-infarct area, and LV-EF were worse in MVO than non-MVO infarcts (LV-EF, MVO: 46.1 ± 7.2%, non-MVO: 50.5 ± 6.6%, $P = 0.038$). At 4M follow-up, MVO infarcts showed more adverse remodeling and lack of functional improvement whereas non-MVO infarcts improved significantly (LV-EF at 4M, MVO, 47.5 ± 7.8% $P = 0.31$; non-MVO, 55.2 ± 10.3%, $P = 0.0028$).

Conclusions: In the majority of patients with successfully reperfused ST-segment elevation MI, MVO is observed, whose present and maximal extent can be best evaluated on early post-contrast MRI. Presence of MVO is typically associated with more extensive infarctions, and is characterized

by greater adverse LV remodeling and lack of functional recovery.

347. WHOLE-HEART SSFP MRCA IN PATIENTS WITH ATRIAL FIBRILLATION: COMPARISON BETWEEN RADIAL AND CARTESIAN K-SPACE SAMPLING

Tarinee Tangcharoen, MD, Sebastian Kelle, MD, Bernhard Schnackenburg, PhD, Steffen Huber, MD, Thomas Kokocinski, MD, Ingo Paetsch, MD, Eckart Fleck, MD, Eike Nagel, MD ***German Heart Institute, Berlin, Germany.***

Purpose: To assess the feasibility of whole-heart magnetic resonance coronary artery imaging (MRCA) radial and cartesian k-space sampling in patients with atrial fibrillation.

Methods: Twenty-two patients with atrial fibrillation were evaluated. Navigator-gated (gating window 7 mm), free-breathing, single 3D-volume MRCA covering the whole heart (T2-preparation, fat saturation pulse, SSFP, TR/TE/flip angle:4.8/2.4/110, in-plane resolution 0.7*0.7 mm, Philips Intera CV 1.5T) was used (see table 1 for more details). In randomized order, each patient was scanned with radial and cartesian (SENSE factor:2) k-space sampling. In each patient, cardiac rest period was individually determined from the minimal RCA motion in a 4-chamber view. Number of slices and acquisition duration per heart beat were adapted individually. Images were evaluated by two independent observers with respect to subjective parameters (number of assessable segments, number of side branch, image quality) and objective parameters (vessel diameter, vessel length and vessel sharpness).

Results: Seventeen patients were completely scanned with both radial and cartesian k-space sampling, 3 only with cartesian and 2 only with radial k-space sampling. Total number of assessable coronary artery segments,using a 7-segment model,were 74.3% (125 from 140 segments) and 73.7% (98 from 133 segments) for cartesian and radial imaging ($p = NS$). In the RCA, radial k-space sampling visualized a larger number of segments (3.18 ± 1.55 vs. 2.41 ± 1.50; $p < 0.05$) and a longer part of the artery (88.74 ± 62.18 mm vs. 73.55 ± 60.17 mm; $p < 0.05$). See table 2 for more details.

Conclusions: MRCA in patients with atrial fibrillation resulted in visualization of 74% proximal and mid-segments using a 7-segment model. In general, radial and cartesian imaging yielded similar results. Significant improvements with radial were only found for the RCA. Results are inferior to those published for patients in sinus rhythm and the diagnostic accuracy needs to be determined in a further study. A potential clinical application would be to rule out high grade CAD before

Table 1.

	Cartesian	Radial	p value
Nominal time (seconds)	237.94 ± 75.34	705.25 ± 291.50	<0.05
Number of slices	114.7 ± 4.9	112.5 ± 5.6	0.359
Acquisition/heart beat	86.9 ± 12.95	95.1 ± 3.25	<0.05
TFE factor	21.38 ± 2.36	17.56 ± 2.53	<0.05

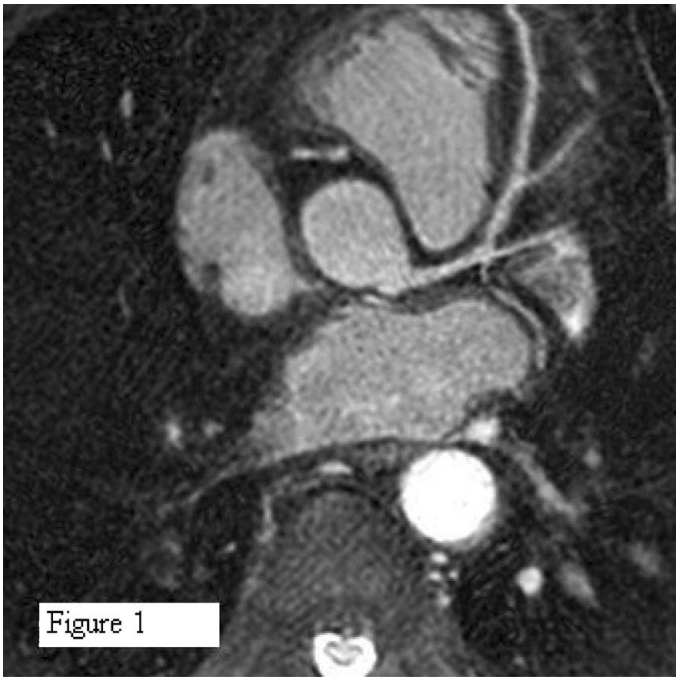

FIG. 1.

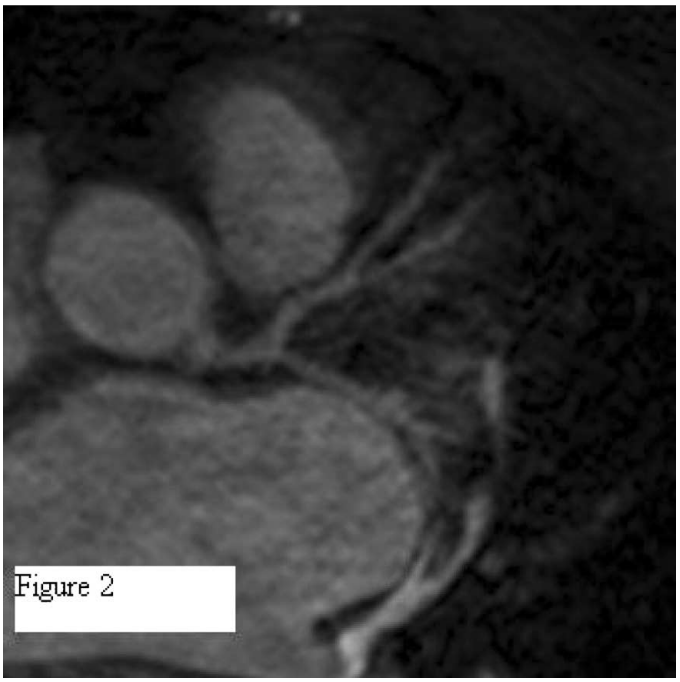

FIG. 2.

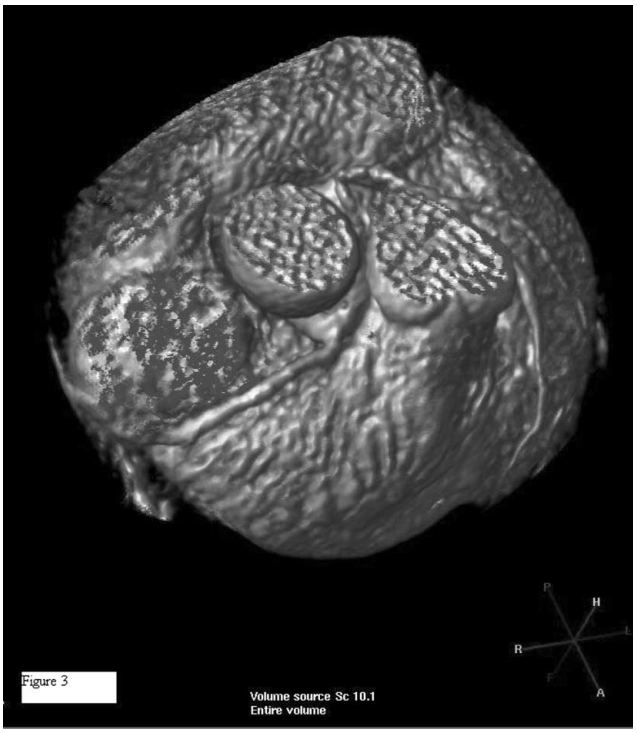

FIG. 3.

mitral valve replacement. In priciple, MRCA is feasible in patients with atrial fibrillation.

Figures 1 and 2 comparison of the left anterior descending artery reconstructed with the soap-bubble program, Fig. 1 = radial; Fig. 2 = cartesian k-space sampling. In this patient a better image quality was achieved by radial k-space sampling.

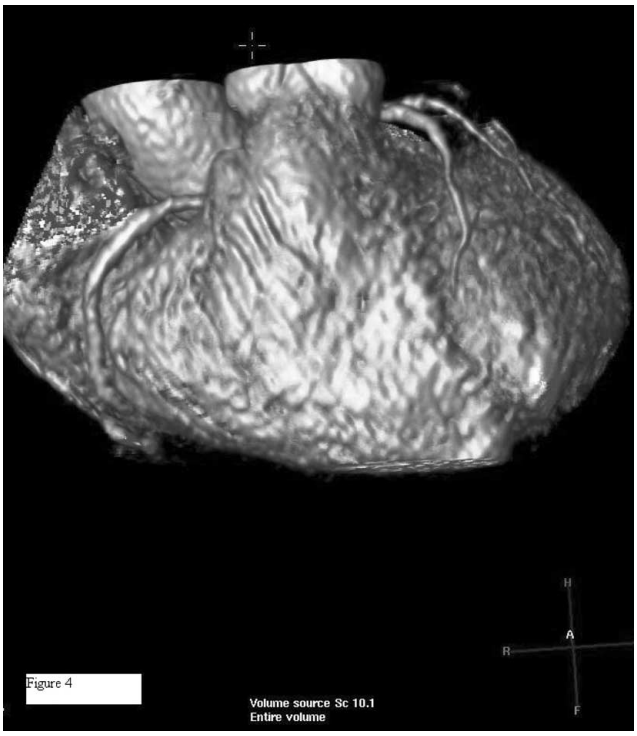

FIG. 4.

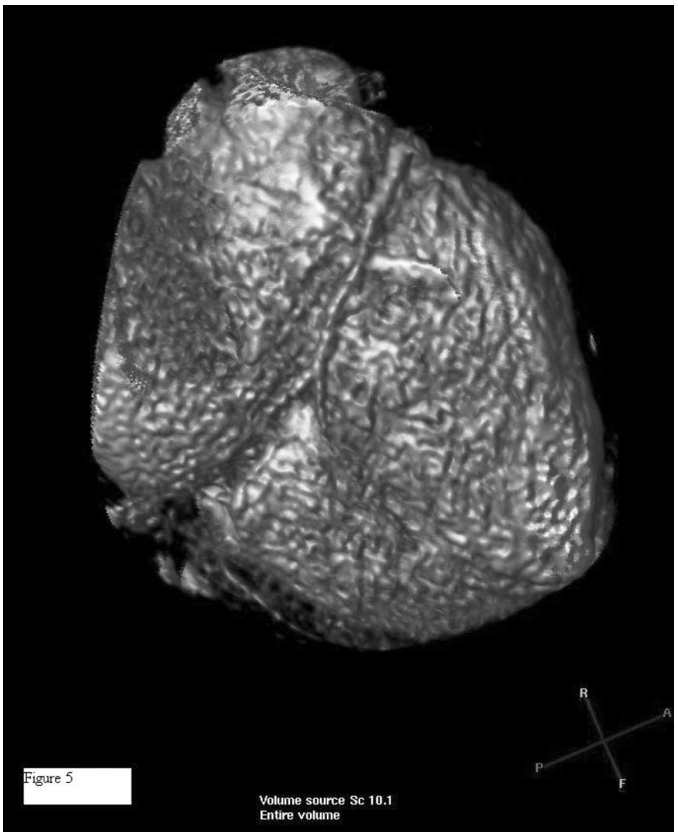

FIG. 5.

Figures 3–5: Shaded surface view of the right coronary artery from proximal (Fig. 3), mid (Fig. 4) to distal (Fig. 5) in patient imaged with radial k-space sampling.

Table 2.

Parameter (per patient)	Cartesian	Radial	p value
1. Total number of segment, using 7-segment model	5.06 ± 2.33	5.06 ± 2.25	1
2. Total number of segment, using 15-segment model	7.71 ± 4.12	8.06 ± 4.44	0.56
3. Total number of side branch	2.06 ± 1.82	2.12 ± 2.15	0.9
4. Image quality	2.34 ± 1.26	2.40 ± 1.34	0.71
5. Vessel length (mm)	38.50 ± 27.21	43.22 ± 25.85	0.09
6. Vessel diameter (mm)	2.34 ± 1.26	2.40 ± 1.34	0.71
7. Vessel sharpness (%)	38.61 ± 17.75	33.26 ± 14.51	0.1

348. VASCULAR MR IMAGING DETECTS IMPROVEMENTS IN CENTRAL & PERIPHERAL VASCULAR FUNCTION AFTER SHORT-TERM FOLIC ACID TREATMENT IN PATIENTS WITH CORONARY ARTERY DISEASE

Cheerag Shirodaria,[1] Justin Lee,[1] Charalambos Antoniades,[1] Clare Jackson,[1] Matthew Robson,[1] Jane Francis,[1] Frank Wiesmann,[1] Stuart Moat,[2] Chandi Ratnatunga,[3] Ravi Pillai,[3] Stefan Neubauer,[1] Keith Channon.[1] [1]***University of Oxford, Oxford, United Kingdom,*** [2]***University of Wales, Cardiff, United Kingdom,*** [3]***John Radcliffe Hospital, Oxford, United Kingdom.***

Background: Homocysteine (Hcy) is an independent predictor of cardiovascular events. Folic acid 400 mcg daily significantly lowers plasma Hcy, but only a daily dose of 5 mg and above has been shown to improve endothelial function as assessed by brachial artery ultrasound. The effects of folic acid on central arterial function are unknown. High-resolution magnetic resonance imaging allows us to quantify vascular function at both central and peripheral sites within the vascular tree during one examination.

Purpose: To test the hypothesis that early changes in arterial function occur with low and high dose folic acid treatment, and that these changes could be assessed accurately and non-invasively using MRI.

Methods: In a double-blind placebo-controlled trial, 27 patients with coronary artery disease (mean age 66 ± 2 y) were randomized to receive folic acid 400 μg daily (n = 9), folic acid 5mg/daily (n = 9), or placebo (n = 9). Non-invasive high-resolution cine MRI at 1.5 Tesla (Siemens Sonata, Erlangen, Germany) was performed to assess distensibility of the aorta (ascending, proximal descending and abdominal) and carotid arteries (CA) before and after 6 weeks of treatment using a TruFISP sequence. Distensibility was measured as the relative change in cross-sectional area per mmHg of pulse pressure. Flow-mediated dilatation (FMD) was measured as the maximum relative change in brachial artery area during post-ischemic hyperemia.

Results: Hcy levels were similarly decreased after treatment with folic acid 400 μg daily (13.0 μmol/L to 11.4 μmol/L, $p < 0.05$) or 5 mg daily (13.7 μmol/L to 11.6 μmol/L, $p < 0.01$) and

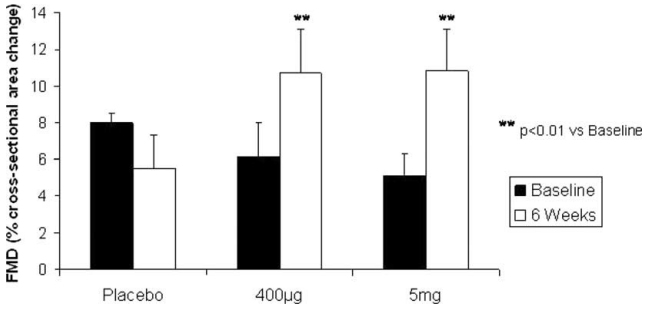

FIG. 1.

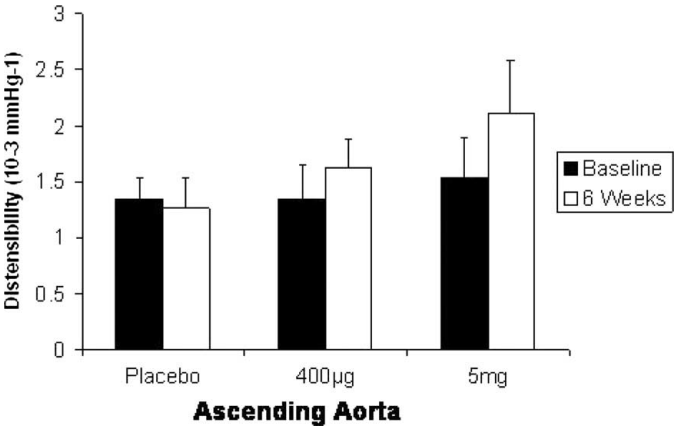

FIG. 2.

were unchanged with placebo (15.0 μmol/L to 14.4 μmol/L, $p = 0.36$). Aortic distensibility was significantly improved in ascending (Fig. 1), proximal descending (2.65 ± 0.64 to $2.69 \pm 0.74\ 10^{-3}$ mmHg^{-1} ($p = 0.82$) with placebo; 2.02 ± 0.22 to $2.35 \pm 0.2\ 10^{-3}$ mmHg^{-1} [$p < 0.05$] with 400 μg; 2.95 ± 0.52 to $3.82 \pm 0.53\ 10^{-3}$ mmHg^{-1} [$p < 0.05$] with 5 mg) and abdominal segments (3.5 ± 0.53 to $3.41 \pm 0.58\ 10^{-3}$ mmHg^{-1} [$p = 0.76$] with placebo; 2.7 ± 0.32 to $3.56 \pm 0.32\ 10^{-3}$ mmHg^{-1} ($p < 0.05$) with 400 μg; 3.25 ± 0.51 to $4.17 \pm 0.57\ 10^{-3}$ mmHg^{-1} [$p < 0.05$] with 5 mg) after daily treatment with both folic acid 400μg and 5mg, but not with placebo (Fig. 1). Distensibility in both carotid arteries also improved with both folic acid 400 μg daily (RCA $2.3 \pm 0.2\ 10^{-3}$ mmHg^{-1} to $3.2 \pm 0.3\ 10^{-3}$ mmHg^{-1}, $p < 0.01$; LCA $2.8 \pm 0.2\ 10^{-3}$ mmHg^{-1} to $3.8 \pm 0.3\ 10^{-3}$ mmHg^{-1}, $p < 0.01$) and 5 mg daily (RCA $3.5 \pm 0.5\ 10^{-3}$ mmHg^{-1} to $4.2 \pm 0.5\ 10^{-3}$ mmHg^{-1}, $p < 0.01$; LCA $3.3 \pm 0.7\ 10^{-3}$ mmHg^{-1} to $4.3 \pm 0.8\ 10^{-3}$ mmHg^{-1}, $p < 0.01$) but not in the placebo group ((RCA $3.5 \pm 0.5\ 10^{-3}$ mmHg^{-1} to $3.3 \pm 0.5\ 10^{-3}$ mmHg^{-1}, $p = 0.37$; LCA $3.9 \pm 0.7\ 10^{-3}$ mmHg^{-1} to $3.7 \pm 0.6\ 10^{-3}$ mmHg^{-1}, $p = 0.49$). FMD was increased in both the 400 μg and 5mg groups but not in the placebo group (Fig. 2).

Conclusion: Both low and high dose folic acid improve arterial distensibility and endothelial function as quantified by MRI. These beneficial actions on vascular structure and function suggest that folic acid treatment may be a promising therapeutic opportunity in patients with coronary artery disease.

349. CAROTID MAGNETIC RESONANCE SCANS PROVIDE CONSISTENT SIGNAL-TO-NOISE RATIO AND CONTRAST-TO-NOISE RATIO IN THE ORION TRIAL

Baocheng Chu, MD, PhD,[1] Niranjan Balu, PhD,[1] Hunter Underhill, MD,[1] Tobias Saam, MD,[1] Norihide Takaya, MD,[1] Joel Raichlen, MD,[2] John Waterton, PhD,[3] Thomas S. Hatsukami, MD,[4] Chun Yuan, PhD.[1] [1]***University of Washington School of Medicine, Seattle, WA, USA,*** [2]***AstraZeneca, Wilmington, DE, USA,*** [3]***AstraZeneca, Macclesfield, United Kingdom,*** [4]***University of Washington***

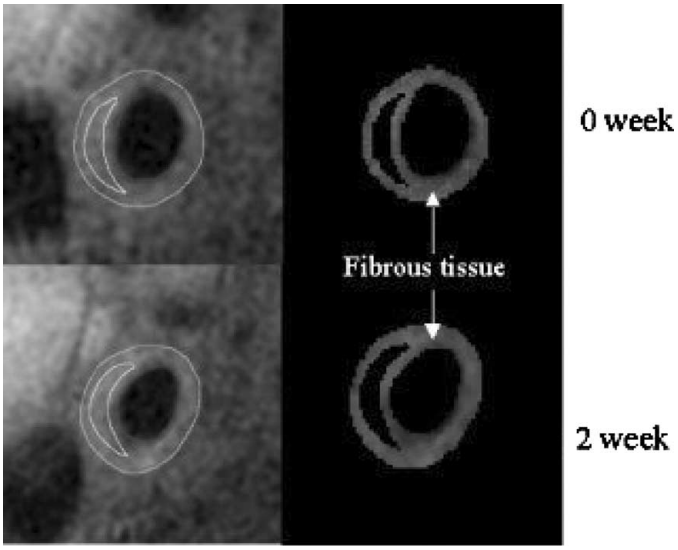

FIG. 1.

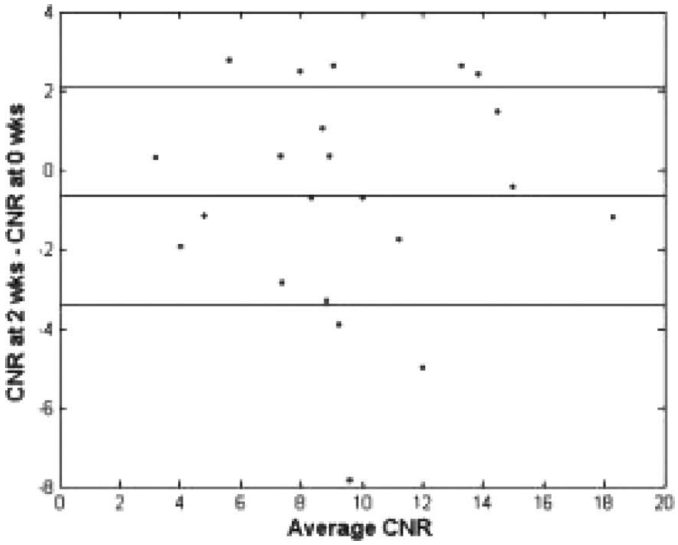

FIG. 3.

School of Medicine and VA Puget Sound Health Care System, Seattle, WA, USA.

Introduction: The ORION (Outcome of Rosuvastatin treatment on carotid artery atheroma: a magnetic resonance Imaging Observation) trial examined the effects of 2 years of treatment with low or high doses of rosuvastatin on carotid plaque size and composition using 5 serial high-resolution magnetic resonance (MR) scans. A primary requirement of serial MR studies is to ensure that the protocol used provides consistent image quality as indicated by signal-to-noise ratio (SNR) and contrast-to-noise ratio (CNR). The purpose of this assessment was to test reproducibility of the two baseline MR scans with respect to SNR and CNR of the carotid artery wall.

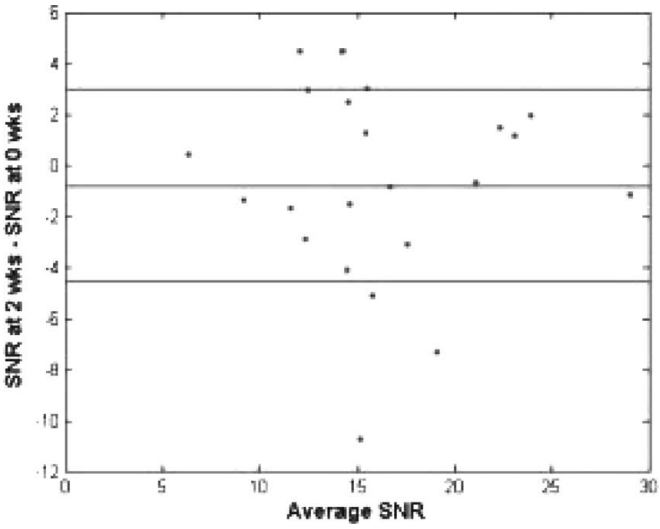

FIG. 2.

Methods: Forty-three hypercholesterolemic patients with 16%–79% carotid stenosis by ultrasound or plaque with a lipid-rich necrotic core (LRNC) by MR were randomized to low- (5 mg) or high-dose (40 or 80 mg) rosuvastatin for 2 years. Serial carotid MR examinations were performed at 1.5T, with phased-array carotid coils, using a multi-contrast weighted protocol (T1, T2, proton density, and 3-dimensional time-of-flight). Two baseline scans (<3 weeks apart) were reviewed by expert readers who evaluated image quality using a 5-point score (1 = poor, 5 = excellent). Studies with image quality $\geq$3 for the two baseline scans were analyzed with outlines of the lumen, the outer wall of the artery, and any area that was not fibrous tissue (LNRC, hemorrhage, calcium, and loose matrix from the artery wall). The SNR and CNR of all matched slices for the two scans were calculated from the arterial wall area on T1-weighted images. On each slice, SNR was calculated by signal intensity (SI) of fibrous tissue area (Fig. 1 [inner circle = lumen; outer circle = outer wall area; crescent shape = LRNC]) divided by the mean SI of background noise, which was determined by finding the standard deviation of the SI of air and multiplying by 1.253. CNR was calculated by the difference between SI of the fibrous tissue and SI of the carotid artery lumen, and dividing by the mean SI of background noise. One-way analysis of variance determinations were performed to examine the differences in mean SNR and mean CNR for both MR scans. Intra-class correlation coefficient and the Bland-Altman plots were used for comparison of SNR and CNR in the two MR scans.

Results: Two hundred and fifty-eight matched slices with image quality $\geq$3 from 22 randomly selected patients were analyzed for the two baseline MR scans. The SNR was comparable between the two scans: 17.09 $\pm$ 5.92 and 16.24 $\pm$ 5.79 (patient-based paired t-test: $p = 0.65$). The CNR also did not show significant differences between the two scans: 10.35 $\pm$ 4.35 and 9.63 $\pm$ 4.33 (patient-based paired t-test: $p = 0.59$). The intra-class

correlation coefficient was 0.77 and 0.76 for the SNR and CNR, respectively. The Bland-Altman plots showed that there was no trend in the difference in SNR and CNR measurements between the two MR scans (Fig. 2 and 3).

Conclusions. Carotid MR can provide images of consistent SNR and CNR and, therefore, consistent image quality for use in serial studies.

350. RIGHT VENTRICULAR FUNCTION AND PULMONARY CIRCULATION IN ARTERIAL SWITCH PATIENTS DURING LONG-TERM FOLLOW-UP, ASSESSED WITH MRI

Heynric B. Grotenhuis, MD, Saskia van Elderen, MD, Lucia J. M. Kroft, MD, Hubert W. Vliegen, MD, Jaap Ottenkamp, MD, Albert de Roos, MD. ***Leiden University Medical Center, Leiden, The Netherlands.***

Introduction: Stenosis in the pulmonary vascular bed in patients with transposition of the great arteries corrected with the arterial switch (AS) operation has been previously described, but its effect on right ventricular (RV) function is unclear.

Purpose: Assessment with MRI of RV function and pulmonary circulation in AS patients during long-term follow-up.

Methods: Fifteen AS patients (age range, 10-20 years) and 15 controls (matched for age and gender) underwent cardiac MRI. RV volumes, ejection fraction and mass indexed for body surface area (RVMi) were assessed, while RV diastolic function was assessed using flow-mapping at the level of the tricuspid valve (TV). Flow dynamics of the pulmonary vascular bed was assessed using flow-mapping at the level of the pulmonary artery (PA), and left and right pulmonary artery (LPA and RPA). Diameter measurements throughout the cardiac cycle of proximal pulmonary branches at the level of the aorta were obtained using cine MR imaging.

Results: Both systolic and diastolic function were normal in AS patients compared to controls (RV EF $p = 0.79$; TV E/A ratio $p = 0.53$). RV hypertrophy was present in AS patients as expressed by a significantly larger RV ventricular mass (RVMi) compared to controls ($p < 0.01$). Supravalvular pulmonary stenosis (PS), with a peak flow velocity (Vmax) exceeding 1.5m/s, was frequently encountered in patients (10 of 15). A significant correlation was observed between PA Vmax and RVMi ($p = 0.05$). Furthermore, increased Vmax in LPA and RPA (12 resp. 9 of 15) was detected as well as compressed pulmonary branches during systole by the aorta (8 and 13 of 15 resp.) (Fig. 1). However, no correlation could be detected between these parameters and RVMi (LPA $p = 0.41$, RPA $p = 0.98$; LPA $p = 0.99$, RPA $p = 0.24$).

Conclusions: AS patients showed normal RV systolic and diastolic function during long-term follow-up. However, significant increased RVMi was frequently encountered, being correlated with supravalvular PS. Frequent pulmonary branch stenoses, (partly) caused by narrowing of the pulmonary branches during systole might contribute to increased RV afterload. The latter mechanism is due to the anatomical relationship between aorta and pulmonary trunc after the Lecompte manoeuvre.

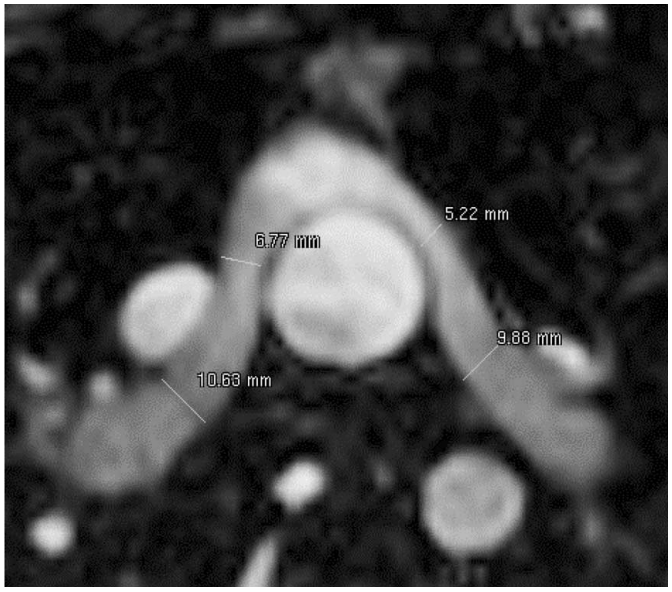

FIG. 1.

351. A MULTIPLE SPIN PREPARATION TECHNIQUE FOR ARRHYTHMIA INSENSITIVE DELAYED ENHANCEMENT IMAGING

Puneet Sharma, PhD, Mushabbar Syed, MD, John N. Oshinski, PhD. ***Emory University, Atlanta, GA, USA.***

Introduction: It is well known that enhancing myocardium due to fibrosis or infiltrative disease can be visualized with MRI following contrast administration. In some cases, however, several technical challenges, such as improper inversion time selection (TI) or variable R-to-R intervals, compromise the high contrast ratio between enhancement and remote (viable) myocardium.

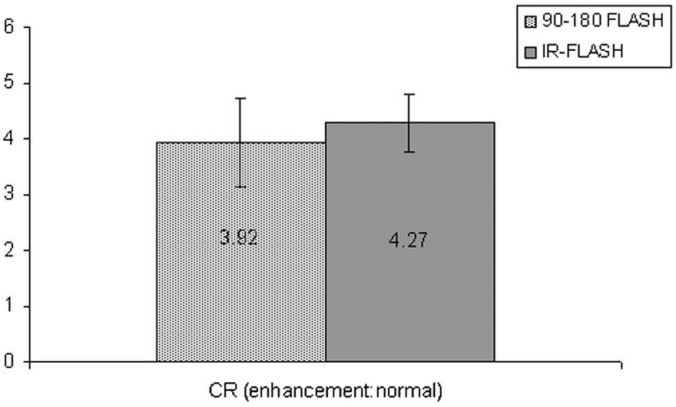

FIG. 1.

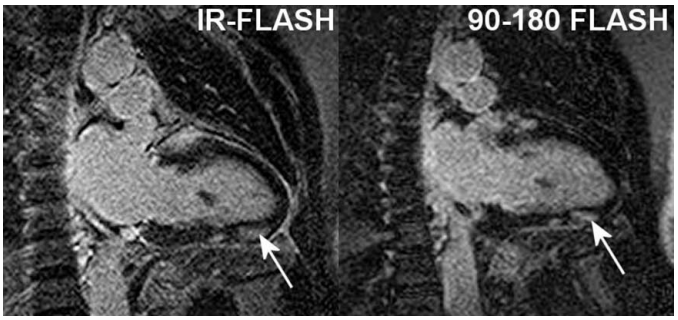

FIG. 2.

This affects the efficiency of the study and requires repeat acquisitions. Arrhythmia insensitivity can be created in delayed enhancement imaging by implementing a non-selective saturation pulse (90 deg) prior to the inversion (IR) pulse. This effect has been shown previously in phantoms and humans (1), but the SNR tradeoff of the technique has not been fully explored in a subset of patients without significant arrhythmia in order to establish its potential use in routine delayed enhancement imaging.

Purpose: The purpose of this study is to compare the image contrast ratio (CR) of the 90–180 arrhythmia insensitive sequence to the tradtional IR delayed enhancement in patients without significant arrhythmia.

Methods: The timing of the 90–180 preparation pulses prior to data acquisition were determined by simulating the expected magnetization available at ky = 0. This was performed in Mathematica computing software (Wolfram) by modeling excitation and relaxation using the Bloch equations. A saturation (TS) and inversion (TI) delay of 600 and 189 ms, respectively, produced low magnetization for expected post-contrast normal myocardium T1s (300–500 ms), while still providing enhancement for expected post-contrast infarct T1s (200–300 ms). Six patients with delayed myocardial enhancement (3 infarction, 3 infiltrative disease) were examined on a Philips 1.5T Intera System using a cardiac phased array coil. Following functional assessment, each patient was administered 0.1-0.2 mmol/kg Gd-DTPA-BMA intravenously. All comparative delayed enhancement images were taken at least 20 minutes after contrast injection. The standard 2D viability sequence was an IR-FLASH technique with TR/TE/flip = 4.1/2.0/15, 40 lines/segment, TI = 250–300 ms, 320 mm FOV, 256 matrix, 10 mm thickness, 2 NSA, and 1 RR segment interval. The proposed arrhythmia insensitive technique utilized a FLASH acquisition with TR/TE/flip = 5.1/2.5/20, 20 lines/segment, TS = 600 ms, TI = 189 ms, 320 mm FOV, 256 matrix, 10 mm thickness, 1 NSA, and 1 RR interval. The mean signal intensity was measured in enhanced and remote myocardium, and divided by the standard deviation of the background noise. The ratio between these two values represented the CR. Since some sequence parameters differed, the SNR/voxel was determined for each method based on the image parameters (2). This value represented a scaling factor in which to normalize the signal intensities for comparison of the two methods.

Results: The pulse timings for the arrhythmia insensitve sequence remained constant throughout imaging, while the TI for the IR-FLASH method spanned 250–300 ms over all subjects. Figure 1 shows the CR between enhancement and normal myocardium using both techniques. There was not a significant difference, depsite a mean drop in CR of the arrhythmia insensitive sequence, which was expected. Figure 2 shows a visual comparison of both techniques in one patient. Both methods clearly reveal the presence and location of the enhanced tissue (arrow). Overall, there was minor visual difference between the two techniques.

Conclusions: Utilizing a 90-180 preparation scheme is a method to overcome image degradation due to cardiac cycle fluctuations. However, this study has also shown its utility in non-arrythmia cases without significant contrast ratio tradeoffs. Furthermore, the proposed method provided greater TI insensitivity than the standard IR-FLASH method post-contrast.

REFERENCES

1. Sharma P, et al. Proc ISMRM 10, 2002.
2. Haacke M, et al. MRI: Physical Principles and Sequence Design. 1999.

352. AUTOMATIC MASKING AND PHASE UNWRAPPING OF DENSE MYOCARDIAL TISSUE TRACKING IMAGES IN HUMAN

Katherine Sinele,[1] Eric Bennett,[2] Han Wen[2]. [1]*Mississippi State University, Starkville, MS, USA,* [2]*National Institutes of Health, Bethesda, MD, USA.*

Introduction: Displacement ENcoding with Stimulated-Echo (DENSE)(1) provides displacement measurements on a continuous scale at high resolution by converting the displacement of each pixel to a proportional phase shift of that pixel. For optimal precision it is desirable to use the highest possible encoding strength, expressed in mm/π, while maintaining image quality.

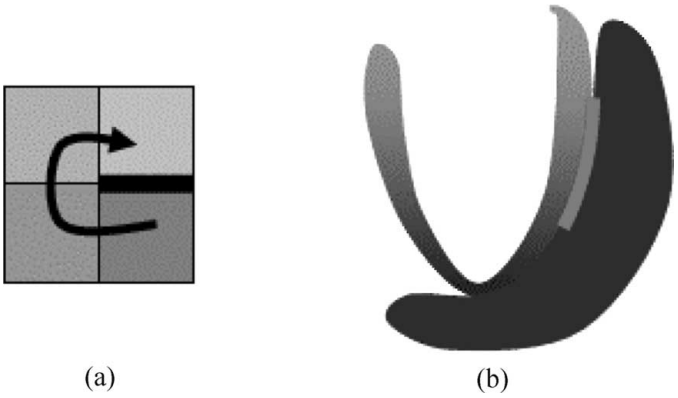

FIG. 1.

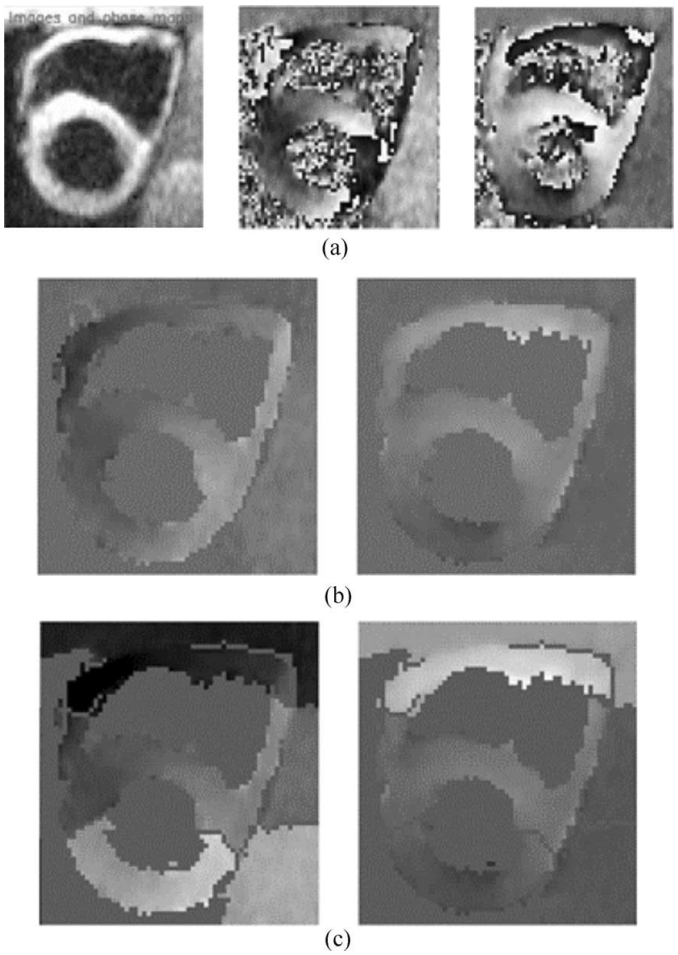

FIG. 2.

The result is that phase shifts may exceed 2π and wrap back onto itself in the form of (θ mod 2π). Previous data processing methods contain manual segmentation of the images before phase-unwrapping (1, 2). Indeed phase-unwrapping can be done automatically based on spatial continuity of phase, provided that the images are properly masked to be free of phase singularities. Image masking and phase-unwrapping are interrelated and we present an automatic masking method that ensures the correct unwrapping of DENSE phase images and demonstrate its effectiveness in DENSE tissue tracking in the human heart.

Methods: A phase singularity is a point or a region surrounded by a closed loop that always contains phase discontinuity despite phase-unwrapping. In DENSE data phase singularities come from low signal, high phase noise pixels, and slip-planes where adjacent tissues have disparate motion and slide relative to each other, such as the interface between the heart and the diaphragm (Fig. 1).

To remove phase singularities, all groups of four-neighboring pixels were checked for singular points of the type Fig.1a, and the pixel of the lowest signal intensity around a singular point was removed. Then the differential motion (ΔD_x/pixel size) and (ΔD_y/pixel size) of adjacent pixels was computed after local

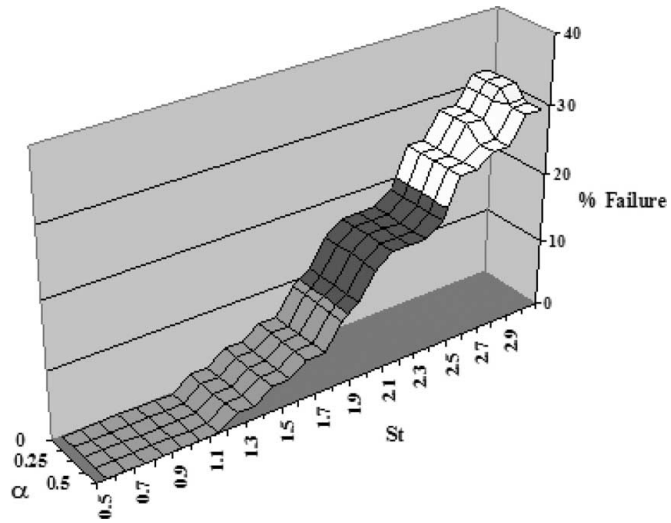

FIG. 3.

phase-unwrapping, and a threshold S_t was used to identify slip-planes (Fig. 1b). The pixel of lower intensity astride a slip-plane is removed. Lastly the average intensity of all removed pixels were used as a measure of the intensity noise level I_N, and a fraction of the noise αI_N was used as an intensity threshold to further mask the image. Afterwards the phase map was unwrapped according to remaining phase discontinuities. Eleven normal volunteers (6M, 5F, age 21–51) were scanned in a clinical 1.5T system (Sonata, Siemens). A respiratory gated version of cine-DENSE scan[2] was developed to improve temporal resolution. Both long and short axis data were acquired with the following parameters: pixel size $1.8 \times 3.5 \times 7$ mm^3, 25 frames at temporal resolution of 21 ms, mean scan time 5 min 46 sec/slice (21% gate acceptance). All data sets were processed with a range of S_t and α values. A failure was defined as incorrect phase-unwrapping of any frame in a data set. Failure rate as a function of S_t and α was plotted to determine their optimal values.

Results: Fig. 2 illustrates the auto-masking and phase-unwrapping process in a short axis data set. Success and failure resulted from two different sets of S_t and α values. Figure 3 plots the failure rate as a function of these two parameters in all volunteers.

The maximum S_t value without failure is 1.1. The value of α has minimal influence on phase-unwrapping, but does affect the number of pixels retained in the mask.

Conclusion: We developed a method for auto-masking and phase-unwrapping of DENSE tissue motion data and optimized parameters for 100% success rate. This method is a core component of an automated processing software of DENSE data, which reduced processing time to 2 minutes/slice and improved inter and intra observer consistency.

REFERENCES

1. Aletras AH, Ding SJ, Balaban RS, Wen H. Journal of Magnetic Resonance 1999;137:247–252.
2. Kim D, Gilson WD, Kramer CM, Epstein FH. Radiology. 2004;230:862–871.

353. RESPIRATORY SELF-GATED 4D CORONARY MRA

Peng Lai, MS, Andrew C. Larson, PhD, Jaeseok Park, PhD, Debiao Li, PhD. ***Northwestern University, Chicago, IL, USA.***

Introduction: In coronary MRA, cardiac motion and respiratory motion are two major sources of artifacts that limit its clinical value. Traditionally, ECG triggering is used to suppress cardiac motion artifacts by synchronizing data acquisition with mid-diastole of a cardiac cycle. However, it is a tedious job to properly set trigger-delay time and acquisition window, which varies a lot from one subject to another (1). Breath-hold freezes respiratory motion of the heart during a scan, but the achievable slice coverage and spatial resolution is restricted as a result. Although diaphragmatic navigator (NAV) enables free-breathing high-resolution coronary MRA, it is incompatible with time-resolved imaging. Furthermore, NAV suffers from hysteretic problems due to indirect measurement of heart position.

Purpose: Our work aimed to investigate the feasibility of a new free-breathing technique for 3D cine (4D) coronary MRA which derives real-time respiratory gating signal directly from the heart motion and yields continuous phase images depicting cardiac motion of the coronary over a whole cardiac cycle.

Methods: A new sequence was implemented based on a SSFP cine sequence with retrospective ECG gating and Cartesian K-space sampling. An additional k-space center line for self-gating was acquired before each segmented data acquisition corresponding to each cardiac phase and acquisition of each segment of K-space lines was repeated for 4∼5 seconds to cover a respiratory cycle. The readout direction was along the maximal in-plane respiratory motion of the heart. Data were continuously acquired throughout the scan and retrospectively remapped into the nearest cardiac phase of 15 evenly spaced cardiac phases based on the ECG time stamp simultaneously recorded. By analyzing 1D projections of the imaging slice reconstructed from the self-gating lines, cardiac phase-dependent templates were generated (2). Heart displacement due to respiratory motion was derived by template matching and used for motion compensation and respiratory gating. A phase-sensitive method was applied for fat saturation (3). To study the effectiveness of this method for suppressing respiratory motion artifacts, images were also reconstructed using simple averaging for comparison. Coronary arteries of 8 healthy volunteers were scanned on a 1.5T Siemens Sonata system during free breathing. Sequence parameters included: FOV: 350 × 250 mm^2, slice number: 8 (interpolated from 4), slice thickness: 1.75 mm, matrix: 256 × 154, in-plane resolution: 1.4 × 1.6 mm^2, flip angle: 60°, TR/TE: 4.30/2.15 ms, lines/segment: 11.

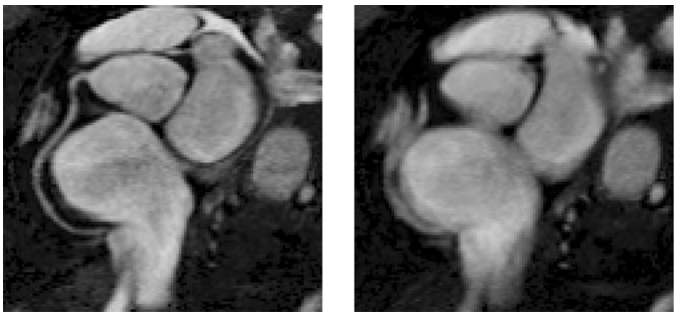

FIG. 2. MIP image reconstructed using self-gating (left) and simple averaging (right).

Results: Coronary images of a volunteer at different cardiac phases are shown in Fig. 1. Position shift of the RCA due to cardiac motion is distinguishable. RCA is clearly delineated in the mid-diastole image. In Fig. 2, a maximum intensity projection (MIP) image at mid-diastole reconstructed using self-gating and the corresponding MIP image reconstructed using simple averaging are shown. Obviously, the coronary is severely blurred by motion artifacts in the image of simple averaging, while it is clearly visualized in the image of self-gating, including the distal portion.

Conclusions: The proposed self-gating technique is promising for suppression of respiratory motion artifacts in free-breathing coronary MRA. Besides, with retrospective ECG gating, cardiac motion is also resolved and no pre-determined trigger-delay time and acquisition window is needed. Images with the best delineation of the coronary artery can be selected retrospectively for diagnosis.

REFERENCES

1. Bi X, et al. MRM 2005;54:470.
2. Larson AC, et al. MRM 2005;53:159.
3. Hargreaves BA, et al. MRM 2003;50:210.

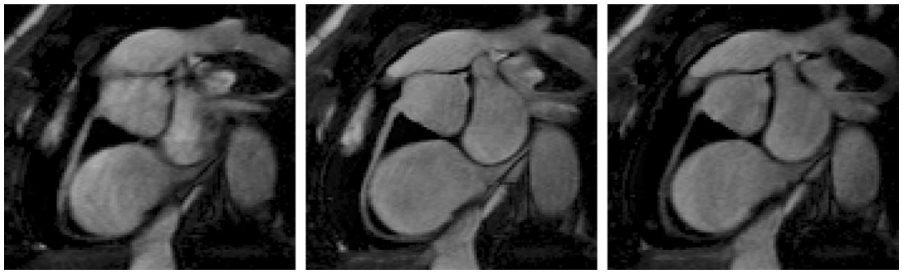

FIG. 1. From the left to the right, Self-gated images of the RCA at early-diastole, mid-diastole, late-diasole, respectively.

354. PROGRESSIVE INFARCT HEALING AND LEFT VENTRICULAR REMODELING 4 MONTHS AND MORE THAN 1 YEAR FOLLOWING AN ACUTE MYOCARDIAL INFARCTION

Jose T. Ortiz, Preeti Kansal, MD, Paula Tejedor, MD, Chiara Bucciarelli-Ducci, MD, Daniel C. Lee, MD, Thomas A. Holly, MD, James C. Carr, MD, Francis J. Klocke, MD, Robert O. Bonow, MD, Edwin Wu, MD. ***Northwestern University, Chicago, IL, USA.***

Background: Previous contrast-enhanced cardiac magnetic resonance imaging (ce-CMR) studies have shown a reduction of infarct size at 3 to 6 months following acute myocardial infarction (MI). We used serial ce-CMR to sequentially assess infarct and left ventricle (LV) remodeling over an extended year follow-up period.

Methods: We imaged 39 patients at 3 different time points following an acute MI (34 patients with ST segment elevation MI and 4 patients with non-ST segment elevation MI). The first CMR exam was obtained at 3 ± 2 days, the second at 4 ± 1 months and the third at 14 ± 3 months after the acute MI. Standard cine and ce-MRI were performed to measure the LV ejection fraction (EF), end-diastolic volume (EDV), end-systolic volume (ESV), total LV mass, non-infarct mass (NI-mass), infarct mass and infarct size as a percentage of the total LV mass. All 117 image sets from each time point were de-identified, randomized and measured by a single analyst.

Results: Initial infarct mass (mean 24 ± 18 g; 20 ± 13% of LV mass) decreased to 17 ± 13 g at 4 months follow-up ($p < 0.001$). At 14 months, infarct mass further decreased to 16 ± 12 g ($p < 0.001$), an overall 34 ± 23% reduction in infarct mass compared to the initial infarct mass. Additionally, between the first and the second CMR study, the NI-mass and total LV mass decreased by 7 ± 13% ($p < 0.001$) and 12 ± 11% ($p < 0.001$) respectively, while the EDV did not change significantly.

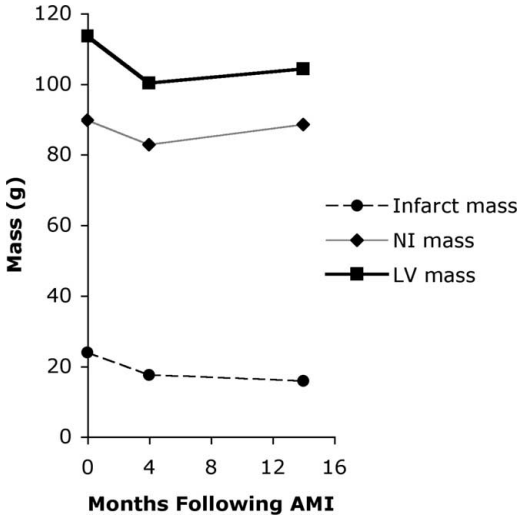

FIG. 1.

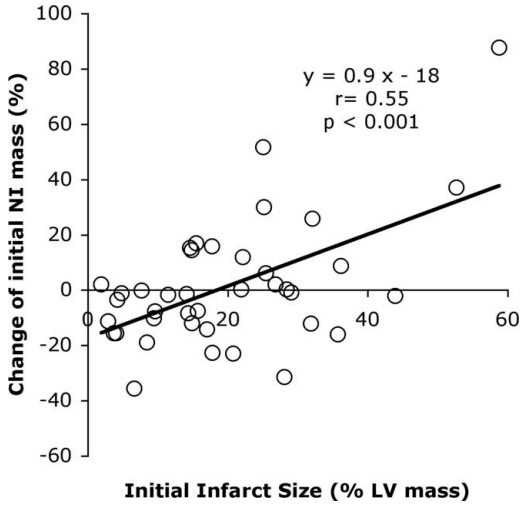

FIG. 2.

However, the NI-mass increased 8 ± 18% between the second and the third study ($p < 0.05$), with a non-significant increase in the total LV mass (4 ± 13%, p = NS). The initial infarct size correlates with the long-term increase in the EDV ($r = 0.38$, $p < 0.05$) and non-infarct mass ($r = 0.55$, $p < 0.001$).

Conclusions: Changes in infarct and non-infarct mass vary depending on the duration of follow-up and the initial infarct size. Infarct healing rapidly occurs within the first several months and continues at a slower rate chronically. Additionally, despite the healing of acute necrotic tissue into a dense collagenous scar, late increases in non-infarct mass may reflect an activation of compensatory hypertrophy mechanisms seen in patients with large initial infarct sizes that would not be evident if follow-up CMR examinations are performed soon after an acute MI.

355. IDENTIFYING DIFFERENT HEART TISSUES FROM COMBINED FUNCTIONAL AND VIABILITY IMAGES USING C-SENC

El-Sayed H. Ibrahim, MSE, Amy Spooner, MD, Matthias Stuber, PhD, Michael A. Jacobs, PhD, Robert G. Weiss, MD, Nael F. Osman, PhD. ***Johns Hopkins University, Baltimore, MD, USA.***

Introduction: Assessment of myocardial viability in patients with Myocardial Infarction (MI) is important for therapeutic decision making. Functional magnetic resonance imaging (MRI) can provide important information about the status of heart muscle. For example, delayed-enhancement (DE) contrast images combined with functional images can identify different tissue types of the heart, using unsupervised clustering techniques. However, seldom are these MR images acquired at the same point in time to allow automatic clustering. Composite Strain-Encoding (C-SENC) MRI technique enables acquiring both DE

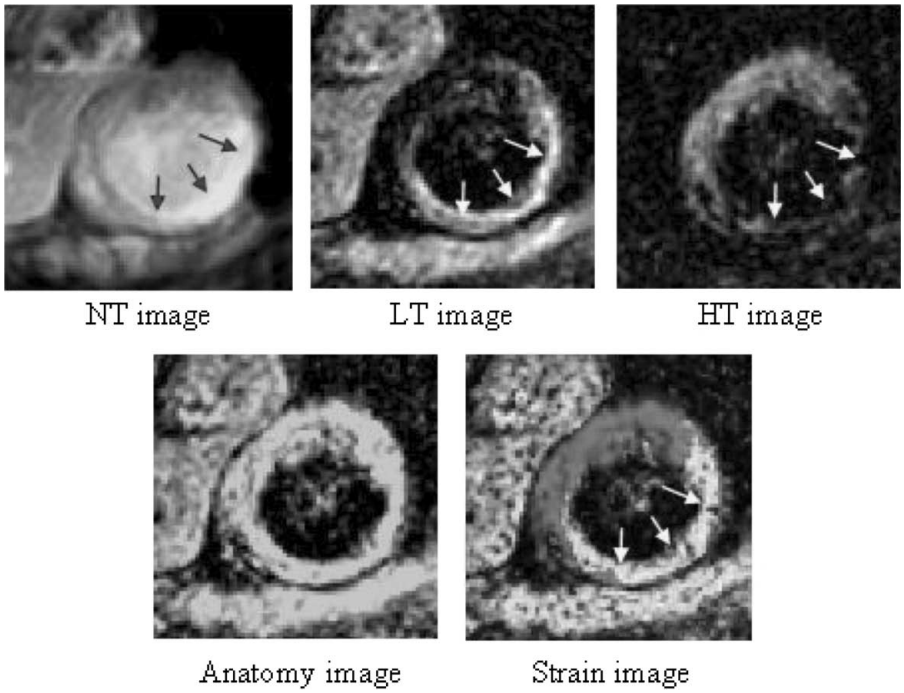

FIG. 1. Representative C-SENC images. Bright regions in the NT, LT, and HT images represent infarcted, akinetic, and kinetic myocardium, respectively. The anatomy and strain images could be computed from the LT and HT images. Infarcted region is marked by arrows.

and functional images simultaneously [1]. In this work, a multi-stage clustering technique was applied to the C-SENC DE and functional images *of volunteers and patients with MI*. The results showed the ability of the proposed technique of identifying different heart tissues.

Methods: Six volunteers (5 males, average-age = 45) were scanned on a 3T Philips scanner. The subjects were injected with 0.2 mmol/kg of GD-DTPA for dynamic imaging followed by a saline flush. C-SENC images were acquired 10–15 minutes post injection. The imaging parameters were: Trigger-Delay (TD) ≈300 ms (depending on heart-rate); TR = 23 ms; TE = 4.9 ms; and flip-angles = 27, 32, and 40 degrees for No-Tuning (NT), Low-Tuning (LT), and High-Tuning (HT), respectively. C-SENC imaging obtains the NT, LT, and HT images in the same acquisition (1). Bright regions in the NT, LT, and HT images represent infarcted, akinetic, and contracting myocardium, respectively. In addition, blood appears bright in the NT image and dark in the LT and HT images. Figure 1 shows representative images from the C-SENC method. These images were used to build a 3-D space of the heart, represented by the NT,

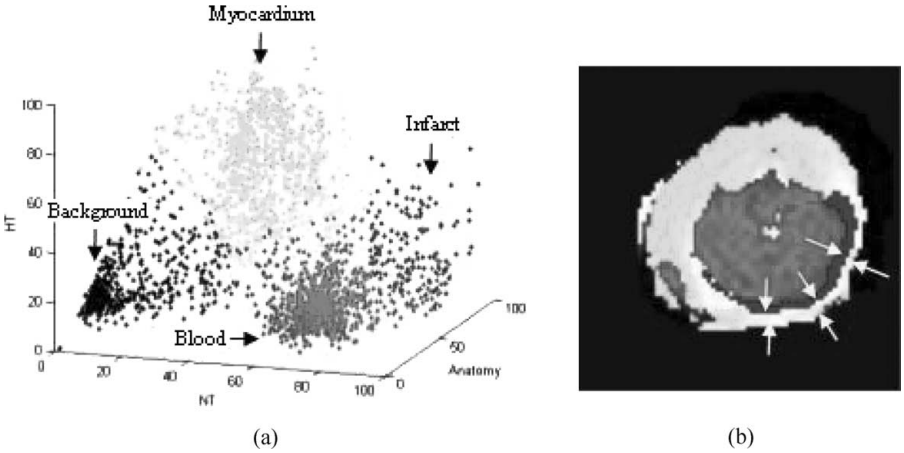

FIG. 2. Results of the clustering process applied to the slice in Fig. 1. Red, blue, and black represent blood, infarct, and background, respectively. Non-infarcted myocardium is represented by colors ranging from white, for non-contraction, to green, for maximum contraction (a) The NT-HT-Anatomy density distribution after clustering. (b) The clustered images. Arrows mark the endocardial infarct, surrounded by a rim of non-contracting (white) epicardium.

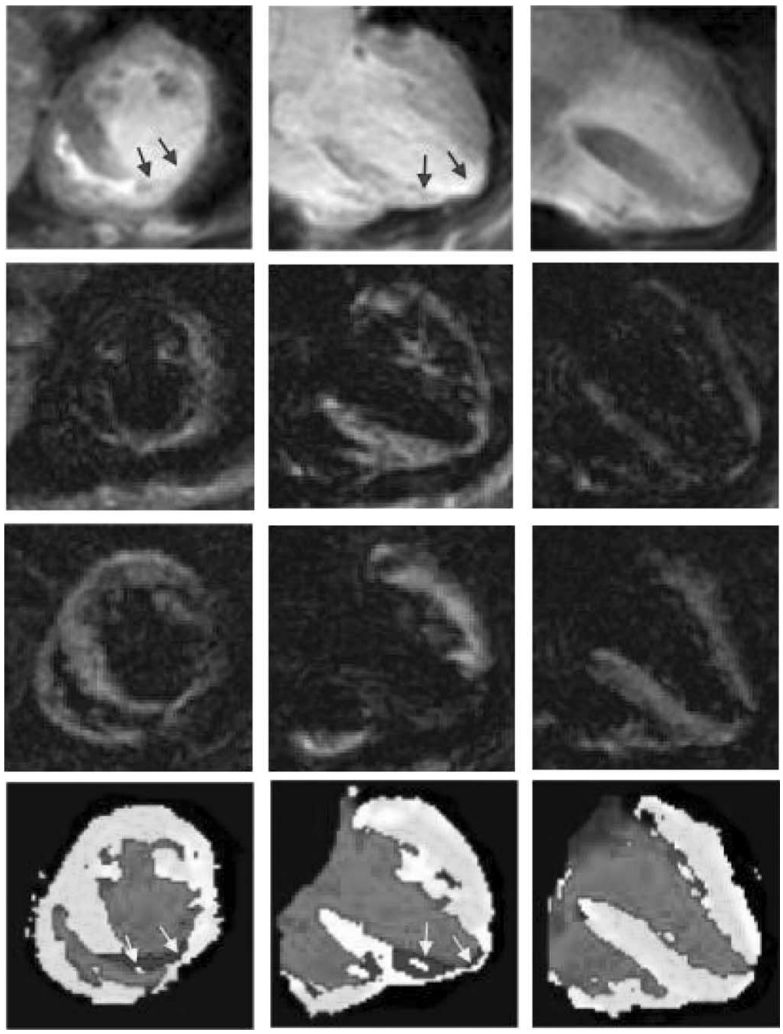

FIG. 3. The rows show NT, LT, HT, and resulting clustered images, from top to bottom. Red, blue, and black represent blood, infarct, and background, respectively, while myocardium is represented by colors ranging from white for non-contraction, to green, for maximum contraction. The images in the third column are for a volunteer who did not have infarct. This is reflected in the clustered image, where the clustering method resulted only in three clusters: blood, background, and myocardium.

HT, and Anatomy (LT+HT) axes. Different tissue types appear well-identified in this 3-D space: Infarcted myocardium shows bright in the NT and Anatomy images, and dark in the HT image. Non-infarcted myocardium shows dark in the NT image, bright in the Anatomy image, and it has a continuum of signal intensities, depending on contractility, in the HT image. Finally, blood uniquely shows bright in the NT image and dark in the Anatomy and HT images. The unsupervised clustering technique consisted of two stages. First, the heart is segmented into three clusters: background, blood, and myocardium using the fuzzy c-means clustering technique (2). Second, the myocardial cluster is further segmented into infarcted, if applicable, and non-infarcted tissues using the ISODATA clustering technique (3). In the non-infarcted tissue cluster, pixels of different contractility patterns are represented by different color grades.

Results: Typical results are shown in Fig. 2, which demonstrates the 3-D distribution of the signal intensities, and the resulting clustered image, of a Region-of-Interest encompassing the heart shown in Fig. 1, after applying the proposed clustering technique. Blood, background, and infarction were represented by red, black, and blue, respectively, while non-infarcted myocardium was represented by colors ranging from white, for non-contraction, to green, for maximum contraction. Figure 3 shows the results of applying the proposed technique to slices from different volunteers.

Conclusions: The proposed technique is capable of characterizing human myocardial function and viability in a single acquisition. The combination of this information with clustering techniques allows the identification of divergent cardiac tissue types. The resulting clustered images could help reveal more information about the heart and possibly allow delineation of viable, but not contracting, myocardium such as that present in hibernating or stunned tissues (outer arrows in Fig. 2).

Acknowledgements: Grants: Donald W. Reynolds Foundation and R01-HL072704.

REFERENCES

1. Ibrahim EH, et al. Magn Reson Med in press.
2. Hoppner F, et al. Fuzzy cluster analysis. John-Wiley; 1999.
3. Jacobs MA, et al. J Magn Reson Imaging, 11:425–437.

356. VENTRICULAR NON-COMPACTION IN IDIOPATHIC DILATED CARDIOMYOPATHY

Andrew McCann, MBBS, Richard E. Slaughter, MBBS, FRACR, Andrew Galbraith, MBBS FRACP, Wendy E. Strugnell, BSc(App), Robyn A. Riley, DipAppSc. ***The Prince Charles Hospital, Brisbane, Australia.***

Introduction: Isolated ventricular non-compaction is thought to represent a rare cardiomyopathy with a high incidence of left ventricular dysfunction, thromboembolism and arrhythmias. Diagnosis has mostly depended on the demonstration of a ratio of trabecular to non-trabecular myocardium of greater than 2:1 on echocardiography. We used steady state free precession (SSFP) cine MR imaging with its excellent definition of ventricular trabecular patterns to compare a group of patients with LV dysfunction with a group of normal subjects. Using adapted echo criteria for ventricular non-compaction to assess the images, it appears the presence of isolated ventricular non-compaction in idiopathic dilated cardiomyopathy (DCM) may be more common than previously thought.

Purpose: To assess the extent of left ventricular trabeculation and to describe the presence of isolated ventricular non-compaction in idiopathic DCM using cardiac MRI. To compare the trabecular patterns in this group with those of a group of normal subjects.

Method: SSFP MR images of 54 consecutive patients with a clinical diagnosis of idiopathic DCM, and 50 normal volunteers were examined to assess the LV trabecular patterns. MR imaging was performed on a 1.5 Tesla Signa Twinspeed system with a 4-element cardiac phased array coil. SSFP images were obtained in the standard orientations for ventricular function assessment. Delayed myocardial enhancement imaging acquired between 8–15 minutes after administration of 0.2 mmol/kg of GD-DTPA, was performed on the DCM group. Two independent observers assessed trabecular patterns in the apex, septum, anterior, lateral and posterior left ventricular walls on images obtained in short axis, vertical long axis and horizontal long axis orientations. They were graded as mild, moderate or severe if the end systolic ratio of trabecular to non-trabecular myocardium was <1, 1–2, or >2 respectively.

Results: The DCM group had a mean ejection fraction (EF) of 21% (normal 47–69%) and a mean end diastolic volume (EDV/m^2) of 180 mL/m^2 (61–116 mL/m^2). The normal group had a mean EF of 58% and mean EDV/m^2 of 88 mL/m^2. A spectrum of trabecular patterns from mild to severe was present in the DCM group. 10 patients (19%) had severe trabeculations in at least one of the five segments, with the apex most commonly involved, followed by the anterior and lateral walls. Moderate trabeculation was present in 35% and mild trabeculation in 46% of patients. No patients showed enhancement on delayed enhancement imaging. In the normal group, no subjects had severe trabeculation, 9% had moderate and 91% mild trabeculation.

Conclusion: In normal subjects moderate or severe trabeculation is uncommon. Prominent trabeculation of the left ventricle is common in idiopathic DCM and exists on a continuum from mild to severe. Using the criteria adapted from transthoracic echocardiography, 19% of DCM patients fulfilled the diagnostic criteria for isolated ventricular non-compaction. The frequency with which we have observed these findings suggests that the use of an arbitrary cut off ratio of greater than 2:1 may not be valid for a diagnosis of ventricular non-compaction. Further studies to evaluate what degree of non-compaction, if any, denotes a higher risk of adverse clinical outcomes are needed.

357. AN APPROACH TO THE QUANTIFICATION OF REGIONAL RIGHT VENTRICULAR WALL MOTION USING CINE MRI

Karen G. Ordovas, MD, Mario Morales, MD, Gautham P. Reddy, MD, MPH, Charles B. Higgins, MD. ***UCSF, San Francisco, CA, USA.***

Introduction: It has been demonstrated that MRI is the best method for assessment of ventricular volumes and function. For

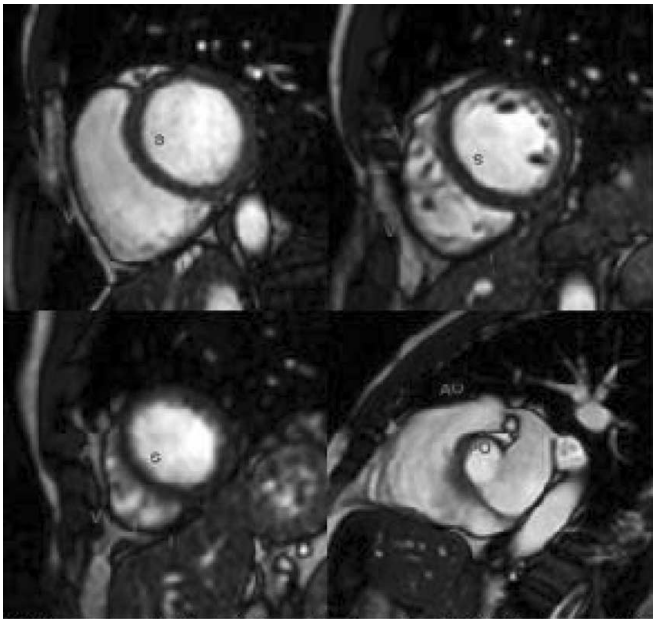

FIG. 1. RV segmentation: Short-axis cine MR images at the basal, midventricular and apical levels as well as in the outflow tract plane (top left to bottom right) demonstrating the segmentation of the right ventricle. S = septal segment, I = inferior segment; V = ventral segment; A = anterior segment; AO = anterior outflow tract; PO = posterior outflow tract.

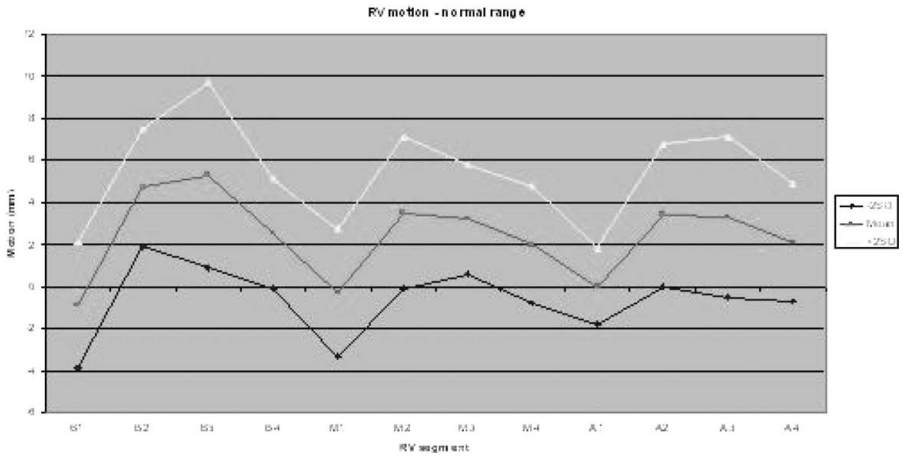

FIG. 2. Normal distribution of right ventricular motion. p = patients; v = volunteers; B1 = septal segment at the base; B2 = inferior segment at the base; B3 = ventral segment at the base; B4 = anterior segment at the base; M1 = septal segment at the midventricle; M2 = inferior segment at the midventricle; M3 = ventral segment at the midventricle; M4 = anterior segment at the midventricle; A1 = septal segment at the apex; A2 = inferior segment at the apex; A3 = ventral segment at the apex; A4 = anterior segment at the apex.

the evaluation of the right ventricle (RV), it has been shown to be more accurate than echocardiography. Right ventricular functional assessment is particularly important in the evaluation of patients with congenital heart disease and arrytmogenic right ventricular dysplasia. To our knowledge, a systematic tomographic approach for evaluating RV regional function has not been established.

Purpose: The purpose of this study was to develop a method of tomographic segmentation of the RV on cine MR imaging and demonstrate the range of normality.

Patients and methods: This is an early phase of a cohort study. Cine MR images were obtained in 10 normal volunteers in the short-axis and vertical long axis planes in order to evaluate RV function. A method of RV wall segmentation was employed in which 14 segments were defined: septal wall, inferior wall, ventral wall and anterior wall segments at the base, midventricle and apex on the short axis plane; anterior and posterior outflow tract wall segments on an oblique vertical long axis plane parallel to the outflow tract (RV outflow tract plane) (Fig. 1). RV regional motion during the cardiac cycle was measured in each of RV segments and a range of normality (mean ± standard deviation) was described.

Results: The range of normal motion of RV segments are shown on Fig. 2. The septal segment had approximately no motion at the midventricular and apical levels and only slight motion away from the center of the RV cavity at the basilar level. Ventral segments demonstrated the greatest motion of all segments at all levels.

Conclusion: The study proposed and implemented a systematic approach for evaluation of right ventricular regional function using cine MRI. At an early phase of this study, the normal pattern of RV regional function was characterized by little or no motion of septal segments and maximal motion of the lateral free wall at all levels.

358. OPTIMIZATION OF DENSE SEQUENCE FOR IMAGING REGIONAL STRAIN DISTRIBUTION IN THE CAROTID ARTERY WALL AND PRELIMINARY TESTS IN HUMANS

Han Wen, Ignacio Rodriguez, PhD, Eric Bennett, MS, Alexandre Vignaud, PhD. ***National Institutes of Health, Bethesda, MD, USA.***

Introduction: Atherosclerotic lesions of the arteries are localized to regions of high stress and excessive stretching of the arterial wall, where strain likely influences endothelial function. Recent results with intravascular ultrasound also showed that high strain in atherosclerotic lesions is a predictor of vulnerability. Noninvasive imaging of vessel wall strain distribution is valuable for studying the progression of atherosclerosis. We tested strain imaging in the carotid artery wall using Displacement Encoding with Stimulated Echo (DENSE). Specifically, SNR optimization was carried out in a phantom study, and preliminary data in human subjects were collected.

Methods: Scans were performed on a 1.5T clinical scanner (Sonata, Siemens). A multi-slice, single phase, 2D DENSE pulse sequence with segmented k-space acquisition (24 k-space lines per heartbeat) was first tested in an agar gel phantom (T_1 = 1.1 sec, T_2 = 140 ms). The signal and noise levels of three different readout schemes were compared. These were: 1. true-FISP readout with ramped flip angle to equalize the echo

Table 1. Signal and noise of three readout schemes

Readout scheme	Signal level	Noise level	SNR
True-FISP	127.1	13.4	9.5
GRE	83.8	12.6	6.7
ET-GRE	142.9	44.2	3.2

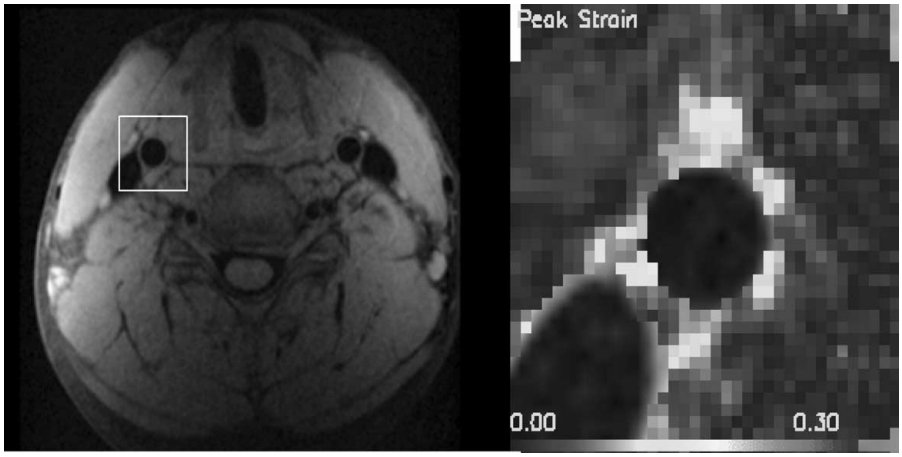

amplitudes, 2. GRE readout with one echo per RF excitation and ramped flip angle, 3. ET-GRE readout with two echoes per RF excitation and ramped flip angle. The imaging parameters were matrix 256 × 240, FOV 154 × 144 × 4 mm^3, displacement encoding strength 1.0 mm/π, RF Phase cycling (n = 11) was used to isolated the stimulated-echo, and 3 slices were acquired in 15 minutes. In 4 volunteers, ECG-triggered scans were performed with a 4-channel neck coil set (Machnet, Netherlands) and the same parameters listed above. A cine movie was acquired to determine the times of minimum and maximum carotid lumen diameter, and tissue displacement between the two time points were measured. This time interval was typically 150 ms.

Results: Table 1 summarizes the signal and noise levels and SNR of the three readout schemes. While ET-GRE gave the highest signal level, it also had the highest noise due to ghosting from the disparity between the first and second echo. Overall, true-FISP readout gave the best SNR and was used for human subjects. The SNR ratio ranged from 4.5 to 9.3 in humans. The displacement noise was 22 to 45 μm, and strain noise 5.1% to 10.6% per pixel. To suppress strain noise, circumferential smoothing was performed for every 4 pixels around the wall. Figure 1 shows a DENSE image and the circumferential strain in color scale aorund a carotid artery.

Conclusion and Discussion: The strain distribution of the carotid artery wall and the surrounding tissue can be mapped non-invasively with DENSE. At 1.5T the scan time is approximately 5 minutes per slice to obtain reasonable SNR. Higher field strength will help to shorten the scan times or provide better strain precision.

REFERENCES

1. Thubrikar MJ, Robicsek F. Annals of Thoracic Surgery 1995;59:1594–1603.
2. Schaar JA, Regar E, Mastik F, McFadden EP, Saia F, Disco C, de Korte CL, de Feyter PJ, van der Steen AFW, Serruys PW. Circulation 2004;109:2716–2719.
3. Aletras AH, Ding SJ, Balaban RS, Wen H. Journal of Magnetic Resonance 1999;137:247–252.
4. Kim D, Gilson WD, Kramer CM, Epstein FH. Radiology 2004;230:862–871.
5. Callot V, Bennett E, Decking UKM, Balaban RS, Wen H. Magnetic Resonance in Medicine 2003;50:531–540.

359. CARDIAC MAGNETIC RESONANCE CONTRAST ENHANCEMENT DIFFERENTIATES PATIENTS AFFECTED WITH FAMILIAL DILATED CARDIOMYOPATHY FROM ASYMPTOMATIC RELATIVES

Michael Jerosch-Herold, Ph.D., David C. Sheridan, B.S., Jessica D. Kushner, MS, C.G.C., Deirdre Nauman, BSN, Donna Burgess, BSN, Diana Dutton, BSN, Ray E. Hershberger, M.D. ***Oregon Health & Science University, Portland, OR, USA.***

Introduction: Idiopathic dilated cardiomyopathy occurring in families, or familial dilated cardiomyopathy (FDC), is characterized by left ventricular (LV) enlargement with systolic dysfunction, other causes excluded. Novel phenotype markers, such as interstitial, diffuse, fibrosis, may be useful for early detection of at-risk kindred in FDC families. Cardiac magnetic resonance (CMR) imaging of myocardial contrast enhancement with gadolinium is used to detect loss of myocardial viability and fibrosis. Its value for the detection of diffuse fibrosis in FDC patients remains unproven.

Purpose: To test the hypothesis that patients diagnosed with FDC demonstrate increased up-take of gadolinium contrast, compared to their kindred without clinical signs of FDC.

Methods: CMR imaging was performed at 3 Tesla in nine family members of one of the 304 families that have been characterized in a FDC research project. The cohort comprised affected family members (N = 3), unaffected first to fourth generation relatives (N = 4), and 2 family members with intermediate phenotype. The myocardial partition coefficient for gadolinium contrast, defined as the ratio of gadolinium contrast concentration at equilibrium in blood and tissue, was determined by multiple T1 measurements with a gradient echo Look-Locker technique (TR/TE/flip angle = 3.4/1.7 ms/12°; slice thickness = 8 mm; 176 × 140 matrix), pre and post contrast administration. Global LV shape and function parameters were assessed by standard CMR methods.

Results: The EDV measured by MRI, and indexed by height was significantly different between the three FDC phenotypes

($p = 0.005$ for ANOVA test), and largest in the FDC patients. There was no evidence of focal contrast hyper-enhancement on images where the myocardial signal intensity was nulled. The global averages of the myocardial Gd-DTPA partition coefficient showed significant differences between the three categories of FDC phenotype (ANOVA $p = 0.007$), and were significantly elevated in affected family members, versus their unaffected kindred (0.56 ± 0.15 vs. 0.33 ± 0.10; adj. $p < 0.05$). The Gd-DTPA partition coefficient correlated with LV enlargement, and increased with impairment of systolic function (correlation with ejection fraction: $r = -0.78$; $p = 0.01$).

Conclusions: The finding of a significantly elevated myocardial Gd-DTPA partition in FDC patients, compared to their at-risk kindred supports the hypothesis of diffuse interstitial fibrosis, seen previously in myocardial biopsy samples of FDC patients. Gadolinium contrast enhancement assessed by CMR may provide a novel marker for phenotyping FDC-affected patients, assessing disease onset and progression in known mutation carriers, and effective monitoring of treatment.

360. A MAXIMUM PREDICTED LEFT VENTRICULAR EJECTION FRACTION IN RELATION TO INFARCT SIZE IN PATIENTS WITH ISCHEMIC HEART DISEASE

Martin Ugander, MD, Bjorn Ekmehag, MD, PhD, Hakan Arheden, MD PhD. ***Lund University Hospital, Lund, Sweden.***

Introduction: An understanding of the relationship between left ventricular ejection fraction (LVEF) and infarct size (IS) is important when assessing the potential benefit of revascularization in patients with ischemic heart disease (IHD).

Purpose: Using cardiac magnetic resonance (CMR) imaging, we sought to explore the relationship between LVEF and IS and to determine a maximum predicted LVEF in relation to IS.

Methods: Reports from 297 patients referred for delayed contrast enhanced CMR were retrospectively reviewed and 156 patients with IHD were identified. LVEF and IS were quantified by manual planimetry at the time of imaging. The maximum predicted LVEF was defined as the linear function delimiting the smallest area encompassing 95% of the data for LVEF vs IS.

Results: For patients with IHD, LVEF and IS had a range of 9–67% and 0–44%, respectively. Patients with a small IS (<10%, $n = 55$) showed a wide range of LVEF (mean 42%, range 9–67%). Patients with a low LVEF (<20%, $n = 27$) showed a wide range of IS (mean 21%, range 3–44%). The maximum predicted LVEF in relation to IS was described by the function $LVEF = 73.1 - [1.21 \times IS]$.

Conclusions: The study population demonstrated a large variation in LVEF in relation to IS over a large range of values. LVEF cannot be used to estimate IS, and vice versa. However, IS can be used to estimate a maximum predicted LVEF and vice versa. Future studies are needed to assess if IS is useful to assess the potential for improvement in LVEF following revascularization.

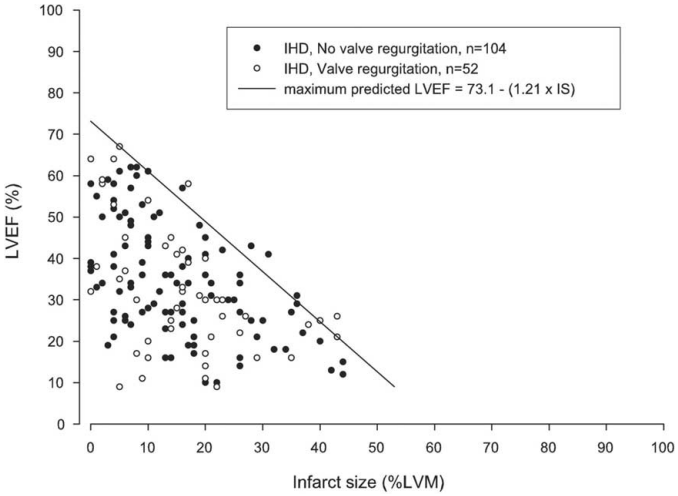

361. AUTOMATED IDENTIFICATION OF MINIMAL MYOCARDIAL MOTION FOR IMPROVED IMAGE QUALITY IN CORONARY MRA AT 3T

Ali O. Ustun, MS,[1] Milind Desai, MD,[2] Matthias Stuber, PhD.[1] [1]***Johns Hopkins University, Baltimore, MD, USA,*** [2]***Cleveland Clinic Heart Center, Cleveland, OH, USA.***

Introduction: For improved motion suppression in coronary MRA, the identification of the period of minimal myocardial motion is very important. Heart rate dependent formulas and visual inspection on cine images have been used for that purpose but these methods are subjective and prone to errors. We hypothesized that a newly developed computer algorithm, FREEZE, for the automatic identification and prescription of the period of minimal myocardial motion, leads to an improved image quality in coronary MRA.

Purpose: The purpose of this study was to test whether the use of FREEZE leads to an improved image quality (when compared to visual inspection) in coronary MRA.

Table 1. Objective and subjective comparision of image quality from coronary MRA obtained with a visually identified (VISUAL) and computer prescribed (FREEZE) trigger delay.

	VISUAL	FREEZE	VISUAL	FREEZE	VISUAL	FREEZE
	Vessel length (mm)		Vessel sharpness (%)		Vessel diameter (mm)	
Mean	65.2	83.1	43.8	46.3	2.9	3
SD	29.3	38.9	5.4	4.8	0.4	0.3
P value	<0.01		<0.02		<0.04	
	SNR(a.u.)		CNR(a.u.)		Visual grading (a.u.)	
Mean	29.5	32	21	23	2.5	3.3
SD	8.6	8.4	6.4	6.3	0.9	0.8
P value	<0.02		<0.04		<0.01	

SD = Standard deviation of the mean.

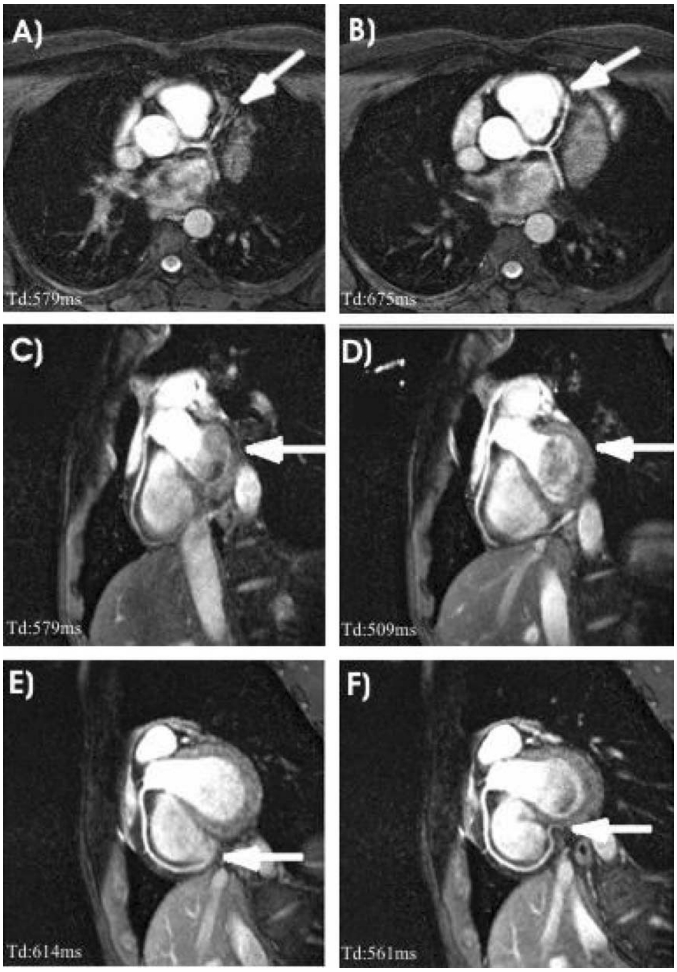

FIG. 1. Improvement in vessel sharpness (A, B), in delineation of the epicardium (C, D) and in vessel length (E, F). The images in the left column were obtained with visual assessment and those in the right column were obtained with FREEZE.

Methods: The image based correlation algorithm, FREEZE, was developed to identify the period of minimal myocardial motion (= trigger delay) on multi-heart phase cine images on a frame-by-frame basis. Preliminary phantom studies demonstrated successful results (1). In the present in-vivo study, 10 healthy adult subjects (9 men, 1 woman; mean age, 25; range, 21–32 years) underwent coronary MRA using a) a visually determined (on cine images) trigger delay (Tdv) and b) a trigger delay that was identified by FREEZE (Tdf). Volume targeted 3D images of the left and right coronary arterial system were acquired on a commercial 3T system (Gyroscan Achieva, Philips Medical Systems, Best, The Netherlands; 80 mT/m, 200 mT/m/ms). After scout scanning, an axial mid-ventricular 2D segmented k-space gradient echo cine sequence (TR = 2.7 ms, TE = 1.4 ms, $\alpha = 25^{\circ}$) with 50 frames/s was acquired to determine the trigger delay for subsequent coronary MRA. For high-resolution coronary MRA, a navigator gated and corrected, double oblique 3D segmented k-space gradient echo imaging sequence (TR = 4.9 ms,TE = 1.7 ms, $\alpha = 20^{o}$, 3 mm slice thickness, 512 matrix, FOV = $36 \times 27\,\text{cm}^2$, 20 slices, fat saturation, T2Prep (TE = 50 ms)) was used. Data were collected at both Tdv and Tdf. Quantitative analysis of the thus obtained coronary MRA was performed using the 'SoapBubble' tool (2) by a blinded reader. Images obtained at Tdv and Tdf were compared for vessel length, vessel sharpness, vessel diameter, signal-to-noise ratio (SNR) and contrast-to-noise ratio (CNR). In addition, a qualitative grading of image quality was performed by two blinded readers using a 1–4 scale (1 = worst, 4 = best) (3).

Results: By the use of the FREEZE prescribed trigger delay Tdf, a significant quantitative and qualitative improvement in image quality was obtained in comparison to images that were obtained using the visually identified trigger delay Tdv (Table 1). In Fig 1 A & B, an improved image quality is readily apparent

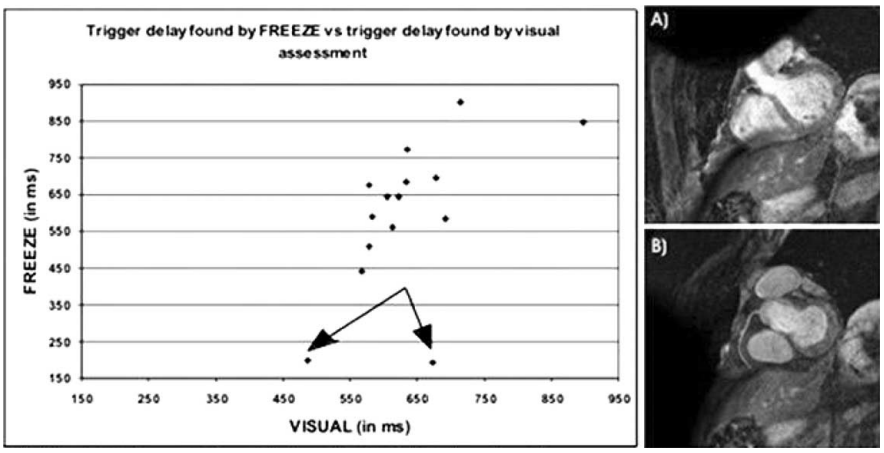

FIG. 2. Left: Trigger delay calculated by FREEZE vs. visual assessment. In two subjects (arrows), FREEZE found end-systolic Td whereas the visual inspection led to a diastolic acquisition interval in the same subjects. A and B: Images obtained in one of these two subjects A) Visual Assessment B) FREEZE.

(B) using Tdf. Similarly, when compared to Fig. 1C, Fig. 1D (that was acquired with FREEZE) shows a sharper delineation of the epicardial contour (arrow). On the right coronary system (RCA) shown in Fig. 1 E & F, the automated identification of the trigger delay led to the visualization of a longer contiguous segment of the RCA. Furthermore, in subjects with high heart-rates, the automated tool found periods of minimal myocardial motion at end-systole (Fig. 2, arrows) leading to better image quality as shown in Fig 2B, while diastolic trigger delays were always identified by visual inspection.

Conclusion: This study demonstrates that an automated algorithm (FREEZE) for the identification of the period of minimal myocardial motion significantly improves objective and subjective image quality in coronary MRA when compared to a more conventional visual inspection of the optimal trigger delay. Periods of minimal myocardial motion can be found objectively and operator dependent variations can be minimized. The use of FREEZE may contribute to an overall improved image quality and reproducibility of coronary MRA in general.

REFERENCES

1. Ustun, et al. *SCMR* 2005;7:194–195.
2. Etinne, et al. *MRM* 2002;48:658–666.
3. McConnel, et al. *AJR* 1997;168:136–175.

362. REAL-TIME SSFP CINE IMAGING FOR REGIONAL WALL MOTION ASSESSMENT IN PATIENTS WITH PERSISTENT CARDIAC ARRHYTHMIA

Okan Ekinci, MD, Baerbel Tiebert, MD, Hans-Peter Tries, MD, Suzan Durmaz, Ulrich Loercher, MD, Heinz Lambertz, MD. ***German Clinic for Diagnostics, Wiesbaden, Germany.***

Background: Cine image acquisition in patients (pts) with cardiac arrhythmia is challenging and necessitates the use of special sequences in order to improve image quality. Sequences with "arrhythmia rejection" are suitable in pts with occasional occurrence of R-R interval irregularities. In pts with high frequency of extrasystoly or persistent atrial fibrillation, though, these sequences do not give satisfying results. We investigated the use of a non-segmented steady state free precession (TrueFISP) cine sequence for real-time image acquisition in comparison to an ECG-gated segmented TrueFISP cine sequence for regional wall motion assessment (RWMA).

Methods: Eighteen pts (13 male, 61 ± 6 y/o) with transthoracic echocardiography (TTE, Siemens Acuson Sequoia) proven wall motion abnormalities and persistent arrhythmia underwent MRI for viability imaging. MRI was performed on a 1.5 T Siemens Avanto Scanner (Siemens, Erlangen, Germany). For cine imaging a retrospectively ECG-gated TrueFISP cine sequence was used in LVOT, 2CV, 4CV and 3 short axis orientations. Additionally, a non-segmented TrueFISP cine sequence for real-time image acquisition was used in the same orientations (SENSE, TR 79 ms, TE 0.9 ms, SLT 10 mm, matrix 66 × 128, FOV typically 260 × 380). For viability imaging, a single-shot phase-sensitive inversion-recovery TrueFISP sequence was used 8–15 min after administration of 0.1 mmol/kg bw Gd-DTPA (Magnevist, Schering, Germany). Images were visually analyzed according to the 17-segment model (AHA). Presence and type of wall motion abnormalities (RWMA) and delayed hyperenhancement (DE) were assessed.

Results: In total, 306 segments of 18 pts were analyzed. By TTE 28 segments (9%) were detected showing RWMA. Mean heart rate was 78 ± 18/min. Segmented TrueFISP cine sequence revealed 24 segments with RWMA. In comparison, RT cine sequence revealed 32 segments with RWMA (8 hypokinesis, 14 akinesis, 10 dyskinesis). Correlation analysis showed moderate correlation between the sequences (R = 0.69). Better correlation was found comparing RT cine sequence results with echo findings (R = 0.82). Viability imaging showed regions with DE in 16 pts. None of the 3 pts with RWMA in TTE but not in RT cine sequence had areas with DE. Blurring artifacts were the main reason, why findings for 16 segments were discordant comparing both MR sequences.

Conclusion: In patients with persistent cardiac arrhythmia non-segmented steady state free precession (TrueFISP) cine sequence for real-time image acquisition allows better assessment of regional function than segmented TrueFISP sequence. Patients with persistent cardiac arrhythmia can undergo cardiac MRI for functional and viability imaging using non-gated sequences. However, further improvement of spatial and temporal resolution is needed.

363. PROSPECTIVE MULTISLICE SHIM CORRECTION FOR SINGLE BREATH-HOLD WHOLE-HEART MRCA

Juan M. Santos,[1] Bob S. Hu,[2] John M. Pauly.[1] [1]***Stanford University, Stanford, CA, USA,*** [2]***Palo Alto Medical Foundation, Palo Alto, CA, USA.***

Introduction: Multi-slice breath-held coronary imaging techniques conventionally lack the coverage of free breathing 3D acquisitions, but use a considerably shorter acquisition window during the cardiac cycle. This produces images with significantly less motion artifact but lower SNR. By using the extra SNR available at 3 Tesla and undersampling k-space without introducing significant aliasing artifacts, we were able to acquire high resolution fat-suppressed images of the whole heart in 17 heart beats, a single breath hold. The basic pulse sequence consists on a spectral-spatial excitation followed by a variable-density spiral readout. Images are reconstructed using gridding, and advanced techniques to reduce aliasing artifacts. Spiral k-space trajectories are sensitive to off-resonance modulation. This can result in severe image blurring. Spectral-spatial excitation is also sensitive to Bo inhomogeneities with a resulting shift in the spectral

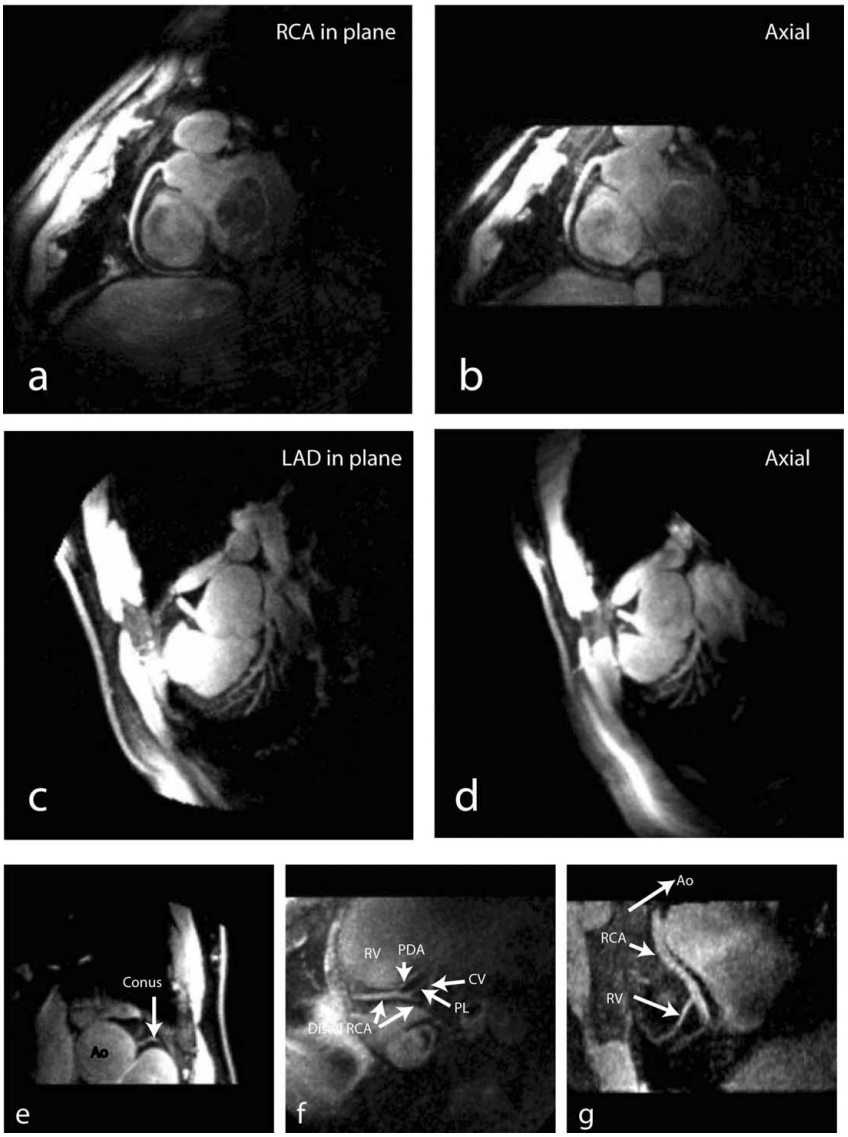

FIG. 1.

selectivity. This can result in sub-optimal fat suppression where in the extreme case, water is suppressed instead of fat. A real-time prospective shim correction was developed to compensate for field variations through the acquisition volume.

Methods: Before each experiment, a high-order volumetric shim calibration was applied over the entire heart. Additionally a dynamic real-time multislice linear shim method was used to individually fine-tune each slice. Two acquisitions per slice, obtained at the beginning of the imaging breath-hold period, were used to calculate a volumetric field map. If each slice is individually corrected, inconsistencies in the through-slice direction can be generated due to abrupt field variations. A compromise exists between obtaining a well-fitted correction for each slice and maintaining a smooth field transition between slices. A global estimate of the first order shim correction is obtained for the whole volume. The center frequency is further corrected individually for each slice. This results on a significant improvement in the off-resonance artifacts maintaining a good transition between slices. To further improve this method, first order correction can be calculated for sub-volumes corresponding to a moving average of consecutive slices. In this manner, a first order correction can be smoothly applied to consecutive slices.

Results: The Fig. shows different images obtained using the proposed correction technique with a resolution of $0.8 \times 0.8 \times 1.6$ mm. The RCA and LAD were acquired with the imaging volume in an in-plane orientation (a, c) as well as an axial orientation (b, d). The images were then reformatted for the same in-plane view. Figure 1 (e, f, g) show details of the conus artery, acute marginal right, posterior left and posterior descending obtained from axial slices reformatting. Consistent fat suppression, smooth field transitions (continuity in axial reformatting) and minimal blurring artifact can be observed.

Conclusions: We have implemented and demonstrated the ability to acquire a whole-heart angiography at 3T in a single breath-hold interval. Because it is essential to minimize the field distortions within the large acquisition volume, we have developed a prospective shim method. The proposed method is able to correct field distortions preserving the continuity between slices.

364. AORTIC DISTENSIBILITY AND DIMENSIONS IN TURNER SYNDROME: BENEFICIAL EFFECTS OF GROWHT HORMONE TREATMENT

Jochem van den Berg, MD,[1] Ellen M. N. Bannink, MD,[1] Piotr A. Wielopolski, PhD,[2] Peter M. T. Pattynama, MD, PhD,[2] Sabine M. P. F. de Muinck Keizer-Schrama, MD, PhD,[1] Willem A. Helbing, MD, PhD[1] [1]***Erasmus MC - Sophia Children's Hospital, Rotterdam, The Netherlands,*** [2]***Erasmus MC, Rotterdam, The Netherlands.***

Introduction: In Turner Syndrome (TS) an increased risk for cardiovascular malformations exists, including aortic dilation of unknown etiology. Abnormal biophysical wall properties may play an important role. MRI has successfully been used to assess aortic size and wall distensibility.

Purpose: Aim of this study was to assess aortic biophysical properties and dimensions in Turner syndrome.

Methods: We enrolled 38 former participants of our growth hormone (GH) dose-response study in TS (age 19.9 ± 2.1, BSA 1.74 ± 0.16), and 27 controls (age 20.6 ± 1.6, BSA 1.80 ± 0.13). Previously patients had been assigned to 1 of 3 groups, treated with different GH-dosages: group A-0.045, B-0.067 and C-0.09 mg/kg/d. All underwent MRI at least 6 months after GH discontinuation to determine aortic dimensions and distensibility at four predefined levels: 1. ascending aorta, 2. descending aorta, 3. level of the diaphragm, 4. abdominal aorta.

Results: Patients had larger aortic diameters at all but level 4, and lower distensibility at levels 1 and 3. Distensibility in group A was significantly lower compared to group C at levels 3 and 4. Compared to controls group A had larger aortic diameters at all but level 4, and lower distensibility at levels 1, 3 and 4. Distensibility results in groups B and C were not different from those in controls.

Conclusions: Patients with TS, formerly treated with GH, have a dilated aorta and signs of impaired wall distensibility.

Aortic distensibility (10^{-3} * mm Hg^{-1})

	Level 1	Level 2	Level 3	Level 4
Controls	5.3 ± 1.2	5.2 ± 1.2	7.5 ± 2.2	8.4 ± 2.2
Total patients	4.7 ± 2.3*	5.7 ± 2.4	6.4 ± 1.9*	7.3 ± 2.5
Group A	4.1 ± 1.7*	5.0 ± 2.3	5.4 ± 2.0*	5.8 ± 2.4*
Group B	4.7 ± 2.5	5.9 ± 2.4	6.5 ± 1.5	8.1 ± 2.4
Group C	5.5 ± 2.7	6.3 ± 2.6	7.4 ± 1.7†	8.6 ± 1.9†

*Statistically significant difference ($p < 0.05$) compared to controls.
†Statistically significant difference ($p < 0.05$) compared to group A.

Aortic diameters (mm/m^2)

	Level 1	Level 2	Level 3	Level 4
Controls	15.2 ± 1.2	10.9 ± 1.2	9.6 ± 0.7	8.5 ± 0.6
Total patients	17.6 ± 2.6*	11.8 ± 1.9*	10.4 ± 1.2*	8.7 ± 0.9
Group A	17.4 ± 2.0*	12.8 ± 2.2*	11.2 ± 1.4*	9.1 ± 1.0
Group B	18.2 ± 3.3*	10.9 ± 1.6	9.8 ± 0.6	8.5 ± 0.7
Group C	16.5 ± 1.6*	11.7 ± 1.4	10.3 ± 1.0	8.6 ± 1.0

*Statistically significant difference compared to controls ($p < 0.05$).

FIG. 1.

Severity of abnormalities seems related to GH dose, with a beneficial effect of a higher GH dose on the abnormalities.

365. A 32 CHANNEL ARRAY FOR OPTIMIZED CARDIAC PARALLEL IMAGING AT 1.5T

Titus Lanz, PhD,[1] Mathias Nittka, PhD,[2] Mark Griswold, PhD,[3] [1]***Rapid Biomedical, Rimpar, Germany,*** [2]***Siemens Medical Solutions, Erlangen, Germany,*** [3]***Department of Physics, University of Wuerzburg, Wuerzburg, Germany.***

Introduction: Parallel imaging has been shown to be an elegant solution to the problem of cardiac and respiratory motion. One significant limitation of parallel imaging is the number of receiver coils available for acceleration. In addition, heart patients are often obese, which demands very thin and flexible RF coils. In this abstract, we propose a highly flexible 32 channel array especially adapted to the needs of cardiac imaging at 1.5T.

Methods: The array coil consists of an anterior and a posterior array. Each of them has 16 receive-only coil elements which are arranged on the surface (Fig. 1). The elements are equal in shape (hexagon) and size (diameter 100.5 mm/116.0 mm). The total extent of the array is 40 cm × 50 cm. The coil elements are arranged in such a way that the head end of the coil is less broad and, thus, does not interfere with the arms of the patient. The posterior, rigid part is flat, while the anterior part can be

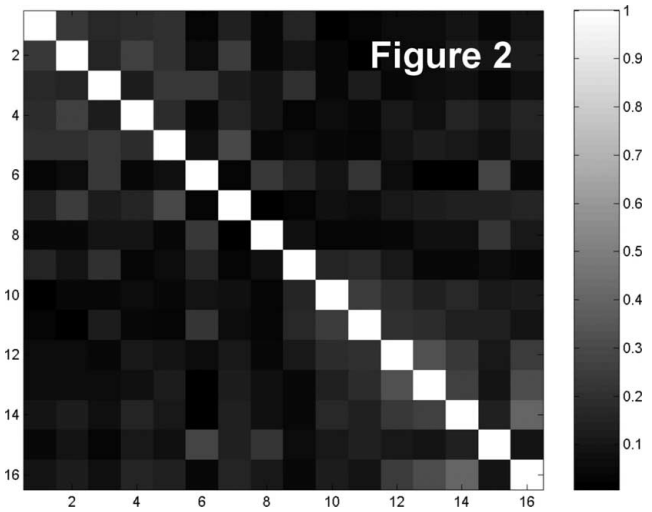

FIG. 2.

curved in a flexible housing. For compactness, the preamplifiers are directly positioned in the middle of each coil element. This results in a total coil thickness of 3 cm. The decoupling of the elements is done by both actively and passively switched trap circuits, one for each coil element. Additional fuses are also integrated into the coil as an additional safety mechanism. The coil was characterized on a Siemens Avanto system with a field strength of 1.5 T and 32 receive channels.

Results: The decoupling of each pair of elements was better than 20 dB. The noise correlation of the coil elements of one array half is shown in Fig. 2. When the self correlation on the diagonal is normalized to be 1, the highest cross correlation

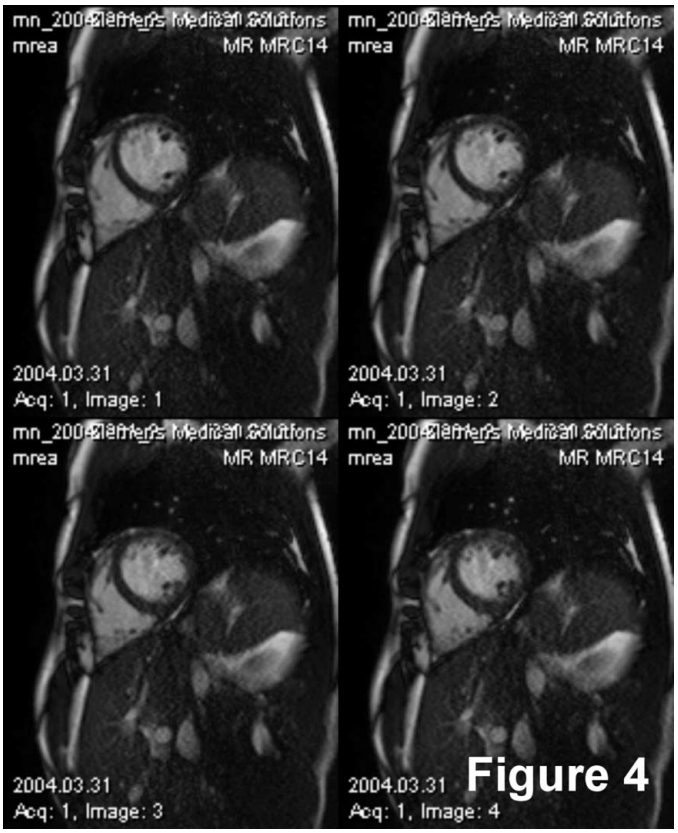

FIG. 4.

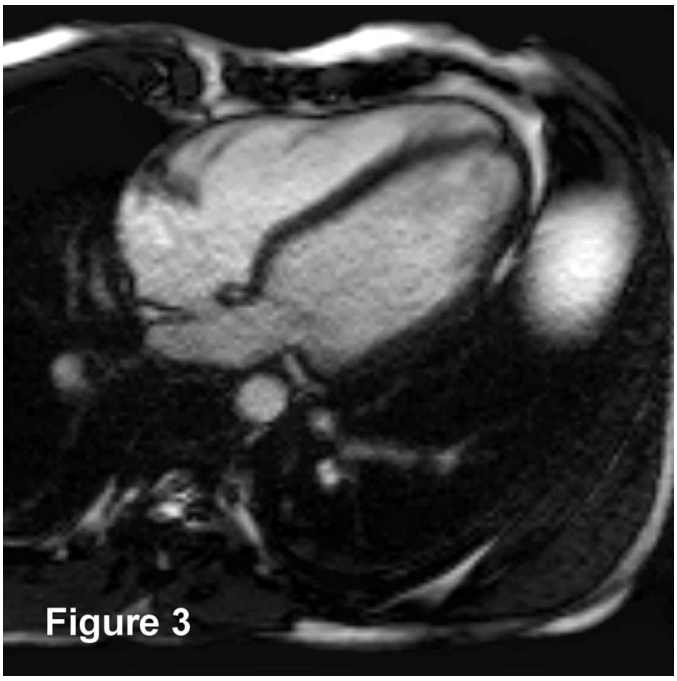

FIG. 3.

FIG. 5.

between any two elements is 0.4. Most pairs of elements show a noise correlation far below this level. To show imaging properties of the coil, various types of imaging was performed. Figure 3 shows one frame of a TrueFISP cine image of the heart (long axis) with an acceleration factor of four. 21 phases were acquired in a 3 s breath hold. Fig. 4 shows the same in a short axis view, except four slices were acquired in a 10 s breath hold. Figure 5 is a single shot HASTE image with a 5x GRAPPA reconstruction which shows the utility of the coil for abdominal imaging as well.

Conclusions: A 32 channel cardiac array for 1.5T was presented which can be used for clinical investigation of the heart. Standard acceleration factors of four are possible for 2D imaging in all directions, while factors of 12 are possible for 3D imaging. In particular, high accelerations in the anterior-posterior direction are possible. These high acceleration factors result in significantly reduced acquisition times and, thus, shorten the breath hold time for patients and potentially allow real-time imaging to be used in standard clinical settings. A prototype version of this array has already demonstrated up to factor of 7 accelerations in vivo with excellent results (3).

Acknowledgement: We want to thank Stefan Kannengießer, Siemens Erlangen for his valuable contribution to this work.

REFERENCES

1. Pruessmann K, et al. *SENSE, MRM* 1999;42:952–962.
2. Griswold M, et al. *GRAPPA, MRM* 2002;47:1202–1210.
3. Reeder S, et al. *MRM* 2004;54:748–754.

366. FIRST PASS CONTRAST-ENHANCED CALF MUSCLE PERFUSION AT PEAK EXERCISE: A METHOD TO IDENTIFY PERIPHERAL ARTERIAL DISEASE

David C. Isbell, MD, Frederick H. Epstein, PhD, Arthur Weltman, PhD, Walter J. Rogers, PhD, Stuart S. Berr, PhD, Craig H. Meyer, PhD, Douglas E. Lake, PhD, Klaus D. Hagspiel, MD, Nancy L. Harthun, MD, Christopher M. Kramer, MD. ***University of Virginia, Charlottesville, VA, USA.***

Introduction: Hypoperfusion of the lower limbs is the hallmark of peripheral arterial disease, a condition that currently affects between 10 and 12 million in the U.S. As a consequence of insufficient tissue perfusion, PAD patients can experience exertional limb pain, reduced exercise capacity, and tissue loss. Improving blood flow is a major therapeutic goal in PAD. A noninvasive technique capable of measuring tissue perfusion would be of great clinical value in PAD for diagnosis, assessing severity, and monitoring response to novel therapeutic interventions designed to enhance skeletal muscle perfusion.

Methods: Eleven patients (age 61 ± 11 yrs) with mild to moderate symptomatic PAD (ankle-brachial index 0.75 ± 0.08) and 22 normal control subjects were studied. All PAD and 11 NL (NL_{max}) (age 46 ± 10 yrs; p = 0.003 vs. PAD) exercised one leg to exhaustion while supine in a 1.5T MRI scanner using

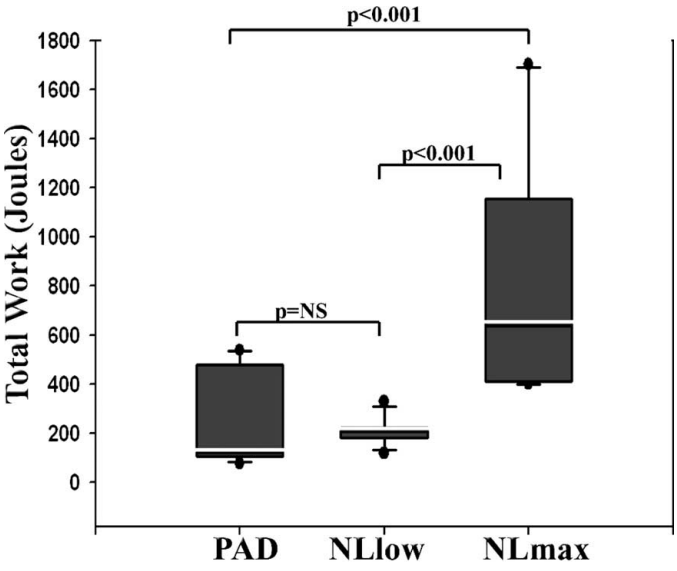

a custom-built mechanical plantarflexion ergometer. An additional 11 normal subjects (NL_{low}) (age 52 ± 6; p = NS vs. PAD) were instructed to exercise to a workload similar to that achieved by the PAD subjects. Gadolinium DTPA at 0.1 mmoL/Kg was infused at 4 mL/sec through a peripheral IV immediately after the cessation of exercise. A gradient echo pulse sequence was modified to accomodate the simultaneous acquisition of muscle perfusion in a distal imaging plane and the arterial input function (AIF) in a proximal plane. Inversion-recovery (TI = 320 ms) was used for muscle imaging and saturation-recovery (TI = 10 ms) was used to image the AIF. This approach was employed to maximize sensitivity to contrast-enhancement in the muscle while avoiding saturation of the AIF signal. Other parameters included FOV 180 × 180, matrix = 64 × 64, flip angle 15 degrees, TR 423, TE 1.86, acquisitions 100, and number of slices = 2. Time intensity curves (TIC) were generated for regions of interest drawn in calf muscle and the input artery. A perfusion index (PI) was defined as slope of the tissue TIC divided by slope of the AIF.

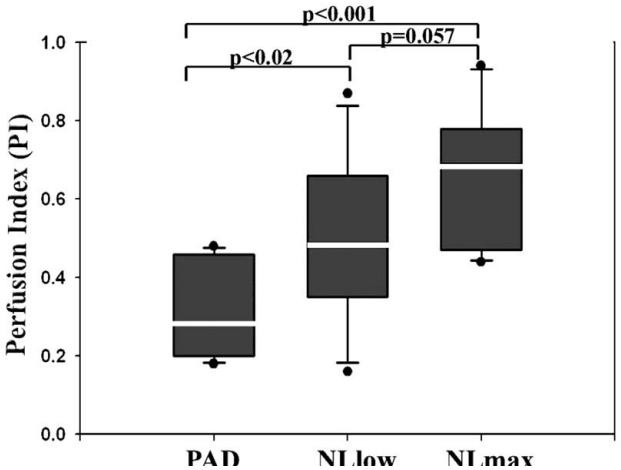

Results: Median work performed was 120 Joules in PAD (25th and 75th percentiles = 100 and 418), 210 Joules in NL_{low}(25th and 75th percentiles = 185 and 221; p = NS vs. PAD), and 698 Joules in NL_{max}(25th and 75th percentiles = 427 and 1425; $p < 0.001$ vs. both Nl_{low} and PAD) (Fig. 1). PI was 0.29 in PAD (25th and 75th percentiles = 0.20 and 0.40), 0.48 in Nllow (25th and 75th percentiles = 0.36 and 0.62; $p < 0.02$ vs. PAD), and 0.69 in Nlmax (25th and 75th percentiles = 0.51and 0.77; $p < 0.001$ vs. PAD). PI compared between the three groups is shown in Fig. 2.

Conclusions: Post-exercise measurement of lower limb perfusion employing a dual-contrast, first-pass gadolinium enhanced MR technique distinguishes mild to moderate PAD from normals. While differences in perfusion are greatest between PAD and normals who acheive their maximal workload potential (NLmax), tissue perfusion remains a discriminating parameter when the workload acheived is similar between PAD and normals (NLlow). This semiquantitative measure of muscle perfusion during physiologic stress may be useful in assessing the severity of PAD and evaluating the impact of novel PAD therapies on end-organ perfusion.

367. MYOCARDIAL T2 MAPPING WITH HIGH SPATIAL RESOLUTION: VALIDATION IN PHANTOMS AND IN HEALTHY VOLUNTEERS

Mirko Fröhlich, MD,[1] Daniel R. Messroghli, MD,[1] Andreas Greiser,[2] Rainer Dietz, MD,[1] Jeanette Schulz-Menger, MD.[1] [1]***Franz-Volhard-Klinik, Charité Campus Buch, Universitätsmedizin Berlin, Helios-Kliniken, Berlin, Germany,*** [2]***Siemens AG Medical Solutions, Erlangen, Germany.***

Background: It has been shown that T2-weighted pulse sequences (eg, short TI inversion recovery, STIR) can be used as a clinical tool to detect myocardial diseaseinjury. We aimed to establish a T2 mapping technique with high spatial resolution in order to assess T2 changes quantitatively.

Methods: T2 mapping was performed using ECG-gated breathhold turbo spin echo pulse sequences (turbo factor 15, field of view 340 mm, matrix 106 × 192) with different TEs (6.5, 39, 46, 52, 59, 65, and 958 ms) on a 1.5T MR system (Magnetom Sonata, Siemens AG Medical SolutionsSiemens AG, Erlangen, Germany). In order to assess T2 accuracy in-vitro, eight Gadolinium-doped agarose gel phantoms with nominal T2 times from 61 to 233 ms (as assessed by a non-gated reference spin-echo technique) were studied at simulated heart rates from 50–100 per minute. In order to optimize T2 accuracy, we furthermore used different numbers of trigger pulses intervals (two, three, and four) and tested the results of those measurements for correlation with reference T2 values. Quantitative T2 maps were computed using an in-house software program allowing manual registration in case of lateral spatial displacement (implemented in IDL 6.1, RSI, Boulder CO, USA). Using the same pulse sequence and post-processing technique, quantitative T2 maps were acquired in mid-cavity short-axis views of 15 healthy subjects (9 men, mean age 24 ± 4 years). All T2 maps were analyzed using a commercial image analysis software package (Mass 5.0, Medis, Leiden, Netherlands).

Results: In the phantoms, the ECG-gated pulse sequence yielded good correlations with reference values over the full range of T2 values studied. There was significant heart-rate dependency, but not within a range of T2 values from 60 to 120 ms. Although there was a significant difference between reference and actually measured T2 times (mean difference = 25.1, t = 5, 39 $p < 0.01$), there were very good correlations between reference and measured T2 values. Best correlation with reference T2 values was achieved by using two trigger pulses intervals (r = 0.995, 95%CI = 0.982–0.999). In-vivo, our approach resulted in T2 maps of good image quality allowing clear delineation of myocardial borders in all cases. Median myocardial T2 was 72 ms, 71 ms, 25th and 75th percentile were 65, 64, and 81 ms 80 ms, so that reference values (3rd to 97th percentile) of 53, 51, 103 ms 99 ms could be deducted.

Conclusion: High-resolution turbo spin-echo pulse sequences can be used to create T2 maps of the myocardium with good image quality and high T2 accuracy. T2 mapping is a promising tool for the quantitative assessment of myocardial diseases without the need for contrast agent. Clinical evaluation of this method is currently being performed in patients with acute myocarditis.

368. TIMING THE DEVELOPMENT OF LEFT VENTRICULAR ABNORMALITIES IN CHRONIC KIDNEY DISEASE—WHEN TO START TREATMENT

Nicola C. Edwards. ***University Hospital Birmingham & University of Birmingham, Birmingham, United Kingdom.***

Background: Premature cardiovascular disease (CVD) is the leading cause of mortality in End-Stage Renal disease (ESRD) accounting for approximately 60% of deaths. Left ventricular (LV) abnormalities are seen in 80% of patients with ESRD at initiation of renal replacement therapy (RRT) and late gadolinium enhancement (LGE) indicative of uraemic cardiomyopathy (fibrosis or infarction) has been documented in 29% of dialysis patients. CV risk increases significantly as glomerular filtration (GFR) declines (particularly below 81 mL/min), yet there is no prospective data regarding onset of LV abnormalities or LGE in milder forms of CKD despite this cohort out-numbering ESRD by 10 times.

Method: Fifteen patients (median age 50 years [range 35–73]; males 73%) with mild-moderate CKD (GFR 30–80 mL/min calculated by the Cockroft-Gault formula) secondary to non-diabetic renal disease and no prior CV history were prospectively studied. All underwent cardiac magnetic resonance imaging (CMR) on a 1.5T scanner (Siemens Sonata Symphony). Serial

contiguous short axis (SA) cines were piloted from VLA/HLA of the RV and LV (ECG-gated, True-FISP; TR 45 ms, TE 1.7 ms, FA60°, slice thickness 7 mm). These slices were repeated 10–15 minutes after intravenous injection of 0.2 mmol/kg gadolinium-DTPA (Magnevist™) with serial contiguous SA segmented inversion recovery T1 weighted cines (TR 800 ms, TR 1.4 ms, TI 200–240 ms, slice thickness 7 mm, fat saturation band across the spine) to detect LGE.

Results: Ten (67%) patients had mild CKD (GFR 60–80 mL/min) and 5 (33%) moderate CKD (GFR 59–30 mL/min). All had 12 lead electrocardiograms within normal limits with no evidence of voltage criteria indicative of LV hypertrophy. Mean 24 hr ambulatory BP was 124/76 (range systolic 112–138, diastolic 61–85). All data was indexed to body surface area (BSA g/m^2). LV mass index (LVMI) was increased in 5 patients (33%), 3 (60%) with mild CKD and 2 (40%) with moderate CKD. Mean LVMI in males with LVH 89.3 g/m^2 (range 88.2–98.5) and female with LVH 71.5 g/m^2. Ventricular dimensions and function were within limits previously reported for the general population. Male End Diastolic Volume (EDV) 64.5 mL/m^2 (50.2–75.9). Female EDV 64.1 mL/m^2 (54.7–77.1). Male LV Ejection Fraction (LVEF) 72% (66–81). Female LVEF 70% (60–77). Male Right Ventricular (RV) EDV 75.6 mL/m^2 (70–86.1). Female RV EDV 72.7 ml/m^2 (65.9–79.9). Male RVEF 63% (62–73). Female RVEF 61% (57–68). None of the patients had evidence of discrete or diffuse subendocardial or mid wall LGE.

Conclusion: LV mass was increased in one third of patients with mild-moderate CKD despite excellent blood pressure control suggesting that LV hypertrophy occurs early in the course of CKD and that there are stimuli to LVH in CKD other than hypertension. The lack of LGE in this cohort suggests that unlike LVH, myocardial fibrosis/infarction may be a late manifestation of CKD related to disease severity and duration. Further studies are required to define the time of onset of LV abnormalities to ensure targeted primary prevention therapies.

369. REPRODUCIBILITY AND RELIABILITY OF HIGH VOLUME ATHEROSCLEROTIC PLAQUE IMAGING IN PERIPHERAL ARTERIAL DISEASE: IMPLICATIONS FOR CLINICAL TRIALS

David C. Isbell, MD, Craig H. Meyer, PhD, Walter J. Rogers, PhD, Frederick H. Epstein, PhD, Stuart S. Berr, MD, Klaus D. Hagspiel, MD, Nancy J. Harthun, MD, Christopher M. Kramer, MD. ***University of Virginia, Charlottesville, VA, USA.***

Introduction: In patients with cardiovascular disease, a direct relationship between atherosclerotic plaque progression and cardiovascular events has been defined. Thus, serial measurement of plaque volume in the vessel wall is increasingly being used as a surrogate end-point in clinical trials of novel therapies for atherosclerosis. CMR has become an important noninvasive alternative to invasive assessment of atherosclerotic plaque volume (APV) with intravascular ultrasound. Peripheral arterial disease (PAD) is a common atherosclerotic condition of the lower limbs. We hypothesized that CMR measurement of APV in the superficial femoral artery (SFA) in PAD would significantly minimize sample sizes needed for trials evaluating serial change in plaque volume.

Sample size estimates

%ΔAPV	Sample size
1	424
2	106
5	19
7	11
10	7

Methods: Fifteen patients (age 61 ± 9 yrs) with mild to moderate PAD (ankle brachial index 0.72 ± 0.11) were studied in a 1.5T Siemens scanner. A custom-built flexible, linear four-element surface coil array (Nova Medical, Wilmington, MA) was placed over the thigh and SFA. A multi-slice spin-echo-train pulse sequence with fat presaturation was used. Flowing blood was suppressed using presaturation, with a combination

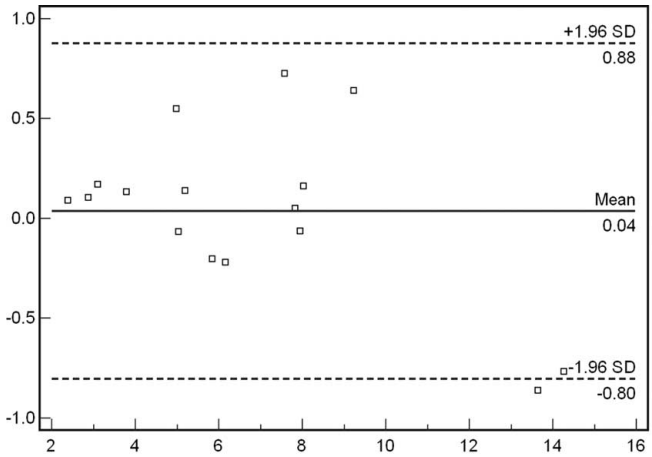

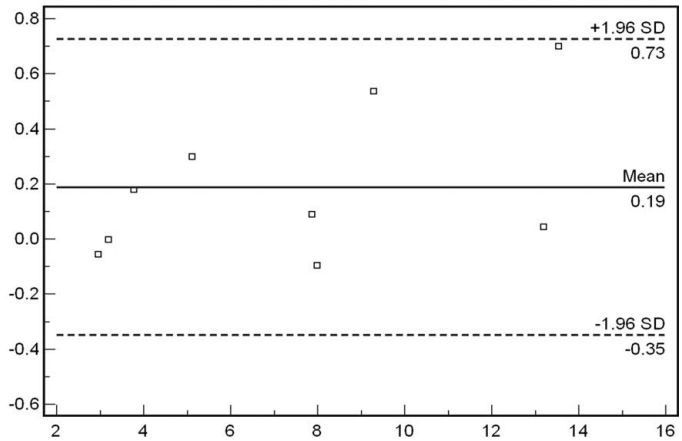

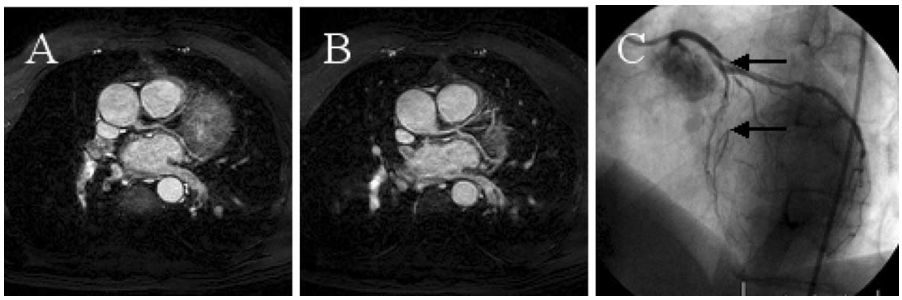

of periodic excitation of upstream slices and spatial presaturation pulses. Other imaging parameters included: TR 715 ms, TE 7.6 ms, voxel size 0.5 × 0.5 × 3 mm, and 4 signal averages. APV of SFA was contoured by two independent operators with VesselMASS software (University of Leiden, NL). Both inter- and intra-observer variability were determined by Bland-Altman analysis on all studies. Nine patients returned (at a mean of 45 days after initial imaging) for evaluation of test-retest reliability using anatomic landmarks and matched number of acquired slices. Sample size calculations for future clinical trials were made using the test-retest reliability data, a paired t-test, and power of 0.80 and alpha 0.05.

Results: Sixteen SFA vessels in 15 patients were studied (mean length 16.7 ± 5.5 cm) with total image acquisition time of 12.8 ± 2.9 minutes per vessel. Mean APV on initial exam was 6.26 ± 3.36 cm^3. Interobserver variability was low with mean bias of 0.04 cm^3 (precision 0.82 cm^3) (Fig. 1). A single operator performed repeat analysis of the 16 vessel segments at a mean of 22 ± 16 days. Intraobserver bias was 0.01 cm^3 (precision 0.50 cm^3). Bland-Altman analysis of test-retest reliability (n = 9) is shown in Fig. 2. Sample size estimates based on the expected standard deviation of 0.49 cm^3 are shown in Table 1.

Conclusion: High resolution, high volume CMR measurement of atherosclerotic plaque volume in the superficial femoral artery in peripheral arterial disease is feasible, rapid, and highly reliable and reproducible. This noninvasive approach could minimize required sample sizes for clinical studies using atherosclerotic plaque progression/regression as an endpoint.

370. MR CORONARY ANGIOGRAPHY BEFORE AND AFTER ADENOSINE STRESS FIRST PASS PERFUSION

Christoph Klein,[1] Tarinee Tangcharoen,[1] Cosima Jahnke,[1] Bernhard Schnackenburg,[2] Eckart Fleck, Prof.,[1] Eike Nagel, PD.[1] [1]***German Heart Institute Berlin, Berlin, Germany,*** [2]***Philips Medical Systems, Hamburg, Germany.***

Introduction: MR coronary angiography (MRCA) is feasible and yields first useful clinical results for the detection of coronary artery disease (CAD). In addition to morphological information MR offers functional information on hemodynamic relevance of CAD, eg, by adenosine stress perfusion. Since there is a waiting period between stress and rest perfusion it could safe time to perform coronary angiography immediately after the application of adenosine and the first pass contrast agent bolus. It is not know, whether this might impair MRCA image quality.

Purpose: Aim of the study was to compare image quality and diagnostic accuracy of standard MRCA before and after adenosine stress perfusion.

Methods: In 27 patients with suspected CAD scheduled for adenosine stress perfusion (0.05 mmol/kg bw Gd-BOPTA) MRCA (SSFP turbo-gradient, SENSE factor 1.7, spatial resolution 0.7 × 0.7 × .0.9 mm, T2 prep, fat suppression, TE/TR/FA 2.3/4.6/100°) was performed before and after the perfusion study. Heart rate had to return to baseline before post contrast MRCA was started. Trigger delay and acquisition duration per heart beat were adjusted to individual diastolic coronary rest period for each MRCA. Image quality was assessed by signal and contrast to noise ratio (SNR/CNR) of the proximal coronaries and vessel length. Stenosis >50% in invasive angiography was considered significant.

Results: Prevalence of CAD was 52%. 15% (4/27) MRCA before and 19% (5/27) after stress perfusion had non diagnostic image quality. Table 1 shows SNR/CNR and vessel length (all not significant), as well as sensitivity and specificity of both tests. Similar to intravascular contrast agents, Gd-BOPTA enhances venous blood, due to inadequate suppression by the T2 prepulse. Figure 1 shows A. MRCA before and B. after stress perfusion. C shows the invasive study. Please note the proximal occlusion of the left anterior descending with retrograde filling of the distal part. MRCA after perfusion has similar image quality with better delineation of the first diagonal branch (stenotic). However, compared with A. the great cardiac vein is enhanced in B.

Conclusion: Image quality of MR coronary angiography is similar, but diagnostic accuracy is increased due to the increased specificity after adenosine stress perfusion. Thus, angiography can be placed after stress perfusion. Drawback is the enhancement of cardiac veins. A larger study population needs to confirm these diagnostic results.

Image quality and diagnostic accuracy of MRCA

	SNR blood	CNR LAD	CNR RCA	Length LAD	Length RCA	Sensitivity	Specificity
Before perfusion	74 ± 15	28 ± 6	15 ± 9	65 ± 21	121 ± 19	92%	45%
After perfusion	89 ± 21	29 ± 9	19 ± 13	68 ± 21	129 ± 21	91%	72%

371. AUTOMATIC PASSIVE CATHETER TRACKING USING REAL-TIME 3D IMAGING—A FEASIBILITY STUDY

Redha Boubertakh, PhD MSc BSc,[1] Nicholas M. I. Noble, PhD MEng,[2] Vivek Muthurangu, BSc MBCHB (Hons),[1] Richard Winkelmann, MSc,[3] Peter Börnert, PhD MSc BSc,[4] Derek L. G. Hill, PhD MSc BSc,[2] Reza S. Razavi.[1] [1]***King's College London, London, United Kingdom,*** [2]***University College London, London, United Kingdom,*** [3]***University of Karlsruhe, Karlsruhe, Germany,*** [4]***Philips Medical Systems, Hamburg, Germany.***

Introduction: Passive catheter visualization in MR guided cardiac catheterization is limited by ambiguity in catheter identification as well as the need for manual tracking. In this paper,

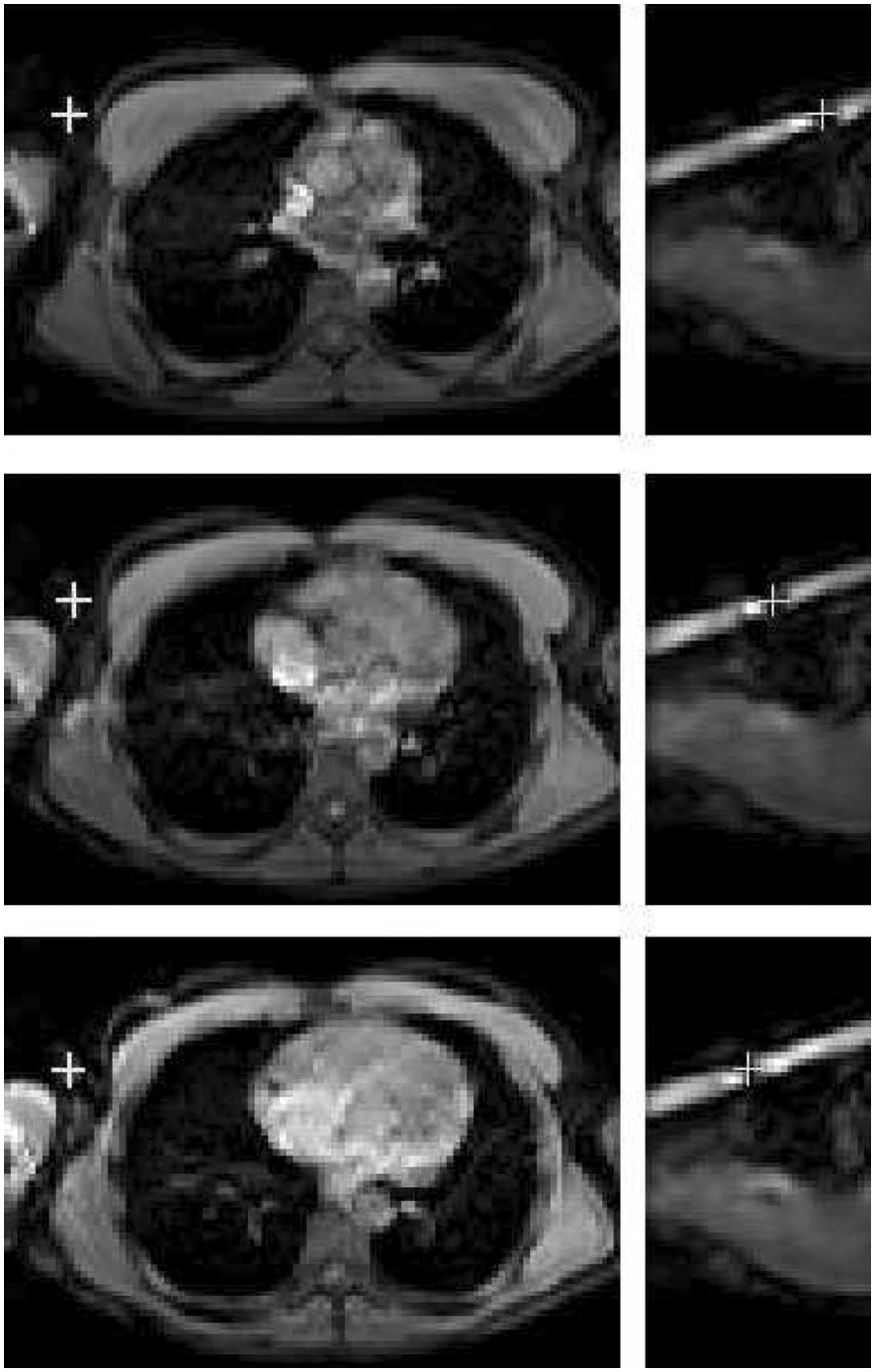

FIG. 1. Sagittal and transverse anatomical views during catheter manipulation.

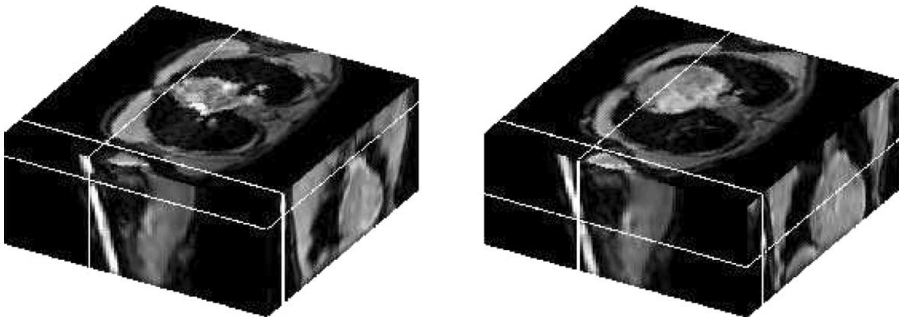

FIG. 2. Volume localization of the catheter tip in three orthogonal reformatted slices at two consecutive time frames.

we present a technique for passive tracking of standard balloon angiographic catheters using real-time volumetric MR imaging on a 32 channel scanner. Prior to catheter insertion, real-time 3D reference volumes are acquired, sampling the cardio-respiratory space. After catheter insertion, the location of the tip of the catheter can be automatically identified in real-time interventional volumes by: 1) calculating difference images by subtracting the current interventional volume from the reference data set, 2) finding the closest reference volume using a similarity measure metric, 3) localizing the catheter in 3D from the selected difference image using simple image analysis operators. Applied to a healthy volunteer with a vessel phantom, this technique was able to track the 3D location of the catheter tip in the presence of both cardiac and respiratory motion.

Methods: A healthy male volunteer was imaged on a 1.5T Philips Achieva equipped with 32 independent receive channels and using a custom built 32 channel coil. A flexible plastic tube, filled with manganese chloride solution, was attached to the volunteer's chest. A reference data set, consisting of 1000 free-breathing 3D whole-heart volumes, was acquired over 4 minutes prior to catheter insertion. Each volume was acquired in 213 ms, a temporal resolution of over four volumes per second. A single shot TFE-EPI sequence was used (FOV $360 \times 255 \times 131$ mm^3, TR 15.2 ms TE 7.5 ms, flip angle 15°) in combination with 2D-SENSE (factors of 3×2) and half-Fourier sampling, reconstructed to $3.75 \times 3.75 \times 3.75$ mm. To simulate catheter manipulation, a balloon angiographic catheter was then introduced in the tube and the balloon inflated. The catheter was maneuvered along the tube whilst an interventional data set consisting of 50 free-breathing volumes was acquired. Subsequent image analysis was performed off-line. For each interventional volume, the closest reference volume was determined. This was achieved by subtracting each reference volume in turn from the interventional volume, and selecting the reference volume with the minimum sum of squares residual in the difference image. The balloon's signal void was localized within the subtracted volume by automatic thresholding. The 3D centroid of this thresholded region localized the catheter tip. For each frame in the dynamic sequence, the automatically identified location of the catheter tip was overlaid as a cross-hair on a reformatted slice passing through the tip.

Results: Figure 1 shows transverse and sagittal slices during catheter manipulation. The tip of the catheter, displayed as a cross-hair, can be clearly seen as it is progressing inside the tube. Figure 2 illustrates the three-dimensional nature of the technique: the tip of the catheter has been successfully localized and tracked as shown in the three orthogonal views.

Conclusions: We demonstrated the feasibility of an adaptive subtraction technique that allows safe and automated 3D catheter tip tracking. This technique relies on fast real-time acquisition of 3D data using high SENSE factors. The cine frames and movies of the automatically identified catheter location and corresponding anatomy clearly highlight the technique's ability to track the catheter tip's trajectory in 3D. The main obstacle to be surmounted before this technique could be applied to real-time tracking in patients is the substantial acceleration of image reconstruction so that the image can be made available in the scanner room with a low latency. We have however provided proof-of-concept that this techniques can be used for passive tracking in the presence of cardio-respiratory motion.

372. CARDIAC MAGNETIC RESONANCE CHARACTERIZATION OF THALASSEMIA INTERMEDIA PATIENTS CONFRONTED WITH THALASSEMIA MAJOR PATIENTS

Alessia Pepe,[1] Eliana Cracolici,[2] Vincenzo Positano,[1] Giovanni Aquaro,[1] Brunella Favilli,[1] Paolo Cianciulli,[3] Aldo Filosa,[4] Luciano Prossomariti,[4] Gianluca Forni,[5] Carmen Lo Pinto,[6] Aurelio Maggio,[7] Massimo Midiri,[2] Massimo Lombardi.[1] ***[1]MR Lab, Institute of Clinical Physiology, CNR, Pisa, Italy, [2]Department of Radiology, University of Palermo, Palermo, Italy, [3]S. Eugenio Hospital, Roma, Italy, [4]Cardarelli Hospital, Napoli, Italy, [5]Galliera Hospital, Genova, Italy, [6]Villa Sofia Hospital, Palermo, Italy, [7]V. Cervello Hospital, Palermo, Italy.***

Introduction: Thalassemia is the most common genetic disorder worldwide and heart disease represents the main determinant of survival. Thalassemia intermedia (TI) is a moderate form. However, it is reasonable to expect a cardiac involvement in

Table 1. Comparison of MRI findings between TI and TM patients

	TI patients (n = 31)	TM patients (n = 70)	*P*
LV EF (%)	65 ± 6	63 ± 5	0.05
Left end-diastolic volume index (mL/m^2)	87 ± 19	75 ± 16	0.002
Left Ventricular stroke volume (mL/m^2)	55 ± 11	47 ± 10	0.0001
Left Ventricular Mass Index (g/m^2)	76 ± 12	69 ± 12	0.008
Left atrial area (cm^2)	24 ± 6	20 ± 5	0.001
RV EF (%)	65 ± 6	62 ± 7	0.02
Right end-diastolic volume index (mL/m^2)	77 ± 19	66 ± 17	0.005
Right Ventricular stroke volume (mL/m^2)	50 ± 12	41 ± 9	0.001
Right atrial area (cm^2)	22 ± 5	19 ± 4	0.01

TI patients due to chronic anemia, resulting in a high cardiac output state; and iron overload, mainly related to the increased gastro-intestinal iron absorption. Little is known about cardiac involvement in TI, in particularly using cardiac magnetic resonance (CMR).

Purpose: Aim of our study was to investigate myocardial and liver iron overload, myocardial fibrosis, atrial dimensions and biventricular function parameters in TI patients and to compare the obtained data with that of thalassemia major (TM) patients, using CMR.

Methods: Thirty-one TI and 70 TM patients were studied using 1.5 T scanner (GE, USA). To evaluate myocardial iron overload, T2* multiecho sequences on three short axis views of left ventricle were obtained and analyzed using custom-written software. The myocardium was automatically segmented into 16 segments and T2* value on each segment as well as the global T2* value were calculated. Liver iron overload was evaluated using T2* multiecho sequences. Myocardial fibrosis was determined by late gadolinium-enhanced sequences. Cine dynamic images (SSFP) were also obtained to evaluate atrial areas and biventricular function parameters quantitatively.

Results: TI patients were significantly older than the TM patients (39 ± 13 yrs vs 27 ± 8; $P = 0.0001$). Mean serum ferritin concentrations and mean Hb-levels were significantly lower in the TI patients vs the TM patients (875 ± 611 ng/mL vs 1846 ± 1562 ng/mL; $P = 0.0001$ and 9.1 ± 0.9 g/dL vs 9.7 ± 0.6 g/dL; $P = 0.002$, respectively). Myocardial iron overload was present in 7(23%) TI patients and the heterogeneous pattern of distribution (segments with T2* >20 ms and segments with T2* <20 ms) was the most frequent (86%). The myocardial iron overload was significantly lower in TI patients: we detected T2* global values and segments' number with normal T2* value significantly higher (36 ± 8 ms vs 24 ± 12; $P = 0.0001$ and 10 ± 3 vs 7 ± 5; $P = 0.0001$, respectively) Severe liver iron overload was found in 18(58%) TI patients. There were no significant differences in liver iron overload between the TI vs the TM patients (6 ± 6 ms vs 5 ± 5; $P = 0.4$) We did not find a correlation between global heart T2* and serum ferritin concentrations ($P = 0.7$; r = 0.06) or liver T2* ($P = 0.5$; r = -0.1). The presence of myocardial fibrosis was not significantly difference in TI (36%) vs the TM patients (31%) ($P = 0.4$). In both groups myocardial fibrosis was predominantly patchy and did not follow a coronary distribution. In TI we found left ventricular (LV) dilatation with increased ventricular stroke volume in 14 (45%) patients, left atrial dilatation in 21 (68%) patients, mild reduction of LV ejection fraction (EF) in 4 (13%) patients, right ventricular (RV) dilatation with increased ventricular stroke volume in 7 (23%) patients, right atrial dilatation in 17 (55%) patients and mild reduction of RV EF in 2 (6%) patients. Left and right end-diastolic volume indexes, ventricular stroke volumes and EF were significantly higher in the TI vs the TM patients. TI patients showed significantly larger left and right atrial area. Table 1 summarizes the findings.

Conclusions: In 1/5 of TI patients we detected myocardial iron overload. The lack of correlation between cardiac iron and serum ferritin or liver iron levels confirms MRI the only non invasive technique to detect heart iron in TI patients. Myocardial fibrosis was detectable in a significant percentage of TI patients. High cardiac output findings was significantly more pronounced in TI patients. These data suggest that the option of starting blood transfusions and chelation therapy in TI patients should be revaluated. CMR re-iterates its role as fitted guide to cardiac managements also in TI.

373. PREOPERATIVE EFFECTIVE FORWARD LEFT VENTRICULAR EJECTION FRACTION IN PATIENTS WITH CHRONIC SEVERE MITRAL REGURGITATION PREDICTS LEFT VENTRICULAR EJECTION FRACTION FOLLOWING MITRAL VALVE SURGERY

Eli V. Gelfand, MD, Thomas H. Hauser, MD, MMSc, Lois Goepfert, RN, Kraig V. Kissinger, RT, Ralph de la Torre, MD, Warren J. Manning, MD ***Beth Israel Deaconess Medical Center, Boston, MA, USA.***

Background: Patients with chronic severe mitral regurgitation (MR) may have subclinical left ventricular systolic dysfunction that is not characterized by global measures of systolic performance such as ejection fraction. An important consideration for the timing of mitral valve surgery is the desire to have preserved post-operative left ventricular (LV) ejection fraction. We hypothesized that pre-operative effective forward LVEF (EF-LVEF = LV forward flow/LV end-diastolic volume) would predict post-operative LVEF and used quantitative cardiovascular magnetic resonance (CMR) to study 12 patients with severe chronic MR prior to and 3 months following mitral valve repair or replacement (MVR).

Purpose and methods: Twelve patients (50% F; age 51 ± 11 yrs; 9 valve repair/3 replacement) referred for MVR underwent quantitative CMR with assessment of LV end-diastolic

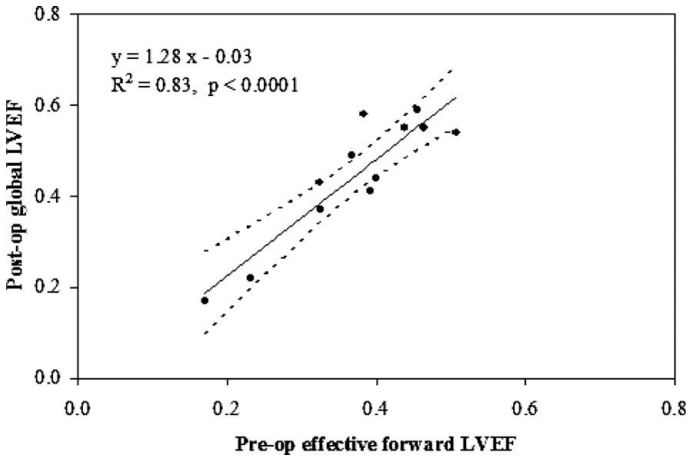

FIG. 1. Linear regression model demonstrating correlation of preoperative effective forward LVEF and postoperative global LVEF.

and end-systolic volumes, ejection fraction and EF-LVEF prior to and 3 months following MVR.

Results: Pre-op LVEF was 60.7 ± 10.1% with preoperative MR regurgitant fraction of 37.1 ± 12.7%, and pre-op EF-LVEF of 37.2 ± 9.7%. Post-operatively, global LVEF declined (absolute decrease 16.2 ± 9.0%, $p < 0.0001$), whereas EF-LVEF minimally increased (4.8 ± 7.2%, $p = 0.04$) with excellent correlation with pre-op EF-LVEF ($R = 0.91$; Fig. 1) that was superior to pre-op global LVEF, LV volumes, and LV end-diastolic and end-systolic dimensions.

Conclusions: Among patients with chronic severe MR, pre-op EF-LVEF is the best predictor of post-operative LVEF. If confirmed in larger series, EF-LVEF may serve as a useful clinical guide for the timing of MVR in this population.

374. CARDIAC MAGNETIC RESONANCE IMAGING FOLLOWING STAGE 1 NORWOOD OPERATION FOR HYPOPLASTIC LEFT HEART SYNDROME

Vivek Muthurangu, MBChB, MRCPCH,[1] Andrew Taylor, MD, MRCP, FRCR,[1] Sanjeet Hegde, MBBS, MRCPCH,[1] Robert Johnson, BA, BM, MRCP,[1] David Anderson, MB-BCh, FRCS,[2] Edward Baker, MD, FRCP,[1] Reza Razavi, MD, MRCP, MRCPCH.[1] ***[1] Kings College London, London, United Kingdom, [2] Guys Hospital, London, United Kingdom.***

Introduction: Hypoplastic left heart syndrome (HLHS) has an incidence of approximately 1 in 5000 births. Staged reconstructive surgery is the preferred treatment option and is performed in 3 stages. The Norwood procedure (Stage 1) involves formation of a neo-aorta as well as placement of a Blalock-Taussig shunt and excision of the atrial septum. In Stage 2, a bidirectional cavopulmonary connection (BCPC) is created, which is converted to a total cavopulmonary connection (TCPC) in Stage 3. Success of the BCPC is dependant on pre-operative assessment currently performed using a combination of cardiac catheterization and echocardiography. However, cardiac catheterization is associated with morbidity and even mortality in this group of patients. A non-invasive method of evaluating these patients is therefore desirable. Cardiovascular magnetic resonance (CMR) is a proven method of assessing anatomy and function in infants with congenital heart disease.

Purpose: The purpose of this study was to demonstrate that CMR can provide complete pre-BCPC assessment in patients with HLHS.

Methods: Thirty-seven infants with HLHS were assessed with CMR and echocardiography prior to BCPC. Gd-MRA and black blood imaging was performed to delineate neo-aortic and branch pulmonary artery anatomy. Any vascular stenosis was noted and categorized as severe (obstruction greater or equal to 40% of the diameter of normal distal vessel), mild/moderate (obstruction 10–39%), or none/trivial (obstruction less than 10%). MR and echocardiographic findings were compared to the 'gold standard' surgical assessment of the vasculature. 2D SSFP cine imaging was used to perform ventricular volumetry and quantify ventricular function. Velocity encoded PC-MR was used to quantify neo-aortic flow. A combination of volumetry and flow data was used to calculate tricuspid and neo-aortic regurgitation. MR assessment of ventricular function and valvar regurgitation were compared to echocardiographic findings.

Results: All patients underwent BCPC, with good post-operative outcome, and no short-term mortality. Volume rendered images of vascular anatomy are shown in Fig. 1. The sensitivity of MR for diagnosis of severe neo-aortic obstruction was 86% and the specificity was 97%. The sensitivity of echocardiographic assessment of the neo-aorta was 42% and the specificity was 97%. The sensitivity of MR assessment of the branch pulmonary artery was 100% and the specificity was 94%. The sensitivity of echocardiographic assessment of the branch pulmonary artery was 20% and the specificity was 100%. Thus MR exhibited a higher sensitivity for the correct identification of vascular obstruction than echocardiography. There was general agreement between MR and echocardiographic measures of ventricular function, and valvar regurgitation.

Conclusions: In this study we have demonstrated that CMR provides anatomical and functional assessment in patients with HLHS prior to formation of a BCPC. We have demonstrated that CMR has a high sensitivity for the identification of vascular obstruction. Operative outcome was good in all patients in this study. This implies that CMR can replace catheterization without adverse affect on outcome. Echocardiography has a low sensitivity for identification of vascular stenoses and is thus not a suitable replacement to cardiac catheterization. CMR assessment of ventricular function and valvar regurgitation is consistent with echocardiographic findings. Therefore, we conclude that CMR represents a comprehensive imaging modality for pre-operative assessment of patients with HLHS. This has major ramifications for the management of this patient group as

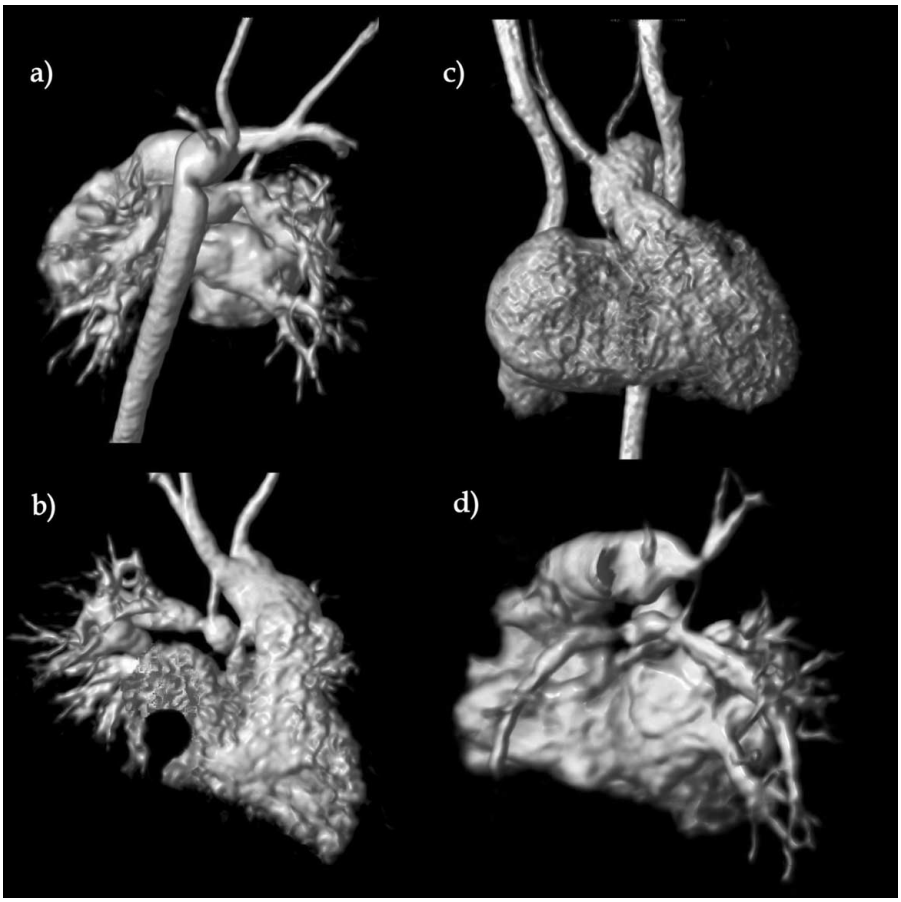

FIG. 1. Volume rendered Gd-MRA's of a) severe neo-aortic narrowing (note the complex 3 dimensional structure) and tenting of the right pulmonary artery (RPA). b) RPA stenosis just distal to the insertion of the modified Blalock-Taussig shunt. c) Bilateral superior vena cava. d) Proximal left pulmonary artery stenosis.

it should avoid morbidity and mortality due to catheterization, and improve pre-operative functional evaluation.

375. AORTIC STIFFNESS OF NORMAL-SIZED AORTAS IN PATIENTS WITH BICUSPID AORTIC VALVES BY MR FLOW MAPPING

Trung H. Tran, MD,[1] Jason Ricci, MD,[1] Michael A. Beardslee, MD,[1] Shelton Caruthers, PhD,[2] Mary Watkins, BS,[1] Samuel A. Wickline, MD,[1] Gregory M. Lanza, MD PhD[1] [1]***Washington University, Saint Louis, MO, USA,*** [2]***Washington University/Philips Medical Systems, Saint Louis/Cleveland, MO, USA.***

Introduction: Patients with congenital bicuspid aortic valves (CBAV) manifest with a higher rate of aortic root dilatation and a nine fold greater risk of aortic dissection. However, clear criteria to identify susceptible individuals are lacking. In Marfan's syndrome aortic dilation and dissection has been shown to correlate with abnormal aortic distensibility and stiffness, which are independent predictors of aortic dilatation.

Purpose: The aim of this study was to determine whether patients with CBAV exhibit early changes in aortic distensibility and stiffness associated with increased aortic dilation.

Methods: CBAV patients with normal aortic diameters (ie, 2 to 4.0 cm) were subdivided into two groups (<3.6 cm, n = 8; >3.6 cm, n = 7) based upon the median aortic diameter and compared to a third control group (<3.6 cm, n = 5) without aortic pathology. Aortic diameter, translumenal area and MR flow mapping was performed at three locations within the aorta (1, ascending aorta; 2, descending aortic arch; 3, abdominal aorta). Blood pressure was measured prior to each scan. Distensibility at each location and flow wave velocity between location 1 to 2 and location 2 to 3 were calculated.

Results: CBAV patients aortic root diameter <3.6 cm (2.9 ± 0.2 cm) had lower flow wave velocities in the ascending arch than did their counterparts with larger root diameters >3.6 cm (3.8 ± 0.6 cm), (4.33 ± 0.31 m/sec versus 6.83 ± 1.01 m/sec, $p < 0.05$). However, no difference in distensibility between the two groups was noted ($3.08 \pm 0.42\ 10^{-3}$ mmHg^{-1} versus $3.69 \pm 0.93\ 10^{-3}$ mmHg^{-1}, respectively, $p > 0.05$) or BSA (1.99 ± 0.21 m^2 vs. 1.83 ± 0.24 m^2; $p = 0.18$). Control patients had aortic diameters < 3.6 cm (3.1 ± 0.1 cm) and flow wave velocities

of 5.04 ± 0.72 m/sec, which did not differ from either CBAV group. In CBAV patients flow wave velocities of the descending aorta (8.16 ± 1.00 m/sec) were greater ($p < 0.05$) than those in the ascending aorta (5.35 ± 0.60 m/sec) with no differences appreciated in the high and low CBAV groups. Similarly, flow wave velocity in control patients increased ($p < 0.08$) in the descending aorta (10.9 ± 2.8 m/sec).

Conclusions: These data suggest that flow wave velocity of the ascending aorta, an integrated measure of stiffness, may be a better indicator of material changes in CBAV patients than is distensibility, which is a more regional index. These results parallel similar abnormalities in Marfan's patients. MR-based flow wave velocity characterization may help identify and characterize patients with congenital bicuspid aortic valves at greater risk for aortic dilatation or dissection.

376. AUTOMATED MAGNETIC RESONANCE IMAGING ASSESSMENT OF COMMON CAROTID ARTERY WALL CHANGES AFTER 2 YEARS OF STATIN THERAPY

Hunter Underhill, MD,[1] Chun Yuan, PhD,[1] William Kerwin, MD,[1] Joel Raichlen, MD,[2] John Waterton, PhD,[3] Thomas S. Hatsukami, MD.[4] ***[1]University of Washington School of Medicine, Seattle, WA, USA, [2]AstraZeneca, Wilmington, DE, USA, [3]AstraZeneca, Macclesfield, United Kingdom, [4]University of Washington School of Medicine and VA Puget Sound Health Care System, Seattle, WA, USA.***

Introduction: Intima-media thickness (IMT) of the carotid artery as measured by B-mode ultrasound (US) has been shown to correlate with extent of systemic atherosclerosis, myocardial infarction and stroke (1). Consequently, IMT has been used in clinical trials to evaluate pharmaceutical efficacy in cardiovascular disease (2). However, due to reproducibility limitations, evaluating changes in IMT by B-mode US is confined to only large population-based studies (3). High-resolution magnetic resonance imaging (MRI) is an emerging, non-invasive modality that has been proven to characterize features of local atherosclerotic disease in the carotid artery (4). Additionally, automated measurements of common carotid artery (CCA) mean wall thickness (MWT) have been shown to have a high correlation to IMT measurements by B-mode US (5). Given the excellent reproducibility of MRI for measuring wall size (6), MRI may have the potential to measure changes in CCA wall thickness, a surrogate for systemic atherosclerosis, within a smaller population.

Purpose: To demonstrate the ability of carotid MRI to detect change in wall measurements in a small population of carotid disease patients receiving statin therapy.

Methods: As part of the ORION (Outcome of Rosuvastatin treatment on carotid artery atheroma: a magnetic resonance Imaging ObservatioN) trial, 43 subjects with fasting low-density lipoprotein cholesterol (LDL-C) >100 and <250 mg/dL and 16%–79% carotid stenosis by duplex US or plaque with a lipid-rich necrotic core by MRI were randomized to low- (5 mg) or high-dose (40 or 80 mg) rosuvastatin (RSV) therapy for 2 years. Subjects underwent serial 1.5T MRI examinations with a protocol that included acquisition of black-blood, T1-weighted axial images. Acquisition parameters were: TR/TE = 800/9.3 msec., echo train length (ETL) = 8, matrix size = 256 × 256, slice thickness 2 mm, and zero-filled interpolation to 512 × 512. Effective resolution was 0.62 mm or better. Analysis was performed on a subgroup that had sufficient coverage of the CCA (2 adjacent slices >6 mm proximal to the bifurcation), and absence of plaque at these sites. Lumen and outer-wall boundaries were automatically detected using a novel algorithm capable of determining thickness measurements with sub-pixel accuracy. Lumen area (LA), wall area (WA), mean wall thickness (MWT), and the wall-to-outer wall percent (W/OWP) were measured from a single artery in 10 patients ($n_{low} = 4$; $n_{high} = 6$) at baseline and 2 years. Inter-scan reproducibility was assessed in 8 arteries from 6 patients with baseline scans separated by less than 3 weeks.

Results: At baseline, mean LA, mean WA, and the mean MWT were 33.3 mm^2, 24.6 mm^2, and 1.02 mm, respectively. The root-mean-square difference between each of the two baseline scans was 2.1 mm^2, 1.0 mm^2, and 0.04 mm, respectively. Two-year results are summarized in Table 1.

Conclusions: These findings suggest that the high inter-scan reproducibility measurement afforded by carotid MRI may enable the detection of vessel wall changes in small populations. Therefore, this technique may be valuable for monitoring changes in the CCA as a systemic marker for atherosclerotic disease.

Table 1. Change in wall thickness measurements of the CCA after 2 years of statin therapy.

	Change ± 95% Cl p value		
	Combined (n = 10)	Low-dose (n = 4)	High-dose (n = 6)
LA (mm^2)	0.1 ± 2.0 0.47	−1.6 ± 2.8 0.17	1.2 ± 2.3 0.17
WA (mm^2)	−3.3 ± 1.7 0.002	−4.2 ± 3.5 0.05	−2.6 ± 1.9 0.02
MWT (mm)	−0.11 ± 0.06 0.002	−0.12 ± 0.11 0.06	−0.10 ± 0.07 0.02
W/OWP (%)	−3.2 ± 2.0 0.008	−2.0 ± 3.0 0.10	−3.4 ± 2.9 0.03

REFERENCES

1. O'Leary DH, et al. NEJM 1999;340:14–22.
2. Taylor AJ, et al. Circulation 2002;106:2055–2060.
3. Kanters SD, et al. Stroke 1997;28:665–671.
4. Yuan C, et al. Circulation 2001;104:2051–2056.
5. Underhill HR, et al. JCMR 2005;7:140–141.
6. Saam T, et al. ATVB 2005;25:234–239.

377. EVALUATION OF CORONARY ARTERY BYPASS GRAFT PATENCY WITH A 2D BREATH-HOLD SPIN ECHO MR SEQUENCE

Thomas Wittlinger,[1] Feyzan Oezaslan,[1] Peter Kalden,[2] Anton Moritz.[1] [1]***University Hospital, Frankfurt, Germany,*** [2]***University Hospital, Mainz, Germany.***

Introduction: The application of previous desript magnetic resonance angiography techniques has enabled noninvasive differentiation between patent and occluded coronary artery bypass grafts. There are few clinical studies, who examine a sufficiently large number of patients with documented graft stenosis or occlusions. The aim of the study was to evaluate in a large patient group the patency of coronary artery bypass grafts and to detect graft stenosis and occlusions with a MR spin echo sequence. We examined furthermore the diagnostic accuracy in the detection of the distal anastomoses.

Methods: Three hundred patients with 840 distal anastomoses were examined with a 1.5 T MR scanner. A 2-dimensional T2-weigthed breath-hold half-Fourier acquisition single-shot turbo spin echo sequence (Haste) was performed. All images were evaluated independently by a radiologist and cardiologist and correlated to the conventional coronary angiography. The observers were blinded to the results of the coronary angiography, but informed about the surgical graft anastomosis.

Results: With the Haste sequence 76% of the distal anastomosis were recognized (640/840). 70 of 84 stenosis and all occlusions were identified. The sensitivity and specificity for the evaluation of the distal anastomosis was 87% and 96%. 24% of the distal anastomoses were not identified due to a poor image quality or motion artefacts.

Conclusion: Using the Haste sequence a reliable assessment of graft patency and evaluation of graft occlusion is possible.The novel finding in the present study with 840 grafts is that MRI enables the detection of vein graft stenosis and occlusions even in the distal segments with a fair diagnostic accuracy. This results offers perspective for noninvasive screening of patients who present with recurrent chest pain after bypass surgery, because 40% of the currently studied CABG patients who underwent diagnostic coronary angiography required no further therapeutic intervention. Further improvements of the spatial resolution and the image quality are necessary to recommend this MR technique for routines clinical use.

Results

Graft	All	IMA	LAD	RCA	PLA	Diagonal branch
Sensitivity%	89.5	68.8	78.6	95.2	90.5	100.0
Specitifity%	98.3	97.3	98.0	97.0	92.3	97.0

378. CSPAMM IN COMBINATION WITH HARP TO ASSESS MYOCARDIAL MOTION IN FABRY PATIENTS

Andrea K. Rutz,[1] Christoph F. Juli,[2] Salome Ryf,[1] Urs Widmer,[3] Sebastian Kozerke,[1] Boris P. Eckhardt,[2] Peter Boesiger.[1] [1]***Institute for Biomedical Engineering, University and ETH, Zurich, Switzerland,*** [2]***Inst. for Clin. Radiology, Kantonal Hospital, Winterthur, Switzerland,*** [3]***Internal Medicine Department, University Hospital, Zurich, Switzerland.***

Introduction: Progressive left ventricular (LV) hypertrophy is the hallmark of cardiac manifestations in patients with Fabry disease. There is a need to accurately assess the effects of Fabry disease on the myocardial function and motion. Myocardial tagging using CSPAMM (1) and harmonic phase-analysis (HARP) (2) is a powerful method to quantify LV functional impairment.

Purpose: To study alterations of myocardial function in patients with Fabry disease using tagged MR images in combination with HARP-analysis. The detection of myocardial motion abnormalities at an early stage of disease was of particular interest for the study.

Methods: Twenty-nine Fabry patients (17 male, 12 female) aged 17–64 years, medium age of 37.6 years (12 with LV hypertrophy vs. 17 with normal LV mass), were compared with an age and sex matched control group of 28 volunteers. For the quantification of LV circumferential shortening and LV torsion (rotation [apex]-rotation [basis]) midwall contours were HARP-tracked on apical, equatorial and basal short-axis CSPAMM-images (Fig. 1), acquired on a 1.5T Philips scanner (2 × lines, 8 mm tag distance, slice following) using a single breath-hold EPI sequence (EPI-factor:11, FOV:330 mm, matrix: 128 × 33, ramped flip angles, 20 cardiac phases, temporal resolution: 35 ms). Furthermore, the onset of LV long axis shortening was assessed

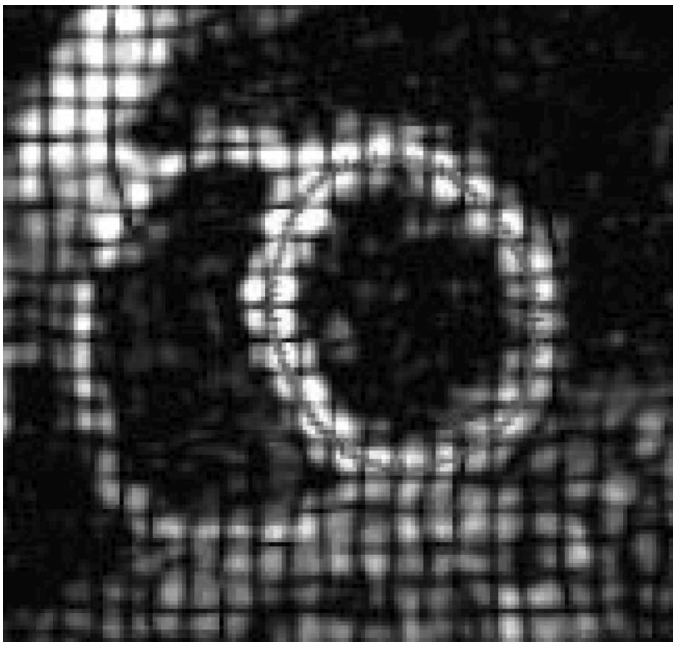

FIG. 1. Midwall contour on a basal short-axis CSPAMM-image.

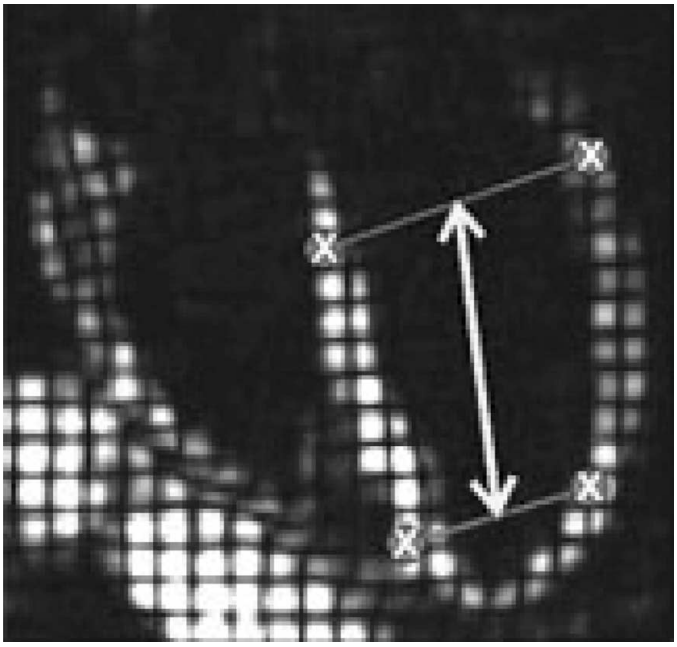

FIG. 2. Measurement of LV long axial shortening after tracking of 4 landmark points (septum&free wall, basal&apical).

for 20 patients (7 with advanced LV mass) vs. volunteers on CSPAMM-images acquired in 4 chamber views with identical scan parameters (Fig. 2). HARP-analysis was applied using peak-combination (3) and the results were compared applying unpaired two tailed t-tests.

Results: Fabry patients with marked LV hypertrophy show significantly reduced LV contraction at end-systole (ES) on all levels ($p < 0.007$) and prolonged diastolic relaxation compared to patients without LV hypertrophy and normal controls. Apical circumferential shortening over the cardiac cycle is shown in Fig. 3 (error bars representing 1SD in all figures). The onset of LV shortening is represented in Fig. 4 with a significant impairment at ES for Fabry patients with advanced LV mass ($p = 0.0025$). No differences could be observed between patients with normal LV mass and controls for LV contraction and shortening. Peak LV torsion is significantly increased for both Fabry patients with normal (Fig. 5a, $p < 0.0025$) and patients with increased (Fig. 5b, $p < 0.02$) LV mass. Accordingly, diastolic back rotation occurs faster and prolonged for patients compared to controls.

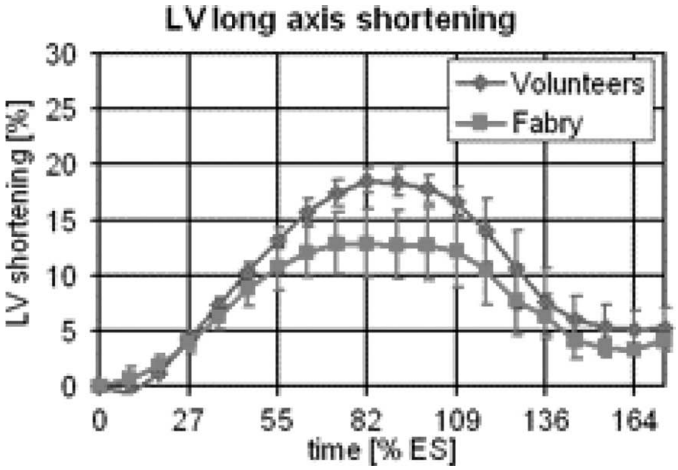

FIG. 4. LV shortening for Fabry patients with LV hypertrophy vs. volunteers ($n = 7$).

Conclusions: For Fabry patients with LV hypertrophy circumferential shortening and LV shortening are significantly reduced, which is consistent with results from other studies [4]. Severity of LV contraction impairment is related to the extent of LV hypertrophy and is compensated for by increased LV torsion. Using CSPAMM combined with HARP, functional changes of the heart can be detected prior to LV hypertrophy in Fabry patients. LV torsion was found to be significantly increased at an

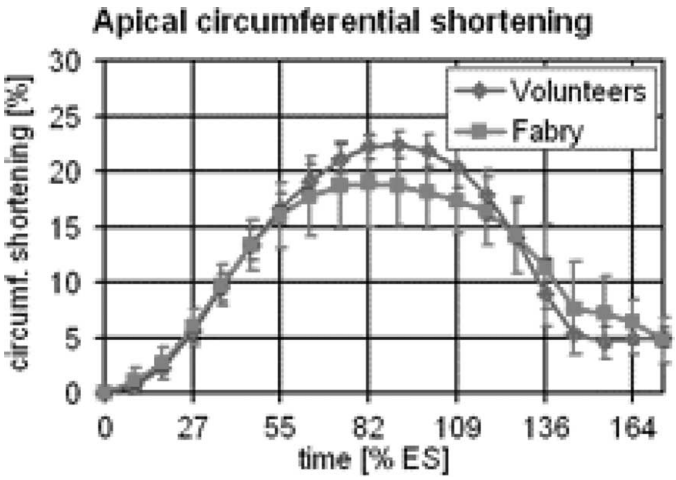

FIG. 3. Apical contraction for Fabry patients with LV hypertrophy vs. volunteers ($n = 12$).

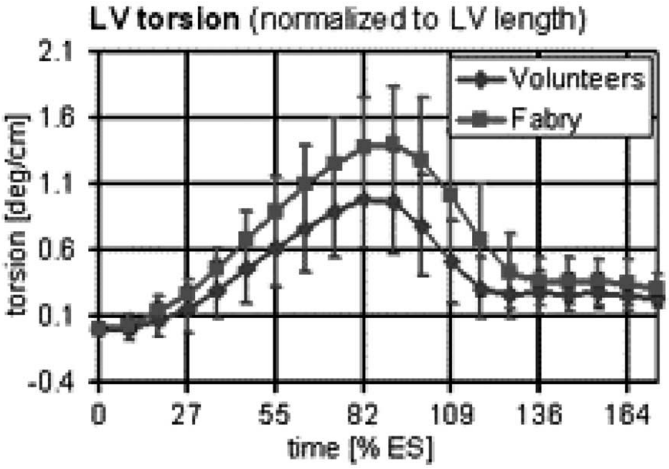

FIG. 5a. LV torsion for Fabry patients with normal LV mass vs. volunteers ($n = 17$).

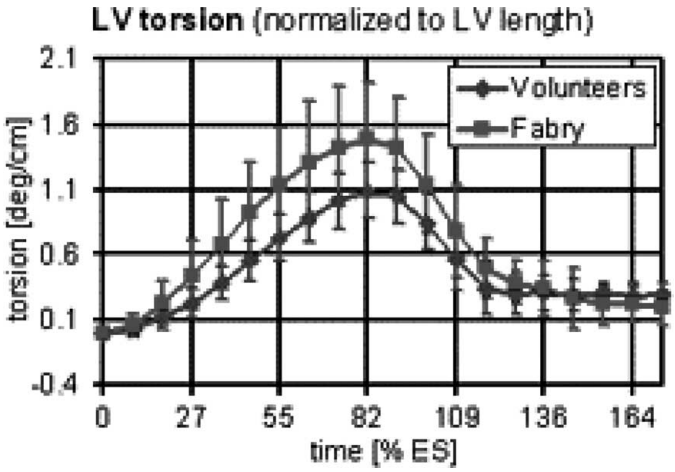

FIG. 5b. LV torsion for Fabry patients with LV hypertrophy vs. volunteers (n = 12).

early stage of disease, ie, in patients without LV hypertrophy. This is a new finding in this group of patients.

REFERENCES

1. Fischer SE, et al. MRM 1993;30:191–200.
2. Osman N, et al. MRM 1999;42: 1048–1060.
3. Ryf S, et al. JMRI 2004;20:874–878.
4. Weidemann F, et al. Eur. Heart J. 2005;26:1221–1227.

379. COIL COMBINATION FOR PEAK-COMBINATION HARP

Andrea K. Rutz, Salome Ryf, Sebastian Kozerke, Peter Boesiger. ***Institute for Biomedical Engineering, University and ETH, Zurich, Switzerland.***

Introduction: Myocardial tagging such as CSPAMM (1) combined with harmonic phase-analysis (HARP) (2) is a powerful method to quantify myocardial motion of healthy and diseased hearts. Typically, CSPAMM data are acquired using a phased array coil. In order to achieve a better SNR and optimal tracking results, combination of all coil elements is desirable. Using the root-mean-square (RMS) combination, images of different coil elements can easily be combined into a modulus image, which could be used for HARP analysis. However, the modulus operation generates additional k-space peaks at zero spatial frequency and at harmonics greater than the tagging frequency. The resultant crowding in k-space may lead to errors in HARP evaluation or may require a very narrow HARP filter, reducing the already limited spatial resolution of HARP analysis. Therefore, complex CSPAMM data should be used for HARP analysis. In order to combine data from different coil elements, an algorithm is required that compensates for phase contributions originating from the different spatial locations of the coil elements.

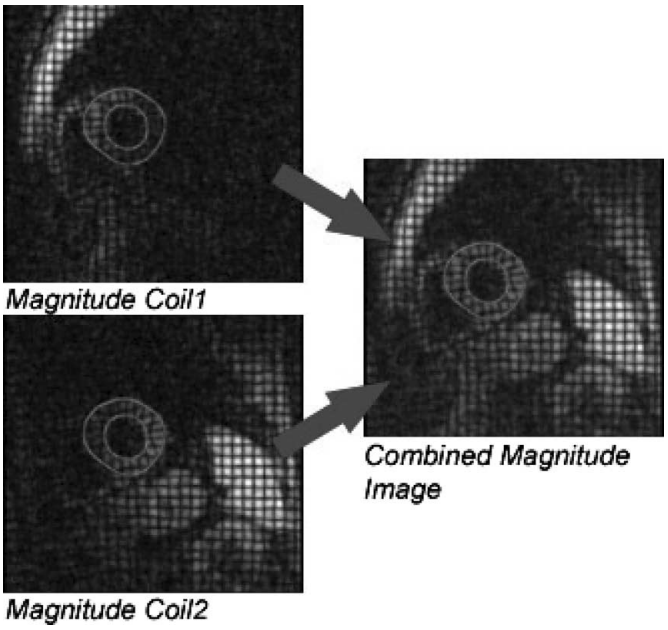

FIG. 1. Root-mean-square combination of tagged magnitude images.

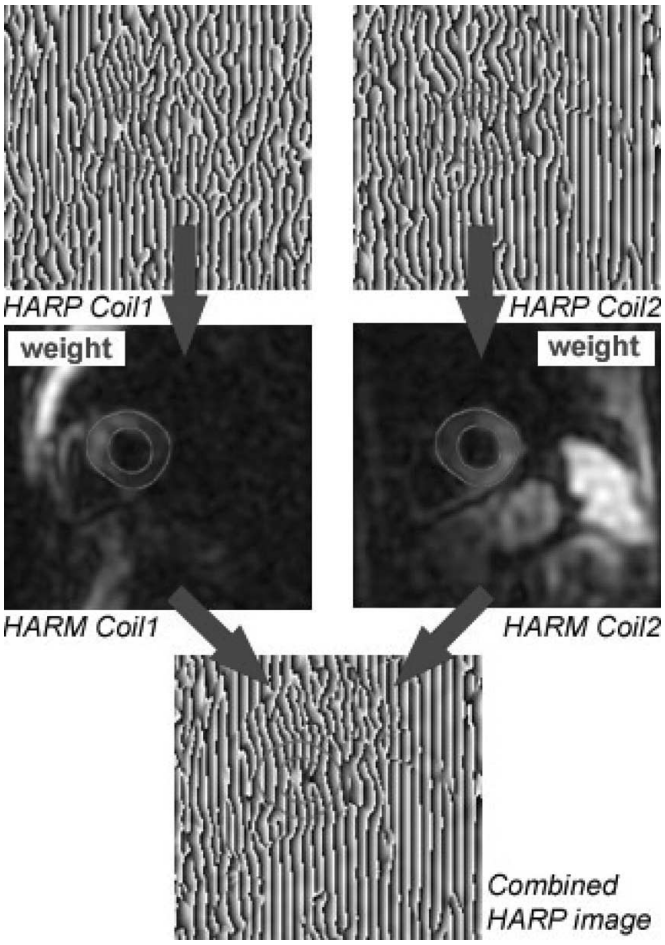

FIG. 2. Combination of HARP images from two different coil elements.

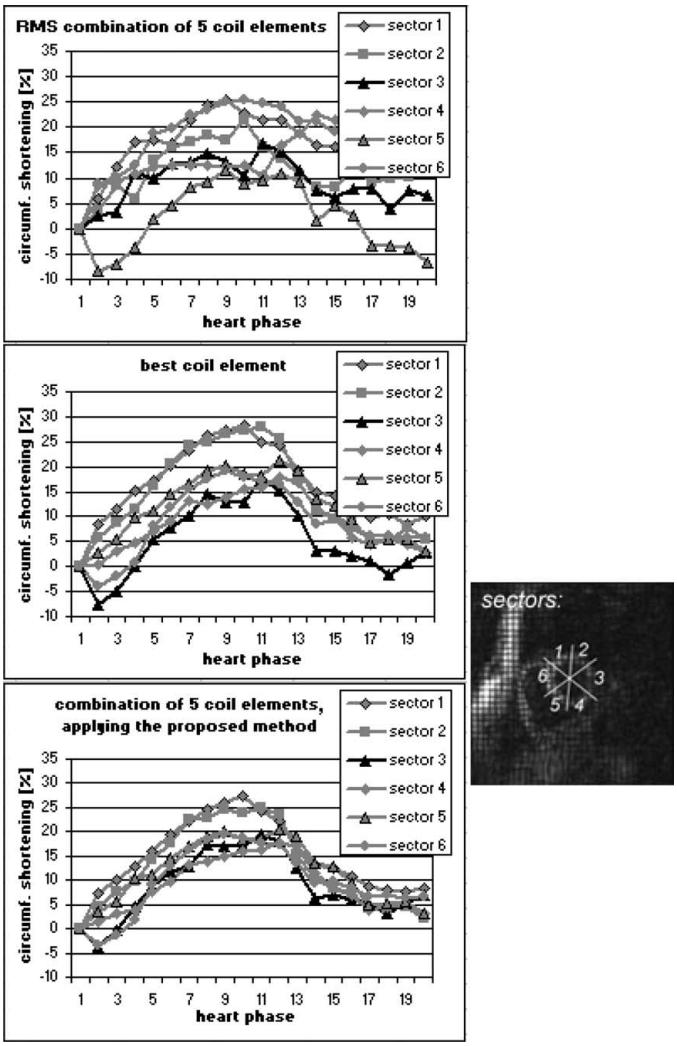

FIG. 3. Circumferential shortening of the midwall tracked with HARP. The contraction pattern for the different sectors is more homogeneous and tracking of more distant sectors (sector 3) is improved for the analysis using the proposed method compared to the RMS combination and the analysis with only one coil element.

Purpose: The purpose of this work was to implement an efficient algorithm to combine the signal of different coil elements in order to improve the HARP images over the whole myocardium for better tracking results and more accurate motion quantification.

Methods: For a better delineation of the myocardial borders, the tagged images of different coil elements are combined using a RMS calculation resulting in a more homogeneous signal and improved harmonic magnitude (HARM) images over the whole myocardium (Fig. 1).

Due to different coil phases, this approach is not suitable for HARP-tracking. For conventional HARP evaluation, either the positive or the negative harmonic peak is extracted in k-space, whereas for peak-combination HARP, both peaks are used (3). The corresponding harmonic phase of the positive ($P^{+}(x)$) and the negative peak ($P^{-}(x)$) is: $P^{\pm}(x) = \pm\varphi(x) + \beta(x)$, where $\varphi(x)$ describes the displacement-encoded phase contrast, resulting from tagging. $\beta(x)$ describes any remaining phase unrelated to motion, including the phase of the coil sensitivity. With peak-combination HARP, $P^{-}(x)$ is subtracted from $P^{+}(x)$: $P^{+}(x) - P^{-}(x) = 2\phi(x)$, thus eliminating any phase contribution from the different spatial locations of the coil elements. Hence, the peak-combined HARP images of different coil elements can be combined in a straightforward fashion as illustrated in Fig. 1. The complex averaging is done after weighing the HARP image of each coil with the square of its corresponding HARM image.

CSPAMM images with a tag-line distance of 8 mm were acquired in a healthy volunteer on a 1.5T Scanner (Philips Medical Systems, Best, NL) using a five-element phased array coil. A midwall contour was HARP-tracked through the cardiac cycle and circumferential shortening was calculated for six sectors over the myocardium.

Results: Fig. 3 shows that HARP-tracking is more accurate when combining all coil elements applying the proposed method compared to the analysis with RMS-combination or with one coil element only. Particularly, myocardial sectors which are more distant from the coil (eg, sector 3 in Fig. 3), benefit from a better SNR due to coil combination, resulting in less tracking errors and smoother curves for the circumferential shortening.

Conclusions: A method was introduced to combine tagged images of different coil elements. It could be demonstrated that better myocardial motion quantification can be achieved when using the proposed coil combination method. Alternatively, coil combination could be used to choose a larger strain resolution (by increasing the size of the HARP-filter) without changing the SNR. Compared to other coil combination methods (4), no further reference scan is needed and no coil sensitivities have to be calculated.

REFERENCES

1. Fischer SE, et al. MRM 1993;30:191–200.
2. Osman N, et al. MRM 1999;42:1048–1060.
3. Ryf S, et al. JMRI 2004;20:874–878.
4. Roemer PB, et al. MRM 1990;16:192–225.

380. ACCURACY OF MEASUREMENT OF INFARCT AND NO-REFLOW ZONE SIZE IN ACUTE MYOCARDIAL INFARCTION USING A SINGLE-SHOT PHASE SENSITIVE INVERSION RECOVERY TECHNIQUE

Sharyn Katz, MD,[1] Susan Ghods, MD,[1] Kambiz Parchamazad, MD,[2] Sayed Hashemi, MD,[1] Robert Wilensky, MD,[1] Harold Litt, MD-PhD.[1] [1]***University of Pennsylvania Medical Center, Philadelphia, PA, USA,*** [2]***Drexel University School of Medicine, Philadelphia, PA, USA.***

Introduction: A method for rapid measurement of infarct and no-reflow zone size in the setting of acute myocardial infarction

would provide useful information for therapeutic decision making and prognosis. Delayed enhancement MR imaging can be used to measure infarct size in patients with acute and chronic myocardial infarction and no-reflow zone size in acute MI using an inversion recovery gradient echo sequence. Usual magnitude reconstruction techniques require precise determination of the optimal inversion recovery time (TI) to null the signal of normal myocardium. Phase sensitive reconstruction imaging (PSIR) avoids the need for precise setting of the TI, maintaining excellent contrast between normal and infarcted myocardial tissue over a wide range of TI values. Using a TrueFISP PSIR sequence, an image is acquired during every two heartbeats, so that short axis imaging through the entire LV can be performed rapidly without the need for additional imaging to determine the optimal TI.

Purpose: To compare the rapid TrueFISP PSIR and traditional segmented k-space IR-FLASH techniques for measurement of acute myocardial infarct and no-reflow zone size in an acute infarction animal model.

Methods: Thirty-three juvenile domestic swine underwent 1 hour balloon occlusion of the proximal LAD followed by reperfusion using a previously validated protocol which results in reproducible infarction of approximately 25% of the LV mass. Cardiac MR was performed 3 days later using a 1.5T magnet and phased array coils. Delayed images were obtained in multiple short axis views covering the entire LV using the IR-FLASH and single-shot PSIR sequences 12–15 minutes after administration of 0.2 mmol/kg gadolinium-DTPA. The IR-FLASH sequence was performed during suspended respiration while the PSIR was performed during free-breathing. A TI scout was used to determine the optimal TI setting for the IR-FLASH sequence by choosing the TI value at which myocardial signal at a site distant from the infarction was nulled. The hyperenhancing area and subendocardial hypoenhancing no-reflow zone were measured for both techniques using manual tracing and compared using a paired t-test. The no-reflow zone was included as part of the total infarct size.

Results: IR-FLASH images could not be evaluated in 2/33 cases, and the PSIR images could not be evaluated in 4/33 cases (neither series could be evaluated in 1 case). There was no significant difference in measured infarct size between the IR-FLASH and PSIR techniques. Infarct sizes were 16.31 ± 4.97 cm^2 and 16.53 ± 5.45 cm^2, respectively. Mean difference in infarct size (IR-FLASH—PSIR) was 0.39 ± 2.39 cm^2. ($p = 0.39$) No-reflow zone sizes measured using IR-FLASH were significantly larger than using PSIR (3.29 ± 1.93 cm^2 vs. 2.62 ± 1.40 cm^2, mean difference 1.39 ± 0.79 cm^2, $p = 0.015$).

Conclusions: Delayed enhancement imaging using the single-shot PSIR technique provides rapid and accurate assessment of infarct size in setting of acute MI without the need for additional imaging to determine optimal inversion time. However, no-reflow zone sizes were significantly underestimated using the PSIR sequence in this animal infarct model.

381. NONINVASIVE CORONARY VESSEL WALL IMAGING USING CONTRAST ENHANCED BLACK BLOOD MRI—INITIAL EXPERIENCES

David Maintz,[1] René Botnar,[2] Murat Ozgun,[1] Roman Fischbach,[1] Walter Heindel,[1] Paulus Kirchhof.[1]
[1] University of Muenster, Muenster, Germany, [2] University of Muenchen, Muenchen, Germany.

Introduction: Published studies on coronary vessel wall imaging using MRI are scarce and have been restricted to non-contrast enhanced (native) techniques.

Purpose: To evaluate contrast-enhanced black blood coronary MRI for vessel wall imaging in patients with different coronary artery disease risk profiles.

Methods: Twenty patients with a different coronary artery disease risk profile (low risk n = 11, intermediate n = 7, high risk n = 2) according to the PROCAM score were studied by free-breathing T1-weighted black blood inversion recovery coronary MRI appr. 30 min. after administration of Gd-DTPA (0.2 mmol/kg). Scan parameters were: voxel size $1 \times 1 \times 3$ mm, TR/TE 6.1/1.9 ms, flip angle 30°. The inversion delay was individually assessed according to the T1 of blood (approx. 300 ms) for optimal signal suppression of the vessel lumen and nonenhancing tissue. Scan orientations were longitudinal and perpendicular to the course of the right coronary artery (RCA). Two readers subjectively classified overall image quality (1 = excellent, 2 = good, 3 = poor, 4 = not evaluable) and vessel wall signal (= contrast uptake) in consensus on a four-point scale (1 = high uptake, 2 = medium, 3 = low/no uptake, 4 = not evaluable).

Results: The average overall image quality was 1.95. The mean RCA vessel wall enhancement score was 2.5 in the longitudinal and 2.74 in the axial scans. In eight patients the RCA

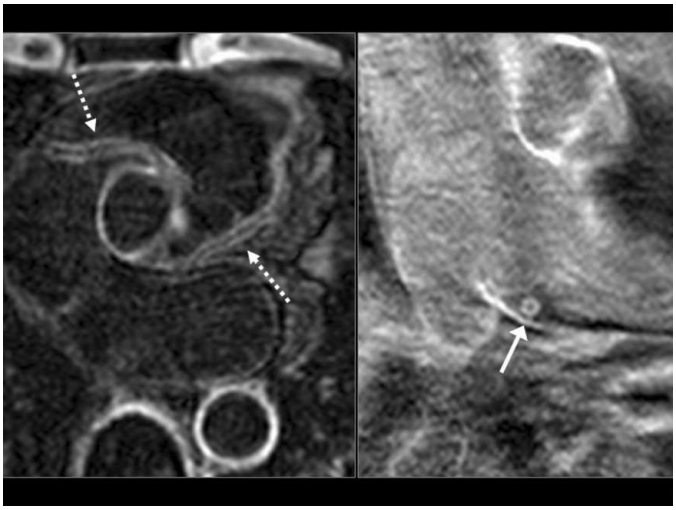

FIG. 1. Diffuse contrast enhancement of left and right coronary artery vessel wall (arrows).

vessel wall did not show contrast uptake on both the longitudinal and the perpendicular post contrast scans (5 with low risk, 2 intermediate, 1 high risk). Of the remaining 12 patients, seven exhibited high or medium RCA vessel wall contrast uptake in both scans. 5 of those had intermediate or high risk according to PROCAM. Of all 9 patients with high or intermediate risk, 6 showed high vessel wall contrast uptake and excellent image quality.

Conclusions: In this study, we demonstrate the use of contrast-enhanced black blood coronary MRI for the visualization of the right coronary artery vessel wall. Initial results suggest that increased vessel wall contrast uptake is associated with cardiovascular risk profile.

382. GADOLINIUM KINETICS OF CHRONIC MYOCARDIAL INFARCTS AS MEASURED BY MAGNETIC RESONANCE

James W. Goldfarb, Marguerite Roth, RN, Nathaniel Reichek, MD. ***St Francis Hospital, Roslyn, NY, USA.***

Introduction: The purpose of this study was to measure the kinetics of gadolinium enhancement over an extended time period in patients with chronic myocardial infarcts. Knowledge of the gadolinium kinetics of myocardial infarcts will allow the determination of necessary changes of TI times over time for optimal nulling of viable myocardium, optimal imaging delay times after contrast agent injection and the accuracy of T_1 times for tissue discrimination. Lastly, this data may allow discrimination of different types of delayed hyperenhancement (DHE), specifically for determination of amalyoiddosis, myocardititis and infarct dating.

Methods: Twenty-five patients having chronic myocardial infarctions (MI) (23 men and two women; age mean $\pm$ STD, 61.5 ± 9.9 years; age range, 43–84 years) underwent MR imaging at 1.5 T. The MI age ascertained from medical history was on average 7.7 years and ranged from 2 to 21 years. Directly after the administration of the contrast agent (0.2 mmol/kg of gadodiamide (Omniscan)), imaging commenced and continued for up to one hour with IR CINE TrueFISP acquisitions for T_1 quantification occurring approximately every two minutes. A single slice was positioned based on MR wall motion imaging to include regions with both injured and normal myocardium and T_1 relaxation times were calculated using a validated technique. Receiver operator characteristic curve analysis was performed to compare the performance of DHE imaging at different times. The Area under the Curve (AUC) was calculated as a measure of the overall imaging performance using T_1 values. A Student t-test was also used to show the statistical significance of T_1 values over time.

Results: All subjects tolerated the examination well. The average imaging time after contrast administration was 47.3 with a range of 20–63 minutes. The difference in detectability of regions was plotted as a difference in mean T_1s of the regions over time (Fig. 1 left). Note how the T_1 difference between infarcts and the LV bloodpool increases over time while the difference between viable myocardium and the LV bloodpool decreases over time. The difference between infarcts and viable myocardium initially sharply increases and then slowly increases over time. Statistical significance of T_1 values is reached after 10 minutes between all regions. After 40 minutes the difference between the LV bloodpool and viable myocardium decreases with statistical significance being lost after 50 minutes. ROC curve analysis (Fig. right) showed a decrease over time in the performance (as measured by the AUC) of a fixed T_1 value to discriminate between the LV bloodpool and viable myocardium while there was a marked increase in the AUC between the LV bloodpool and infarcted myocardium. The discrimination between viable and infarcted myocardium remained essentially constant. A plot of the optimal TI to minimize signal from viable myocardium showed an increase from 200 to 285 over the hour time period.

Conclusions: After a delay of approximately 10 minutes, gadolinium concentrations fall progressively in blood and viable myocardium creating increased image contrast with infarcted myocardium. The rate of change of T_1 decreases over time such that smaller changes in the TI need to be made. The performance

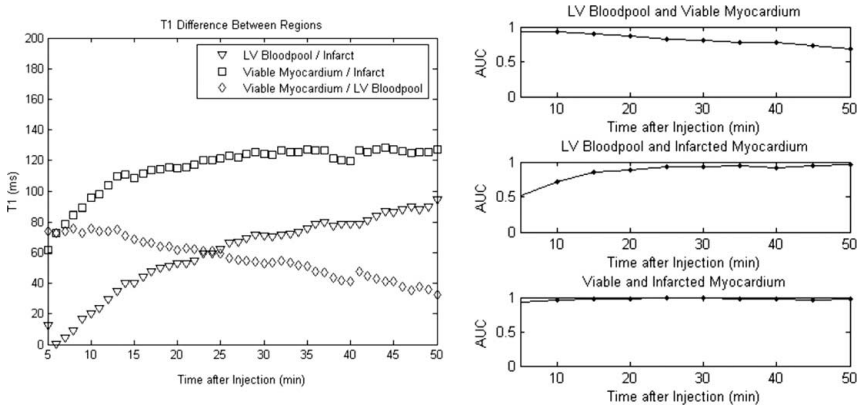

FIG. 1.

of T_1 times as a means of identifying infarcted myocardium increases over time and performs best in discriminating viable from infarcted myocardium.

383. COMPARISON OF MRI AND ECHOCARDIOGRAPHIC PARAMETERS AS DIAGNOSTIC CRITERIA FOR LEFT VENTRICULAR DIASTOLIC DYSFUNCTION

Giso von der Recke, MD, Karol Miszalski-Jamka, David Hardung, MD, Christoph Hammerstingl, MD, Harald Schmidt, MD, Jan Schnapauff, Bernd Saxler, Heyder Omran, MD, PhD. ***St.-Marien-Hospital, Bonn, Germany.***

Introduction: Heart failure is a major disease in elderly patients. For further therapy and prognosis a thorough assessment of ventricular function and discrimination between diastolic and systolic function is necessary. Echocardiographic assessment of mitral flow profiles and tissue Doppler imaging of the lateral mitral valve annulus (LMVA) have been demonstrated to provide insights into filling dynamics of the left ventricle, and thus allow for diagnosing left ventricular diastolic dysfunction. MRI on the other hand is becoming a major diagnostic tool for several different aspects of congestive heart failure and underlying aetiology.

Purpose: The aim of this study was to demonstrate, that MRI is capable of providing the same diagnostic approach to left ventricular diastolic dysfunction as echocardiography.

Methods: The study was planned as a prospective study in a primary cardiac investigational centre. All consecutive patients referred for cardiac MRI (1.5T Magnetom Avanto, Siemens, Germany) were included. Patients were investigated by an adapted phase contrast (pc) MR sequence and Doppler echocardiography for mitral flow and tissue velocity at LMVA. pcMR measurement took two breath holds to complete. Investigators for MR data and echocardiography were blinded for each others data.

Results: During the one month study period 78 consecutive patients were included (NYHA I: 15 pts, NYHA II: 41 pts, NYHA III, 16 pts, NYHA IV 6pts). Doppler echocardiography and pcMR correlated very well for the overall category of diastolic dysfunction. There was a strong correlation for peak flow E/A and Ea of LMVA. Correlation was less for deceleration time and duration of A.

Conclusions: Diastolic dysfunction as defined by criteria of mitral flow and LMVA tissue velocity is well accessible by cardiac MRI. The assessment can be done in two breath holds and provides diagnostic criteria that correlate very well with established echocardiographic markers for left ventricular diastolic dysfunction.

384. MRI-GUIDED NAVIGATION FOR ELECTROPHYSIOLOGICAL INTERVENTIONS USING MRI-TRACKED CATHETERS OVERLAID ON PRE-ACQUIRED IMAGES

Ehud J. Schmidt, PhD,[1] Godtfred Holmvang, MD,[2] Renee Guhde, MS,[3] Robert D. Darrow, MS,[3] Glenn Slavin, PhD,[4] Maggie Fung, MS,[4] Richard Mallozzi, PhD,[3] Charles L. Dumoulin, PhD,[3] Gregory Kampa,[5] Jeremy D. Dando,[5] Thomas K. Foo, PhD,[3] Srinivas Dukkipati, MD,[2] Zachary Malchano, BS,[2] Christina D. McPherson, BS,[2] Jeremy N. Ruskin, MD,[2] Vivek Y. Reddy, MD.[2] ***[1]GE Healthcare ASL East, Newton, MA, USA, [2]Cardiology, Massachusetts General Hospital, Boston, MA, USA, [3]GE Global Research, Niskayuna, NY, USA, [4]GE Healthcare ASL East, Hannover, MD, USA, [5]Saint Jude Medical, Minnetonka, MN, USA.***

Introduction: X-ray guided access to the left atrium and left ventricle serves as a gold-standard for mapping and ablative electrophysiology (EP) procedures. MRI-guided EP intervention could benefit from high-resolution pre-procedural imaging. The images may be utilized as roadmaps for rapid navigation to the left atrium (LA) and the left ventricle (LV) utilizing deflectable MRI-tracked EP catheters.

Purpose: Provide pre-procedural essential images, at minimum imaging time, on vascular approaches to the heart, on wall motion and on scar geometry. Incorporate images into an MR-tracking workstation and utilize them for high-frame rate navigation.

Methods: This study involved the use of 7 infarcted and 3 normal swine. The initial transseptal puncture procedure was performed under fluoroscopic guidance; the remainder of the procedure was performed under MRI-guidance. MR angiography was acquired with contrast-enhanced 3D gradient-echo. 12–15 ECG-gated, short axis FIESTA-SP cine slices, provided wall-motion. 3D myocardium delayed enhancement (3D-MDE) provided scar position. Reformatted coronal and sagittal data sets, loaded into separate workstation windows, provided simultaneous multi-directional and multi-contrast roadmaps for use during the intervention. A deflectable EP catheter outfitted with five MR tracking microcoils was used for navigation, with its position and shape overlaid on each window at 10–15 frames-per-sec. The displayed slices coincided with the instantaneous catheter position and ECG phase.

Results: MRI-tracked EP venous (transseptal) or retrograde aortic navigation to the LA and LV was completed in <2 minutes using the deflectable catheters. Access to LV scar was immediate, allowing selective ECG mapping. Two small infarcts, not identified by standard X-ray guided electroanatomical mapping (CARTO, Biosense-Webster, Inc), were detected by 3D-MDE and ECG mapped using MR guidance.

Conclusions: MRI-tracked navigation using multiple contrast, multi-directional roadmaps is efficient and provides anatomical and physiological information not available with X-ray guided navigation.

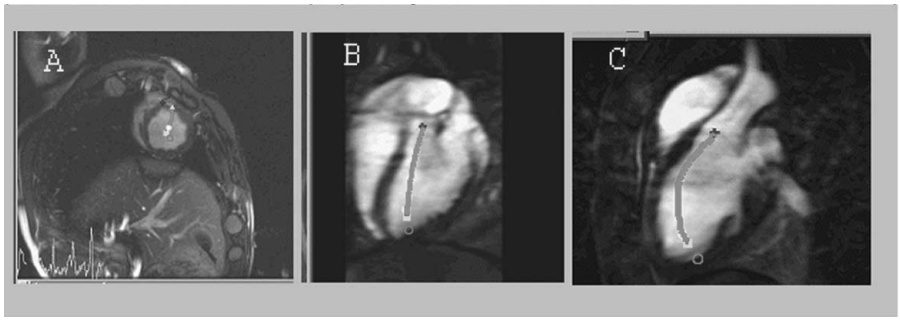

FIG. 1. MRI-guided LV simultaneous navigation (A) Short-axis ECG-gated cine, (B) AP MR angiography, (C) Lateral MDE. Overlays depict instantaneous position of a deflectable EP catheter with 5-MR tracking coils during *in vivo* mapping of the porcine left ventricle.

385. MULTISLICE MULTIECHO T2* MRI APPROACH FOR THE DETECTION OF MYOCARDIAL IRON DISTRIBUTION: VALIDATION IN HEALTHY SUBJECTS AND THALASSEMIA MAJOR PATIENTS

Alessia Pepe,[1] Eliana Cracolici,[2] Maria Filomena Santarelli,[1] Brunella Favilli,[1] Mariolina Deiana,[1] Aurelio Maggio,[3] Paolo Cianciulli,[4] Gianluca Forni,[5] Zelia Borsellino,[6] Aldo Filosa,[7] Massimo Midiri,[2] Massimo Lombardi.[1] ***[1]MR Lab, Clinical Institute of Physiology, CNR, Pisa, Italy, [2]Department of Radiology, University of Palermo, Palermo, Italy, [3]V. Cervello Hospital, Palermo, Italy, [4]S. Eugenio Hospital, Roma, Italy, [5]Galliera Hospital, Genova, Italy, [6]G. Di Cristina ARNAS Hospital, Palermo, Italy, [7]Cardarelli Hospital, Palermo, Italy.***

Introduction: Thalassemia is the most common genetic disorder worldwide and iron-induced cardiomyopathy represents the main determinant of survival. T2* magnetic resonance imaging (MRI) with a single measurement in the mid-ventricular septum has been validated as a quantitative evaluation of myocardial iron overload. However, histological and MRI studies have suggested a marked heterogeneity of iron distribution in the myocardium. We set-up a multislice multiecho T2* MRI approach for the detection of this heterogeneity. However, T2* values could be affect by magnetic susceptibility near the boundaries with cardiac veins, liver and lung or by artefacts depending on the orientation and the motion of the heart.

Purpose: Aim of our study was to validate the multislice, multiecho T2* MRI technique by a complete test of reproducibility and evaluating the spatial heterogeneity of cardiac T2* in healthy subjects and to assess the tissue iron concentration of left ventricle using this segmental approach in thalassemia major (TM) patients.

Methods: T2* multiecho MRI was performed in 20 healthy subjects and in 53 TM patients (1.5 T GE scanner). Three short axis views of left ventricle were obtained and analyzed with custom-written software. The myocardium was automatically segmented into 12 segments. T2* value on each segment and the global T2* value were calculated. In order to assess the endocardial and epicardial distribution of the T2* values, each segment was divided in the inner and outer half. The inter-study reproducibility was performed within the same day.

Results: On T2* global value the coefficient of variation for intra- and inter-observer, and for inter-study reproducibility were 3.9%, 5.5%, and 4.7% respectively. Figure 1 showed the random fluctuation in cardiac T2* among the slices (A) and the segments (B) in the 20 healthy subjects. The percentage of deviation of the slices from the global heart T2* mean was not statistically significant. The percentage of deviation of the segments from the global heart T2* mean ranged from −20 in anterior apex to 18 in lateral apex. The percentage of deviation of the mid-ventricular septum from the global mean was 9%. Among the 66 possible combination in the analysis of variance, significant differences were observed only in 5 cases, among the segments with higher percentage of deviation from the global heart T2* mean. The TM patients had considerable individual variation in the T2* values among the slices and the segments. The epimyocardial iron concentration was significantly higher than the endomyocardial iron concentration in the slices ($P < 0.0001$) and in all segments, excepting in the basal and medium septal segments. Based on T2* segmental analysis, three groups of patients were identified: 8(15%) patients with homogeneous myocardial iron overload (T2* < 20 ms in all segments); 25(47%) patients with no heart iron overload (T2* > 20 ms in all segments); 20(38%) patients with an heterogeneous iron distribution (segments with T2* < 20 ms and segments with T2* > 20 ms). A correlation between the mean global heart T2* value and the T2* value in the mid-ventricular septum was found ($r = 0.94$, $P < 0.0001$). The mean serum ferritin, the liver iron concentration and urinary iron excretion were significant different among groups.

Conclusions: Our data did not account for rejecting certain slices or segments. T2* gradient from endocardium to epicardium is consistent with patterns of iron deposition described in prior histological studies. Cardiac iron overload showed an heterogeneous distribution in a significant percentage of TM patients. The group with heterogeneous myocardial iron overload seems to be different in proved prognostic indicator as serum ferritin and liver iron concentration. Multislice multiecho T2*

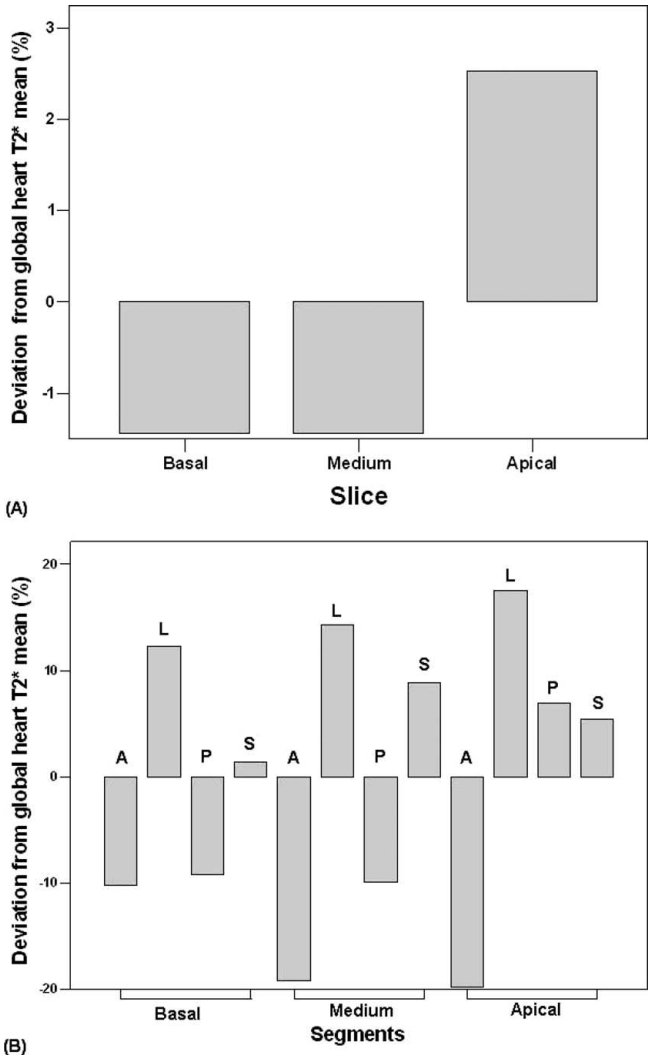

FIG. 1.

MRI approach provides a non-invasive and reproducible way for assessing myocardial iron distribution which may play a role in clinical arena.

386. QRS DURATION IN THE PEDIATRIC PATIENT AFTER REPAIR OF TETRALOGY OF FALLOT

Jason T. Su, DO, Michael D. Puchalski, MD, Lloyd Y. Tani, MD. ***University of Utah, Salt Lake City, UT, USA.***

Background: Pulmonary regurgitation and RV volume overload are common problems after repair of Tetralogy of Fallot (TOF) and contribute to late morbidity and mortality. Recent studies in adults have shown that increased ECG-derived QRS duration correlates with an increased RV size and an increased risk of life-threatening ventricular arrhythmias. In another study that included both adults and children, QRS duration correlated with increased age, RV end-diastolic volume (EDV) and end-systolic volume (ESV), RV mass, and pulmonary regurgitation. For cardiologists taking care of the children after repair of TOF, the usefulness of QRS duration remains unclear.

Purpose: The purpose of this study is to compare QRS duration to functional parameters measured by cardiac MRI in pediatric patients after TOF repair.

Methods: We reviewed our database to identify post-operative TOF patients who had an ECG within 3 months of a cardiac MRI. Left and right ventricular volumes, ejection fraction (EF), mass, and pulmonary regurgitation were determined by the standard techniques using steady-state free precession and phase contrast imaging on one of two available 1.5 T General Electric systems. Maximum QRS duration was measured from each patient's ECG. Correlation and multivariate regression analysis were performed with a p value of <0.05 being significant.

Results: A total of 68 patients were identified. Of these, 53 patients (78%) were less than 19 years old (pediatric group). The mean age was 14.3 yrs (range, 1–32 yrs) for the entire group, and 11.4 yrs (range, 1–18 yrs) for the pediatric subset. For the entire group, QRS duration correlated significantly with RV EDV, RV ESV, indexed and non-indexed RV mass, and RV EF. However, for the pediatric group, there was no correlation between QRS duration and RV EDV, indexed RV EDV, or indexed RV mass. In the pediatric subset, QRS duration did correlate with RV ESV ($p = 0.026$, $r = 0.32$), non-indexed RV mass ($p = 0.016$, $r = 0.34$), LV ESV ($p = 0.017$, $r = 0.34$), and was inversely correlated with RV EF ($p = 0.018$, $r = -0.33$). In addition, RV EF significantly correlated with both LV EF ($p < 0.001$, $r = .46$) and LV EDV ($p = .009$, $r = 0.36$).

Conclusion: This study showed significant differences in the correlation of QRS duration and MRI parameters when comparing the pediatric subset to the entire group of patients with TOF. The lack of correlation with indexed RV EDV in the pediatric group suggests that QRS duration is not a good predictor of RV size for children, and suggests a multifactorial contribution to this ECG interval. Additionally, the strong correlation between the left and right ventricular ejection fractions suggests that ventricular-ventricular interaction may be underestimated in this subset of the pediatric population. These factors influencing QRS duration, ventricular interaction, and function in children after TOF warrants further investigation.

387. AORTIC REGURGITATION: QUANTIFICATION WITH CMR CAN PREDICT PATIENTS LIKELY TO UNDERGO AORTIC VALVE REPLACEMENT SURGERY

Saul G. Myerson, MRCP, Jane Francis, Stefan Neubauer, FRCP. ***Oxford University, Oxford, United Kingdom.***

Introduction: Quantifying aortic regurgitation is feasible with CMR. However, the usefulness of this information in determining clinical practice has not been addressed.

Purpose: This study seeks to examine whether quantifying aortic regurgitation and other accurate CMR parameters of LV

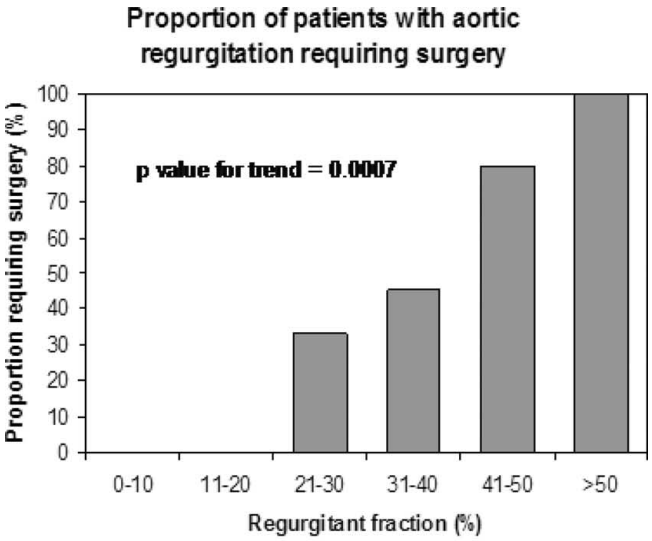

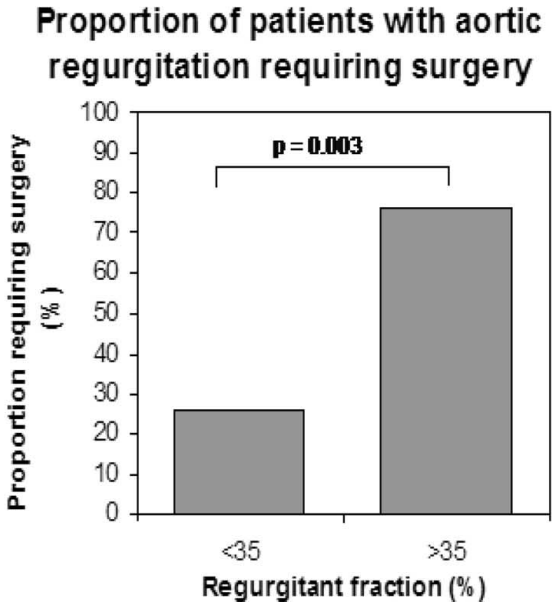

FIG. 1.

function provide useful information with which to potentially guide clinical practice.

Methods: Patients with isolated aortic regurgitation (AR) and without significant coronary artery disease (either clinically or angiographically) were identified from clinics and surgical operating lists (for aortic valve replacement). Thirty-six patients were identified and underwent CMR scanning, including LV volumetric and aortic flow mapping analysis, prior to any planned surgery. The conservatively-treated group were followed for up to two years to determine if the need for surgery arose. Characteristics of the surgical and conservatively treated groups were compared.

Results: Patients requiring surgery (n = 18) had a higher mean aortic regurgitant volume (80 vs 43 mLs; p = 0.0009), regurgitant fraction—AR volume/LV stroke volume × 100% (45 vs 28%; p = 0.0004), LV end-diastolic volume (308 vs 237 mLs; p = 0.008), LV end-systolic volume (132 vs 86 mLs; p = 0.009) and LV mass (293 vs 239 g; p = 0.03). Aortic regurgitant fraction proved to be the best discriminator between the surgical and conservative groups, with the likelihood of surgery increasing in line with regurgitant fraction (Fig. 1, p value for trend = 0.0007). A cut off at 35% regurgitant fraction best separated the two groups (Fig. 2), and 3 of the 6 patients initially treated conservatively with regurgitant fractions above this required surgery over the course of the study.

Conclusions: Quantification of aortic regurgitation with CMR is able to predict those patients who will ultimately undergo valve replacement surgery. A cut off value of 35% regurgitant fraction seems to be a threshold above which surgery is likely to be required in the near future.

388. SUBENDOCARDIAL VERSUS TRANSMURAL BLOOD FLOW INDEX IN PATIENTS WITH DIABETES MELLITUS: RELATIONSHIP TO CORONARY CALCIUM SCORES

Ola Akinboboye, MD, Yi Wang, DSc, Ken Nichols, PhD, Raphael Dim, MD, Kathy McGrath, RN, Margurite Roth, RN, William Schapiro, RT, Nathaniel Reichek, MD. ***St. Francis Hospital, Roslyn, NY, USA.***

Introduction: It has been suggested but not previously proven that the earliest manifestation of perfusion abnormalities in patients with diabetes mellitus (DM) occurs in the subendocardium. First pass perfusion imaging by MRI provides a unique opportunity to study subendocardial myocardial perfusion (MP) because of its high spatial resolution. We hypothesized that subendocardial MP is more impaired and has a stronger relationship with coronary calcification than subepicardial and transmural MP.

Methods: We studied 30 patients without history or symptoms of coronary artery disease, but who were diabetic (DM+, N = 24) or non-diabetic with metabolic syndrome (DM−, N = 6). MP was assessed during adenosine induced hyperemia (HMP) and at rest (RMP) with first pass MRI, using saturation recovery TurboFLASH imaging sequence: TR/TE/TI/FA = 2.9 ms/1.3 ms/90 ms/6°, data matrix 128 × 70, and voxel spatial resolution 3.5 × 1.9 × 8 mm.^{3} Contrast dose was 0.05 mmol/kg (Omniscan, Amersham) for each injection. The steepness of the first pass signal intensity curve's upslope, determined by a linear fit, normalized to blood pool upslope (relative upslope) was determined both at hyperemia and at rest in the inner 50% (subendocardium), outer 50% (subepicardium) and transmural regions using MASS software (Medis Imaging Systems Inc, Leiden, The Netherlands). All subjects also underwent EBCT on the same day for assessment of coronary calcification.

Results: Subendocardial HMP was significantly lower than subepicardial HMP and transmural HMP (12.1 ± 3.6 versus

13.5 ± 4.2 and versus 13.5 ± 3.8, paired t-test p = 0.007 and p = 0.007). Subendocardial HMP predicted calcium score with accuracy = 78 ± 9% and specificity = 100%, and sensitivity of = 63% (HMP threshold <11.13; calcium score threshold >7, based on ROC analysis). The strongest associations with calcium score were for subendocardial HMP (Fisher exact test p = 0.0006), while there were no significant associations with calcium score for subendocardial, subepicardial or transmural RMP values (Table).

	Subendocardial		Subepicardial		Transmural	
	HMP−	HMP+	HMP−	HMP+	HMP−	HMP+
−calcium score	11	0	8	3	8	3
+calcium score	7	12	5	14	6	13
P	0.0006		0.02		0.06	

Conclusion: Subendocardial flow is lower than subepicardial or transmural hyperemic flow in our studied population. Myocardial perfusion measured by CMR corresponded significantly to calcium scores, but only during stress, and most strongly for the subendocardium.

389. MRI IS SUPERIOR TO PET IN THE ASSESSMENT OF MYOCARDIAL VIABILITY IN PATIENTS WITH IMPAIRED LEFT VENTRICULAR FUNCTION

Peter Hunold, MD, Alexander Marcin, Thomas Schlosser, MD, Katja Brandt-Mainz, MD, Roman Pink, MD, Holger Eggebrecht, MD, Parwis Massoudy, MD, Jörg Barkhausen, MD. ***University Hospital, Essen, Germany.***

Introduction: The assessment of myocardial viability is important in coronary artery disease (CAD) patients with impaired left ventricular (LV) function in view of the prediction of functional recovery after revascularization. Late enhancement (LE) in contrast-enhanced MRI has been proven to accurately detect and quantify myocardial scar. [^{18}F]-FDG-PET as the method of reference in this respect lacks sufficient spatial resolution.

Purpose: To evaluate MRI and PET for the assessment of myocardial viability in CAD and to compare the technique's reliability in patient groups with different LV function states.

Methods: One hundred and five CAD patients (87 m/18 f; age, 61 ± 11 yrs) were examined by MRI and PET prior to CABG. The MRI (1.5T, Magnetom Sonata, Siemens) protocol consisted of a segmented TrueFISP functional study (TR, 3.0 ms; TE, 1.5 ms; FA, 60°; slice thickness, 8 mm) in long and contiguous short axis scans of the entire left ventricle. 8–15 min after application of 0.2 mmol/kg BW of Gd-DTPA

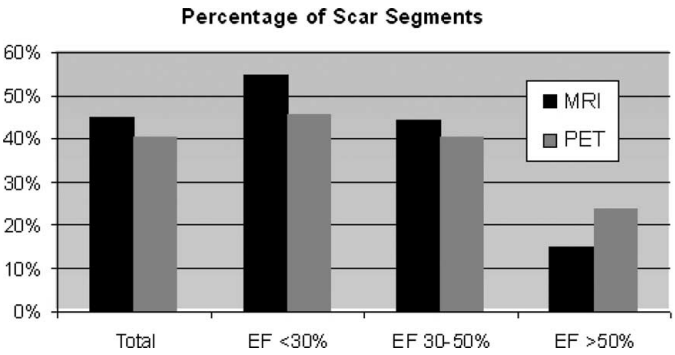

(Magnevist™, Schering), short axes were again scanned with a segmented inversion-recovery TurboFLASH sequence (TR, 8 ms; TE, 4 ms; TI, 200–240 ms) to detect LE. LE was classified on a 4-point scale (1 = no LE; 2 = subendocardial LE <50% of wall thickness; 3 = non-transmural LE >50%; 4 = transmural LE) based on a 6-segment model in all short axes. PET scans (ECAT HR+, Siemens) were performed following application of 370 MBq of [^{18}F]-FDG. The corresponding 8 mm short axis slices were reformatted from the 3D data set. FDG uptake in the same short axis segments was analysed using an analogous scale (1 = normal; 2 = reduced but >50% of maximum; 3 = reduced and <50% of maximum; 4 = no uptake). The detection of scar by MRI and PET and the quantification in terms of prediction of functional recovery were compared in patients with ejection fractions (EF) of <30%, 30–50%, and > 50%.

Results: Of 105 patients, 45, 44, and 16 had EF <30%, 30–50%, and >50%, respectively. A total of 5508 myocardial segments were analysed in MRI and PET separately in a blinded manner. Two thousand four hundred seventy-four of 5508 (45%) segments provided LE in MRI (score 2: 915, 3: 679, 4: 880), whereas PET revealed uptake deficits in 2220 (40%) segments (score 2: 1108, 3: 581, 4: 531). In the group of patients with EF <30%, MRI and PET detected any kind of scar (score 2, 3, and 4) in 1341 (55%) and 1116 (46%) of 2453 segments, respectively. In this group, functional recovery (score 1 and 2) was predicted in 1456 (66%) of 2453 segments by MRI vs. 1834 (75%) by PET. In patients with EF 30–50%, scar was detected by MRI and PET in 1022 (44%) and 927 (40%) of 2301 segments. Functional recovery was predicted in 1674 (72%) and 1852 (80%). In patients with EF >50%, scar was detected in 111 (15%) and 177 (23%) of 754 segments. Functional recovery was predicted in 687 (91%) and 710 (94%) of 754 segments by MRI and PET.

Conclusions: Contrast-enhanced MRI detects more scar in patients with severely and moderately impaired LV function than does PET. Therefore, less segments are predicted to recover function after revascularization by MRI, the MRI outlook is less optimistic. As known from literature, PET seems to overestimate "viability" also in this very important patient group.

390. MYOCARDIAL PERFUSION IMAGING AT 3 TESLA IN INFANTS AND CHILDREN WITH CONGENITAL HEART DISEASE: INITIAL EXPERIENCE

Michael Silberbach, MD, William J. Woodward, BS, Michael Jerosch-Herold, PhD, David J. Sahn, MD. ***Oregon Health & Science University, Portland, OR, USA.***

Introduction: Myocardial perfusion imaging is particularly challenging in infants and pediatric patients, due to limited spatial resolution, and the need to assess pre- and post-operatively right ventricular perfusion in patients with congenital heart disease. CMR perfusion imaging in pediatric patients at field strengths of 3 Tesla and higher, may address some of these current shortcomings, and also provide an alternative to nuclear perfusion scans, with their well-known drawbacks for pediatric patients.

Purpose: To evaluate the benefits of myocardial perfusion imaging at 3T in pediatric patients, both for LV and RV assessment.

Methods: Myocardial perfusion imaging was performed in patients (N = 6, age range: 3 months to 12 years), on a 3 Tesla CMR scanner (Philips Intera), using a gradient echo sequence (TR/TE/flip angle = 2.6/1.1 ms/ 20°; slice = 8 mm; 192 × 176 matrix; FOV = 240–320 mm; rect. FOV factor = 60–80%) with SENSE parallel imaging (mean speed-up of 1.7), and a 0.03 mmol/kg bolus of Gd-DTPA contrast (Omniscan) injected at 2 mL/s. Indications for the perfusion scans were post-operative assessment of arterial switch, anomalous origin of a coronary artery, and status post right ventriculotomy (post TET), and status post Kawasaki disease with aneurysms. A phased-array cardiac coil, or a dual-loop extremity coil were used for patients of ages greater and less than approx/years, respectively. For two patients a perfusion scan was performed during maximal hyperemia (iv adenosine for 4 minutes at 0.14 mg/min per kg BW). Images of delayed contrast enhancement of delayed contrast enhancement for assessment of viability were also acquired, following the perfusion scans, and injection of additional 0.1–0.15 mmol/kg of Gd-contrast.

Results: Figure 1 shows an example for a 3-month-old male who was born with complete transposition of the great arteries, poor left coronary flow after anatomic correction (arterial switch) and poor cardiac function (EF = 28%). The myocardial perfusion scan, with an in-plane spatial resolution of 1.1 × 1.6 mm, shows a defect (highlighted by arrows) in the anterior territory, with delayed contrast enhancement (DCE) seen at 15 minutes after perfusion scan. Similar results were obtained in all patients. No adverse side-effects were observed during iv. adenosine in an infant and a 12 year old patient. 3 slices could be imaged during every heart beat at rest with an average heart rate of 63 bpm, and 2 slices during hyperemia (HR = 120 bpm). The average peak contrast to noise (C:N) was (mean ± SD) 27 ± 14, with the highest C:N observed in infants, compared to older pediatric patients. Peak contrast enhancement (peak SI/baseline SI) with 0.04 mmol/kg of Gd-contrast was 86 ± 16% at rest, and 135 ± 34% for hyperemic perfusion.

Conclusions: This study demonstrates the feasibility of myocardial perfusion imaging at 3 Tesla in infants and pediatric patients, both at rest and during hyperemia, and with sufficient spatial resolution to depict sub-endocardial perfusion defects.

391. COMPARISON OF INVERSION RECOVERY STEADY-STATE FREE PRECESSION AND FAST LOW ANGLE SHOT SEQUENCES FOR 3D CORONARY MAGNETIC RESONANCE ANGIOGRAPHY

Kai-Uwe Waltering, Holger Eggebrecht, Kai Nassenstein, Thomas Schlosser, Peter Hunold, Jörg Barkhausen. ***University Hospital Essen, Essen, Germany.***

Introduction: For the diagnosis of coronary artery disease (CAD), invasive coronary artery angiography must still be considered the standard of reference. However, within the last 5 years, hard and software developments have made magnetic resonance coronary angiography (MRCA) feasible, but the sensitivity and specificity of current approaches remains insufficient for broad clinical use. Recent developments have launched different intravascular contrast agents, which have shown to improve the image quality and the diagnostic accuracy of MRCA. However, the search for the perfect imaging sequence for contrast enhanced MRCA is not yet over.

Purpose: The purpose of our study was to compare inversion-recovery steady state free precession (3D-IR-SSFP)

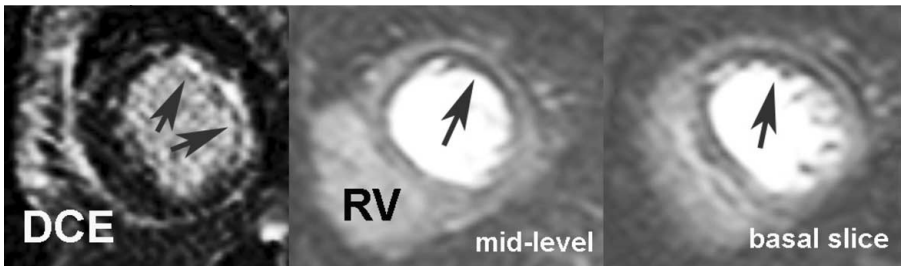

FIG. 1.

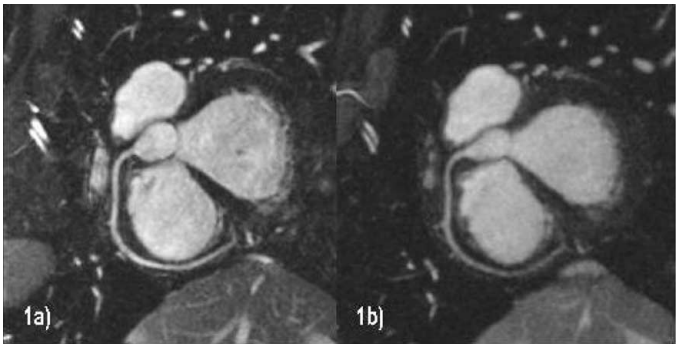

FIG. 1. MRCA images of the RCA show higher SNR and CNR values for SSFP (a) compared to FLASH (b).

and inversion recovery fast low angle shot (3D-IR-FLASH) sequences for contrast enhanced MRCA using an intravascular contrast agent.

Methods: Twenty-eight healthy volunteers (17 male, 11 female, mean age 28 ± 5 years) and 6 CAD patients (6 male, mean age 61 ± 9 years) were included in this study. All examinations were performed on a 1.5T MR scanner (Siemens Magnetom Sonata) in accordance with the regulations of the local ethics committee. In all subjects a dose of 0.150 mmol/kg body weight SH L 643A (Gadomer, Schering AG, Berlin, Germany) was injected. Thereafter, MRCA of all three mayor coronary arteries was performed using an IR-SSFP (TR 3.8 ms, TE 1.6 ms, FA 65°, 540 Hz/pixel bandwidth, voxel size 1.8–2.3 mm^3) sequence and an IR-FLASH sequence (TR 3.8 ms, TE 1.6 ms, FA 25°, 490 Hz/pixel bandwidth, voxel size 1.8–2.3 mm^3) in random order. For all sequences the inversion time was set to minimize the signal intensity of the myocardium and the acquisition time was adjusted to the subjects' breath-hold capabilities. Signal-to-noise-ratio (SNR) and contrast-to-noise-ratio (CNR) values were calculated based on signal intensity (SI) measurements in regions-of-interest (ROI) within the vessels, the myocardium and an artefact-free area outside the subjects. Image quality for the proximal and middle coronary segments was assessed based on a 5-point scale ranging from 1 = excellent, 2 = good, 3 = equivocal, 4 = poor to 5 = non-diagnostic.

Results: The mean acquisition time was comparable for both sequences (39.5 ± 8.2 s for FLASH versus 38.8 ± 4.7 s for SSFP). The mean image quality score for SSFP MRCA was higher compared to FLASH sequences (2.6 ± 1.1 versus 3.3 ± 1.0); Fig. 1. The signal intensity measurements showed higher SNR and CNR values for SSFP imaging (SNR blood pool: 6.6 ± 1.7 versus 6.1 ± 1.5; CNR 5.2 ± 1.7 versus 4.9 ± 1.4; Fig. 2).

Conclusions: Although hard- and software developments have dramatically improved image quality of MRCA within the last three years, limited signal to noise and contrast to noise ratios are still an issue. Several studies have shown that intravascular contrast agents can help to overcome these limitations. However, different sequences are currently available for contrast enhanced MRCA, which have not been compared so far. Following injection of extracellular contrast agents, SNR and CNR rapidly decrease due to the short plasma half-life time. Therefore intravascular compounds with constant T1 times of blood and myocardium over several minutes are a prerequisite for the comparison of different breath-hold sequences for contrast-enhanced MRCA. Our results show an overall improved image quality for IR-SSFP sequences and therefore we recommend this technique for contrast enhanced MRCA.

392. THE REGURGITANT JET AREA ON STEADY STATE FREE PRECESSION CORRELATES WITH AORTIC REGURGITATION REGURGITATANT VOLUME

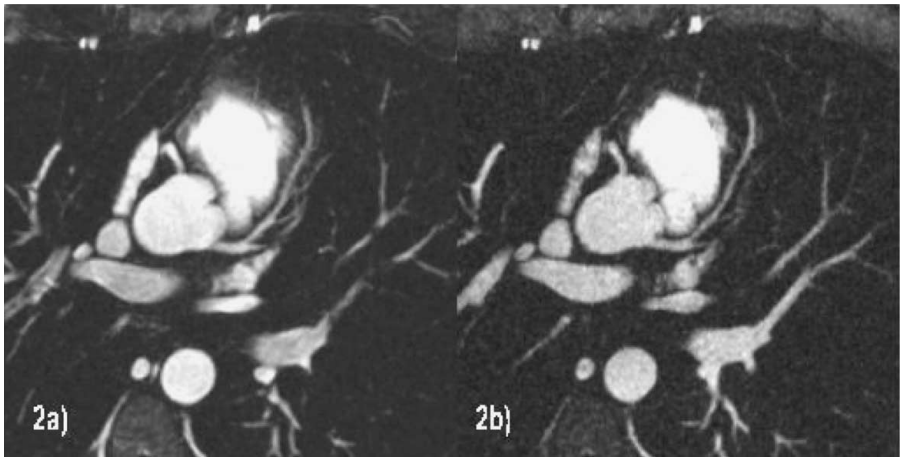

FIG. 2. Improved image quality of SSFP MRCA (a) compared to FLASH (b). Side branches of the LAD can better be delineated on the SSFP image.

Vijayasree Kudithipudi, MD, Rajan D. Bhatt, MD, MBA, Jose Gonzales, MD, Vincent L. Sorrell, MD. ***University of Arizona School of Medicine, Tucson, AZ, USA.***

Background: Most common technique used for diagnosing the severity of aortic regurgitation (AR) is Doppler echocardiography. 2D echo determined LV size is used for timing aortic valve surgery. Since cardiac MRI is the reference standard for LV cavity size determination, this may be a better tool to time aortic valve surgery. However, determination of AR is complex and time-consuming relative to 2D echo. This project was designed to investigate simpler CMR markers of AR severity.

Methods: Sixteen patients with AR underwent comprehensive, clinical cardiac MRI (1.5T GE Fiesta Scanner with advanced cardiac software). Steady state free precession (SSFP) imaging was performed per protocol to obtain short axis images and calculate the right and left ventricular stroke volumes. AR was determined as the difference of the LV-RV stroke volume (regurgitant volume). Patients with suboptimal images or significant MR were excluded. Additionally, the ratio of the diameter of signal loss from AR on SSFP imaging in left ventricular out flow tract (LVOT) to the diameter of the LVOT (jet width ratio) and the ratio of the area of the AR signal loss to the short axis LVOT area (jet area ratio) were determined. Using phase

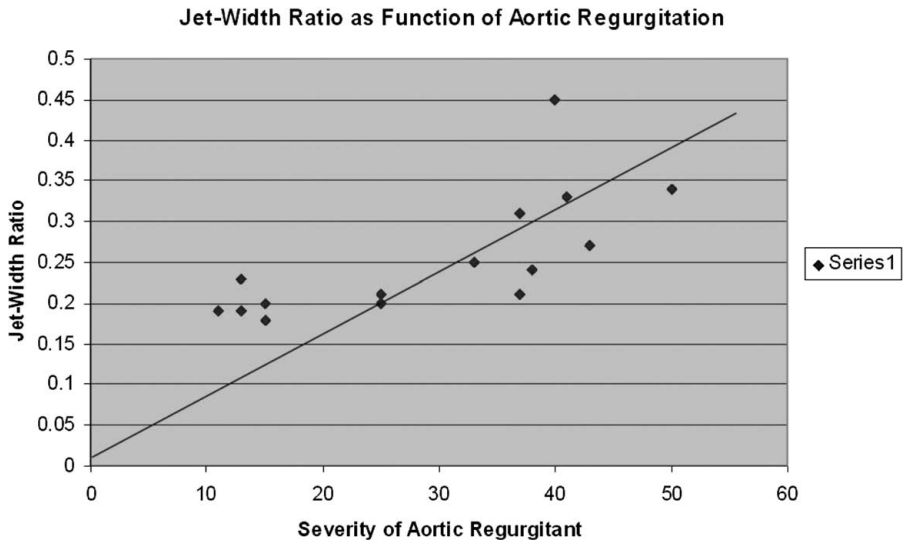

FIG. 1.

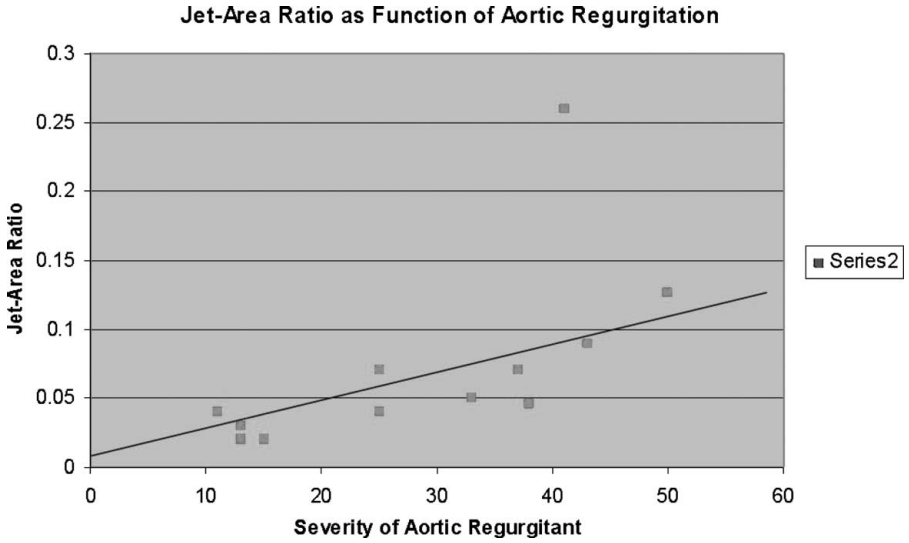

FIG. 2.

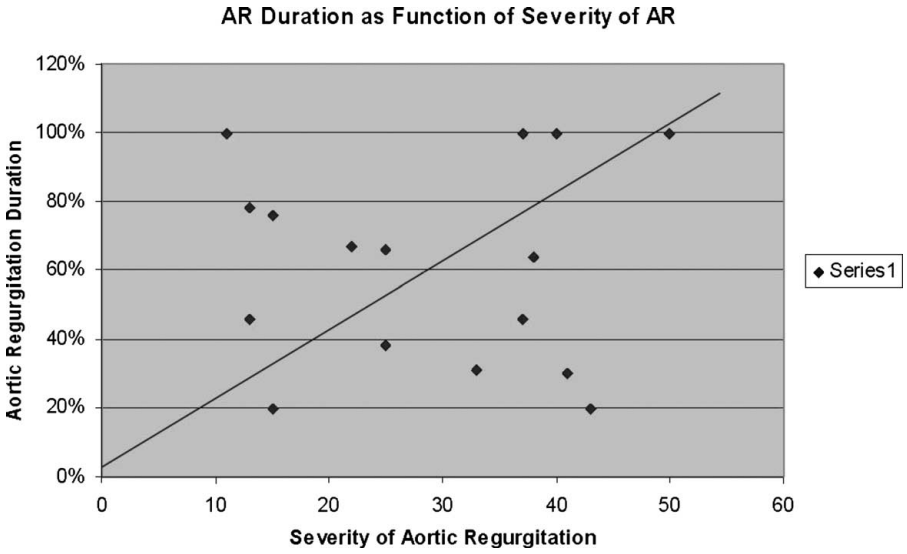

FIG. 3.

contrast velocity encoding of the ascending aorta, the duration of aortic regurgitation (flow volume/time curves) relative to the total duration of diastole was determined.

Results: Figures 1 and 2 show an excellent correlation of the regurgitant volume (RV) with the SSFP jet width ratio and jet area ratio, respectively. Figure 3 shows that there is no correlation between the RV and the duration of AR determined by phase contrast imaging.

Conclusion: The SSFP-determined jet area ratio has the best correlation with the volume-determined severity of AR and is a simple, rapidly acquired method.

393. PATTERN RECOGNITION WITH THE 17-SEGMENT MODEL ALLOWS IDENTIFICATION OF THE IRA WITH DELAYED-ENHANCEMENT MRI

Manesh Patel, MD,[1] Timothy S.E. Albert, MD,[2] Robert M. Judd, PhD,[2] Raymond J. Kim, MD.[2] [1]*Duke University, Hillsborough, NC, USA,* [2]*Duke University, Durham, NC, USA.*

Introduction: The American Heart Association (AHA) recommends a 17-segment model for myocardial analysis for consistency across different imaging modalities. While specific segments have been assigned to coronary arteries, data is limited on the correlation between the proposed segments and coronary artery territories.

Purpose: To determine the utility of the 17-segment model with delayed-enhancement MRI (DE-MRI) for identification of the infarct related artery (IRA).

Methods: We prospectively performed DE-MRI on 86 patients after an acute myocardial infarction (AMI) and cardiac catheterization (mean day 4). Each patient's DE-MRI was read blindly for the presence of myocardial infarction on a segmental basis using the 17-segment model. Each angiogram was read blindly to identify the IRA, defined as an artery with less than TIMI 3 flow and evidence of acute occlusive stenosis. A segmental analysis was performed by IRA to determine if >50% of involved segments were included in the AHA proposed scheme.

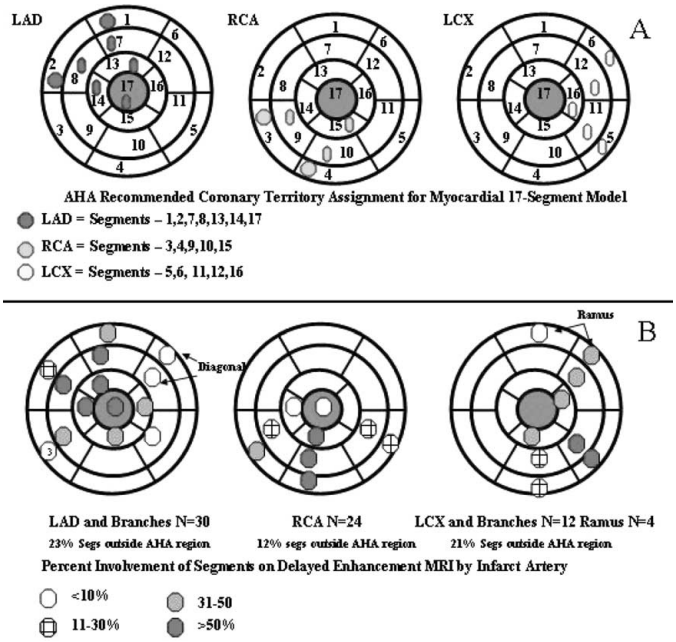

FIG. 1. Panel A demonstrates the AHA recommended coronary artery territories for the 17-segment model. Panel B demonstrates the results of masked road of DE-MRI 70 patients with initial acute myocarcial infarction and single identified infarct related artery (IRA). Although the majority of patients 93% (65/70) had over 50% of segments captured by the recommended AHA model, 12% of RCA, 21% of LCX, and 23% of LAD infarcted segments on DE-MRI were outside recommended AHA region. Primary branch vessels infarcts such as the diagonal and ramus artery account for some of the variability.

Results: Of the 86 AMI patients, 70 patients had angiograms where the IRA could be conclusively identified. The mean age of the group was 56 years, 71% were male, and 66% presented with ST-segment elevation on electrocardiogram. Although blinded analysis of IRA segments demonstrated that 65 (93%) of patients had greater than 50% of segments fall within the AHA scheme, 12% of RCA, 21% of LCX, and 23% of LAD infarcted segments on DE-MRI were outside recommended AHA region. The misidentified patients (N = 5) had infarctions of the first diagonal (N = 2) and ramus artery (N = 3) (Fig. 1).

Conclusion: Use of the pattern recognition with the 17-segment model and DE-MRI allows identification of the IRA. Branch vessels such as diagonal and ramus arteries lead to unique infarct patterns.

394. CMR ASSESSMENT OF REGIONAL BLOOD FLOW DISTRIBUTION DURING EXERCISE IN ELDERLY HEART FAILURE PATIENTS

W. Gregory Hundley, MD, Stephen Kritchevsky, PhD, Nicklas Barbara, PhD, Craig Hamilton, PhD, Xiaoyan Leng, PhD, Brubaker Peter, PhD, Dalane Kitzman, MD. ***Wake Forest University, Winston-Salem, NC, USA.***

Introduction: Reduced lower extremity blood flow during exercise contributes to exercise intolerance. Understanding the relationship between forward cardiac output and peripheral arterial blood flow during exercise would be useful for designing treatment strategies that could improve exercise tolerance. However, current assessment techniques are invasive and require ionizing radiation, and therefore ill-suited for normal subjects or serial evaluations during interventions.

Purpose: Therefore, we sought to design a cardiovascular magnetic resonance (CMR) imaging technique to measure cardiac output (thoracic aorta) and peripheral arterial blood flow (femoral artery) in elderly patients with and without congestive heart failure (CHF) during bicycle exercise.

Methods: We studied 13 healthy/normal (NML) persons (6 men/7 women weighing 77 ± 10 kg, aged 60–78 years) and 13 individuals with CHF (6 men/7 women weighing 76 + 16 kg, aged 55–82 years). Potential participants with obstructive or restrictive lung disease, renal insufficiency, peripheral arterial disease, or a contraindication to CMR were excluded. Exercise tolerance was assessed by measuring peak exercise oxygen consumption with expired gas analysis during maximal bicycle ergometry. Within 1 week, subjects underwent CMR for measurement of blood flow in the central aorta and superficial femoral artery before and after exercise (30% of maximal capacity) on an electronically braked bike attached to the end of the CMR table. CMR blood flow measures were acquired using phase-contrast CMR with a 30 cm FOV (aorta) or 16 cm FOV (femoral artery), a 256 × 256 matrix, a temporal resolution of 40 msec, a 30° flip angle, and a VENC of 2 m/sec.

Results: CHF participants had reduced peak exercise oxygen consumption and workload compared to NML subjects: 16 ± 6 versus 12 ± 3 mL/kg/min, respectively ($p = 0.008$), and 1.1 ± 0.2 versus 0.7 ± 0.2 watts/g[W1], respectively ($p = 0.0003$). At rest and with stress, cardiac output in the descending thoracic aorta was similar in the 2 groups of participants: 3.4 ± 0.7 increasing to 5.0 ± 0.7 L/min in NMLs and 3.0 ± 1.0 increasing to 5.1 ± 1.0 L/min in CHFs (p = NS). Importantly however, compared to NMLs, blood flow in the femoral artery of CHFs did not augment to a similar degree: 0.2 + 0.1 increasing to 0.4 + 0.2 L/min in NMLs versus 0.2 + 0.1 increasing to 0.3 + 0.1 in CHFs ($p < 0.003$). The stress-rest difference in femoral flow between NMLs and CHFs was correlated with peak exercise oxygen consupmption ($r = 0.52$; $p = 0.008$) and this remained significant after adjustment for age and body size.

Conclusions: CMR provides a safe, feasible, noninvasive method for assessing both cardiac output and leg arterial blood flow during exercise in older healthy and impaired subjects. Preliminary data using this novel technique provide potentially important insights into the symptoms of severe exercise intolerance experienced by elderly CHF by suggesting that leg arterial blood flow may be inappropriately reduced compared to healthy individuals.

395. ACCELERATED WHOLE VOLUME MR ANGIOGRAPHY AT 3 TESLA

Robert R. Edelman, MD,[1] Wei Li, MD,[1] John Salanitri, MD,[1] Andres Carrillo, PhD,[2] Anthony Vu, PhD.[2] ***[1]Evanston Northwestern Healthcare/Northwestern University School of Medicine, Evanston, IL, USA, [2]GE Healthcare, Waukesha, WI, USA.***

Introduction: Contrast-enhanced magnetic resonance angiography (MRA) is well established as a valuable diagnostic tool for the evaluation of vascular disease. Although the vast majority of MRA studies have been performed at 1.5 tesla, there is growing interest in the use of 3 tesla systems because of the potential for a two-fold improvement in the signal-to-noise ratio as well as superior vascular enhancement with paramagnetic contrast agents. Whereas 3 tesla MRI systems have already shown promise for neurovascular MRA, the challenges for body MRA are different and formidable. Foremost is the four-fold greater level of power deposition at the higher field strength, which necessitates the use of longer TR or lower flip angles, thereby increasing scan time to an unacceptable degree or reducing vessel conspicuity.

Purpose: Traditional approaches for contrast-enhanced MRA use spatially-selective RF pulses to excite a thick slab of tissue. We have applied an entirely different approach using a combination of spatially non-selective RF excitation, k-space undersampling in conjunction with parallel imaging, and fat suppression to optimize contrast-enhanced MRA at 3 tesla.

Methods: A non-selective RF excitation of 100 microsecond duration was applied along with a sampling bandwidth of

FIG. 1. 65 year old with normal arteries. (a) Frontal projection of the abdominal aorta. (b) Lateral projection. Contrast-enhanced spatially non-selective MRA acquired at 3T using TR/TE/flip angle of 2.3/1.6/25 degrees, slice thickness of 1 mm after interpolation, field of view 30 cm, 192 × 320 matrix, asymmetric sampling in z, ASSET acceleration factor of two, fat suppression, breath-hold acquisition. *Note*: excellent depiction of all vessels including peripheral branches; no vessels were excluded from the acquired data.

125 kHz. For a flip angle of 25 degrees, the minimum TR/TE was 2.3 msec/0.6 msec within first level SAR limits. Typically, the 3D acquisition used 100–128 3D partitions, slice thickness of 2 mm before interpolation or 1 mm after interpolation, field of view of 30–34 cm and a 192 × 320 acquisition matrix (interpolated to a display matrix of 512 × 512). Asymmetric sampling with zero filling was applied in the slice-select direction. Parallel imaging (ASSET) was applied with an acceleration factor of two and an eight channel phased array torso coil. Typical scan time was 18–23 seconds. Timing of the acquisition was determined using a 2 cc test bolus.

Results: An example of a contrast-enhanced MRA study using this technique at 3 tesla is given in Fig. 1. Preliminary comparisons of MRA performed at 1.5 tesla and 3 tesla in healthy volunteers and patients show a marked improvement in image quality at 3 tesla using the non-selective technique. Moreover, setup time for the non-selective study was reduced, particularly for multi-station acquisitions, because the entire thickness of the body along with all the vessels was necessarily encompassed without the need for individual positioning of the imaging volumes.

Conclusions: The use of non-selective RF excitation in combination with k-space undersampling and fat suppression offers promise to improve the quality and ease of contrast-enhanced MRA at 3 tesla.

396. INFLUENCE OF HIGH MAGNETIC FIELD STRENGTHS AND PARALLEL ACQUISITION STRATEGIES ON IMAGE QUALITY IN CARDIAC 2D CINE MAGNETIC RESONANCE IMAGING: COMPARISON OF 1.5T VS. 3.0T.

Birgit Spors, MD,[1] Kerstin Schwinge, MD,[1] Patrick Freyhardt, MD,[1] Matthias Grothoff, MD,[1] Claudia Seibt, MD,[1] Ralph Noeske,[2] Thoralf Niendorf, PhD,[3] Roland Felix, MD,[1] Matthias Gutberlet, MD.[1] [1]***Charité, Campus Virchow Klinikum, Berlin, Germany,*** [2]***GE Health Care, Berlin, Germany,*** [3]***Radiology Department University Aachen, Aachen, Germany.***

Purpose: Examine signal-to-noise ratio (SNR), contrast-to-noise ratio (CNR) and image quality of cardiac CINE imaging at 1.5 and 3.0 Tesla.

Methods: Twenty volunteers underwent cardiac MRI examinations using a 1.5T and 3.0T scanner. Three different sets of breath-held, ECG-gated CINE imaging techniques were employed including (i) unaccelerated SSFP (steady state free precession), (ii) accelerated SSFP imaging and (iii) gradient echo based myocardial tagging.

Results: 2D CINE SSFP imaging at 3.0T revealed a SNR (103%) and CNR increase (19%) as compared to the results obtained at 1.5T. The SNR reduction in accelerated 2D CINE SSFP imaging was larger at 1.5T (37%) as compared to 3.0T (26%). The mean SNR/CNR increase at 3.0T obtained for the tagging sequence was 88% and 187%. At 3.0T the duration of the saturation bands persisted throughout the entire cardiac cycle. For comparison, the saturation bands were significantly diminished at 1.5T during enddiastole. For 2D CINE SSFP imaging no significant difference in the left ventricular volumetry and in the overall image quality was obtained. For myocardial tagging image quality was significantly improved at 3.0T.

Conclusions: The SNR reduction in accelerated SSFP imaging was overcompensated by the increase in the baseline SNR at 3.0T and did not result in an image quality degradation. 3.0T was highly beneficial for cardiac tagging techniques, which holds the promise to improve its diagnostic value.

397. USPIO IS A MAGNETIC RESONANCE DUAL CONTRAST AGENT ABLE TO IDENTIFY BOTH FIBROUS CAP AND MACROPHAGE BURDEN IN-VIVO IN CAROTID ATHEROMA: A TOOL FOR RISK STRATIFICATION

Simon P. Howarth, BM, BCh MRCS,[1] Rikin Trivedi, MRCS,[1] Jean U-King-Im, MRCS,[1] Martin J. Graves, MA,[1] Peter J. Kirkpatrick, FRCS (SN),[2] Jonathan Gillard, MD.[1] [1]***University Department of Radiology, Cambridge, United Kingdom,*** [2]***University Department of Neurosurgery, Cambridge, United Kingdom.***

Introduction: It is well described that "vulnerable" atheromatous plaque has a thin, fibrous cap and extensive lipid core with associated inflammation. This inflammation can be detected as areas of signal drop on high resolution MR imaging using a novel contrast medium, Sinerem, an Ultrasmall Super-Paramagnetic Iron Oxide (USPIO). Studies using USPIO have, thus far, not reported its additional T1 effect of enhancing fibrous cap.

Methods: Twenty patients with carotid stenosis (10 symptomatic, 10 asymptomatic) were imaged at 1.5T, pre and 36 hours post USPIO infusion. Images were anonomysed, plaque seen was manually segmented into quadrants (CMR tools, London) and focal regions of signal drop post contrast. Signal change was normalised to adjacent muscle.

Results: There were 9 males and 11 females and mean ages were 71 (symptomatics) and 73 (asymptomatics). Mean stenoses were 82% (symptomatics) and 72% (asymptomatics). Symptomatics had significantly more quadrants with signal drop post USPIO than asymptomatics (75% vs 32%, $p < 0.01$) and more focal regions of signal drop (0.68 vs 0.26 regions/image, $p < 0.01$). Asymptomatics had more quadrants with signal enhancement than symptomatics (68% vs 25%, $p < 0.05$).

Conclusions: Symptomatic plaques had more focal areas of signal drop than asymptomatic plaques, suggesting that they harboured a greater inflammatory burden. Asymptomatic plaques showed more enhancement than symptomatic plaques, suggesting thicker fibrous caps and greater stability, although some focal areas of signal drop were noted suggesting vulnerability. If validated by larger studies, USPIO may be a useful dual contrast medium, able to enhance risk stratification of patients with carotid stenosis, improving selection for intervention.

398. DIAGNOSIS OF ACUTE RIGHT VENTRICULAR INFARCTION: A COMPARISON OF ECHOCARDIOGRAPHY TO LATE-ENHANCEMENT MAGNETIC RESONANCE IMAGING

Andreas Kumar, MD,[1] Hassan Abdel-Aty, MD,[1] Ilka Kriedemann,[2] Jeanette Schulz-Menger, MD,[2] Michael Gross, MD,[2] Rainer Dietz, MD,[2] Matthias G. Friedrich, MD.[1] [1]***University of Calgary, Calgary, AB, Canada,*** [2]***Humboldt University, Berlin, Germany.***

Introduction: Right ventricular involvement can complicate acute inferior myocardial infarction, putting the patient at increased risk for acute phase mortality. Recent reports suggested that late enhancement cardiac magnetic resonance imaging (LE-CMR) can diagnose right ventricular infarction.

Purpose: To compare echocardiography to LE-CMR for the diagnosis of acute right ventricular infarction.

Methods: Patients presenting to the emergency room with the diagnosis of acute inferior myocardial infarction (meeting AHA infarction criteria with inferior lead ST-elevation) were prospectively included. All patients underwent an echocardiogram using a commercially available system (Acuson Sequoia, Siemens Medical, Erlangen Germany). The following parameters were assessed: RV free wall motion, interventricular septal motion, and right ventricular dilatation. The echocardiogram was rated positive when any one or more of these parameters showed abnormality. After successful reperfusion therapy, LE-CMR was performed in all patients using a commercially available 1.5 Tesla system (Sonata, Siemens Medical, Erlangen, Germany). In short axis views of the right ventricle, a LE-CMR sequence was applied (IR-GE, TR 7.1 ms, TE 3.1 ms, TI individualized to null remote myocardium at 200–300 ms). RV infarction was rated positive when the late enhancement zone extended from the inferior left ventricle into the right ventricular free wall. In a second step, RV infarction was quantified using a 12-segment model for the right ventricle. Patients with RV infarction were divided in two groups, one with small RV infarctions (involving four segments or less) and one with large infarctions (involving five segments or more). Qualitative as well as quantitative LE-CMR data were compared to echocardiography.

Results: Thirty-seven patients with acute inferior infarction were included (9 female, age 54 ± 11). LE-CMR detected right ventricular infarction in 21 patients, echocardiography was positive in six patients. Using LE-CMR as a standard of truth, echocardiography had a sensitivity of 24% and a specificity of 94% to detect right ventricular infarction. When patients with RV infarction as defined by LE-CMR were divided in large and small RV infarcts, echocardiography yielded a sensitivity of 0% to diagnose small RV infarcts (0/8) and a sensitivity of 38% to diagnose large infarcts (5/13).

Conclusion: Echocardiography has low sensitivity to diagnose RV infarctions defined by LE-CMR criteria, especially when the RV infarction is small.

399. RETROSPECTIVE DETERMINATION OF THE AREA AT RISK FOR REPERFUSED ACUTE MYOCARDIAL INFARCTION WITH T2-WEIGHTED CARDIAC MAGNETIC RESONANCE IMAGING: HISTOPATHOLOGICAL AND DENSE FUNCTIONAL VALIDATIONS OF ISCHEMIC MEMORY IMAGING

Anthony H. Aletras,[1] Gauri S. Tilak,[1] Alex Natanzon,[2] Li-Yueh Hsu,[1] Felix M. Gonzalez,[1] Robert F. Hoyt,[1] Andrew E. Arai.[1] [1]***National Institutes of Health, Bethesda, MD, USA,*** [2]***Mount Sinai School of Medicine, New York, NY, USA.***

Purpose: The aim of this paper was to determine whether edema imaging by T2-weighted CMR could be used as an 'ischemic memory' imaging tool for retrospectively delineating the hypoperfused area at risk in reperfused myocardial infarction. We hypothesized that the area at risk by microspheres during a transient occlusion would be of similar size to the T2 abnormality observed two days later and that the T2-weighted hyper-intense region would resolve and would show partial functional recovery after two months.

Methods and Results: Seventeen dogs underwent a 90 minute coronary artery occlusion followed by reperfusion. The area at risk, as measured with fluorescent microspheres ($n = 9$), was comparable to the size of the hyper-intense zone on T2-weighted images 2 days later ($41.3 \pm 2.7\%$ LV area vs. 43.4 ± 2.5, $p = \text{NS}$) but was significantly larger than the infarcted zone (25.4 ± 5.1, $p = 0.018$). Bland Altman analysis showed a bias of -2.1% LV area. To test if the hyper-intense myocardium on T2-weighted images would exhibit partial functional recovery over time, another 8 animals were imaged on day 2 and two months later with

DIR-FSE and systolic strain was mapped with DENSE (displacement encoding with stimulated echoes). Edema resolved and regional radial systolic strain partially improved from 4.9 ± 0.7 to 13.1 ± 1.5 ($p < 0.005$) over two months suggesting that the T2 abnormality consisted of both reversibly and irreversibly injured myocardium as expected for a partially infarcted area at risk.

Conclusions: The "ischemic memory" associated with edema allows T2-weighted CMR to delineate the area at risk 2 days after reperfused myocardial infarction.

400. IMPORTANCE OF RIGHT VENTRICULAR END-SYSTOLIC REGIONAL WALL STRESS IN IDIOPATHIC PULMONARY ARTERIAL HYPERTENSION: NOVEL MRI METHOD FOR ESTIMATION OF RIGHT VENTRICULAR WALL STRESS

Marcus Y. Chen, MD, David B. Badesch, MD, Norbert F. Voelkel, MD, Eugene E. Wolfel, MD, Bertron M. Groves, MD, Tatiana Tsvetkova, MD, Robert A. Quaife, MD ***University of Colorado Health Sciences Center, Denver, CO, USA.***

Background: Cardiac dysfunction in idiopathic pulmonary arterial hypertension (IPAH) is characterized by chamber dilation, ventricular hypertrophy and impaired systolic function. Studies in animal models and humans suggest that cardiac myocyte and ventricular chamber remodeling exhibit distinct phenotypic characteristics in response to increased afterload and wall stress. Techniques to serially and non-invasively assess right ventricular (RV) wall stress are limited. Therefore, we modified regional wall stress measurements of the left ventricle to assessments of RV free wall stress.

Objective: To characterize RV chamber size, end-diastolic volume (EDV), end-diastolic wall thickness (EDT), end-systolic RV wall stress (RVWS), RV myocardial mass, RV ejection fraction (RVEF), cardiac output (CO) and pulmonary artery systolic pressures (PAS) in human subjects with chronic heart failure from three different patient populations, severe idiopathic pulmonary arterial hypertension (IPAH, n = 14), after recent heart transplantation for idiopathic dilated cardiomyopathy (TX, n = 4) and normal controls (n = 4).

Methods: All subjects underwent single-breathhold, gated cine cardiac magnetic resonance imaging using 10 mm serial short-axis slices from 20 mm behind the tricuspid valve through the RV apex. From the mid RV short-axis slice at the end of the papillary muscles, the mid RV short axis radial lengths (originating from the center of the RV major and minor axis) and RV free wall thickness at end-diastole (EDT) at each radial point were obtained at 45 degree increments. RV free wall thickness and radial length in conjunction with RV systolic pressure measured by right heart catheterization were used to calculate regional RVWS. Standard measurements of RV EDV, mass, RVEF were obtained from short-axis oblique images using Simpson's technique. Routine measurements of CO and PAS were made from right-heart catheterization. Data were analyzed using unpaired t-test and linear regression methods.

	IPAH (n = 14)	IDC (n = 4)	p value
PAS (mmHg)	91.3 ± 24.6	22.7 ± 4.6	0.003
CO (L/min)	3.7 ± 0.3	4.2 ± 0.4	NS
RVEF	34.4 ± 9.3%	57.4 ± 3.8%	0.0002
EDV (ml)	131.9 ± 37.3	68.8 ± 26.0	0.006
EDT (mm)	0.85 ± 0.28	0.44 ± 0.16	0.01
Mass (g)	99.6 ± 43.3	47.0 ± 31.6	0.04
RVWS (kdynes/cm^2)	101.6 ± 54.1	17.3 ± 3.9	0.008

Results: There was no significant difference between normal controls and patients following heart transplantion (TX). RVWS was significantly elevated in the IPAH group as compared to controls ($p = 0.008$). RVWS also demonstrated an inverse correlation ($y = 0.535 - 0.002x$, $R = 0.79$, $p < 0.0001$) to RV systolic function as measured by RVEF. However, wall stress values did not correlate with PAS.

Conclusions: Application of this MRI method to estimate RV circumferential wall stress will likely improve our understanding of RV dysfunction in IPAH and describes a technique to assess the effects of different therapeutic interventions on RV function.

401. AUTOMATIC REFORMATTING OF 32-CHANNEL NON-ANGULATED CARDIAC VOLUMES

Nicholas M. I. Noble, PhD, MEng,[1] Vivek Muthurangu, BSc, MBCHB (hons),[2] Redha Boubertakh, PhD, MSc, BSc,[2] Richard Winkelmann, MSc, BSc,[3] Sanjeet Hedge, MBBS, MRCPCH,[2] Robert A. Johnson, MRCP, BM, BA,[2] Peter Börnert, PhD, MSc, BSc,[4] Reza S. Razavi, MD, MRCP, MRCPCM,[2] Derek L. G. Hill, PhD, MSc, BSc.[1] ***[1] University College London, London, United Kingdom, [2] King's College London, London, United Kingdom, [3] University of Karlsruhe, Hamburg, Germany, [4] Philips Medical Systems, Hamburg, Germany.***

Introduction: In this paper, we address two of the major obstacles to the uptake of cardiac MR as a high throughput diagnostic tool; the required presence of a highly skilled operator to identify scan planes, and the long scan duration. A typical exam for analysis of cardiac function contains short-axis, two-chamber and four-chamber images acquired during 6-8 breath-holds. We acquired non-angulated whole-heart volumes in a single breath-hold using SENSE acceleration on a 32-channel scanner. Two-chamber, four-chamber and short-axis images were subsequently created by automatically reformatting the non-angulated volumes. This approach has two benefits; firstly it reduces total scan time by reducing the number and duration of scans acquired; only one scan is obtained, secondly it removes the need for clinician interaction during scanning planning.

Methods: Nine healthy male volunteers (age 34 ± 6 years, weight 76 ± 7 kg) were imaged on a Philips Achieva 1.5T with 32 receive channels using a prototype 32-element thoracic

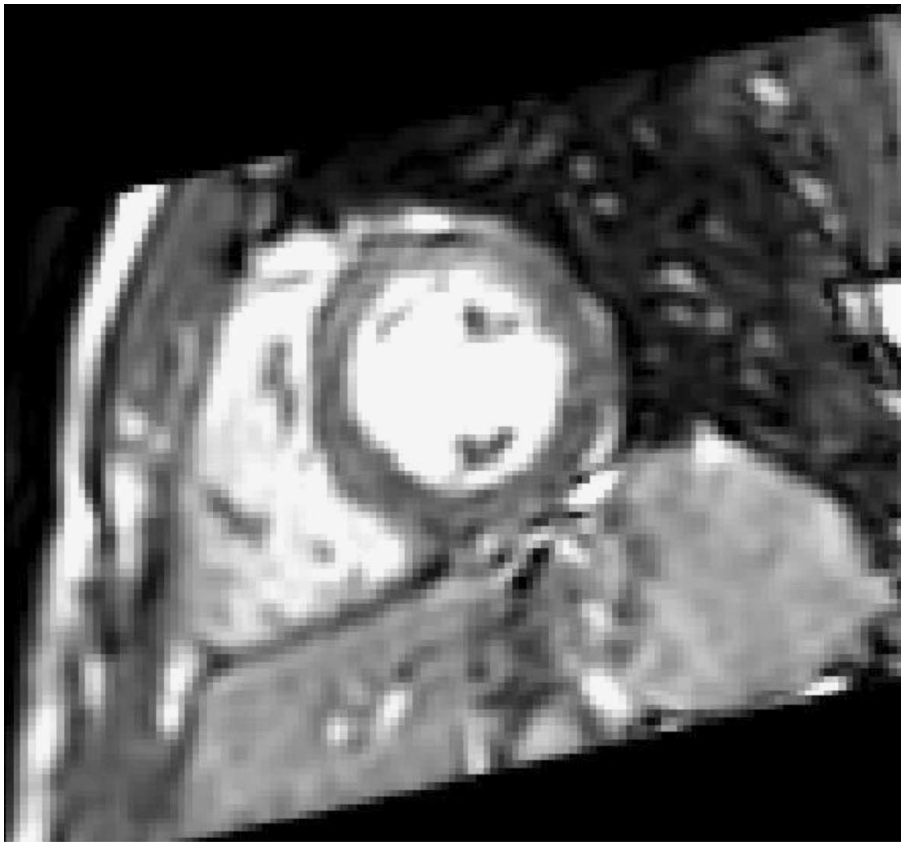

FIG. 1. Automatically identified views, showing the short axis (*top*), two-chamber (*middle*) and four-chamber (*bottom*).

coil. Non-angulated SSFP SENSE factor 4 half-Fourier 3D volumes were acquired during a single breath-hold. Reconstructed resolution was 1.52 × 1.52 × 1.50 mm with 20 cardiac phases. To enable subsequent comparison, the short-axis, two-chamber and four-chamber views were manually identified during real-time interactive scanning. To automatically identify the viewing planes, each end-diastolic non-angulated volume was registered to a 3D cadaver atlas of the heart. The atlas came from the visible human data set and had been manually segmented and labeled (http://voxel-man.de). An initial average orientation was used as a starting estimate for a rigid plus scaling registration using normalised mutual information as the similarity measure. Scan planes identified in the atlas were then transformed according to the registration results to determine the short-axis, two-chamber and four-chamber views. The non-angulated volumes were reformatted into these orientations using tri-linear interpolation. The results were evaluated both qualitatively and quantitatively. For the qualitative analysis, three clinicians with experience of reporting cardiac MR images were shown movies of both manually and automatically identified short-axis, two-chamber and four-chamber orientations in a random blinded manner. The observers were asked to identify whether the orientations were

FIG. 2. Bland-Altman plot of EDV.

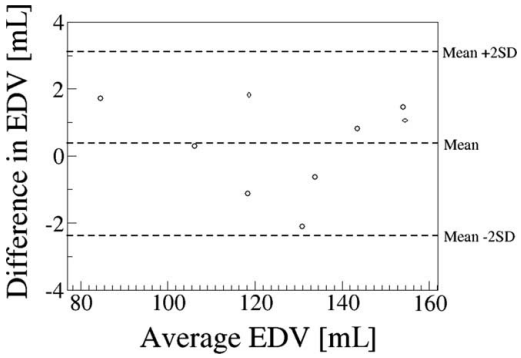

FIG. 3. Bland-Altman plot of ESV.

clinically acceptable (1) or not (0). A combined score of two or more indicated a consensus of acceptability. Quantitative analysis was performed by expert delineation in the short axis of the manually and automatically reformatted images to determine left ventricular End-Diastolic Volume (EDV) and End-Systolic Volume (ESV). These results were then assessed using Bland-Altman analysis.

Results: Figure 1 shows reformatted example images following automatic planning. View identification took 50 ± 23 s on a 2 GHz AMD Athlon64 3000+. All of the automatically reformatted images were judged to be clinically acceptable. Figure 2 and 3 show Bland Altman plots for EDV and ESV. The biases were 0.34 mL and -0.37 mL for EDV and ESV. The Bland-Altman limits of agreement were [-2.38,3.12] mL and [-3.73, 3.05] mL for EDV and ESV respectively. If 10 mL is taken as the minimum clinically significant change in EDV or ESV, we can say that EDVs and ESVs evaluated following automatic planning are equivalent to those evaluated following manual planning.

Conclusions: A new technique has been introduced to automatically reformat non-angulated cardiac volumes. Only a single cine volume need be acquired to obtain short-axis, two- and four-chamber views. This can be performed in a single breath-hold which considerably reduces total scan time. Our technique automatically identifies and reformats the volumes into conventional orientations, removing the need for skilled anatomical planning. It is quick, reliable, and there is no clinically significant difference in EDV or ESV when compared to manual planning.

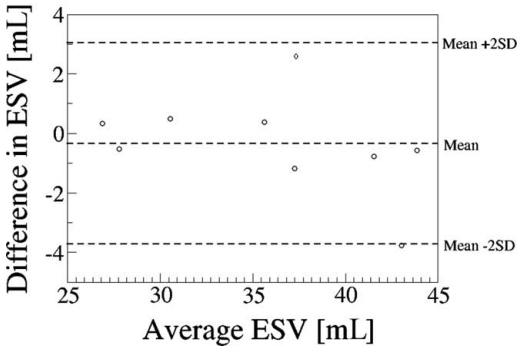

FIG. 4.

402. PROPAGATION OF MYOCARDIAL CONTOURS IN LONG AXIS CINE CARDIAC MAGNETIC RESONANCE IMAGES

Gilion Hautvast,[1] Steven Lobregt,[2] Marcel Breeuwer,[2] Frans Gerritsen.[1] [1]***University of Technology Eindhoven, Eindhoven, The Netherlands,*** [2]***Philips Medical Systems, Best, The Netherlands.***

Introduction: Long axis cine cardiac MRI acquisitions usually consist of 15–25 phases for both the 2 and 4 chamber views. These image sequences are used for quantification and diagnosis of the cardiac function. This requires delineation of the valve plane contour and the left ventricular endo- and epicardial contours in each image, involving up to 150 contours per patient. Therefore, computer assistance is desirable. Large partial volume effects near the papillary muscles due to the usually large acquisition slice thickness complicate fully automatic methods, which often provide many incorrect contours requiring elaborate user interaction.

Purpose: The purpose of our work is to reduce the required user interaction to only drawing initial contours at the end diastolic phase. These initial contours are then propagated automatically to all other phases. The resulting contours should reflect the preferences of the user, as specified in the initial manual contour, specifically near the papillary muscles.

Methods: To achieve our goal, we optimize a contour propagation algorithm for the propagation of cardiac contours in long axis images. The algorithm, previously developed for short axis images, propagates contours by repositioning contour vertices in order to optimize the match between gray-value profiles in subsequent phases, perpendicular to the contour. Consequently, constant gray-value neighborhoods are maintained as much as possible and the 'initial behavior' of the contour is copied, until each phase in the dataset is segmented. The performance of

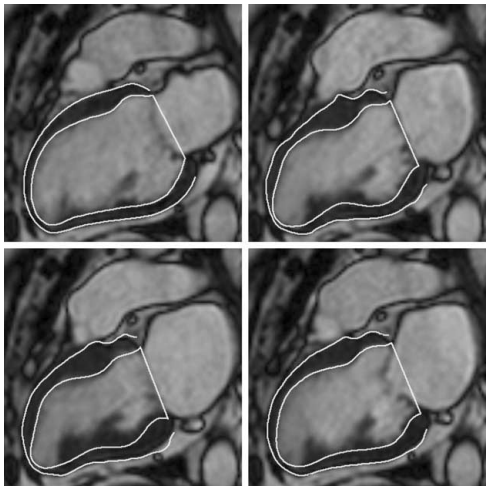

FIG. 1. Initialization (upper left) and propagated segmentations of long axis cardiac MR images.

the contour propagation depends on a number of parameters, for which an optimal configuration is determined in an extensive search of the parameter space, including 5040 parameter configurations. Proper definition of positioning errors allows Analysis of Variances to be used to determine main effects and interactions of the parameters. Ultimately, an optimal parameter configuration is concluded. The method is optimized and technically validated using 300 long axis ECG-triggered cine cardiac MR images, obtained in 7 acquisitions containing 25 phases. The images are acquired using the BTFE protocol with slice thickness 10.0 mm, FOV 350 × 350−410 × 410 mm; image size 256 × 256; flip angle 60°; TE 1.5–1.6 ms; TR 3.1–3.2 ms. We are grateful to Eike Nagel of the Deutsches Herzzentrum, Berlin, for supplying image data. Golden standard segmentations are obtained by averaging six manual expert segmentations. We observed an average positioning RMS inter-user-variability of 1.16 mm for the LV endocardium contour and 0.94 mm for the LV epicardium contour.

Results: After optimization, the average positioning RMS error observed throughout a complete heart cycle is 1.19 ± 0.68 mm for the LV endocardium contour, 0.84 ± 0.34 mm for the LV epicardium contour, which is within inter-user-variability of manual segmentation. The average angle between the propagated and reference valve plane is 5.7 ± 6.7 degrees. Within 1 second, an initial long axis segmentation is propagated to all phases.

Conclusions: The presented algorithm for automatic propagation of cardiac contours in long axis images demonstrates to be robust, fast and accurate for the delineation of LV endocardium, LV epicardium and the valve plane in 2 and 4 chamber long axis cine cardiac magnetic resonance images. Additionally, the analysis time is reduced significantly with respect to complete manual segmentation.

403. NEW PHARMACOKINETIC APPROACHES FOR QUANTIFYING BINDING OF $\alpha_v\beta_3$-INTEGRIN TARGETED NANOPARTICLES TO ATHEROSCLEROTIC VASA VASORUM

Anne M. Neubauer,[1] Patrick M. Winter, PhD,[1] Shelton D. Caruthers, PhD,[2] Ralph W. Fuhrhop,[1] Tood A. Williams,[1] J Stacy Allen,[1] Gregory A. Lanza, MD, PhD,[1] Samuel A. Wickline, MD.[1] [1]***Washington University, St. Louis, MO, USA,*** [2]***Philips Medical Systems, Best, The Netherlands.***

Introduction: Atherosclerosis is associated with upregulation of myriad biomarkers, including signals for angiogenesis, which is manifested as expansion of the vasa vasorum. Molecular imaging enables detection of these unique biomarkers based on specific binding of contrast agents targeted to the tissue of interest. We have developed a liquid perfluorocarbon nanoparticle that can be targeted to $\alpha_v\beta_3$-integrin, a protein associated with angiogenic endothelial cells. By incorporating paramagnetic contrast agents into the particle, MRI can register signals from these molecular beacons of angiogenesis. We have shown previously that signal quantification of the concentration of nanoparticles bound at sites of plaque angiogenesis can provide a handle on the extent and growth rate of early plaque (1). We now introduce new multicompartmental pharmacokinetic approaches for characterizing vasa vasorum imaging that could be useful for establishing optimum imaging times and dosing regimens.

Methods: Perfluorocarbon nanoparticles contained approximately 90,000 paramagnetic chelates (Gd-DTPA-BOA) and a peptidomimetic vitronectin antagonist targeted to the $\alpha_v\beta_3$-integrin (2). As previously described (3), thirteen male New Zealand white rabbits were fed a 1% cholesterol diet (n = 9) for ~80 days. Targeted (n = 6) or control (n = 4) nanoparticles were injected intravenously (0.5 ml/kg), and the aortas of all animals were imaged with a multislice T1-weighted spin echo imaging sequence at baseline and after 15, 60, 90 and 120 min, and at 24 hours. MRI contrast enhancement was quantified with a MatLab program. Three control diet rabbits were dosed with 0.5 ml/kg of non-targeted nanoparticles, and blood samples were analyzed at several timepoints for gadolinium content with a Bruker MiniSpec spectrometer. The data from these two experiments were used as an input to the ADAPT II software (Biomedical Simulations Resource, Los Angeles, CA) for multicompartmental pharmacokinetic analysis (4).

Results: A two-compartment pharmacokinetic (1: blood, and 2:peripheral) model was used to analyze the blood concentration over time in the normal animals, resulting in good agreement with the data (R^2 of 0.974). The parameters derived are given in the Fig. 1 (left). Next, to model the effect of the nanoparticle targeting to vasa vasorum, MRI signal enhancement was converted to concentration of gadolinium with the use of previously published signal models[1] and used as a input to a 3 compartment model in which the vasa vasorum was treated as a third compartment. We made the reasonable assumptions that this compartment does not appreciably affect the kinetics of the other two, and our high avidity particles bind irreversibly to the $\alpha_v\beta_3$-integrins. Non-specific binding and passive transfer (parameters K_{13} and K_{31}) were quantified using data from rabbits given non-targeted particles, while targeting was modeled using the kinetic constants k_b*[R] (binding) and k_r (removal). The Fig. 1 below (right) shows the model-generated curves for the targeted and non-targeted data. The exact values of these kinetic constants can change under a variety of conditions including increased or decreased clearance. For instance, a decrease in K_e of 43% would lead to an increase in K_{31} and K_r of 30 and 70% respectively, illustrating modest sensitivity to exact input parameters.

Conclusions: We have shown that by modeling both targeted and non-targeted nanoparticles used for imaging angiogenesis, it is possible to noninvasively quantify kinetic processes that might dictate nanoparticle binding to atherosclerotic vasa vasorum with MRI. Although the model could be improved with more comprehensive data (timepoints between 2–24 hours and more animals) and additional estimates of clearance parameters, we surmise that this approach may allow pharmacodynamic characterization of targeted nanoparticle drug delivery systems in the near future.

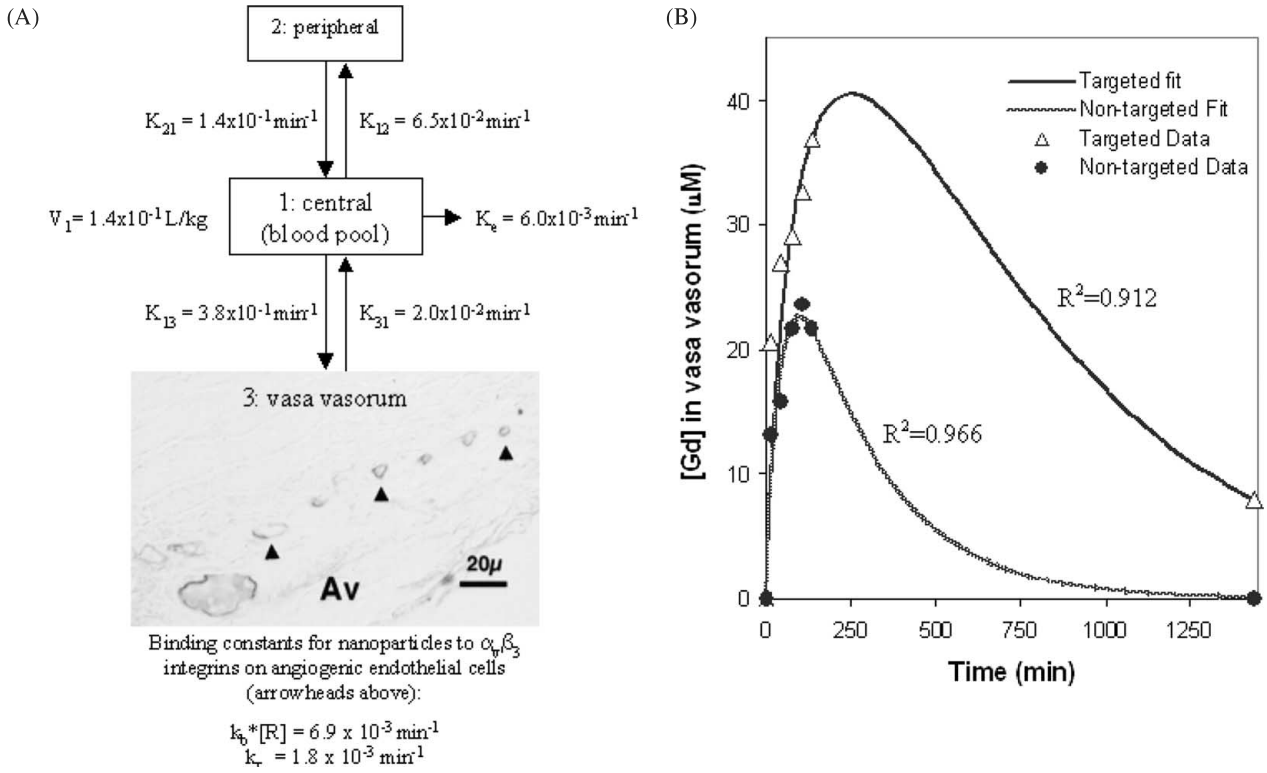

FIG. 1.

REFERENCES

1. Morawski, et al. Magn Reson Med, 2004;51:480–486.
2. Lanza, et al. Circulation, 1996;94:3334–3340.
3. Winter, et al. Circulation, 2003;108:2270–2274.
4. D'Argenio, et al. Computer Programs in Biomedicine, 1979;9:115–1134.

404. GADOFLUORINE M BASED IN-VIVO MRI FOR ATHEROSCLEROTIC PLAQUE DETECTION IN APOLIPOPROTEIN E KNOCKOUT MICE: COMPARISON OF MRI AND CONFOCAL MICROSCOPY FOR ASSESSMENT OF CONTRAST ENHANCEMENT MECHANISM

Esad Vucic, MD,[1] Juan Gilberto Aguinaldo, MD,[1] Marc Sirol, MD,[1] Vardan Amirbekian,[1] Joerg Meding,[2] Hanns-Joachim Weinmann,[2] Zahi A. Fayad, PhD.[1] [1]***Mount Sinai School of Medicine, New York, NY, USA,*** [2]***Schering AG, Berlin, Germany.***

Introduction: Gadofluorine M (Schering AG) as an MR contrast agent has been shown to improve atherosclerotic plaque detection in rabbit models of atherosclerosis. The purpose of this study was to determine the efficacy of Gadofluorine M for *in vivo* MRI of atherosclerotic plaque in Apolipoprotein E KO (ApoE KO) mice at several time points post-injection and to determine the underlying biological mechanism leading to contrast enhancement using confocal microscopy.

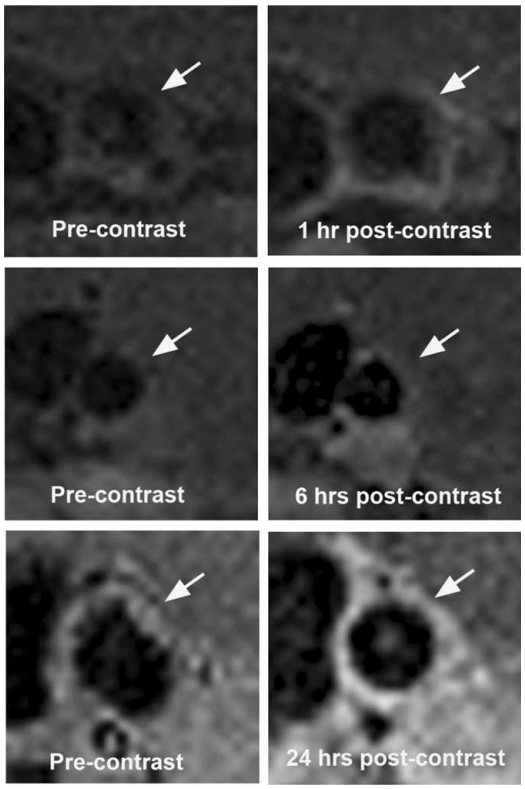

FIG. 1. Matched pre- and post contrast MR image of the abdominal aorta of ApoE KO mice at different time points.

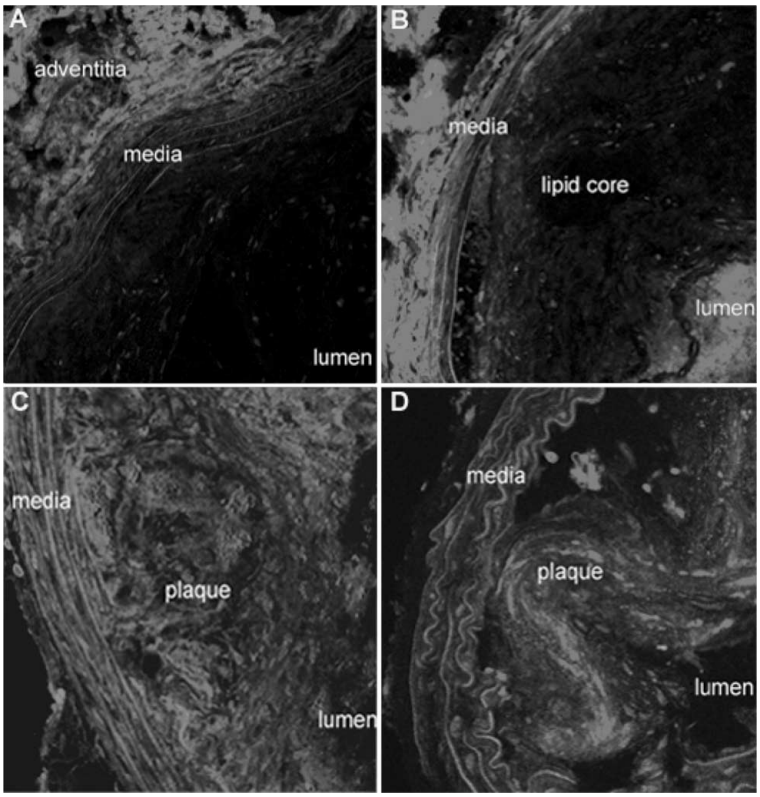

FIG. 2. Confocal images at different time points (A: 1 h, B: 2 h, C: 6 h and D: 24 h) post-injection with Gadoflourine-carbocyanine: red and DAPI nuclei stain: blue. Magnification: top row: 20×; bottom row: 40×.

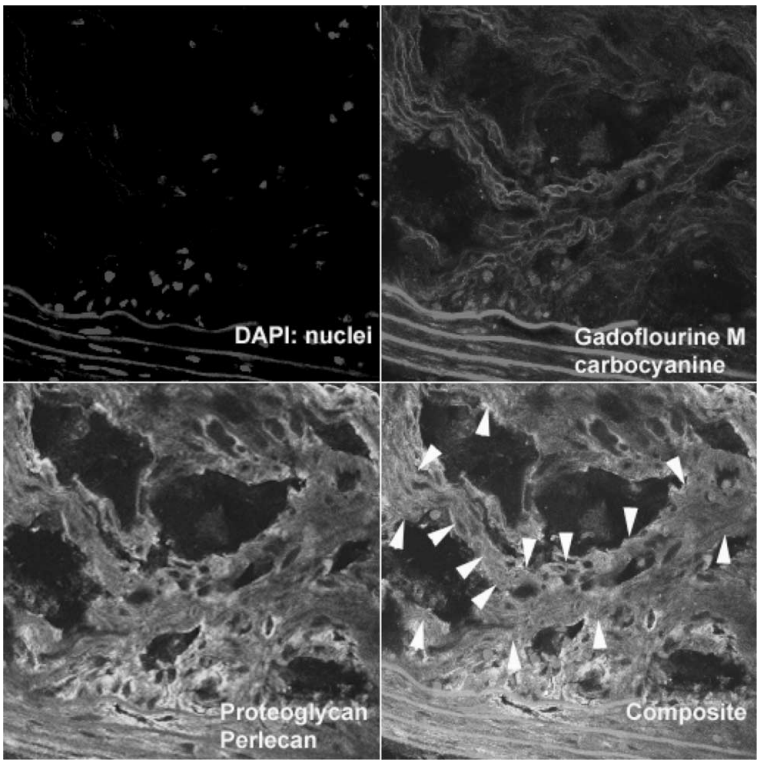

FIG. 3. Confocal Images of Atherosclerotic Plaque with Proteoglycan-Perlecan co-staining. Individual channels (red, green and blue) and composite image are shown. Perlecan co-staining reveals areas of association of Gadoflourine M with Perlecan on composite image (yellow-orange areas shown with arrowheads). Magnification 40×.

Methods: Fifteen-month-old ApoE KO mice (n = 6) and wild type (WT) (n = 6) underwent *in vivo* MRI of the abdominal aorta using a 9.4T MR system. Carbocyanine conjugated Gadofluorine M was injected in the tail vein (100 μmol/kg) and pre- and post-contrast enhanced MR at different time points: 1, 2, 6, 12, 24 and 48 hours using a T1W black blood sequence was performed. After MRI, the aortas were removed and fixed. Frozen sections were obtained and stained for tenascin, perlecan, smooth muscle actin, macrophages, and imaged using confocal microscopy for co-localization studies.

Results: Heterogeneous enhancement was seen in all ApoE KO mice after Gadofluorine M injection at different time points ($p < 0.001$) with significant increase in contrast-to-noise ratio (CNR) on post contrast enhanced images at 12, 24 and 48 hours post-injection. No enhancement was detected in the WT control group (Fig. 1). Confocal imaging demonstrated an increase in Gadofluorine M penetration from the adventitia after 1 hour through the media and intima after 2 to 6 hours (Fig. 2). Simultaneously, there was a delayed increase of Gadofluorine M penetration from the luminal side earliest seen after 2 hours (Fig. 2). After 24 to 48 hours, Gadofluorine M is associated with extracellular matrix proteins seen with perlecan staining and remained strictly extracellular (Fig. 3). No association was found with smooth muscle actin, and macrophages.

Conclusions: Gadofluorine M based contrast MRI improves plaque detection in ApoE KO mice. The enhancement of Gadofluorine M in atherosclerotic plaque probably originates at early time points from the adventitia, which may suggest increased neovascularization. A delayed, direct penetration of Gadofluorine M through the plaque itself is the second mechanism of enhancement in atherosclerotic plaque. Finally, the association with extracellular matrix, mainly arterial proteoglycans is demonstrated at later time points. All these temporal processes may explain the mechanism of Gadofluorine M contrast enhancement and retention in atherosclerotic plaque. Gadofluorine M may be useful in the delineation of plaque burden and molecular composition in vivo.

405. MORPHOLOGIC MRI IN SMALL INFANTS WITH CONGENITAL HEART DISEASE AT 1.5T USING A 3D TRUEFISP SEQUENCE

Michael Fenchel, MD, Gerald F. Greil, MD, Petros Martirosian, PhD, Ulrich Kramer, MD, Fritz Schick, MD, PhD, Claus D. Claussen, MD, Ludger Sieverding, MD, Stephan Miller, MD. ***Eberhard-Karls-University, Tuebingen, Germany.***

Introduction: For assessment and follow-up of patients with congenital heart disease (CHD) the importance of MR examinations has increased over the last several years. So far, mainly 2D spin-echo sequences have been used for the depiction of cardiac morphology. However, isotropic 3D datasets acquired in standardized planning procedures allow arbitrary reformatting of any desired imaging plane without loss of resolution. Presently, these 3D datasets yield only poor image quality in young patients ($\leq$6 years) and/or heart rates $>$100 bpm.

Purpose: Aim of the study was to optimize a 3D TrueFISP sequence for the assessment of cardiac morphology in newborns and small infants.

Methods: Eighteen patients (age 29.4 ± 26.6 months, 1 month to 76 months) were examined at 1.5T using a navigator-gated 3D TrueFISP sequence with T2 preparation triggered to the end-diastole (TE = 1.95–2.25 ms, FA = 110°, TE(T2prep) = 48 ms, acquisition window 40–60 ms). A constant steady-state preparation was used in order to increase the blood-myocardial contrast. Image quality was assessed by two observers in a consensus reading (1 = not diagnostic, 3 = diagnostic information present, 5 = excellent image quality).

Results: Acquisition time for the navigator-gated 3D sequence was 884 ± 263 seconds having a navigator efficiency of $75 \pm 15\%$. Although the heart rate of the patients was relatively high (110 ± 20 bpm, range 80–160 bpm) all 3D datasets yielded diagnostic image quality. Rating of the image quality yielded a mean value of 4.18 ± 0.73. The minimal achievable voxel size was 1 mm^3.

Conclusions: The presented 3D MR sequence allows the exact assessment of intra- and extracardiac morphology even in infancy and childhood in spite of high heart rates and small anatomical structures. The sequence provides high spatial resolution as well as high blood-myocardial contrast within an acceptable measurement time. Therefore, it may improve the diagnostic efficiency in the assessment of CHD in young patients.

406. IS RENAL MRI/MRA A USEFUL SCREENING TOOL FOR ALL AGE GROUPS IN THE WORKUP OF PATIENTS SUSPECTED TO HAVE RENOVASCULAR HYPERTENSION?

Rajiv Agarwal, MD,[1] Raja Muthupillai, PhD,[2] Scott Flamm, MD.[3] ***[1] University of Texas Health Science Center Houston, Houston, TX, USA, [2] Philips Medical Systems, Cleveland, OH, USA, [3] St. Luke's Episcopal Hospital/Texas Heart Institute, Houston, TX, USA.***

Table 1. Breakdown of RAS by age

Age group	Total patients in age group	Number of significant stenosis	Number of patients with significant stenosis	% patients with significant stenosis
11–20	2	0	0	0%
21–30	6	0	0	0%
31–40	21	0	0	0%
41–50	42	1	1	2.4%
51–60	63	7	6	9.5%
61–70	78	12	11	14.1%
71–80	91	43	32	35.2%
>80	36	25	18	50.0%
Total	339	88	68	20.1%

Table 2. Analysis based on age threshold

Age group	Total patients in age group	Number of patients with significant stenosis	% Patients with significant stenosis
≤50	71	1	1.4%
>50	268	67	25.0%
≤60	134	7	5.2%
>60	205	61	29.8
<70	212	18	8.5%
>70	127	50	39.4%
Male	165	40	24.2%
Female	174	28	16.1%

Introduction: Secondary hypertension (HTN) remains a common and treatable diagnosis. Patients in all age groups who display specific clinical clues to suggest a renovascular etiology of HTN require further workup. X-ray digital subtraction angiography is currently considered the gold standard; however, this technique is invasive with potential for significant vascular complications. Therefore, physicians are increasingly screening patients for renovascular HTN with renal MRI/MRA. The utility of renal MRI/MRA as a screening test for patients of different age groups suspected to have renovascular HTN is unknown.

Purpose: The aim of this study was to determine if renal MRI/MRA is a useful screening tool for all age groups in the workup of suspected renovascular HTN.

Methods: From January 2002 to January 2004, 339 patients (165 males, 174 females) underwent renal MRI/MRA on a 1.5T Philips MR system for evaluation of possible renovascular HTN. T1 and T2 weighted axial and coronal images were obtained pre and post gadolinium administration. In addition, a non-ECG gated, contrast enhanced MRA and 3D phase contrast MRA was performed. Main renal arteries were assessed for degree of stenosis by an experienced physician. Any stenosis reported as ≥ moderate was considered significant. Patients were grouped based on decade of life (Table 1).

Results: Of 339 patients who underwent renal MRI/MRA for suspected renovascular HTN, 68 patients (20.1%) had 88 significant renal artery stenosis (RAS) lesions. Only 1.4% of patients ≤50 years old had significant RAS (Table 2). However, 25% of patients >50 years old had significant RAS ($p < 0.01$). Furthermore, 29.8% of patients >60 years old, 39.3% of patients >70 years old, and 50.0% of patients >80 years old were discovered to have significant RAS. The incidence of significant RAS in males (24.2%) trended higher than in females (16.1%), although it was not statistically significant.

Conclusions: In patients ≤50 years of age and suspected to have renovascular HTN, the likelihood of encountering significant RAS by renal MRI/MRA is low. On the contrary, diagnosis of significant RAS is more frequently established in patients >50 years of age. Our study suggests that the current use of Renal MRI/MRA in suspected renovascular HTN is likely unwarranted in patients ≤50 years of age.

407. CONTRAST ENHANCED MR IMAGING OF THE HEART IN PATIENTS WITH END-STAGE RENAL DISEASE

Ulrich Kramer, MD, Sabine Wolf, MD, Michael Fenchel, MD, Teut Risler, MD, Claus D. Claussen, MD, Stephan Miller, MD. ***Universiy of Tuebingen, Tuebingen, Germany.***

Introduction: Cardiac disease has a high incidence in patients undergoing long term hemodialysis (HD). The survival rate is influenced by myocardial function, left ventricular (LV) ejection fraction (EF), severity of left ventricular dilatation (LVD) and hypertrophy (LVH) which can be accurately determined by MR imaging. Autopsy studies revealed that myocardial fibrosis is an additional factor for LV functional impairment.

Purpose: Purpose of this study was the evaluation of Gd-DTPA contrast enhanced MR imaging in correlation to myocardial morphology and function in order to detect fibrotic myocardial changes in patients with end-stage renal disease (ESRD).

Methods: Ten healthy volunteers and 25 patients with ESRD were examined at 1.5T (Magnetom Sonata, Siemens) including cine trueFISP 2D and contrast enhanced inversion-recovery prepared segmented turboFLASH sequences (0.15 mmol Gd-DTPA/kg). Based on a 16 segment model of the LV and 6 segment model of the RV an individual score was determined by segmentally rating myocardial contrast enhancement from 0 (= normal) to 3 (= markedly elevated) for each study subject. Contrast to noise (CNR) was measured in reference regions of interest (ROI's) and regions with visually detectable enhancement. Cardiodynamic parameters like EF, LV mass and end-diastolic volumes (EDV) were calculated based on the modified Simpson rule.

Results: Patchy, stripe like or focal endocardial contrast enhancement of the LV was present in 22/25 and of the RV in 10/25 patients (volunteers 6/10 and 2/10). The following parameters were found in patients/ volunteers: EDV 146 ± 47 mL/ 117 ± 38 mL ($p < 0.001$), myocardial mass 144 ± 46 g/ 92 ± 31 g ($p < 0.001$), mean rating of segmental enhancement 0.84 ± 0.98/ 0.30 ± 0.47 ($p < 0.001$), mean score 13.08 ± 8.53 (range 0–31)/ 4.60 ± 3.58 (range 0–9, $p < 0.001$). Markedly elevated CNR of post contrast myocardium was observed in patients (3.08 ± 2.77) compared to controls (1.2 ± 0.8, $p < 0.001$). Close correlation was found comparing EF and CNR ($r = 0.75$, $p < 0.0001$) and was inferior for enhancement score and EF ($r = 0.52$, $p < 0.008$).

Conclusions: Different types of contrast enhancement can be detected in patients with ESRD compared to control subjects. Referring to results from autopsy studies we suppose that contrast enhancement is consistent with focal and/ or diffuse myocardial fibrosis, respectively. Close correlation of CNR and EF suggests that the diffuse type is more relevant for cardiac functional impairment than the focal pattern.

408. THE NATURAL HISTORY OF CARDIOMYOPATHY IN THE *db/db* MOUSE

Patrick Yue, MD, Takayasu Arai, MD, Masahiro Terashima, MD, Michael McConnell, MD, MSEE, Philip S. Tsao, PhD, Phillip C. Yang, MD. ***Stanford University Medical Center, Stanford, CA, USA.***

Introduction: The *db/db* mouse develops severe obesity due to a defective leptin receptor. It is a well-established model of insulin-resistance diabetes mellitus. However, only limited studies of cardiac function in *db/db* mice using M-mode echocardiography have been performed to demonstrate evidence of contractile dysfunction (i.e. diabetic cardiomyopathy). These data provide few insights into the cardiac structure, function, and natural history of the development of diabetic cardiomyopathy.

Purpose: To use cardiovascular magnetic resonance (CMR) imaging to determine the longitudinal changes in cardiac anatomy and function in *db/db* mice over time.

Methods: CMR studies were performed on 6 female *db/db* mice and 4 heterozygous *db*/+ control animals at 5, 9, 13, and 17 weeks of age. Unity Inova console (Varian, Inc., Palo Alto, CA) controlling a 4.7T, 15 cm horizontal bore magnet (Oxford Instruments, Ltd., Oxford, UK) with GE Techron Gradients (12G/cm) and a volume coil with an inner diameter of 3.5 cm (Varian, Inc., Palo Alto, CA) was used. The ECG gating was optimized using 2 subcutaneous precordial leads with respiratory motion and body temperature monitoring (SA Instruments, Inc., Stony Brook, NY). LV function was evaluated using ECG-triggered cine sequence (TE 2.8-ms, TR 160-ms, FA 60°, FOV 3.0 cm^2, matrix 128 × 128, slice gap 0-mm, slice thickness 1.0-mm, 8 NEX, and 12 cardiac phases). Imaging plane was localized using scout images in an axial plane followed by double-oblique acquisition. The data were analyzed using MR Vision software (Winchester, MA). LV ejection fraction (LVEF), end-diastolic (LVED), and end-systolic (LVES) volumes were calculated by tracing the endocardial and epicardial borders in end-systole and -diastole. Cardiac index (CI), and stroke volume were then derived from these data. At each time point, body weights were measured. Additionally, tail-cuff blood pressures were obtained at 5 and 9 weeks.

Results: CMR of *db/db* mice and their controls revealed no notable qualitative differences in cardiac morphology, with the exception of a dramatically increased amount of pericardial fat (Fig. 1). At 5 and 9 weeks, there were no significant differences between the two groups in left ventricular end diastolic volume (LVEDV). However, LVEDV increased significantly in *db/db* mice relative to control over the next 8 weeks (Table 1). In addition, CI was consistently decreased relative to control at each time point and was significantly decreased compared to week 5. There were no significant differences in heart rate, blood pressure, or left ventricular ejection fraction at all time points.

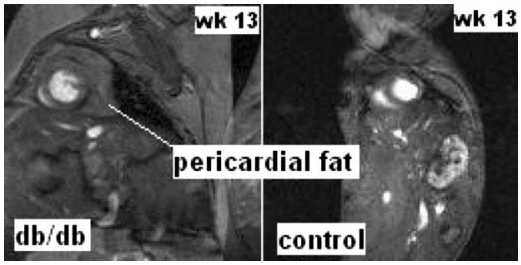

FIG. 1.

Conclusions: Consistent with echocardiographic studies, cardiac structure and function in *db/db* mice as assessed by CMR worsen over time, indicative of progressive ventricular remodeling. However, hemodynamic evidence of contractile dysfunction is manifest much earlier than previously appreciated. These data support the *db/db* mouse model as an ideal platform to study the pathogenetic mechanisms of diabetic cardiomyopathy and evaluate potential therapeutic modalities for this condition.

Table 1. Morphometric and functional data, db/db vs. control

	db/db week 5	Control week 5	*db/db* week 9	Control week 9	*db/db* week 13	Control week 13	*db/db* week 17	Control week 17
LVEDV (mL)	36.6	34.6	35.2	34.4	45.0*,†	34.4	49.2*,†	36.3
Body weight (g)	28.3*	17.0	37.2*,†	18.3	46.5*,†	19.3	43.2*,†	21.0
Cardiac index (mL/min/$g^{2/3}$)	136*	161	89*,†	152	79*,†	142	120*,†	161
Ejection fraction (%)	68.5	68.2	68.0	70.1	69.0	70.1	68.3	68.7

*$p < 0.05$ vs. control. †$p < 0.05$ vs. 5 weeks.

409. RAPID PROTOTYPING THREE-DIMENSIONAL MODEL BUILDING OF THE RIGHT VENTRICULAR OUTFLOW TRACK AND PULMONARY TRUNK FROM MAGNETIC RESONANCE DATA—CLINICAL UTILITY FOR PERCUTANEOUS PULMONARY VALVE IMPLANTATION

Silvia Schievano,[1] Francesco Migliavacca,[2] Louise Coats,[1] Sachin Khambadkone,[1] Wendy Norman,[1] John Deanfield,[1] Philipp Bonhoeffer,[1] Andrew M. Taylor.[1] ***[1] UCL Insitute of Child Health & Great Ormond Street Hospital for Children, London, United Kingdom, [2] Politecnico di Milano, Milan, Italy.***

Introduction: Percutaneous pulmonary valve implantation (PPVI) is a catheter-based technique for treating pulmonary valvular disease (Fig. 1). Patient selection for PPVI is dependent on the three-dimensional (3D) anatomy and size of the right ventricular outflow tract (RVOT) and pulmonary trunk (14–22 mm).

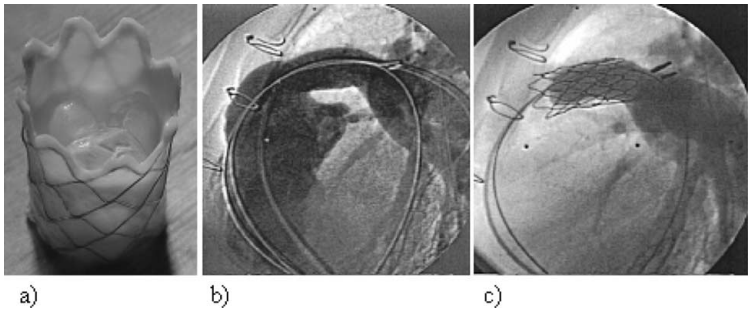

FIG. 1. a) Valved stent, and pulmonary angiograms b) before and c) after PPVI.

We use 3D magnetic resonance (MR) to plan these procedures; however, in borderline cases, interpretation of these images can be difficult.

Purpose: To describe the application of computer aided design (CAD) and rapid prototyping (RP) for building 3D models of the RVOT and pulmonary trunk from MR data, and to demonstrate the potential clinical utility of such models.

Methods: Gadolinium-enhanced 3D MR data from 6 phantoms and 12 patients was analysed. The 12 patients had repaired congenital heart disease, and were symptomatic and in need of conduit replacement (58% males, median age 20 years ranged between 9 and 39). The raw DICOM MR data was imported into CAD software and converted to standard steroelithography format and inputted into a RP system. A rigid, nylon model was then printed. Phantom volumes and pulmonary trunk dimensions were compared between the MR images and the models. For the 12 patients, PPVI was performed and the success of the PPVI noted. Two expert cardiologists, blinded to the result of PPVI, and not involved with the original decision to perform PPVI, were retrospectively presented the 3D MR images and models in random order, and were asked if they would attempt PPVI. These responses were compared with the outcomes of PPVI.

Results: 3D models were successfully built from all 18 MR datasets (Fig. 2). Five separate operators performed the CAD, with good agreement in the final STL files (mean variation 4%). The 3D models were an accurate representation of the MR data, with good agreement between the parameters measured from the MR data and from the models (phantom volumes $r = 0.97$, $p < 0.001$; patient dimensions $r = 0.97$, $p < 0.001$). The cardiologists made the correct decision, based on the known clinical outcome, respectively in 66% and 50% of the cases using conventional MR assessment and improved to 75% and 75%, with the availability of the 3D models.

Conclusions: 3D rapid prototyping is a novel, inexpensive method of model building that allows for complete appreciation of 3D anatomy. Such models can be used to select patients for PPVI more accurately than 3D MR images. Furthermore, the physical models of the RVOT and pulmonary trunk can be used as a trial for device implantation, to ensure that the device will 'fit' the implantation site prior to the actual procedure. The main limitation of the models that we have built to date is their lack of compliance: A property that has to be taken into account during the actual procedure. We are now in the process of building models from more compliant materials to address this issue.

410. QUANTIFICATION OF LEFT VENTRICULAR VOLUMES AND EJECTION FRACTION BY REAL-TIME THREE-DIMENSIONAL ECHOCARDIOGRAPHY: COMAPRISON WITH CARDIOVASCULAR MAGNETIC RESONANCE

Sandra Pujadas, Eduard Claver, Ruben Leta, Francesc Carreras, Guillem Pons-Llado. ***Hospital de la Santa Creu i Sant Pau, Barcelona, Spain.***

Background: Three-dimensional echocardiography (3DE) has become a useful tool for the assessment of left ventricular (LV) volumes and function, providing greater accuracy than

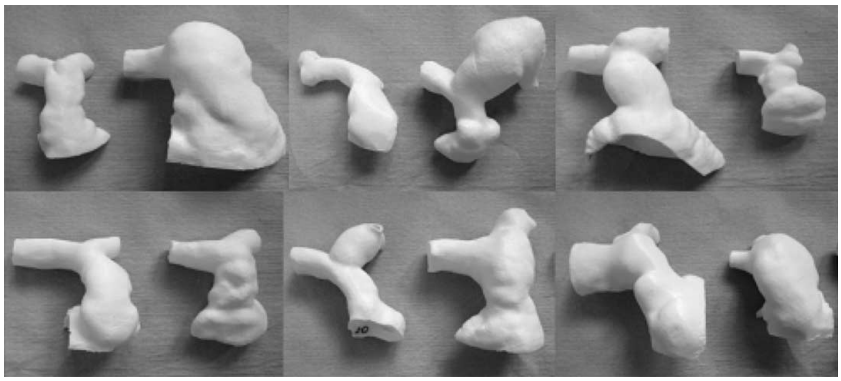

FIG. 2. RP models from the 12 patients.

Table 1.

	3DE		CMR		r		
	N: 43	N:32*	N:43	N:32*	N:43	N:32*	3DE interobserver variability (%)
EDV (mL)	132 ± 50	131 ± 44	155 ± 52	158 ± 54	0.71	0.79	6 (SE 5.4)
ESV (mL)	60 ± 32	59 ± 32	66 ± 39	71 ± 43	0.77	0.92	0.54 (SE 5.9)
EF (%)	57 ± 13	57 ± 14	59 ± 14	58 ± 15	0.74	0.84	4.5 (SE 2.2)

*Results considering only those 32 patients with adequate acoustic window for automatic border detection.

two-dimensional echocardiography. However, its reliability could be conditioned depending on the acoustic window of the patients.

Aim: We sought to analize the ability of 3DE in the assessment of LV volumes and ejection fraction (EF) in non selected patients, using cardiovascular magnetic resonance (CMR) as the gold standard technique.

Methods: Forty-seven patients (38 male; age 53 ± 18 years), in whom a CMR study (Philips Intera 1.5T) including a complete assessment of LV function (B-FFE multiphase-multislice sequence) was performed, were studied immediately after by 3DE (Philips Sonos 7500, Andover, MA). LV end-diastolic volume (EDV), LV end-systolic volume (ESV), and LV EF were calculated by both techniques by two independent observers blinded to the results of each other. 3DE images were postprocessed off-line using the software TomTec 4D LV Analysis® 1.2 (TomTec Imaging Systems, Germany). The semi-automatic border detection was used in all cases, even though it could be modified manually, according to the investigator criteria. The analysis using 3DE was performed in all cases by a second investigator blinded to the results of the first one and to those from the CMR. Results are expressed as mean ± standard deviation (SD), except for accuracy (mean ± 2 SD, following Bland-Altman analysis for the agreement). SE means standard error.

Results: In 43/47 patients (91%) acoustic window was judged as adequate. Four patients were excluded for extremely poor acoustic window. Results from the study group are shown in Table 1.

Conclusions: In non selected patients 3DE reaches CMR accuracy to estimate global LV EF. However, 3DE underestimates absolute LV volumes. When patients with poor acoustic window are excluded, correlations improve, because both systolic and diastolic LV volumes are systematically underestimated, resulting in a more precise determination of the LV EF.

411. LEFT ATRIAL APPENDAGE VOLUMES IN SINUS RHYTHM AND ATRIAL FIBRILLATION BY CARDIAC MAGNETIC RESONANCE IMAGING

Peter Bernhardt, Günter Pilz, Markus Klos, Eman Ali, Gerhard Bräuner, Berthold Höfling. ***Cardiac MRI at the Hospital Agatharied, Hausham, Munich, Germany.***

Background: Left atrial appendage (LAA) emptying velocities are an important predictor for cerebral embolism in patients with atrial fibrillation. Transesophageal echocardiography (TEE) is able to determine this risk factor accurately. Aims of our study were to assess LAA volumes and ejection fraction with cardiac magnetic resonance imaging (CMR) and to correlate with LAA velocities as quantified by TEE.

Methods: Twenty consecutive patients with atrial fibrillation scheduled for TEE prior to cardioversion were included to the study. Patients with sinus rhythm and TEE indication served as controls. All patients were scanned in a 1.5-T whole body scanner. Contiguous functional images covering the entire LAA in long axes orientation were performed. LAA ejection fraction was correlated to LAA velocities as determined by TEE.

Results: Fourteen patients with atrial fibrillation and 6 patients with sinus rhythm were included into our study. Patients with atrial fibrillation had significantly reduced LAA velocities as evaluated by TEE compared to patients with sinus rhythm (0.41 ± 0.19 m/s versus 0.80 ± 0.06 m/s, $p = 0.0001$). LAA velocities highly correlated with LAA ejection fraction as determined by CMR ($\kappa = 0.91$, $p < 0.0001$) in all patients, in patients with sinus rhythm ($\kappa = 0.89$, $p = 0.01$) and in patients with atrial fibrillation ($\kappa = 0.83$, $p < 0.0001$). Maximal LAA volumes correlated with LAA velocities and LAA ejection fraction, too ($p < 0.0001$, $p = 0.0002$, respectively).

Conclusion: CMR is able to determine LAA ejection fraction with a high correlation to LAA velocities. Maximal LAA volume is also highly correlated to LAA velocities and ejection fraction. Thus, CMR could detect patients with increased embolic risk due to low LAA velocities.

412. SHAPE COMPLEXITY OF THE AORTIC ROOT USING STEREOLOGY BASED CONTOUR GENERATION FROM MR IMAGES

Michael D. Taylor, MD, PhD, Colin J. McMahon, MBBS, Rajesh Krishnamurthy, MD, John P. Kovalchin, MD, Taylor Chung, MD, Giles Wesley Vick, III, MD, PhD. ***Baylor College of Medicine, Houston, TX, USA.***

Introduction: Aortic root dilation is an important cardiovascular complication of Marfan syndrome as well as other connective tissue syndromes and certain forms of congenital heart disease. Current methods for quantifying aortic root dilation, which typically employ single linear measurements with a potentially biased direct technique, may be inadequate for defining the complicated shape of the aortic root. Shape complexity can be calculated as a dimensionless parameter based on the surface area and volume properties of an object. For a two-dimensional

object such as a digital image of the aortic root, the complexity can be described by the parameter $\Omega = kP/A^{1/2}$, where $k = 1/2\pi$, P = perimeter, and A = area This function varies from 1 for perfect circle to ∞ for non-rectifiable structures.

Purpose: The purpose of this study was to evaluate the shape complexity of the aortic root in these patients from MR images. We employed an unbiased stereological technique to evaluate the MR images. We compared these measurements with standard two-dimensional echocardiographic assessments.

Methods: Eighteen patients (Marfan = 11, transposition status-post arterial switch = 4, congenital dilated root = 3) were evaluated with cardiac MR as part of their routine clinical management. The 20 patients underwent 28 MR studies. The MR images were acquired with a standard Philips 1.5 T MR scanner. Aortic root images were generated using a cine gradient echo sequence without breath-holding. The images were analyzed off-line using ImageJ (NIH, Bethesda, MD) and Matlab (Mathworks; Natick, MD). Short axis, end-systolic aortic root images perpendicular to the aorta at the level of the coronary arteries were selected for each patient. Three chords were drawn on each root to measure the distance between each aortic cusp. Next, contours describing the shape of the root were generated with an unbiased stereology algorithm. From these contours the following geometric parameters were extracted: area, perimeter, Feret's diameter (maximum diameter of an arbitrarily shaped contour), circularity and Ω. Echocardiographic aortic root dimensions were measured from the standard parasternal long axis view between the right and non-coronary cusp from two dimensional echocardiograms obtained within 2 months of the MRI study.

Results: All of the studies provided interpretable images. The MRI data showed that the right to left aortic cusp distance is consistently greater than the other two chords in virtually all patients (RL 89%, RN 15%, LN 7%, $p < 0.005$). In addition, Feret's diameter was consistently greater than any of the three user defined distances, although the difference was only 4%. There was excellent agreement between the MR measurement of the right to non-coronary cusp dimension compared to the echocardiography measurements with a correlation coefficient = 0.97 ($y = 0.99\times + 0.1$). The shape complexity parameter Ω was distinct for the three patient groups. Patients with Marfan syndrome had the most geometrically complex root shape compared to the other groups ($p < 0.01$). Upon multiple applications of the stereology contour algorithm and generation of Ω the intra-observer variance was <5% verifying this as a robust method of measuring aortic root diameter.

Conclusions: Magnetic resonance is well suited to follow aortic root dilation in pediatric patients. Aortic root contours can be drawn with little observer interaction with a novel unbiased stereological algorithm. Using these contours, multiple robust metrics describing both the shape complexity and size of the aortic root can be measured. These metrics can be employed for phenotypic analysis. Our data demonstrate that standard two-dimensional echocardiography systematically underestimates the true maximal dimension of the aortic root in a non-linear fashion due to the complex shape of the aortic root.

413. INTERACTIVE REAL TIME MULTI SLICE IMAGING

Sven Zuehlsdorff, PhD,[1] Peng Hu, MSc,[2] Peter Speier, PhD.[3] [1] ***Siemens Medical Solutions, Inc., Chicago, IL, USA,*** [2] ***University of Virginia, Charlottesville, VA, USA,*** [3] ***Siemens AG Medical Solutions, Erlangen, Germany.***

Introduction: In interventional MRI, interactive real time sequences are used to track devices such as catheters or needles (1). A multi-slice approach has been successfully applied to simultaneously visualize the anatomy of the target region and device using active receiver coils for intra-arterial contrast injections (2). Some interventional applications require updating a first central slice more frequently than outer slices. This is a common scenario during interventional procedures: A central slice can be used for device tracking, whereas outer slices can be used to visualize the anatomy. Furthermore, the procedure may require switching off the outer slices in real time update depending on the complexity of the anatomy and stage of the intervention. In this work, a generalized multi-slice sequence is presented that enables arbitrary slice acquisition schemes using the standard user interface of the scanner that can be changed in real time. The sequence was tested in a volunteer study.

Material and Methods: The multi-slice capability was integrated into an existing interactive sequence that provides

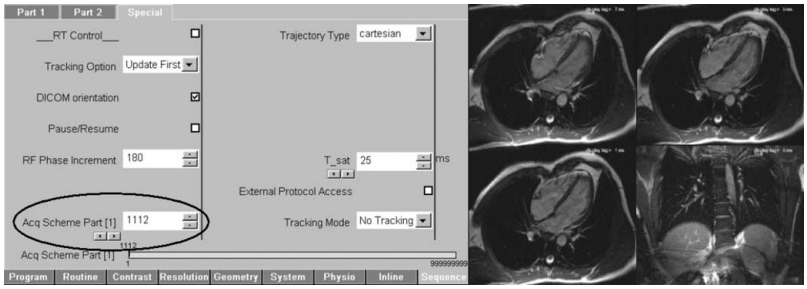

FIG. 1. Interactive multi-slice acquisition: User Interface and single shot images were acquired. Here the slice acquisition scheme '1112' was used that acquires three images of the first slice and one of the second slice in a continuous loop. Slice 1 represents the long axis view that is updated often. Slice 2 shows the diaphragm to monitor the respiratory motion and is updated less frequently.

dedicated functionality for interventional applications (3). A real time parameter was added to the standard user interface describing the slice acquisition scheme. Slice acquisition is defined as the basic building block of recurring slice order. A number, e.g. 112, is indicating a doubled update rate of slice 1 with respect of slice 2 (Fig. 1). Slice 2 could be switched off in real time by changing the building block from 112 to 1. A volunteer study was performed to demonstrate the multi-slice capability. In a first step, a series of long axis single shot images was acquired and the slice orientation was optimized interactively (TE/TR = 1.4/2.8 ms, 120 × 192 matrix, ~3 fps). In the second step, an additional slice was interactively switched on in real time. The slice acquisition scheme was selected to 1113 to acquire three long axis views and one image to monitor the respiratory motion using the diaphragm in a continuous loop. Slice orientation of both slices could be changed in real time using the standard user interface of the scanner.

Results: This study demonstrated the feasibility of interactive multi-slice imaging using arbitrary slice acquisition schemes (Fig. 1). This presented approach improves the workflow of interventional procedures since slices and corresponding updates rates can be changed in real time.

Discussion: The visualization of real time images with different orientations is a challenge. Using a mosaic format of the images compromises inherently 3D character of the images. Consequently, a platform for graphical MR scanner control (4) will be used that offers a dedicated user interface for interactive real time imaging.

REFERENCES

1. Guttman MA, et al. Magn Reson Med 2003;50:315-321.
2. Guttman MA, et al. Proc Intl Soc Mag Reson Med 2005;13:2169.
3. Zuehlsdorff S, et al. Proc Intl Soc Mag Reson Med 2005;13:2157.
4. Kirchberg KJ, et al. Proc Intl Soc Mag Reson Med 2005;13:2170.

414. LEFT VENTRICULAR REMODELING OCCURS IN MORBIDLY OBESE WOMEN: A CARDIOVASCULAR MAGNETIC RESONANCE (CMR) IMAGING STUDY

Kyle K. Pond, MD, Tom Hauser, MD, Kraig V. Kissinger, RT, Lois Goepfert, RN, Daniel Jones, MD, Benjamin Schneider, MD, Warren J. Manning, MD. ***Beth Israel Deaconess Medical Center, Boston, MA, USA.***

Introduction: Due to poor acoustic windows, few data are known regarding ventricular anatomy in the morbidly obese. In this population, volumetric CMR is a superior imaging technique (vs. echocardiography) for the evaluation of left ventricular (LV) morphology and function. Using CMR in men, morbid obesity has been associated with cardiac remodeling, but few data are known regarding obese women. We sought to use CMR to characterize LV anatomy and systolic function in this population.

Methods: Seventeen morbidly obese women (BMI 45 ± 5 kg/m^2; BSA 2.20 ± 0.14 m^2) were recruited from an obesity clinic. Cine steady-state free precession CMR was performed using contiguous short axis imaging. Data were compared to a control group of 79 women (BMI 25 ± 5 kg/m^2; BSA 1.69 ± 0.18 m^2) from the Framingham Heart Study offspring cohort.

Results: There was a significant increase in absolute LV wall thickness, volumes, and mass in the study population (all $p < 0.001$; Table 1) that persisted when values were indexed for height (all $p < 0.001$; Table). However, when indexed for body surface area, only LV volumes remained significantly larger in the morbidly obese group ($p < 0.0001$; Table).

Conclusions: The morbidly obese female manifests unique remodeling of the LV that can be quantified by CMR. It is uncertain if this remodeling is an adaptation to a larger body size or the result of other comorbidities (e.g. hypertension).

Table 1.

Variables	Control	Obese	Control/height	Obese/height	Control/BSA	Obese/BSA
Septal wall (cm)	8.9 ± 0.6	9.7 ± 0.6	5.5 ± 0.5	6.0 ± 0.4	5.3 ± 0.6	4.5 ± 0.4
Inferolateral wall (cm)	8.7 ± 0.6	9.3 ± 1.2	5.4 ± 0.4	5.7 ± 0.8	5.2 ± 0.6	4.2 ± 0.6
LV end-diastolic volume (mL)	84 ± 16	166 ± 37	52 ± 9	102 ± 22	50 ± 8	76 ± 14
LV end-systolic volume (mL)	25 ± 8	61 ± 28	16 ± 5	38 ± 17	15 ± 5	28 ± 12
LV mass (g)	103 ± 16	120 ± 22	64 ± 9	74 ± 13	61 ± 7	55 ± 8

All values presented as mean ± SD.

415. CORRELATION OF CARDIOVASCULAR RISK SCORES WITH MYOCARDIAL HIGH-ENERGY PHOSPHATE METABOLISM DETERMINED BY 31-PHOSPHOROUS CHEMICAL SHIFT IMAGING

Ralf Zwick, Gert Klug, Michael F. Schocke, Christian Wolf, Matthias Frick, Werner Jaschke, Otmar Pachinger, Bernhard Metzler. ***University Hospital Innsbruck, Innsbruck, Austria.***

Introduction: Preliminary data suggested a relationship between human myocardial, high-energy, phosphate metabolism and cardiovascular risk factors such as hypercholesterolemia or diabetes.

Purpose: Therefore we intended to prove its association to validated cardiovascular risk scores.

Methods: We compared established cardiovascular risk scores- PROCAM, SCORE and Framingham- with the myocardial high-energy phosphate metabolism (PCr-β-ATP ratios) determined by phosphorus-31 2-dimensional chemical shift imaging in ninety nine healthy, asymptomatic male patients (mean age 52.2 ± 8.8). All underwent echocardiography and cycle

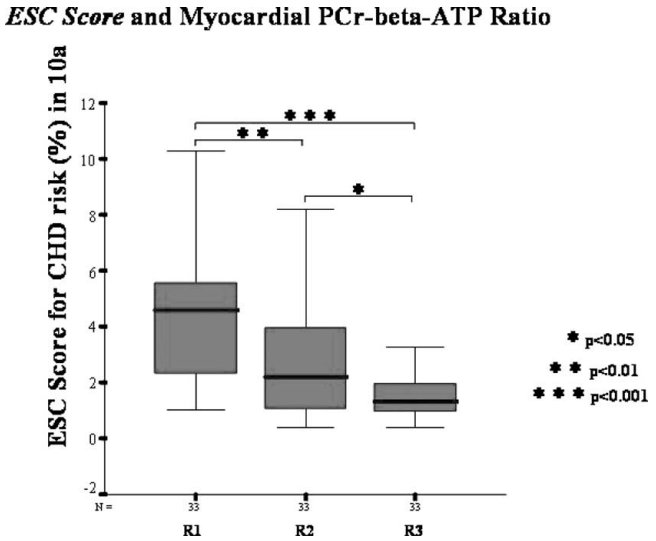

FIG. 1.

ergometry to exclude a latent coronary insufficiency and/or reduced left ventricular function.

Results: For all 3 algorithms, patients at highest estimated risk of events showed lower PCr-beta-ATP ratios than patients at lower risk ($P < 0.003$ to <0.001) (Fig. 1). Bivariat analysis revealed a negative linear relationship between myocardial PCr-beta-ATP ratios and the PROCAM ($P < 0.02$, $r = -0.251$), SCORE ($P < 0.001$, $r = -0.503$), and Framingham ($P < 0.001$, $r = -0.455$) score.

Conclusions: We are the first to show a correlation between the myocardial high-energy phosphate metabolism and established cardiovascular risk scores.

416. TWO WEEKS OF A HIGH-FAT, LOW-CARBOHYDRATE DIET REDUCES CARDIAC HIGH-ENERGY PHOSPHATE METABOLISM AND CAUSES DIASTOLIC DYSFUNCTION IN NORMAL SUBJECTS

Michaela Scheuermann-Freestone, MD,[1] Damian J. Tyler, PhD,[2] Jane M. Francis,[1] Gillian C. Watson,[2] Stefan Neubauer, MD,[1] Kieran Clarke, PhD.[2] [1]***OCMR, University of Oxford, Oxford, United Kingdom,*** [2]***University Laboratory of Physiology, University of Oxford, Oxford, United Kingdom.***

Introduction: In patients with heart failure, cardiac muscle high-energy phosphate metabolism and function are strong predictors of mortality and correlate negatively with circulating free fatty acid (FFA) concentrations. We hypothesised that increased FFA concentrations, caused by a high-fat, high-protein, low-carbohydrate (Atkins) diet, may alter cardiac energy metabolism in healthy subjects and may affect cardiac function.

Methods: We measured fasting circulating metabolites and cardiac high-energy phosphate metabolism (phosphocreatine PCr/ATP ratios) and function using magnetic resonance spectroscopy and imaging, respectively, in 19 healthy subjects before and after two weeks on a high-fat, low-carbohydrate diet and two weeks after returning to their normal diet. Circulating metabolites and cardiac PCr/ATP were also measured daily in a subgroup of 6 subjects for the first week of diet.

Results: Two weeks of the diet resulted in 3.2 ± 0.5 kg (4%) weight loss and a 1.9-fold increase in fasting plasma FFA concentrations from 0.41 ± 0.04 to 0.77 ± 0.12 mmol/L ($p < 0.01$). Cardiac PCr/ATP decreased from 2.34 ± 0.07 to 2.01 ± 0.20 ($p < 0.05$) after the first day of the diet, remained low throughout the diet and correlated negatively with plasma FFA concentrations ($r = -0.38$, $p < 0.01$). Left ventricular peak filling rate decreased from 90 ± 6 to 75 ± 4 ml/s ($p < 0.05$) after two weeks of diet, indicating diastolic dysfunction, and correlated positively with cardiac PCr/ATP. All metabolic and functional effects reversed after returning to a normal diet for two weeks.

Conclusion: A high-fat, low-carbohydrate diet increased plasma FFA concentrations, impaired cardiac high-energy phosphate metabolism and caused diastolic dysfunction within two weeks, suggesting that such a diet may have long-term detrimental effects on the heart.

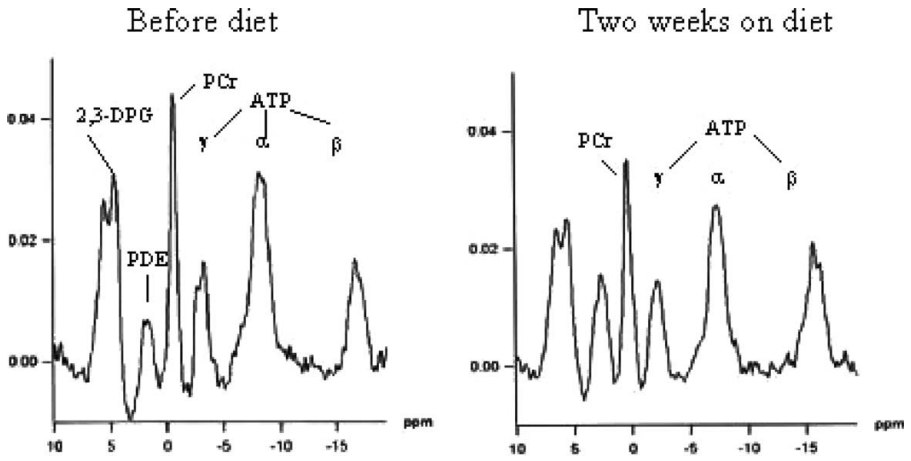

FIG. 1.

417. ALTERED CARDIAC HIGH-ENERGY PHOSPHATE METABOLISM AND ABNORMAL DIASTOLIC FUNCTION IN PATIENTS WITH OBSTRUCTIVE SLEEP APNOEA

Michaela Scheuermann-Freestone, MD,[1] Sophie West, MD,[2] Gillian C. Watson,[3] Damian J. Tyler, PhD,[3] Jane M. Francis,[1] John Stradling, MD,[2] Stefan Neubauer, MD,[1] Kieran Clarke, PhD.[3] [1]***OCMR, University of Oxford, Oxford, United Kingdom,*** [2]***Churchill Hospital, University of Oxford, Oxford, United Kingdom,*** [3]***University Laboratory of Physiology, University of Oxford, Oxford, United Kingdom.***

Introduction: Obstructive sleep apnoea (OSA) is associated with increased cardiovascular morbidity and mortality. We have found that abnormal cardiac function and energy metabolism correlate with free fatty acid levels in patients with heart failure, but it is unknown whether cardiac energetics or function are altered in patients with chronic OSA.

Methods: We measured fasting circulating metabolites and cardiac high-energy phosphate metabolism (phosphocreatine PCr/ATP ratios) and function using magnetic resonance (MR) spectroscopy and imaging, respectively, in 19 patients with chronic OSA and compared them with 15 age-, sex- and body mass-index matched control subjects.

Results: Fasting plasma concentrations of free fatty acids (FFA) were significantly increased from 0.37 ± 0.04 mmol/L in healthy control subjects to 0.51 ± 0.06 mmol/L in patients with chronic OSA ($p < 0.05$), without any changes in fasting plasma glucose or insulin concentrations. Cardiac PCr/ATP was significantly reduced, from 2.11 ± 0.10 to 1.77 ± 0.07, in patients with chronic OSA compared with healthy control subjects ($p = 0.01$), and correlated negatively with circulating concentrations of FFA ($r = -0.38$, $p < 0.05$). Left ventricular systolic function was preserved, but diastolic function was impaired in patients with chronic OSA compared with control subjects.

Conclusion: Obstructive sleep apnoea is associated with increased plasma FFA concentrations, reduced cardiac high-energy phosphate metabolism and diastolic dysfunction. These results suggest that the increased morbidity and mortality in OSA may be due to alterations in myocardial energetics caused by metabolic abnormalities.

418. IS ECHOCARDIOGRAPHY A SUFFICIENT SCREENING METHOD FOR DIAGNOSING MYOCARDIAL SCARRING? A PROSPECTIVE COMPARISON OF DELAYED ENHANCEMENT CARDIAC MAGNETIC RESONANCE IMAGING AND ECHOCARDIOGRAPHY

Heyder Omran, MD, PhD, David Hardung, MD, Karol Miszalski-Jamka, Christoph Hammerstingl, MD, Harald Schmidt, MD, Bernhard Saxler, Jan Schnapauff, Giso von der Recke. ***St. Marien-Hospital, Bonn, Germany.***

Introduction: Echocardiography is regarded the method of choice for screening for coronary heart disease and myocardial scarring. More recently, delayed enhancement cardiac magnetic resonance imaging (deCMR) has been demonstrated to provide very accurate imaging of even small subendocardial infarction by high contrast to noise ratio between infracted and normal myocardium.

Purpose: The aim of this study was to evaluate current echocardiographic parameters for diagnosing myocardial scarring as compared to deCMR.

Methods: The study was planned as a prospective study in a primary cardiac investigational centre. All consecutive patients referred for cardiac MRI for evaluation of coronary heart disease were included and investigated by deCMR and second harmonic echocardiography. The following echocardiographic parameters were regarded as indicative of myocardial scarring: wall thickness <7 mm, wall motion abnormalities, and increased echogenicity.

Results: Six hundred forty-five consecutive patients were included in this study. deCMR deteced myocardial scarring in 109 of those patients. Of the latter patients, 55 pts had transmural myocardial infarction, and 12 subendocardial (<25% wall thickness) infarction. The remaining patients had between 25 and 75% of wall thickness. Of patients with myocardial infarction echocardiography was feasible in 92%. A regional wall thickness <7 mm was found in 45 pts, increased echogenicity

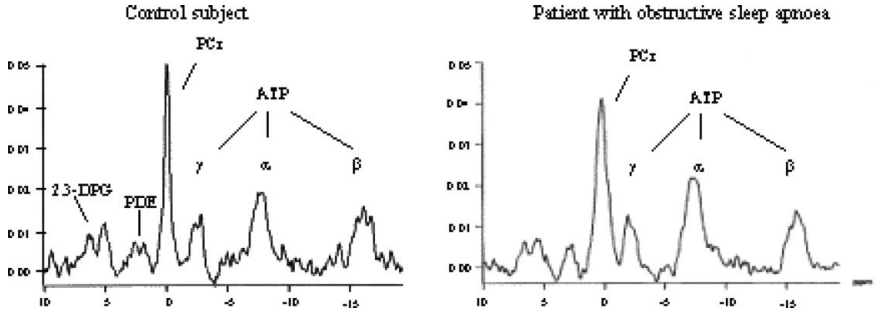

FIG. 1.

in 31 pts., and wall motion abnormalities in 81pts. Transmural infarction was diagnosed by echocardiography in 74%. Whereas subendocardial infarction was only suspected in one patient (8%).

Conclusions: The accuracy for diagnosing myocardial scarring by standard echocardiographic criteria in nonselected cardiac patients is acceptable for transmural infarction. However, the recognition of subendocardial infarction is insufficient.

419. FEASIBILITY OF VASODILATOR STRESS TESTING IN A 70 CM WIDE BORE SCANNER AT 1.5T

Federico E. Mordini, W. Patricia Bandettini, Peter Kellman, Christine Mancini, Andrew E. Arai. ***National Institutes of Health, Bethesda, MD, USA.***

Introduction: The small bore size of standard 1.5T scanners prohibits MR imaging of certain patient populations. Obesity, claustrophobia, and heart failure complicated by orthopnea are all conditions that limit feasibility of cardiac MR examinations in standard bore scanners. Also, obese patients are technically difficult to image by other means. Furthermore, pharmacologic stress testing requires close monitoring of the patient and would be safer and easier to perform in a less confined setting. Many of these problems might be alleviated by a novel 70 cm bore magnet design. We describe our initial experience with performing vasodilator stress MRI exams with a wide bore 1.5T scanner.

Objective: To test the feasibility of performing pharmacologic stress MRI exams in a 70 cm wide bore 1.5T scanner.

Methods: Thirteen patients with clinical indications for cardiac stress testing underwent vasodilator stress with dipyridamole 0.56 mg/kg IV over 4 minutes. Imaging consisted of steady state free precession (SSFP) localization, SSFP short and long axis cine, gradient echo accelerated echoplanar (GRE-EPI) first pass perfusion with a TSENSE factor of 2, and phase sensitive delayed enhancement. Images were acquired with a Siemens 1.5 Tesla Magnetom Espree system with a 70 cm bore size and 125 cm length which is 10 cm wider in diameter and 35 cm shorter in length than traditional scanners.

Results: Image quality was deemed good for all cine function studies. Perfusion was judged good in all but 3 cases which were fair due to artifact (2 ghost and 1 gating artifact). Delayed enhancement was of good quality except for 2 cases which were fair due to arrhythmia or poor gating. No portion of the imaging protocol was non-diagnostic in any patient.

Artifacts during first pass perfusion imaging were common, but did not interfere with image interpretation due to the peripheral location of the artifacts (Fig. 2).

Conclusions: Vasodilator stress MRI exams can be performed on a large bore system with high image quality but with some off-resonance artifacts near the edges of the field of view. In our broader experience with stress and rest MRI studies, we have scanned a patient weighting 404 lbs, a patient requiring

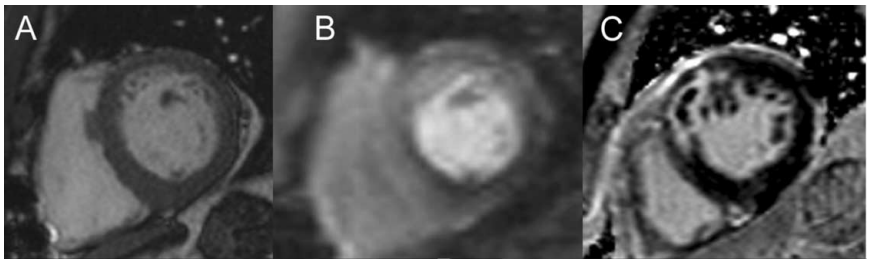

FIG. 1. Examples of cine (A), stress perfusion (B), and delayed enhancement imaging (C) acquired from different patients. Note the severe stress perfusion defect in the inferoseptal, inferior, and inferolateral walls. The delayed enhancement image demonstrates an anterior and anteroseptal infarct with microvascular obstruction.

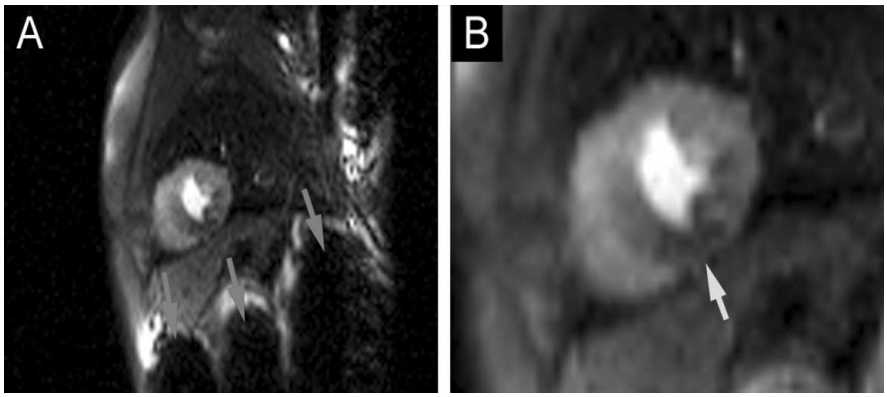

FIG. 2. Panel A demonstrates a true positive perfusion exam in full field of view which shows peripheral off-resonance artifacts (red arrows) that do not interfere with interpretation of the inferior perfusion defect (green arrow) as shown in panel B.

3 pillows for orthopnea, and a patient previously claustrophobic in a traditional bore scanner demonstrating that imaging patients previously unsuitable for MRI is possible. In an era where obesity and heart failure are increasing clinical problems, the feasibility of performing high quality non-invasive cardiac testing in these populations is a clinically important advance.

420. CHANGES OF B-TYPE NATRIURETIC PEPTIDE FOR THE DETECTION OF MYOCARDIAL ISCHEMIA IN PATIENTS UNDERGOING HIGH-DOSE DOBUTAMINE STRESS MRI

Oliver Bruder,[1] Peter Hunold,[2] Markus Jochims,[1] Kai U. Waltering,[2] Georg V. Sabin,[1] Jörg Barkhausen.[2] ***[1] Department of Cardiology and Angiology Elisabeth Hospital, Essen, Germany, [2] Department of Diagnostic and Interventional Radiology and Neuroradiology University Hospital, Essen, Germany.***

Background: High-dose dobutamine stress MRI has been established as a reliable technique for the assessment of myocardial ischemia in patients with coronary artery disease. Dobutamine increases contractility and rate-pressure product, thus increasing myocardial oxygen demand. Dobutamine-induced myocardial ischemia during stress MRI results in increased wall stress and development of regional wall motion abnormalities. Additionally, B-type natriuretic peptides are released by ventricular myocytes in response to wall stress.

Objectives: Aim of this study was to investigate whether the induction of ischemic wall motion abnormalities during dobutamine stress MRI (DSMR) results in changes of the inactive N-terminal fragment of B-type natriuretic peptides (NT-pro-BNP).

Methods: A total of 59 consecutive patients with known or suspected coronary artery disease underwent DSMR for the detection of myocardial ischemia. All examinations were performed using a 1.5 T MR System (Magnetom Sonata; Siemens Medical Solutions; Erlangen, Germany). A dobutamine/atropine stress protocol (10, 20, 30 and 40 μg/kg per min dobutamine and up to 1 mg of atropine) was used until 85% of the age-predicted heart rate was achieved. Imaging at each stress level was performed in at least 3 long and 3 short axis views using a segmented steady state free precession sequence (TR 3 ms, TE 1.5 ms, FA 60°). All examinations were evaluated by an experienced radiologist and a cardiologist in consensus. Myocardial ischemia was defined by new or worsening wall motion abnormalities in more than one myocardial segment. Additionally, late enhancement imaging was performed in all patients following injection of 0.2 mmol/kg of contrast using a segmented 2D inversion recovery fast low angle shot sequence (TR 8 ms, TE 4 ms, FA 25°). Blood samples were taken before and immediately after stress imaging and analysed for NT-pro-BNP.

Results: Fifteen patients with atrial fibrillation, impaired left ventricular function (ejection fraction at rest <50%) or prior myocardial infarction, defined by late enhancement were excluded. Of the remaining 44 patients, 19 had ischemia on DSMR, 25 patients did not. Median baseline NT-pro-BNP values of 104.7 pg/mL (Q1 64.9; Q3 151.6) were significantly higher ($p < 0.01$) in the ischemia group than in the non-ischemia group with median NT-pro-BNP values of 30.8 pg/mL (Q1 21.7; Q3 111.1) (interquartile range). Median NT-pro-BNP values rose from 104.7 pg/mL (Q1 64.9; Q3 151.6) at rest to 147.0 pg/mL (Q1 70.5; Q3 164.7) after dobutamine stress in the ischemia group and from 30.8 pg/mL (Q1 21.7; Q3 111.1) to 30.4 pg/mL (Q1 24.0; Q3 110.8) in patients without inducible ischemia on DSMR. A Wilcoxon signed rank test was performed to compare both groups. Relative stress-induced increase of NT-pro-BNP was significantly lower (median 0.4; Q1 −0.4; Q3 2.00) in non-ischemic than in ischemic patients (median 6.7; Q1 2.0; Q3 16.9); $p < 0.0001$.

Conclusions: Release of NT-pro-BNP after dobutamine stress MRI is higher in patients with myocardial ischemia. Further studies are needed to investigate whether measurement of NT-pro-BNP can improve the diagnostic accuracy of DSMR.

421. ANGIOGRAPHIC CORRELATIONS OF PATIENTS WITH SMALL-VESSEL DISEASE DIAGNOSED BY ADENOSINE-STRESS MAGNETIC RESONANCE IMAGING

Günter Pilz, Markus Klos, Eman Ali, Berthold Höfling, Peter Bernhardt. ***Cardiac MRI at the Hospital Agatharied, Hausham, Munich, Germany.***

Background: Cardiac magnetic resonance imaging (CMR) with adenosine-stress myocardial perfusion is gaining importance for non-invasive detection and quantification of coronary artery disease. However, its high sensitivity values are weakened by lower specificity (false positive CMR assessment). In this context, there is little knowledge about those patients with CMR-detected myocardial ischemia, but no coronary artery stenosis as seen on coronary angiography. Aims of our study were to detect and characterize these patients with small-vessel disease by both CMR and coronary angiography, evaluate correlations and reasons for the ischemic findings.

Methods: Consecutive patients with indication for coronary angiography were scanned on a 1.5-T whole-body scanner. After three minutes of adenosine infusion (140 μg/kg) myocardial first-pass sequence in 4-5 continuous short-axis orientation using Gadolinium-based contrast agent (0.1 mmol/kg) was performed. Images were analyzed by two independent and blinded investigators for abnormal myocardial perfusion. All patients underwent coronary angiography and corrected TIMI frame count was evaluated for the left anterior descending (LAD), circumflex (RCX) and right coronary artery (RCA). Patients with perfusion deficit were classified as having relevant perfusion deficit affecting >1/3 of myocardial wall thickness and persisting for >5 heart beats after maximal signal intensity in the left ventricular cavity or subendocardial deficit ($\leq$ 1/3 wall thickness).

Results: We included 50 patients into our study: 15 with subendocardial perfusion deficit (study group), 17 without

(control I) and 18 with relevant perfusion deficit (control II). All patients with relevant perfusion deficit had coronary artery stenosis >70% as seen by coronary angiography. Study group and control I patients showed no pathological coronary findings. Corrected TIMI frame count in the LAD and RCX was significantly increased in study group patients compared to both control II patients (1.45 ± 0.29 sec. versus 1.10 ± 0.11 sec. in the LAD, $p < 0.0001$; 1.33 ± 0.26 sec. versus 1.1 ± 0.16 sec. in the RCX, $p = 0.001$) as well as compared to control I patients (1.16 ± 0.25 sec. in the LAD, $p = 0.005$; 1.03 ± 0.21 sec. in the RCX, $p = 0.001$). Patients did not differ significantly for TIMI frame count in the RCA. Study group patients had more commonly hypertension (9 (75%) versus 14 (37%), $p = 0.02$) or diabetes (7 (58%) versus 8 (21%), $p = 0.01$) compared to both control groups.

Conclusion: Subendocardial perfusion deficit as seen by CMR highly correlates to slowed coronary artery flow most likely due to coronary microangiopathy. Coronary artery flow in patients with subendocardial perfusion deficit was significantly reduced not only compared to the normal controls, but also to patients with coronary artery stenosis. Hence, the false positive CMR with regard to detection of relevant coronary stenosis seems to be due to "suprasensitivity" in detecting even coronary microangiopathy. Therefore, criteria for differentiating relevant ischemia from subendocardial ischemia could reduce the false positive rate and yield a higher specificity for CMR. Hypertension and diabetes seem to be also cardiovascular risk factors for small-vessel disease detected by subendocardial ischemia and reduced coronary flow.

422. DETERMINATION OF CARDIAC VOLUMES AND MASS IN PATIENTS WITH IMPAIRED VENTRICULAR FUNCTION AT 1.5 AND 3 TESLA

Adrian S.H. Cheng, MBBS, MRCP, Damian J. Tyler, PhD, Matthew D. Robson, PhD, Stefan Neubauer, MD, FRCP, Joseph B. Selvanayagam, DPhil, FRACP. ***University of Oxford, London, United Kingdom.***

Introduction: Cardiac magnetic resonance imaging (MRI) is the gold standard for determination of cardiac volumes and mass. At 1.5 Tesla (T), steady state free precession (SSFP) imaging is the technique of choice for assessment of ventricular volumes and mass in clinical practice. The increased signal-to-noise ratio at 3 T could enhance cardiac MRI applications that have restrictive temporal and/or spatial resolution at 1.5 T, such as perfusion and spectroscopy. Analysis of cardiac volumes and mass would be required to interpret the parameters generated.

Purpose: To compare cardiac cine MRI using the same SSFP sequence at 1.5 and 3 T in patients with impaired left ventricular (LV) function.

Methods: Thirteen patients (12 male, 1 female; mean age 68 ± 12 years) with impaired LV function (determined by previous echocardiography or ventriculography) were recruited. Each participant was scanned by the same operator at both 1.5 T (Sonata, Siemens Medical Solutions, Erlangen, Germany) and 3 T (Trio, Siemens Medical Solutions) with the scans 30 minutes apart and done in random order. Based on frequency pilots in the

Table: Left and right ventricular measurements at 1.5 T and 3 T in patients with impaired left ventricular function

	1.5 T	3 T	Difference	p value
LV ejection fraction (%)	33 ± 13	32 ± 13	0.6 ± 1.7	0.17
LV end-diastolic volume (mL)	271 ± 82	271 ± 80	0.0 ± 11.7	1.00
LV end-systolic volume (mL)	185 ± 83	184 ± 82	0.5 ± 8.2	0.82
LV stroke volume (mL)	84 ± 24	82 ± 28	1.6 ± 9.7	0.53
LV mass (g)	162 ± 44	160 ± 44	1.3 ± 19.5	0.80
RV ejection fraction (%)	41 ± 10	42 ± 11	1.2 ± 6.6	0.49
RV end-diastolic volume (mL)	191 ± 86	189 ± 84	1.3 ± 11.3	0.65
RV end-systolic volume (mL)	114 ± 63	115 ± 67	0.6 ± 9.6	0.82
RV stroke volume (mL)	78 ± 32	75 ± 29	2.5 ± 6.9	0.16
RV mass (g)	68 ± 40	66 ± 38	1.7 ± 4.4	0.15

Paired t-test used to compare effect of field strength and $p < 0.05$ considered significant. All data presented as mean ± standard deviation. LV = left ventricle; RV = right ventricle.

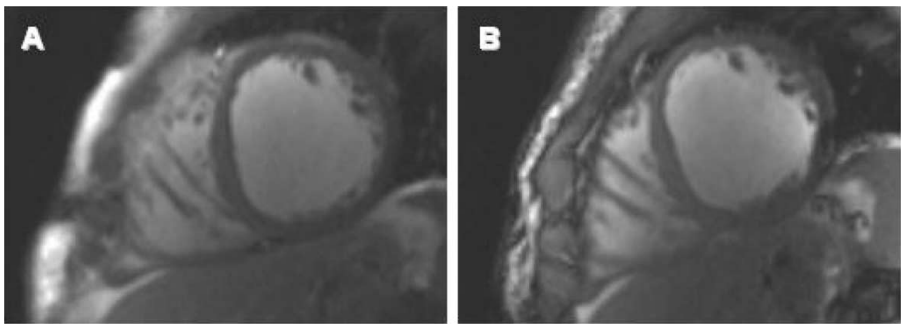

FIG. 1. End-diastolic short-axis slice at 1.5 T (A) and 3 T (B) from a patient with left ventricular ejection fraction of 20%.

mid-ventricular short-axis and horizontal long-axis orientations, the optimum frequency offset was selected and short-axis images (slice thickness 7 mm, inter-slice gap 3 mm) covering the entire heart were acquired with the SSFP sequence using retrospective electrocardiographic gating. Identical sequence parameters were used on each system wherever possible.

Results: All images acquired were of sufficient quality for analysis despite the presence of sternal wires in 3 of 13 (23%) patients and coronary stents in 3 of 13 (23%) patients. No problems with electrocardiographic gating were encountered despite 2 of 13 patients (15%) being in atrial fibrillation. Two investigators blinded to the field strength traced the endocardial and epicardial contours of both ventricles in all end-diastolic and end-systolic short-axis images in the standard way. Mean LV ejection fraction at 1.5 T was 33 ± 13%. There were no significant differences in quantification of volumes, mass or function of either ventricle at 1.5 T or 3 T ($p > 0.05$ for all parameters). Intra-observer coefficient of variability for LV ejection fraction was 6.1% at 1.5 T and 6.0% at 3 T, while inter-observer variability was 2.6% and 3.5% at 1.5 T and 3 T respectively. Right ventricular ejection fraction variability was higher than that for the LV.

Conclusions: Cardiac cine MRI at 3 T using SSFP is feasible and reproducible. There were no significant differences in quantification of cardiac volumes or mass at 1.5 or 3 T. Normal values for cardiac volumes and mass established in patients at 1.5 T can be applied to scans obtained at 3 T.

423. GADOMER-ENHANCED WHOLE HEART CORONARY MAGNETIC RESONANCE ANGIOGRAPHY FOR DETECTION OF CORONARY ARTERY DISEASE

Sebastian Kelle, MD,[1] Tarinee Tangcharoen, MD,[1] Ingo Paetsch, MD,[1] Bernhard Schnackenburg, PhD,[2] Katharina Strach, MD,[3] Uwe Köhler, PhD,[1] Eckart Fleck, MD,[1] Torsten Sommer, MD,[3] Eike Nagel, MD.[1] [1]***German Heart Institute Berlin, Berlin, Germany,*** [2]***Philips Medical Systems, Berlin, Germany,*** [3]***University Hospital Bonn, Bonn, Germany.***

Introduction: Magnetic resonance (MR) coronary artery imaging is rapidly gaining adequate quality for clinical use. It is, however, hampered by low signal to noise ratios and limited coverage of the coronary artery tree, which might be significantly improved by intravascular contrast agents.

Purpose: The aim of this multicenter trial (2 Philips centers) was to evaluate the accuracy of contrast-enhanced MRCA using the intravascular contrast agent Gadomer (Schering, Berlin, Germany) in comparison to invasive angiography.

Methods: Nine patients (6 men, 3 women; age range: 57–80 years; mean age, 69 ± 7 years) with suspected or known coronary artery disease underwent free-breathing navigator whole heart MR coronary angiography before and after injection of Gadomer (0.150 mmol gadolinium per kilogram body weight). Signal intensity vs. native imaging, image quality (five-point scale: 0—no visualization, 1—nondiagnostic, 2—moderate, 3—good, 4—excellent) vs. native imaging and stenosis detection of MR angiograms (6 segment model: left main, proximal and middle left anterior descending, proximal left circumflex and proximal and middle right coronary artery segment) vs. invasive angiography were evaluated.

Results: Contrast (signal intensity blood/signal intensity myocardium) increased significantly after administration of Gadomer (8.5 ± 4.3 vs. 2.4 ± 0.3; $p = 0.004$). Image quality improved significantly from 2.3 ± 0.8 to 3.2 ± 0.4 ($p = 0.006$). Overall sensitivity and specificity of contrast enhanced MRCA vs. native images for detection of coronary artery disease were 91.7% and 86.7%,vs. 35.7% and 88.9%, accuracy was 88.1% vs. 70.7%.

Conclusions: Contrast-enhanced whole-heart coronary MR angiography with Gadomer is feasible and significantly improves image quality, contrast and accuracy for detection of coronary artery disease compared with non-enhanced sequences.

424. B-TYPE NATRIURETIC PEPTIDE EARLY AFTER ACUTE MYOCARDIAL INFARCTION: RELATION TO DIASTOLIC FUNCTION AND EXTENT OF MYOCARDIAL DAMAGE STUDIED BY MR IMAGING

Bernard P. Paelinck,[1] Christiaan J. Vrints,[1] Jeroen J. Bax,[2] Johan M. Bosmans,[1] Albert de Roos,[2] Hildo J. Lamb.[2] [1]***University Hospital Antwerp, Edegem, Belgium,*** [2]***Leiden University Medical Center, Leiden, The Netherlands.***

Introduction: Plasma B-type natriuretic peptide (BNP) levels increase markedly after acute myocardial infarction and have been correlated to left ventricular (LV) systolic dysfunction. However, in these patients, the relation between BNP and the extent of myocardial scar formation and LV diastolic dysfunction remains unclear.

Purpose: To investigate whether BNP levels are associated with the extent of myocardial scar formation and LVdiastolic dysfunction in recent myocardial infarction.

Methods: Thirty-two consecutive patients early (5 ± 3 days) after a first acute myocardial infarction were studied. Delayed contrast-enhanced magnetic resonance (MR) imaging was performed to define myocardial scar. Diastolic function was assessed using phase-contrast MR measurements of mitral flow and septal tissue velocities (tissue MR imaging) to estimate LV filling pressures. MR study was immediately followed by BNP measurement.

Results: LV ejection fraction ranged from 27% to 65% and myocardial scar ranged from 4% to 62% of the LV mass. BNP ranged from 14.6 pg/mL to 1390 pg/mL. BNP related to LV ejection fraction ($r = -0.52$, $P = 0.002$), extent of myocardial scar (% delayed hyperenhancement of the LV mass, $r = 0.49$, $P = 0.005$, transmurality index, $r = 0.58$, $P < 0.001$) and estimated LV filling pressures (E/Ea or ratio of early diastolic mitral flow velocity (E) and early diastolic mitral annular velocity (Ea),

r = 0.51, P = 0.003)). In multivariate analysis transmurality index and E/Ea were independent predictors of BNP levels (P < 0.05, power of 0.99 at alpha = 0.05).

Conclusions: In conclusion, among patients with recent myocardial infarction elevated BNP levels are independently associated with both the extent of myocardial scar tissue and diastolic dysfunction.

425. CONTRAST-DOSE RELATION IN TURBOFLASH AND ECHOPLANAR FIRST PASS PERFUSION IMAGING

Wolfgang Utz, Ralf Wassmuth, Rainer Dietz, Jeanette Schulz-Menger. ***Franz-Volhard-Klinik, CharitÃ Campus Buch, University Berlin, Helios-Kliniken, Berlin, Germany.***

Background: Myocardial perfusion imaging is an interesting tool for the detection of coronary artery disease. However, the ideal dosage of contrast agent (CA) is still unknown. Both visual and semiquantitative evaluation methods rely on a linear relation between CA concentration and signal intensity (SI) of blood and myocardium. We report on the relation of SI enhancement in human first pass perfusion over a broad range of contrast doses with two different pulse sequences.

Methods: Ten healthy volunteers (4 female, range 25–43 years) were studied in a 1.5 T clinical MR scanner (Siemens Sonata). They received incremental dosages of Gd-DTPA, ranging from 0.00125–0.1 mmol/ kg of bodyweight. Doses were administered as equal bolus volumes doped with incremental CA. For doses >0.01 mmol/kg, a resting period of 15 minutes was allowed for CA washout. Using a standard three-slice short-axis protocol, volunteers were examined on two separate occasions with two different MR perfusion pulse sequences:

1) TurboFLASH (TR 172 ms; TE 1.25 ms; flip angle 12°; inversion time 100 ms; parallel imaging (iPAT GRAPPA) acceleration rate 2; FOV 320 mm; matrix size 94 × 192; in plane resolution 1.7 × 2.6 mm; slice thickness 10 mm; bandwidth 500 Hz/Px).
1) Echo Planar Imaging (EPI) (TR 5.6 ms; TE 1.17 ms; EPI factor 4; flip angle 25°; saturation delay 70 ms; FOV 370 mm; matrix size 80 × 128; in plane resolution 2.9 × 3.5 mm; slice thickness 8 mm; bandwidth 1860 Hz/Px).

Maximum contrast enhancement normalized to baseline (MCE_{norm}) as well as contrast-to-noise ratio (CNR) were obtained from time-intensity curves of a mid-ventricular myocardial slice (in total) and blood in the LV cavity. Noise was defined as standard deviation of the pre-contrast MR signal.

Results: Blood MCE_{norm} showed a strong saturation behaviour with increasing CA doses for both sequences (Fig. 1). For dosages <0.01 mmol/kg the MCE_{norm}-dose relation was almost linear with both sequences. EPI obtained 64% of full contrast saturation at slightly lower CA dosage than turbo-FLASH (0.013 vs. 0.018 mmol/kg). For higher doses, contrast saturation resulted in underestimation in relation to a linear approach, e.g. at 0.025 mmol/ kg of 22% for EPI and 24% for turboFLASH, at 0.05 mmol/L 49% for EPI and 46% for turboFLASH. For doses higher than 0.01 mmol/kg, turboFLASH resulted in significantly higher blood contrast ($p < 0.001$). In the myocardium a linear dynamic range could be observed up to a dose of 0.05 mmol/kg for both sequences with no significant difference in contrast magnitude (Fig. 2). At 0.1 mmol/kg an underestimation of 33% (EPI) and 29% (turboFLASH) was detectable. Predominantly due to lower noise of the turboFLASH sequence, the myocardial CNR was about twofold ($p < 0.001$) and the blood CNR was about threefold ($p < 0.001$) higher compared to EPI in CA doses higher than 0.01 mmol/kg.

Conclusion: For semiquantitative perfusion analysis, our data favor contrast doses up to 0.01 mmol/kg for the assessment of arterial input function and up to 0.05 mmol/kg for myocardial perfusion. Given the pulse sequence parameters used in our study, turboFLASH with parallel imaging resulted in a myocardial CNR that was two times higher than that of EPI.

426. MYOCARDIAL MR PERFUSION IMAGING FOR GUIDANCE OF INTERVENTIONAL REVASCULARIZATION IN PATIENTS WITH CORONARY ARTERY DISEASE AND SUSPECTED RE-STENOSIS

Stephan Miller, MD, Tobias Hövelborn, MD, Bernhard Klumpp, MD, Michael Fenchel, MD, Uwe Helber, MD, Ulrich Kramer, MD, Claus D. Claussen, MD, Andreas May, MD, Meinrad P. Gawaz, MD. ***University of Tuebingen, Tuebingen, Germany.***

Introduction: The detection of coronary re-stenosis is very important for the decision of invasive coronary re-angiography and -intervention in symptomatic patients after myocardial revascularization.

Purpose: In our study, cardiac MR imaging (MRI) was used in order to detect relevant coronary artery stenoses (CAS) and guide re-intervention in patients after myocardial revascularization.

Methods: Prior to invasive coronary angiography 73 consecutive patients (mean age 64 ± 12, range 24–85y) with recurrent symptoms of myocardial ischemia after interventional or operative coronary revascularization were examined (1.5 T Magnetom Sonata, Siemens, Erlangen). Myocardial wall motion was evaluated by cine trueFISP imaging and left ventricular functional parameters were determined based on the modified Simpson rule by using a dedicated postprocessing software (ARGUS, Siemens, Erlangen, Germany). Myocardial perfusion imaging was obtained at stress (140 μg Adenosin per kg BW per min.) and rest using a turboFLASH 2D sequence. A dose of 0.1 mmol Gd-DTPA (Magnevist, Schering, Berlin, Germany) was injected at both times. Myocardial viability was assessed by delayed enhancement imaging (segmented IR turbo FLASH 2D sequence). Qualitative consensus reading of two experienced observers who were blinded for clinical data was applied for image analysis. Catheter coronary angiography was used as standard of reference for the diagnosis of hemodynamically relevant CAS (>75% of luminal narrowing).

Results: Stress induced myocardial malperfusion was detected in 51/73 patients and corresponding to relevant CAS requiring re-intervention in 42/44 patients (=sensitivity 94%, specificity 69%). In 20 patients absence of relevant CAS was correctly diagnosed. Sensitivity/specificity for MRI detection of the target region corresponding to the ischemia related artery was 94%/85% for the RCA, 89%/80% for the LAD and 56%/91% for the Lcx. Mean ejection fraction of the patient group was normal with 53 ± 12% (range 22–78%). Delayed contrast enhancement was observed in 49 patients and consistent with unsuspected myocardial infarction in 21 cases.

*Conclusions:*Cardiac MRI allows the detection of hemodynamically relevant stenosis in patients with known CAD after revascularization. Correct identification of Lcx stenosis is limited whereas RCA and LAD lesions can be predicted in most cases. Our study suggests that MRI prior to invasive coronary angiography is helpful to guide re-intervention in this group of patients.

427. EXTENT OF RIGHT VENTRICULAR INFARCTION PREDICTS RIGHT VENTRICULAR DILATATION

Theodorus A.M. Kaandorp, MD, Jeroen J. Bax, MD, PhD, Eric P. Viergever, MD, Ernst E. van der Wall, MD, PhD, Albert de Roos, MD, PhD, Hildo J. Lamb, MD, PhD. ***Leiden University Medical Center, Leiden, The Netherlands.***

Introduction: Right ventricular (RV) infarction is associated with considerable morbidity and mortality, and its presence defines a high-risk subgroup of patients with inferior left ventricular (LV) infarction. Accurate diagnosis is important for acute management and may also be predictive for RV dilatation. The diagnosis of RV infarction is based on the clinical presentation and typical abnormalities in the right precordial (e.g. 1 mm ST-segment elevation in lead V4R) leads on the ECG. Also, contrast-enhanced magnetic resonance imaging (ce-MRI) has a high accuracy for non-invasive assessment of scar tissue.

Purpose: To evaluate the accuracy of ce-MRI to assess RV infarction using the ECG criteria as the gold standard. In addition, the extent of RV scar formation was determined and related to RV remodeling at 6 months follow-up.

Methods: Consecutive patients with a first acute inferior myocardial infarction were included. RV ECGs were obtained at presentation to assess RV infarction. The study protocol consisted of a resting cine MRI, within 1 week after infarction to evaluate RV function and volumes, followed by ce-MRI, to determine the extent of scar tissue in the RV. To evaluate the impact of scar formation on RV remodeling, cine MRI was repeated at 6 months to re-assess RV function and volumes.

Results: Eighteen patients (mean age 42 ± 11 years) were included and 7 (39%) exhibited RV infarction using the ECG (V4R) criteria as the gold standard. All were identified by ce-MRI; in addition, ce-MRI demonstrated scar tissue in 2 patients without ECG abnormalities. Using the ECG as gold standard, ce-MRI had a sensitivity of 100% with a specificity of 78%. At 6 months follow-up, RV end-diastolic volume increased significantly (from 171 ± 25 mL to 182 ± 26 mL, $P < 0.05$) whereas RV end-systolic volume (94 vs. 87, NS) and RV ejection fraction (46 ± 6% vs. 52 ± 5%, NS) remained unchanged A good correlation was shown between extent of the scar in the RV and the increase in RV end-diastolic volume (as marker of RV remodeling) was noted ($y = 0.04\times + 0.03$; $n = 18$, $r = 0.84$, $P < 0.05$); patients with extensive scar formation exhibited significant RV dilatation.

Conclusion: A high accuracy of ce-MRI for detection of RV infarction was shown; ce-MRI may even allow scar detection in patients without typical ECG (V4R) abnormalities on presentation. A good correlation was observed between the extent of scar formation in the RV and the subsequent RV dilatation at follow-up.

428. SENSITIVITY AND SPECIFICITY OF ADENOSINE STRESS CARDIAC MAGNETIC RESONANCE FOR DETECTION OF SIGNIFICANT CORONARY ARTERY STENOSIS: COMPARISON WITH CORONARY ANGIOGRAPHY

Karol Miszalski-Jamka, MD, Giso von der Recke, MD, David Hardung, MD, Bernhard Saxler, Jan Schnapauff, Christoph Hammerstingl, MD, Harald Schmidt, MD, Heyder Omran, MD, PhD. ***St.-Marien-Hospital, Bonn, Germany.***

Introduction: Adenosine stress cardiac magnetic resonance (CMR) is highly accurate imaging modality for evaluating myocardial perfusion. The assessment of myocardial perfusion makes it possible to detect indirectly significant coronary stenosis. The sensitivity and specificity of adenosine CMR has been established in several studies but with relatively small populations.

Purpose: To evaluate sensitivity and specificity of stress CMR with adenosine for detection of significant coronary artery stenoses.

Methods: One hundred twenty-two consecutive patients with known or suspected myocardial ischaemia referred for coronary artery catheterization underwent adenosine CMR using a 1.5 T scanner. The myocardial perfusion was assessed using the standard adenosine protocol (stress and rest perfusion, late enhacement). An experienced observer assessed visually the perfusion deficit transmurality score of each segment using a 16-segment model and a 5-point scale (0—no deficit, 1—transmurality ≤25% of left ventricle wall thickness, 2–26% to 50%, 3–51% to 75%, and 4–76% to 100%). Using a 17-segment model the transmurality of scars was graded analogically. After CMR all patients underwent successfully coronary artery catheterization by an independent blinded experienced observer. Only stenosis ≥70% of lumen diameter were classified as hemodynamically significant.

Results: Eighty-one patients were male (66.4%), 41 female (33.6%) with a mean age of 67.6 years. Interpretable CMR images were obtained in all patients. Nine patients (7.4%) have no inducible perfusion deficits, 18 patients (14.8%)—mild subendocardial ischaemia, 53 patients (43.4%)—relevant ischaemia, 14 patients (11.4%)—myocardial scar without additional relevant ischaemia, and 28 patients (23.0%)—myocardial scar with additional relevant ischaemia. Angiography showed significant stenosis in 56 (45.9%) patients. Only 2 patients from 43 (4.6%), who had no relevant inducible ischaemia in CMR, had significant coronary artery stenosis. On the other hand, 25 of 79 (31.6%) patients, who had relevant inducible myocardial ischaemia in CMR (with and without myocardial scar), had no significant coronary lesions. Sensitivity for detection of angiographically significant coronary artery stenosis was 96.4% with a specificity of 62.1%. Negative and positive predictive value were 95.3% and 68.3%, respectively.

Conclusions: Adenosine CMR has a very high negative predictive value for excluding significant coronary artery stenosis. This finding has important implications for selecting patients for coronary angiography.

429. MYOCARDIAL FIRST PASS PERFUSION DYNAMIC SIGNAL EVALUATION IN NORMALS

Yi Wang, DSc, Bin Luo, BS, Sunil T. Mathew, MD, Ola Akinboboye, MD, Nathaniel Reichek, MD. ***St. Francis Hospital, Roslyn, NY, USA.***

Introduction: MR first-pass perfusion images are difficult to interpret due to poor signal to noise and the presence of susceptibility and motion artifacts. A simple approach to quantification of perfusion signal uses dynamic signal upslope, based on averaging myocardial signal amplitude change in a myocardial segment over a time series. Upslope evaluation algorithms include a global method which evaluates the full range of pixel values in the upslope, a constrained global method and a piecewise method which evaluates a limited subset of upslope pixel values. To systematically compare the performance of these two methods in upslope calculation, we applied both algorithms to the same perfusion image data with the same contours acquired from normals. Variations in regional estimates of flow reserve (FR) taken as the ratio of stress/rest upslope were studied to see which algorithm is more susceptible to artifacts based on the assumption that physiological FR variation is small in normal volunteers.

Methods: To ensure the normality of the perfusion data, strict exclusion criteria were used in volunteer recruitment, including exclusion of hypertension, diabetes, family history of cardiac disease, and EBCT coronary calcium score ≤ 1. Five volunteers (ages: 20 to 37, 3 females) were enrolled after IRB approval. First pass perfusion studies were performed on a 1.5 T Siemens scanner using a saturation recovery TrueFISP technique with a voxel resolution of $1.9 \times 2.8 \times 8$ mm^3 at three slices per heartbeat over 50 heart beats with an acquisition time of 160 ms. After the epi and endo myocardial contours were determined by MASS (Medis, Leiden, the Netherlands), the myocardium was divided clockwise into 6 equal segments. Mean signal intensities of all pixels in each segment at each time point were transferred to Matlab (The MathWorks Inc., Natick, MA) program which calculated relative upslope according to the following algorithms. Piecewise: From start to end of the time series, segmental upslope was calculated for each time point by taking signal intensity from neighboring time points using least square means. The maximal relative upslope was selected as the largest upslope among all time series; Global: Points at the foot and the peak of the upslope were identified and all points in between were used to find upslope using linear least square fitting; Constrained global: To select correct foot and peak values, two constraints were added to the global method: Myocardial peak values had to fall within 15 heartbeats after blood peak and myocardial foot value had to fall after blood foot. The same algorithm was applied to ventricular cavity blood signal to calculate its upslope, which was used to normalize myocardial upslope for each slice. Relative upslope of each myocardial segment in each slice was calculated and evaluated with each algorithm. The FR was determined as the ratio of stress to rest upslopes.

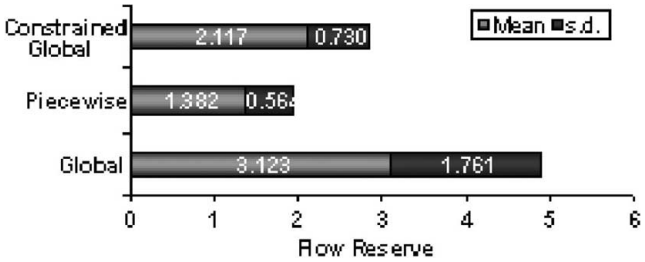

FIG. 1. Upslope algorithm comparison.

Results: The mean and s.d. of FR in all segments (n = 90) for each algorithm is shown in Fig. 1. One-way ANOVA showed significant difference among 3 groups and between each algorithm. Normalized s.d. (NSD = s.d./mean) was low (40.8%) using the piecewise method, but the mean FR was also low compared to other two methods and to reference methods such as PET and invasive Doppler flow wire. The FR is highest with the global method, but the NSD (56.4%) is also highest. The constrained global method gives normal FR values closer to reference methods with lowest variability (NSD = 34.5%).

Conclusion: Regional flow reserves vary with the algorithm chosen for upslope calculation. Results from a constrained global algorithm showed absolute values closer to reference methods than the Piecewise algorithm with smaller normalized variability than the global algorithm, suggesting it may be the most useful approach.